

University of Nebraska - Lincoln

DigitalCommons@University of Nebraska - Lincoln

Dissertations & Theses in Earth and Atmospheric
Sciences

Earth and Atmospheric Sciences, Department of


7-2018

Evaluating 21st Century Climate Change for Bolivia: a Comprehensive Dynamical Downscaling Strategy Using the WRF Regional Climate Model

Azar Mohammad Abadi

University of Nebraska-Lincoln, azar@huskers.unl.edu

Follow this and additional works at: <http://digitalcommons.unl.edu/geoscidiss>

 Part of the [Earth Sciences Commons](#), and the [Oceanography and Atmospheric Sciences and Meteorology Commons](#)

Mohammad Abadi, Azar, "Evaluating 21st Century Climate Change for Bolivia: a Comprehensive Dynamical Downscaling Strategy Using the WRF Regional Climate Model" (2018). *Dissertations & Theses in Earth and Atmospheric Sciences*. 107.
<http://digitalcommons.unl.edu/geoscidiss/107>

This Article is brought to you for free and open access by the Earth and Atmospheric Sciences, Department of at DigitalCommons@University of Nebraska - Lincoln. It has been accepted for inclusion in Dissertations & Theses in Earth and Atmospheric Sciences by an authorized administrator of DigitalCommons@University of Nebraska - Lincoln.

EVALUATING 21ST CENTURY CLIMATE CHANGE FOR BOLIVIA: A
COMPREHENSIVE DYNAMICAL DOWNSCALING STRATEGY
USING THE WRF REGIONAL CLIMATE MODEL

by

Azar M. Abadi

A DISSERTATION

Presented to the Faculty of
The Graduate College at the University of Nebraska

In Partial fulfillment of Requirements
For the Degree of Doctor of Philosophy

Major: Earth and Atmospheric Science
(Meteorology/Climatology)

Under the Supervision of Professor Clinton M. Rowe

Lincoln, Nebraska

July, 2018

EVALUATING 21ST CENTURY CLIMATE CHANGE FOR BOLIVIA: A COMPREHENSIVE DYNAMICAL DOWNSCALING STRATEGY USING THE WRF REGIONAL CLIMATE MODEL

Azar M. Abadi, Ph.D.

University of Nebraska, 2018

Advisor: Clint M. Rowe

Bolivia is a low-latitude, developing country at grave risk for the effects of human-induced climate changes. This means evaluating the consequences of projected future climate changes is of significant importance. Unfortunately, the complex topography and high elevation of much of the country pose particular challenges, as these effects cannot be suitably resolved at the approximately 100 km spatial resolution of current global climate models (GCM). Therefore, a comprehensive suite of high-resolution climate change simulations was made focused on Bolivia are run using three different GCMs with three different emission scenarios for each to drive the Weather Research and Forecasting (WRF) regional climate model. Beyond the results specific to Bolivia, this study is a demonstration of a robust yet viable approach to providing high-resolution, practical, and useable climate change information for any region regardless of global location.

GCM performances in Bolivia show three Coupled Model Intercomparison Project Phase 5 (CMIP5) GCMs of MPI-ESM-LR, MIROC5 and CCSM4 are among the models that can successfully regenerate the large-scale atmospheric circulation over South America and more specifically over Bolivia. Initializing the WRF model by the above mentioned GCMs and the NCEP/NCAR reanalysis data then provides us with finer resolution climatic data at 36, 12 and 4 km that are later used for the climate change assessment over Bolivia. The results for the WRF model evaluation confirm the added

value of the regional climate model in capturing the effects of topography and local features, on simulating more realistic weather and climate especially on the mountainous regions.

Finally, the outcomes of the climate change assessment confirm that the climate mean and extreme patterns are changing in Bolivia as the precipitation is predicted to increase over the Amazon, particularly in the flood-prone region to the west, and decrease in the drier Altiplano. The temperature is predicted to increase across the country with more pronounced warming on the higher elevations where water availability is already a challenge. As one of the costliest hazards in the country, drought patterns are projected to change in the lowlands by having shorter lengths with greater severity while in the highlands conditions are worsening where drought events are predicted to last longer with enhanced severity.

To my mom,
My sweetest home and inspiration

To my dad,
Who was the first to believe in me

ACKNOWLEDGEMENTS

First of all, I take it upon myself to thank my advisor, Dr. Clint Rowe. I owe you a huge debt of gratitude for your fatherly support that kept me motivated and energetic to pursue the better future that I dreamt of and also for your thoughtful feedbacks and guidance throughout this process. Writing this dissertation would not have been possible without your ceaseless help. I would like to sincerely thank my retired advisor, Dr. Robert Oglesby who kindly and persistently conveyed his vast knowledge and experience in the field of climate science to me and helped me to develop my research questions.

I would like to express gratitude to my committee members, Dr. Mark Anderson, Dr. Mathew Van Den Broeke and Dr. Mike Hayes for kindly accepting to serve on my doctoral committee and for providing me with constructive comments in the progress of my research and on the written dissertation.

I want to thank Cynthia Hays who graciously provided her technical and knowledgeable expertise in working with models, and Dr. Marcos Andrade, for his constructive comments and providing me with the observational dataset in Bolivia.

I thank the Earth and Atmospheric Sciences Dept. and the University of Nebraska-Lincoln for funding me during my study period, through teaching assistantship. I also would like to thank Inter-American Development Bank (IDB) for the developments of tools and techniques used in this research, Daugherty Water for Food Global Institute for support to my advisors during the overall project, and the UNL Holland Computing Center for their computational support.

My deepest appreciation belongs to my parents who stuck with me along the way and never stopped supporting and loving me. To whom they have shared my best and

worst moments and have always been there to comfort me, and to my brother, Arash, who shared my nostalgia.

Finally, I would love to thank my boyfriend, Mohsen, for his constant encouragement and support, and my lovely friends Saeideh, Babak and Foad, my favorite siblings away from home.

TABLE OF CONTENTS

| | |
|--|----|
| CHAPTER 1- Introduction | 1 |
| References..... | 6 |
| CHAPTER 2- Evaluation of GCMs Historical Simulations of Monthly and Seasonal Climatology over Bolivia | 8 |
| 2.1. Introduction | 9 |
| 2.2. Data and Methodology | 11 |
| 2.2.1. Study Area | 11 |
| 2.2.2. Models and Observations | 11 |
| 2.3. Results | 13 |
| 2.3.1. Continental and Regional Climatology | 13 |
| 2.3.2. Precipitation Climatology | 15 |
| 2.3.3. Surface Air Temperature | 16 |
| 2.3.4. Upper and Lower Level Atmospheric Circulation Patterns | 18 |
| 2.3.5. Moisture Budget of the Atmosphere | 20 |
| 2.4. Discussion | 22 |
| 2.5. Summary | 24 |
| 2.6. References..... | 26 |
| CHAPTER 3- Climate Classification in Bolivia: A Combination of Nonhierarchical and Consensus Clustering Analyses Based on Precipitation and Temperature | 50 |
| 3.1. Introduction | 51 |
| 3.2. Data and Methodology | 53 |
| 3.3. 3.2.1 Study Area | 53 |
| 3.2.2 Data | 53 |

| | |
|---|----|
| 3.2.3 Methodology | 54 |
| 3.4. Results and Discussion | 58 |
| 3.3.1 Nonhierarchical Clustering | 58 |
| 3.3.2 Consensus Clustering | 59 |
| 3.5. Concluding Remarks | 63 |
| 3.6. References | 65 |
| CHAPTER 4- Climate Change Impact Assessment over Bolivia Using the WRF | |
| High-Resolution Dynamical Downscaling I: Evaluation of the Present-Day Climate | |
| 4.1. Introduction | 78 |
| 4.2. Models, Observation and Experiment Design | 80 |
| 4.2.1. Study Area and Climate Subregions | 80 |
| 4.2.2. Models | 81 |
| 4.2.2.1. NNRP | 81 |
| 4.2.2.2. The Driving CMIP5 Global Models | 82 |
| 4.2.2.3. The WRF Regional Climate Model | 82 |
| 4.2.3. Observational Dataset | 83 |
| 4.2.3.1. Station Measurements | 83 |
| 4.2.3.2. Gridded Observations | 83 |
| 4.2.4. Experimental Scheme | 84 |
| 4.3. Results and Discussion | 86 |
| 4.3.1. Verification against Station Measurements | 86 |
| 4.3.2. Mean Climate Pattern | 89 |
| 4.3.3. Interannual Variability | 92 |

| | |
|---|------------|
| 4.4. Summary and Conclusion | 94 |
| 4.5. References | 98 |
| CHAPTER 5- Climate Change Impact Assessment over Bolivia Using the WRF | |
| High-Resolution Dynamical Downscaling II: A Case Study for Drought | 119 |
| 5.1. Introduction | 120 |
| 5.2. Data and Experiment Design | 122 |
| 5.2.1. Study Area and the Climate Subregions | 122 |
| 5.2.2. Reanalysis and Observational Datasets | 123 |
| 5.2.2.1. Gridded Observations | 123 |
| 5.2.2.2. NCEP/NCAR Reanalysis Project | 124 |
| 5.2.3. Forcing CMIP5 Global Models | 124 |
| 5.2.4. Regional Climate Model | 125 |
| 5.2.5. Experiment Design and Methodology | 125 |
| 5.3. Results and Discussion | 129 |
| 5.3.1. Changes in Mean Climate | 129 |
| 5.3.2. Changes in Extremes | 130 |
| 5.3.3. Drought Assessment | 132 |
| 5.3.3.1. Drought Event Identification | 132 |
| 5.3.3.2. Statistical Properties of the Drought Events under Climate Change | |
| | 134 |
| 5.4. Summary and Concluding Remarks | 135 |
| 5.5. References | 139 |
| CHAPTER 6- Conclusion | 163 |

| | |
|-----------------|-----|
| References..... | 168 |
|-----------------|-----|

| | |
|-------------------------|------------|
| APPENDICES | 169 |
|-------------------------|------------|

List of Figures

| | |
|---|---|
| Figure 1.1 Bolivia's topography with geographical location of a few selected regions..... | 7 |
|---|---|

| | |
|--|----|
| Figure 2.1 Topography of Bolivia | 33 |
|--|----|

| | |
|---|----|
| Figure 2.2 Large-scale atmospheric circulation in South America | 34 |
|---|----|

| | |
|---|----|
| Figure 2.3 Precipitation climatology for CMIP5 models | 35 |
|---|----|

| | |
|--|----|
| Figure 2.4 Precipitation seasonal cycle over Bolivia | 37 |
|--|----|

| | |
|---|----|
| Figure 2.5 Frequency distribution of January precipitation in Bolivia | 38 |
|---|----|

| | |
|---|----|
| Figure 2.6 Temperature climatology for CMIP5 models | 39 |
|---|----|

| | |
|--|----|
| Figure 2.7 Temperature seasonal cycle over Bolivia | 41 |
|--|----|

| | |
|---|----|
| Figure 2.8 Wind climatology at 850 hPa for CMIP5 models | 42 |
|---|----|

| | |
|---|----|
| Figure 2.9 Wind climatology at 200 hPa for CMIP5 models | 44 |
|---|----|

| | |
|---|----|
| Figure 2.10 Climatology of vertically integrated moisture transport | 46 |
|---|----|

| | |
|--|----|
| Figure 2.11 Taylor diagram for models comparison | 48 |
|--|----|

| | |
|--|----|
| Figure 2.12 Heat map for models comparison | 49 |
|--|----|

| | |
|--|----|
| Figure 3.1 Topography of Bolivia | 69 |
|--|----|

| | |
|---|----|
| Figure 3.2 Cluster identification | 70 |
|---|----|

| | |
|---|----|
| Figure 3.3 Precipitation clusters | 71 |
|---|----|

| | |
|---|----|
| Figure 3.4 Statistical properties of the precipitation clusters | 72 |
|---|----|

| | |
|---|----|
| Figure 3.5 Precipitation clusters | 73 |
|---|----|

| | |
|--|----|
| Figure 3.6 Climate subregions in Bolivia | 74 |
|--|----|

| | |
|---|----|
| Figure 3.7 Statistical properties of Bolivia's climate subregions | 75 |
|---|----|

| | |
|---|----|
| Figure 3.8 Seasonal climate variation in Bolivia's climate subregions | 76 |
|---|----|

| | |
|---|-----|
| Figure 4.1 Topography of Bolivia. WRF domain extents | 106 |
| Figure 4.2 Bolivia's climate subregions and station spatial distribution | 107 |
| Figure 4.3 Trinidad, model evaluation vs station measurements | 108 |
| Figure 4.4 San Jose, model evaluation vs station measurements | 109 |
| Figure 4.5 San Antonio, model evaluation vs station measurements | 110 |
| Figure 4.6 Sucre, model evaluation vs station measurements | 111 |
| Figure 4.7 El Alto, model evaluation vs station measurements | 112 |
| Figure 4.8 Potosi, model evaluation vs station measurements | 113 |
| Figure 4.9 WRF evaluation in producing present day mean climate during DJF..... | 114 |
| Figure 4.10 WRF evaluation in producing present day mean climate during JJA | 115 |
| Figure 4.11 WRF evaluation in producing present day seasonal cycle of precipitation . | 116 |
| Figure 4.12 WRF evaluation in producing present day seasonal cycle of temperature .. | 117 |
| Figure 4.13 WRF evaluation in producing DJF precipitation distribution in QQ-plots . | 118 |
| Figure 5.1 Topography of Bolivia. WRF domain extents | 144 |
| Figure 5.2 Bolivia's climate subregions | 145 |
| Figure 5.3 Drought characteristics using Run theory | 146 |
| Figure 5.4 DJF mean seasonal change of precipitation between present day and future | 147 |
| Figure 5.5 DJF mean seasonal change of temperature between present day and future | 148 |
| Figure 5.6 JJA mean seasonal change of precipitation between present day and future | 149 |
| Figure 5.7 JJA mean seasonal change of precipitation between present day and future | 150 |
| Figure 5.8 Present day and future climate RX5day index values | 151 |
| Figure 5.9 Present day and future climate R10mm index values | 152 |
| Figure 5.10 Present day and future PDF of precipitation during DJF | 153 |

| | |
|--|-----|
| Figure 5.11 Present day and future PDF of temperature during DJF | 154 |
| Figure 5.12 Present day and future PDF of precipitation during JJA | 155 |
| Figure 5.13 Present day and future PDF of temperature during JJA | 156 |
| Figure 5.14 1-month SPEI time series | 157 |
| Figure 5.15 6-month SPEI time series | 158 |
| Figure 5.16 12-month SPEI time series | 159 |
| Figure 5.17 Temporal change in the number of droughts | 160 |
| Figure 5.18 Drought characteristics change | 161 |

List of Tables

| | |
|--|-----|
| Table 2.1 CMIP5 models attributions | 31 |
| Table 2.2 Observational and reanalysis datasets | 31 |
| Table 2.3 CMIP5 precipitation mean biases | 32 |
| Table 2.4 CMIP5 temperature mean biases | 32 |
| Table 3.1 Categorical intersection of precipitation and temperature clusters | 68 |
| Table 3.2 Summary of Wilcoxon-Mann-Whitney rank-sum test | 68 |
| Table 4.1 Attributes of the selected GCMs | 101 |
| Table 4.2 Stations geographical details | 101 |
| Table 4.3 Verification of the statistics for selected regions | 102 |
| Table 5.1 Attributes of the selected GCMs | 143 |
| Table 5.2 Downscaling Simulations Summary..... | 143 |
| Table 5.3 Selected climate extreme indices' attributions | 143 |
| Table 5.4 Drought classification..... | 143 |

Appendix Figures

| | |
|---|-----|
| Figure A.1 Trinidad, model evaluation for precipitation (36, 12, 4 km) | 169 |
| Figure A.2 Trinidad, model evaluation for temperature (36, 12, 4 km) | 169 |
| Figure A.3 San Jose, model evaluation for precipitation (36, 12, 4 km) | 170 |
| Figure A.4 San Jose, model evaluation for temperature (36, 12, 4 km) | 170 |
| Figure A.5 San Antonio, model evaluation for precipitation (36, 12, 4 km) | 171 |
| Figure A.6 San Antonio, model evaluation for temperature (36, 12, 4 km) | 171 |
| Figure A.7 Sucre, model evaluation for precipitation (36, 12, 4 km) | 172 |
| Figure A.8 Sucre, model evaluation for temperature (36, 12, 4 km) | 172 |
| Figure A.9 El Alto, model evaluation for precipitation (36, 12, 4 km) | 173 |
| Figure A.10 El Alto, model evaluation for temperature (36, 12, 4 km) | 173 |
| Figure A.11 Potosi, model evaluation for precipitation (36, 12, 4 km) | 174 |
| Figure A.12 Potosi, model evaluation for temperature (36, 12, 4 km) | 174 |
| Figure A.13 Present day climate model evaluation for DJF precipitation | 175 |
| Figure A.14 Present day climate model evaluation for JJA precipitation | 176 |
| Figure A.15 Present day climate model evaluation for DJF temperature | 177 |
| Figure A.16 Present day climate model evaluation for JJA temperature | 178 |
| Figure A.17 NNRP-WRF evaluation, DJF precipitation distribution | 179 |
| Figure A.18 Similar to A.17 for MPI-WRF | 180 |
| Figure A.19 Similar to A.17 for MIROC5-WRF | 181 |
| Figure A.20 Similar to A.17 for CCSM4-WRF | 182 |
| Figure B.1 Mean seasonal average of precipitation during DJF over 2006-2020 | 183 |
| Figure B.2 Mean seasonal average of precipitation during DJF over 2066-2080 | 184 |

| | |
|---|-----|
| Figure B.3 Mean seasonal average of precipitation during JJA over 2006-2020 | 185 |
| Figure B.4 Mean seasonal average of precipitation during JJA over 2066-2080 | 186 |
| Figure B.5 Mean seasonal average of temperature during DJF over 2006-2020 | 187 |
| Figure B.6 Mean seasonal average of temperature during DJF over 2066-2080 | 188 |
| Figure B.7 Mean seasonal average of temperature during JJA over 2006-2020 | 189 |
| Figure B.8 Mean seasonal average of temperature during JJA over 2066-2080 | 190 |

Chapter 1

Introduction

Bolivia is a developing country located in the tropical region and is at grave risk to the effects of human-induced climate changes where has been listed as one of the top twenty at-risk countries (Wheeler 2011). Topographically, the Plurinational State of Bolivia, is divisible to four macro-regions of lowlands to the east with altitudes less than 500 meters, inter-Andean high and low valleys with a range of altitudes from 500 to 3800 meters, higher valleys with altitudes exceeding 3800 meters, and the higher plateau of Altiplano surrounded by the higher mountains (Fig. 1.1).

The lowlands encompass the wet and humid Amazonia basin to the north and dry and warm El Chaco region to the south. Land cover type varies from rainforest in the north to more croplands to the east and south. Soybean and maize cultivation are the main agricultural activities of the lowlands and represent more than 10 percent of agricultural GDP and are mainly produced for export purposes. Rainfall rates vary from higher amounts of values up to 2000 mm in the summer months in the north to much lower values in the southern El Chaco region. Thus, in the lowland communities particularly from Chaco and cropland regions to the east, adaptation measures prioritize improved agricultural and livestock practices, followed by enhanced water management.

The high rainfalls, coupled with deforestation and expansion of the croplands, makes the lowlands more vulnerable to flooding with potential damage to crops and infrastructure and other consequences, such as landslides. The most vulnerable populations in the lowlands are the poor communities along the riverbeds who mainly subsist on rainfed agriculture, livestock farming, forest harvesting, hunting and fishing.

The high potential exposure to climate change impacts and low income and economic resources places these societies in a more challenging situation to invest in and prepare a more practical adaptation strategy.

Higher terrains and Altiplano region are generally more sensitive to water shortages as the rainfall rate drops to a range of 100 to 600 mm in the rainy season, compared to the wet lowlands. According to a census conducted in 2002, approximately 30 percent of the rural population of Bolivia resides in the higher valleys and Altiplano, where access to water is a challenge and the rate of poverty is highest, and rely on agricultural production for subsistence. The main agricultural products in these regions are potato and quinoa that supply the main diet source of the small families in the highlands. Due to the natural constraints on rainfall in these regions, these societies depend on glacial meltwater as their source for drinkable water and irrigation purposes. The alarming rate of glacier shrinkage and their fast retreat has already reduced the water supply for millions of people living in the major cities downstream, such as La Paz. Thus, in contrast to the lowlands, communities from the higher terrain put the highest priority for climate adaptation on water management compared to agricultural and livestock practices. Drought frequency is higher in the elevated regions and recurring droughts have damaged crops and livestock and persuaded many residents to migrate to the lowlands (World Bank 2010).

As mentioned above, Bolivia is already suffering the effects of anthropogenic climate change and its limited capacity to adapt, a product of its socio-economic context, makes it highly vulnerable (IPCC AR5 2014). The complex topography and high

elevation of much of the country in particular pose challenges in identifying key climate changes and vulnerabilities to them at the local to regional level.

As it becomes increasingly clear that human-induced climate change is occurring, the Intergovernmental Panel on Climate Change (IPCC) (2007; 2014) emphasizes that the focus is shifting from basic global climate science into understanding and coping with the impacts of climate change. A fundamental aspect of this shift is the need to produce accurate and precise information on climate change at local and regional scales. IPCC and other current projections of climate change rely on global models of climate change, which, due to demanding computational resources on even the most powerful supercomputers, must be run at a coarse spatial resolution (approximately 100 km for most of the models used in the IPCC 5th Assessment Report).

As stressed by IPCC, results at the global scale are useful for indicating the general nature and large-scale patterns of climate change, though not very robust at the local or regional scale (typically 4-12 km), where impacts are actually felt. This is for two key reasons: (i) global models can only explicitly resolve those physical processes operating over several hundred kilometers or larger and (ii) especially over land, spatial surface heterogeneities can be very large and occur on small spatial scales (e.g. regions of complex topography or different land use patterns). These spatial heterogeneities can have a profound influence on regional climate, however it can be difficult or even impossible to represent them realistically at the 100 km resolution of the global models. Yet it is precisely at this smaller 4-12 km scale that most of the impacts from climate change will occur, and where they need to be understood and mitigated.

A key question then becomes how best to downscale the results of coarse global models to individual regions and localities in a manner that produces verifiable and physically accurate results and, hence value for addressing impacts. We do this via a regional climate model (RCM). RCMs are essentially versions of the Global Climate Models (GCM), except run at high spatial resolution over a limited area (domain), rather than for the entire globe. These models are used to address the horizontal scale limitations of the GCM. Essentially they can be used to dynamically downscale global model results to the regional and even local scale. Depending on the domain size and resolution, RCM simulations can be quite computationally demanding, which has limited the length of many experiments to date.

To help address these issues, we made a comprehensive series of simulations using the Weather Research and Forecasting (WRF) regional climate model driven by three Coupled Model Intercomparison Project Phase 5 (CMIP5) GCMs with three different representative concentration pathways (RCPs). Three different GCMs were chosen to capture the uncertainty in the future climate projections and different scenarios were used to cover all the alternative futures. To evaluate the performance and qualitatively assess the internal biases of the regional climate model, a historical simulation forced by a global reanalysis was also made.

This work is done in three phases. Since incorrect or poor quality input will always produce faulty output and to perform a more robust assessment, in phase one the GCMs historical simulations were evaluated to show how the GCMs (input) are reproducing the large-scale patterns of the atmosphere over South America and Bolivia in particular. The evaluation is presented in terms of mean and seasonal climatology (Abadi et al. 2018a).

The second phase evaluates the performance of the WRF downscaled data in recreating the present-day climate in higher spatial resolutions, mainly focused at 4 km (Abadi et al. 2018c). This part is done comparing (i) the downscaled outputs of the WRF model forced by reanalysis data with the station measurements and gridded observational dataset over the country to verify the WRF regional climate model, and (ii) GCM-driven WRF output versus the observed present-day climatology to gain a better understanding on the combined WRF/GCM biases. Prior to such effort and to render a more robust evaluation at a regional scale where the extreme impacts are felt, a regionalization framework is desired. Therefore, separate nonhierarchical *k*-means clusterings of temperature and precipitation, using a consensus clustering technique, were combined to create a climate regionalization framework to be used in further impact studies (Abadi et al. 2018b).

In the third and the last phase of this project, we provide an overview of projected changes sixty years into the future as well as how the impact will be felt in different regions from Amazonia in the lowlands to the higher plateau of Altiplano (Fig. 1.1). Finally, as a case study to show the extent of climate change impacts on the country, we studied potential changes in drought characteristics in more detail under different emission scenarios. Drought in the region is of significant concern among the international community and has recently forced Bolivia's government to declare a state of emergency due to water shortages in large swaths of the country (Abadi et al. 2018d).

References

- Abadi AM, Oglesby RJ, Rowe CM et al (2018a) Evaluation of GCMs historical simulations of monthly and seasonal climatology over Bolivia. *Clim Dyn* (2018) 51:733–754
doi: 10.1007/s00382-017-3952-y
- Abadi AM, Rowe CM, Andrade MF (2018b) Climate classification in Bolivia: A combination of nonhierarchical and consensus clustering analyses based on precipitation and temperature
- Abadi AM, Rowe CM, Oglesby RJ (2018c) Climate change impact assessment over Bolivia using the WRF high-resolution dynamical downscaling I: Evaluation of the present-day climate
- Abadi AM, Rowe CM, Hayes M (2018d) Climate change impact assessment over Bolivia using the WRF high-resolution dynamical downscaling II: A case study for drought
- IPCC (2013) Climate change 2013: The physical science basis. In: Stocker TF, Qin D, Plattner GK, Tignor M, Allen SK, Boschung J, Nauels A, Xia Y, Bex V, Midgley PM (eds) Contribution of working group I to the fifth assessment report of the intergovernmental panel on climate change. Cambridge University Press, Cambridge
- Wheeler D (2011) Quantifying vulnerability to climate change: Implications for adaptation assistance. *SSRN Electronic Journal*. doi: 10.2139/ssrn.1824611
- World Bank (2010) Adaptation to climate change vulnerability assessment and economic aspects - Plurinational state of Bolivia (English). Washington, DC: World Bank.
<http://documents.worldbank.org/curated/en/642891468162260845/Adaptation-to-climate-change-vulnerability-assessment-and-economic-aspects-BR-Plurinational-state-of-Bolivia>

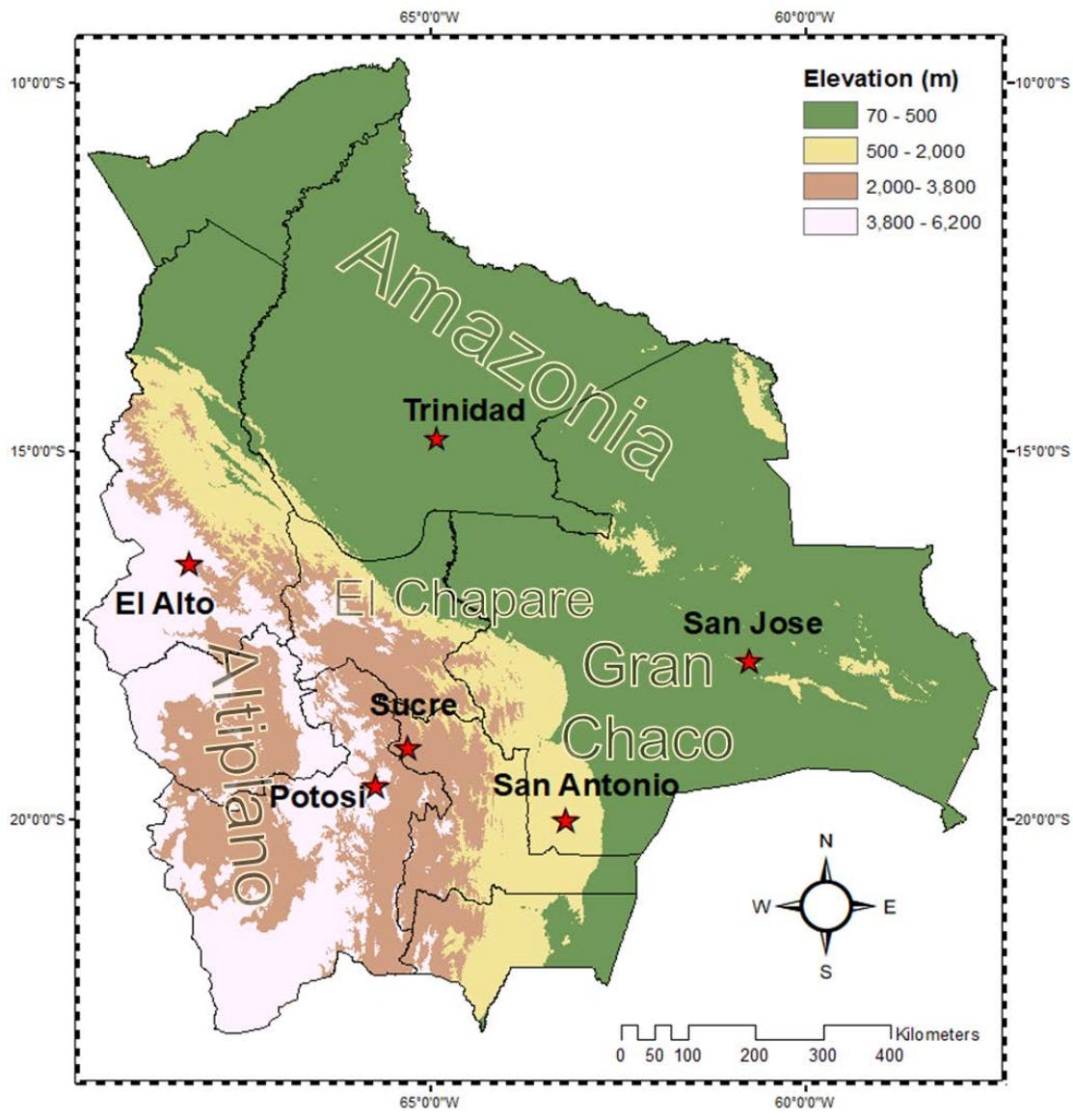


Figure 1.1 Topography of Bolivia in meters. The stars represent the stations used in this study.

Chapter 2

Evaluation of GCMs Historical Simulations of Monthly and Seasonal Climatology over Bolivia

Azar M. Abadi¹, Robert Oglesby¹, Clinton Rowe¹, Rachindara Mawalagedara²

¹Department of Earth and Atmospheric Sciences, University of Nebraska-Lincoln,
Lincoln, Nebraska

²Department of Geological and Atmospheric Sciences, Iowa State University, Ames,
Iowa

Abstract

Bolivia is a low-latitude, developing country at grave risk to the deleterious effects of human-induced climate changes. Due to the complexity of the topography in Bolivia, it is difficult to capture future impacts of the climate change on the regional scale with the coarse resolution of current GCMs. A robust strategy has been developed to dynamically downscale the GCM outputs to a more appropriate temporal and spatial resolution for impact studies. Prior to downscaling, however, evaluation of the GCMs used to provide large-scale forcing is a necessary step to ensure physically meaningful results from regional climate models. This study represents the first part of a broader project on evaluating climate change impacts over Bolivia. We examined precipitation, temperature, wind patterns and moisture transport to evaluate the performance of eight CMIP5 GCMs in simulating the continental and regional climate patterns. Phenomena including the seasonal and monthly positions of the Intertropical Convergence Zone, South Atlantic Convergence Zone, Bolivian high, Chaco low and South American low-level jet, were analyzed. Our results confirm that, in general, all the GCMs do reasonably well in simulating the basic patterns of the variables with some discrepancies in magnitude

across models, especially in the regional scale. Some models outperform the others for the variables and the region of our interest. Finally, the results of this research will help improve quantifying the uncertainty range of further regional downscaling outputs.

2.1. Introduction

According to the Fifth Assessment Report (AR5) of the Intergovernmental Panel on Climate Change (IPCC 2013), the world's growing demand for food and biofuels has led to ongoing land cover change and increasing agricultural expansion in regions experiencing rapid development, including South America. Regional feedbacks of land surface-atmosphere interactions due to altering natural ecosystems, along with the anthropogenic climate impacts owing to greenhouse gas emissions pose a significant threat to countries susceptible to water scarcity.

Bolivia is one of these vulnerable countries expected to face increases in temperature and dry spells, although of varying intensity and with different degrees of confidence in different regions of the country (Wheeler 2011). The country already appears to be suffering from global climate change impacts. Retreating glaciers in the Andes pose a threat to the regions with limited water resources over the Andes (Cook et al. 2016), and there is evidence of more frequent extreme events such as drought and flooding in regions such as Altiplano and La Plata basin in recent decades (Vicente-Serrano et al. 2014; Marengo et al. 2014; Ovando et al. 2016).

Local and regional land surface-atmosphere interaction can also exacerbate the anthropogenic global warming impacts. According to a Food and Agriculture Organization report (FAO 2010), among the countries in South America, Bolivia has the second highest rate of deforestation in its lowland tropical rainforests after Brazil. The

lowlands in eastern Bolivia are also facing other stressors such as cattle ranching, agricultural expansion by indigenous colonies and urbanization. Studies show that the dry tropical forests of South America presently cover only approximately 40% of their former extent. The dry tropical forests of Chiquitano in southern Bolivia have also undergone extensive deforestation, largely by conversion to croplands rather than to a tree plantation/crop mix as in Brazil (Grau and Aide 2008; Sánchez-Azofeifa and Portillo-Quintero 2011; Salazar et al. 2015). The negative impacts of combined anthropogenic and land use change can cause large-scale water imbalances, which in turn can result in significant feedbacks in the regional climate that may not be captured by coarse resolution global circulation models (GCMs).

The complicated topography and high elevation of much of the country pose particular challenges, as these effects cannot be suitably resolved at the approximately 100 km spatial resolution of current global models. To assess any potential impacts of future climate change at a local scale, downscaling efforts are needed to describe these future climate changes better and to provide better input into the development of adaptation strategies. Even though regional climate models like the Weather Research and Forecasting (WRF) model can depict local features more accurately, they are still dependent on their parent GCMs to simulate the larger scale climate patterns properly. Henceforth, selecting the proper GCM would be the first step for any downscaling job, and that motivates this study in advance of downscaling GCMs for Bolivia.

Section 2 provides an overview of the study area, the models, and observational datasets, and the general methodology for evaluating the climate models. In section 3 we analyze the climate model depictions of continental and regional climate patterns of

precipitation, air temperature, moisture budget and wind patterns in both lower and upper atmospheric levels. In Section 4 we discuss each models' ability to simulate the circulation patterns of the area, and in Section 5 we provide a summary of the study.

2.2. Data and Methodology

2.2.1. Study area

Bolivia is a tropical country extending roughly from 10°S to 24°S in latitude and 56°W to 72°W in longitude (Fig. 2.1). Topography mainly dominates the climate in Bolivia.

According to the Köppen climate classification, lowlands in the northern and southeastern Bolivia have equatorial and dry tropical savanna types of climate, respectively. Higher valleys of the Cordillera Real, Cordillera Occidental and Altiplano in the middle are dominated by cold semi-arid to cold desert climate.

2.2.2. Models and Observations

The Coupled Model Intercomparison Project phase 5 (CMIP5; Taylor et al. 2012) multi-model experiment provides climate data on which to examine climate predictability and assess climate change and variability. We evaluated one ensemble member for each of eight different CMIP5 GCMs from their historical runs. This subset of GCMs was selected based on their documented performances in generating realistic climate patterns in South America (Vera, Baez et al. 2006; Vera, Silvestri et al. 2006; Chou et al. 2011; Jones and Carvalho 2013; Seiler et al. 2013a,b). Table 2.1 summarizes the eight selected models, along with their spatial resolutions.

In this paper, we focus on the wet and dry months of January and July, respectively. The GCM outputs are verified using observational model reanalysis datasets of ERA-Interim for temperature, wind patterns and the moisture budget of the atmosphere, and

the gauge-based product of Global Precipitation Climatology Project (GPCP) dataset for precipitation (summarized in Table 2.2) during 1979-2005.

The key question we address is the extent of each model's ability to reproduce the large-scale atmospheric features in terms of several statistical measures including mean, variability and pattern correlation. We first evaluate the seasonal climatology of these variables: precipitation, surface temperature, the lower level and upper level wind fields, and the moisture budget of the atmosphere. Finally, we summarize overall model performances in a matrix against all variable relative biases. All the statistical calculations have been done over two regions; one covering boundaries of Bolivia (8.4 to 24°S and 55.8 to 72.2°W as shown in Fig. 2.1) and the second one covering a larger area representing the continental-scale circulation (56°S to 14°N and 31 to 84°W as shown in Fig. 2.3).

2.3. Results

2.3.1 Continental and regional climatology

While the Altiplano and western Cordillera receive limited precipitation in wet months due to the complex topography of the Andes (Garreaud et al. 2003), the portion of Bolivia located to the east of Andes receives a large amount of precipitation in the summer months (DJF, with the peak in January) interacting with the South American Monsoon System (SAMS; Zhou and Lau 1998; Nogues-Paegle et al. 2002; Raia and Cavalcanti 2008; Marengo et al. 2012) and that is why we are mainly focused on the eastern side of the Andes. The significant seasonal change in the wind regime over South American tropics and subtropics as part of this monsoon system is responsible for the seasonal variability of rainfall (Wanzeler da Costa and Satyamurty 2016) which brings little to no precipitation to Bolivia in the austral winter (JJA, with July as the driest month).

The circulation around the subtropical high pressure in the Atlantic Ocean (South Atlantic Subtropical High; SASH) drives warm and moist air via the trade winds to the northeastern part of South America (Arraut and Satyamurty 2009, Marengo et al. 2012), leading to precipitation in most of the Amazon basin, including Bolivia's northern lowlands (Fig. 2.2). Closer to the eastern Andes, the near surface wind is channeled between the tropics and mid-latitudes into the South American Low Level Jet (SALLJ; Campetella et al. 2002; Liebmann et al. 2004; Marengo et al. 2012). This low-level jet reaches its maximum at 1-2 km above the surface, with the strongest winds observed over Santa Cruz de la Sierra in Bolivia (Vera, Baez et al. 2006). The SALLJ is a characteristic of the warm monsoonal season and plays an important role in transporting moisture from

the tropics to the higher latitudes, bringing convection and rainfall at the exit region of the jet (Haylock et al. 2006). Several studies have shown that the dynamical modification to the mean circulation introduced by the Andes sustains the maximum wind over Bolivia all year (Byerle and Peagle 2002; Vera, Baez et al. 2006).

The latent heat released from the Amazonian precipitation during the wet months and the seasonal heating of Altiplano combine to give rise to an upper level anticyclone known as the Bolivian high (Lenters and Cook 1997, 1999; Zhou and Lau 1998). At the surface, a thermally driven low pressure system (*i.e.*, the Chaco low) strengthens over southeastern Bolivia and northern Paraguay which, along with the strengthened low-level jet, increases downstream moisture advection from the Amazon basin towards La Plata basin (Berbery and Barros 2002; Marengo et al. 2004; Vera, Baez et al. 2006; Salio et al. 2007; Liebmann and Mechoso 2011).

Moisture-laden counterclockwise circulation around the Atlantic subtropical high pressure accompanied by the Chaco low's clockwise circulation creates convergent winds and a northwest-southeast oriented region of clouds and precipitation known as South Atlantic Convergence Zone (SACZ; Liebmann et al. 2004; Carvalho et al. 2011; Marengo et al. 2012;). In July (austral winter), this thermal low, the Bolivian high and the SACZ all dissipate. This results in reduced moisture transport from the Amazon basin to the Bolivian lowlands, causing less rainfall in the interior of the continent. As the Intertropical Convergence Zone (ITCZ) travels northward and westerly winds replace easterlies in the upper troposphere over Bolivia, moisture transport is inhibited from the lowlands to the Andes, causing precipitation to be limited to the northern part of the

country (Garreaud et al. 2003). Fig. 2.2 shows a schematic illustration of atmospheric circulations during the austral summer (January).

2.3.2. Precipitation climatology

Fig. 2.3 compares the climatology of the modeled and observed precipitation for January and July, respectively, for the period 1979-2005. All the models simulate the large-scale spatial patterns of precipitation fairly well, with higher precipitation in the Amazon region during January, and mainly drier conditions in July over central parts of the continent (Zhou and Lau 2001; Vera et al. 2002; Gan et al. 2004; Grimm 2011, Blacutt et al. 2015). Though the GCMs are broadly similar at the largest scales, there are substantive differences at regional scales. In the wet season most of the models get the ITCZ and SACZ's geographical locations and extensions close to observations (the exceptions being CanESM2, MPI-ESM-LR and CNRM-CM5), though the intensity of the precipitation differs between models. During the austral winter (Fig. 2.3) which is the dry season for most of the study area, the regions of maximum precipitation are confined to the northern parts of the continent, associated with the northward shift of ITCZ, and southeastern South America, reflecting the role of synoptic phenomena and frontal passages (Vera et al. 2002; Raia and Cavalcanti 2008).

The main difference among the models is in the simulated intensity of the precipitation. All of the models overestimate precipitation to some extent over the Andes during the wet months (as shown in Table 2.3 and Fig. 2.3), a common behavior of the models over elevated terrains which is likely due to deficiencies in capturing the actual extent of the topography. This may also be in part due to the precipitation underestimation in gridded observations, especially over mountainous regions where the

reliability of the gridded observational datasets is questionable. According to the observations, higher rainfall occurs in the northern lowlands of Amazonia with lower amounts of rainfall at higher elevations. Table 2.3 represents the spatially averaged biases in modeled precipitation divided by the observation (% of observed mean).

Fig. 2.4 charts the seasonal cycle of precipitation in Bolivia. All eight GCMs reproduce the seasonal pattern of precipitation very well in terms of the timing of the maximum and minimum precipitation rate. However, some discrepancies occur among models for the magnitude of precipitation. All of the models except MIROC-ESM overestimate the amount of precipitation to some degree during the wet months, but simulate the precipitation in drier months closer to that observed except the HadGEM2-ES. Fig. 2.5 shows the frequency distribution of rainfall over Bolivia in the month of January. As it is evident in this figure, some models, including MIROC5, IPSL-CM5A-LR and HadGEM2-ES, show some skewness towards a higher amount of precipitation compared to observations, in agreement with Fig. 2.3 and 2.4. That shows the abovementioned models underestimate the frequency of lighter precipitation and overestimate moderate to heavier precipitation events (Solman et al. 2013).

2.3.3. Surface air temperature

Fig. 2.6 depicts the January and July temperature climatology for the GCMs and observations over the period 1979-2005. Following the terrain, lower temperatures are observed in the higher elevations (Cordillera Real, Cordillera Occidental and Altiplano), with higher temperatures in the lowlands (Solman et al. 2013). During the warm season, all the models simulate the basic large-scale spatial pattern of temperature—warmer over the lowlands and cooler over the mountains. In July, models follow the observation with

highest temperatures over the Amazon region with and a well-defined north-south temperature gradient.

In January there is also a local temperature maximum in Chaco region (southeastern Bolivia and northern Paraguay) leading to the presence of the thermal Chaco low that is replaced by cold air in the winter (Garreaud et al. 2009). There are warm biases over the Andes in most of the models, especially in July, likely due to the coarse resolution of the GCMs that cannot resolve sufficiently the vertical extent of the mountain ranges.

The difference between the models and observations in some areas exceeds 2-3°C, and is most evident in MIROC-ESM and CanESM2 overestimating the temperature in January over Andes and northern part of the continent, respectively. There are also warm biases along the western coast of the continent from northern Chile to northern Peru in almost all of the GCMs (the one exception being IPSL-CM5A-LR) which shows that the models likely are underestimating the intensity of the cold Peru/Humboldt current (Penven et al. 2005). Considering the fact that sea surface temperature exerts a significant control on precipitation in regions adjacent to the ocean, this warm bias then helps to explain the modeled wet biases over the Andes. Table 2.4 summarizes the mean biases of the temperature averaged over Bolivia and Continent regions. By comparing the values between the two regions, it is evident that reducing the size of the region increases the averaged error due to improper physics of the GCMs at a regional scale. This is further evidence that motivates the authors to downscale GCMs to study the impacts at a local scale. MPI-ESM-LR, HadGEM2-ES and CNRM-CM5 tend to underestimate the temperature over Bolivia while the other models overestimate it.

The annual cycle of the temperature is shown in Fig. 2.7. Most of the models follow the observed annual cycle of temperature reaching a maximum in December-January and a minimum in July. However, the amplitudes vary among models with some mainly underestimating the surface temperature including HadGEM2-ES, CNRM-CM5 and MPI-ESM-LR while the rest of them overestimate the temperature (Table 2.4).

2.3.4. Upper and lower level atmospheric circulation patterns

Fig. 2.8 and 2.9 show the lower (850 hPa) and upper (200 hPa) level atmospheric mean circulation patterns for January and July, respectively. In January (Fig. 2.8a), trade winds that blow onto the continent from the northeast are channeled by the Andes, creating the SALLJ. As described earlier, the SALLJ carries tropical warm and moist air into the central part of the continent, which then fuels deep convective precipitation. In austral winter the ITCZ migrates north, pushing the trade winds northward as well, which leads to less moisture advection onto the continent (Fig. 2.8b; Zhou and Lau 2001; Liebmann et al. 2004; Marengo et al. 2004; Marengo et al. 2012). All the GCMs capture this wind pattern, with some discrepancies among models in the magnitude of trade winds. The greater the magnitude of the simulated winds, the more moisture they will carry farther south, leaving Amazonia with less available water vapor. That might help explain some of the dry biases over the Amazon basin and wet biases farther south toward the Andes during the summer in models including CanESM2, CNRM-CM5, IPSL-CM5A-LR and MPI-ESM-LR (bias maps not shown).

Fig. 2.9 summarizes the observed and simulated features of the upper level circulation in South America including the Bolivian high. Excluding CanESM2 and IPSL-CM5A-LR, the remaining models reproduce the anticyclone's location and

intensity close to that in the reanalysis dataset. The position and the intensity of the upper level Bolivian high combined with favorable conditions for convective developments in the lower level atmosphere (sufficient water vapor) play an important role (Garreaud et al. 2003) in the heavy convective precipitation during summer over the Altiplano. Insel et al. (2013) showed that the upper level easterlies, resulting from the northern branch of Bolivian high, not only can provide basic horizontal moisture advection, but also can modulate and strengthen upslope circulations, leading to even more moisture transport into the Altiplano. Heating of the elevated terrain also creates a regional up-slope circulation focused on the eastern cordillera slopes, which helps transport moisture to the Bolivian highlands. In winter (Fig. 2.9b), westerlies and a stronger jet stream prevail in the upper levels, hindering moisture transport from the lowlands to higher valleys, with the impact on precipitation noticeable in Fig. 2.3.

2.3.5. Moisture budget of the atmosphere

To understand the above effects better, we investigated the moisture budget of the atmosphere was investigated by examining the climatology of moisture transport over the continent, especially Bolivia, as well as the vertically integrated moisture flux convergence for the period of 1979-2005 with a continued focus on January and July. Newman et al. (2012), ignoring relatively small interannual variations of precipitable water, concluded that the vertically integrated moisture flux convergence can be used to estimate the moisture budget, therefore the imbalance between precipitation and evaporation. In the same research, they also studied the contribution of transient and low frequency eddies, as well as the time-mean circulation, to the total moisture transport. They summarized the mean moisture transport as

$$\bar{Q} = \bar{Q}^m + \bar{Q}^{LF} + \bar{Q}^s$$

where the right hand side terms represent transport by the time-mean flow, low frequency anomalies and synoptic anomalies, respectively. Since their results show clearly that the moisture transport is dominated by time-mean flow in the lower latitudes, we have focused on the mean term in the equation, for the present study. For analysis of the moisture field climatology, horizontal wind components and specific humidity fields from the surface to 300 hPa were extracted from GCMs and ERA-Interim reanalysis datasets for the period 1979-2005.

Fig. 2.10 compares the climatology of CMIP5 models' vertically integrated moisture fluxes (vectors) and associated convergences (contours) to the observational estimates from ERA-Interim for the months of January and July. The mean moisture flow over Amazonia during the warm season is dominated by the interhemispheric

northeasterly trade winds which, as described above, are also associated with convergence over the Andes. This transport is then deflected by the Andes and intensified in the SALLJ so the moisture can reach La Plata basin (Marengo et al. 2004; Soares and Marengo 2009). In January, almost all the models compare well with the reanalysis in the position and intensity of the moisture transport by trade winds and the subtropical high, with the convergence mainly over Amazonia and the Andes, where the maximum precipitation is observed in ITCZ and SACZ, respectively. These results are consistent with other studies in South America including Berbery and Barros (2002), Raia and Cavalcanti (2008), Carvalho et al. (2011), Satyamurty et al. (2013) and Wanzeler da Costa and Satyamurty (2016). The models also simulate the strong divergence in the tropics and east coast of Brazil where the Brazilian plateau blocks the low-level circulation. Comparing the spatial patterns of the models and the observations, it is clear that some models have deficiencies in simulating the strength of the ITCZ, including MPI-ESM-LR, CNRM-CM5, IPSL-CM5A-LR and CanESM2, which was also evident in the precipitation underestimation in the same region (Fig. 2.3). The strong moisture convergences represent the places where precipitation exceeds evaporation. These regions act as a sink of atmospheric moisture and overlap the regions with the maximum precipitation (Fig. 2.3). On the other hand, places with strong divergence serve as moisture sources to the atmosphere, with evaporation exceeding the precipitation (Trenberth et al. 2011), which is the case over Amazonia in the austral winter. There is a reasonable agreement on the locations and intensities of precipitation and convergence among all the GCMs.

In austral winter, with the subtropical high traveling farther north and west, southeasterly winds replace northeasterly trade winds in the northeastern part of the continent. This southeasterly flow leaves Amazonia drier with less moisture transport (Fig. 2.10b).

2.4. Discussion

We evaluated the credibility of eight CMIP5 models in terms of simulating the large-scale circulation over South America, with a particular focus on Bolivia and surrounding regions. Our emphasis is on the implications of these large-scale circulation features for local temperatures and precipitation at the surface. We presented the mean spatial distribution of precipitation, surface temperature, upper and lower level wind components, and the moisture budget of the atmosphere. No one standard performance tool has been found to apply for all types of evaluations (Glecker et al. 2008; Sheffield et al. 2013). For the purpose of this study, therefore, we have focused on comparative assessments including spatial correlations (Pearson correlation coefficient) and standard deviations in the form of Taylor diagram and normalized biases in the form of a matrix of climate model credibility (Rupp et al. 2013).

A Taylor diagram (Fig. 2.11) compares the spatial correlation (shown with regard to the azimuthal angle) and the normalized standard deviation of the models' simulated January mean precipitations and temperatures versus observation (radial distance from the origin) over Bolivia. We choose January since it represents the rainy season for most of our region of interest. Most of the models very closely reproduce the spatial distribution of precipitation and temperature over Bolivia, as the correlation is above 0.88 for all the models for both variables. However the models are more successful in

simulating the spatial distribution of temperature than that of precipitation (Oglesby et al. 2016), with higher correlation values (≥ 0.98).

The normalized standard deviation is the standard deviation of the model data normalized by the standard deviation of the observations, such that the closer a model is to the observation point (Ref point), the lower the RMS error would be (Gleckler et al. 2008). The January diagram shows that more than half of the models underestimate the spatial variability of both precipitation and surface temperature over the larger region, and the remaining models overestimate it. Among these models, MPI-ESM-LR, IPSL-CM5A-LR, CNRM-CM5 and MIROC5 stand out as they have relatively high spatial correlations and lie closer to the Ref point that indicates perfect agreement with observations. In July (not shown), we find high correlations on temperature among the aforementioned outstanding models, with lower agreements on precipitation among models, which is not surprising considering the low amount of precipitation during this dry season.

Finally, Fig. 2.12 summarizes the model biases for precipitation, temperature and moisture convergence with respect to the observations over the two regions, one focused on Bolivia and the other a broader region covering most of central South America so as to capture the larger scale. The biases for each variable are normalized, as

$$Score = \frac{B_i - B_{min}}{B_{max} - B_{min}}$$

where B_i is the bias for model i for a certain variable and B_{min} and B_{max} are the minimum and maximum biases, respectively, across all the models. Thus, a model gains a score between 0 and 1 (Fig. 2.12) with a score closer to 0 (1) meaning a better (worse) performance of that model for that variable (Sheffield et al. 2013). We conclude that

MPI-ESM-LR, MIROC5, CCSM4 perform the best specifically for precipitation and temperature in the wet season and IPSL-CM5A-LR and HadGEM2-ES are doing the worst.

2.5. Summary

Bolivia is a country in South America with a historically small contribution to global greenhouse gas emissions. Yet the effects of climate change are already a reality for Bolivia. This study is the first phase of a more comprehensive project on climate change assessment on Bolivia. One source of uncertainty in possible future climate change is related to the parent GCMs used to drive high-resolution downscaling models. In this research, we evaluated historical simulations from eight CMIP5 GCMs, with the goal of selecting the three best available models in terms of their performance to provide large-scale forcing for dynamical downscaling. In this analysis, only the impact-related variables of surface temperature, precipitation, wind fields and moisture fluxes were investigated and compared against reanalysis datasets. Overall, the GCMs evaluated all perform reasonably well over South America at the large scale while regionally they differ.

Our major findings indicate that, in general, the selected CMIP5 GCMs have more difficulty simulating precipitation comparing to other analyzed variables, especially in the wet months of the summer. Finally, the primary aim of this study is to identify better-performing GCMs in order to reduce the inherited biases in the downscaling process. Future work will focus on evaluating downscaled outputs from WRF for present-day climate and future climate change in Bolivia.

Acknowledgements

This work was initially supported by the Ministry of Environment and Water (MMAyA) of the Plurinational State of Bolivia (contract MMAyA/PPCR No 117/2012 to RO and CR). We acknowledge further support from the Inter-American Development Bank (to RO and CR) for the development of tools and techniques used in this research, the Daugherty Water for Food Global Institute (postdoctoral support to RM), and the UNL Holland Computing Center. We also acknowledge the World Climate Research Programme's Working Group on Coupled Modelling, which is responsible for CMIP, and we thank the climate modeling groups (listed in Table 2.1 of this paper) for producing and making available their model output. For CMIP the U.S. Department of Energy's Program for Climate Model Diagnosis and Intercomparison provides coordinating support and led development of software infrastructure in partnership with the Global Organization for Earth System Science Portals.

2.6. References

- Adler RF, Huffman GJ, Chang A, et al (2003) The version-2 Global Precipitation Climatology Project (GPCP) monthly precipitation analysis (1979–Present). *J Hydrometeorology* 4:1147–1167. doi: 10.1175/1525-7541(2003)004<1147:tvgpcp>2.0.co;2
- Arora VK, Scinocca JF, Boer GJ, et al (2011) Carbon emission limits required to satisfy future representative concentration pathways of greenhouse gases. *Geophys Res Lett.* doi: 10.1029/2010gl046270
- Arraut JM, Satyamurty P (2009) Precipitation and water vapor transport in the Southern Hemisphere with emphasis on the South American region. *J Applied Meteorology and Climatology*, 48(9), 1902–1912. <https://doi.org/10.1175/2009JAMC2030.1>
- Berberly EH, Barros VR (2002) The hydrologic cycle of the La Plata basin in South America. *J. Hydrometeorol.*, 3, 630–645. [https://doi.org/10.1175/1525-7541\(2002\)003<0630:THCOTL>2.0.CO;2](https://doi.org/10.1175/1525-7541(2002)003<0630:THCOTL>2.0.CO;2)
- Blacutt LA, Herdies DL, Gonçalves LGGD, et al (2015) Precipitation comparison for the CFSR, MERRA, TRMM3B42 and Combined Scheme datasets in Bolivia. *Atmos Res* 163:117–131. doi: 10.1016/j.atmosres.2015.02.002
- Byerle LA, Paegle J (2002) Description of the seasonal cycle of low-level flows flanking the Andes and their interannual variability. 10th Conference on Mountain Meteorology and MAP Meeting 2002, 27, 71–88.
- Campetella CM, Vera CS (2002) The influence of the Andes mountains on the South American low-level flow. *Geophys Res Lett*, 29(17), 1826. <https://doi.org/10.1029/2002GL015451>
- Carvalho LMV, Silva A, Jones C, et al (2011) Moisture transport and intraseasonal variability in the South America monsoon system. *Clim Dyn* 36(9), 1865–1880. <https://doi.org/10.1007/s00382-010-0806-2>
- Chou SC, Marengo JA, Lyra AA, et al (2011) Downscaling of South America present climate driven by 4-member HadCM3 runs. *Clim Dyn* 38:635–653. doi: 10.1007/s00382-011-1002-8
- Cook SJ, Kougkoulos I, Edwards LA, et al (2016) Glacier change and glacial lake outburst flood risk in the Bolivian Andes. *The Cryosphere* 10:2399–2413. doi: 10.5194/tc-10-2399-2016
- Dee DP, Uppala SM, Simmons AJ, et al (2011) The ERA-Interim reanalysis: configuration and performance of the data assimilation system. *Quarterly J Royal Meteor Soc* 137:553–597. doi: 10.1002/qj.828
- Dufresne JL, Foujols MA, Denvil S, et al (2013) Climate change projections using the IPSL-CM5 Earth System Model: from CMIP3 to CMIP5. *Clim Dyn* 40:2123–2165. doi: 10.1007/s00382-012-1636-1
- FAO (2010) Global forest resources assessment 2010. FAO forestry paper 163. doi: ISBN 978-92-5-106654-6

- Gan MA, Kousky VE, Ropelewski CF (2004) The South America Monsoon circulation and its relationship to rainfall over west-central Brazil. *J Clim*, 17(1), 47–66. [https://doi.org/10.1175/1520-0442\(2004\)017<0047:TSAMCA>2.0.CO;2](https://doi.org/10.1175/1520-0442(2004)017<0047:TSAMCA>2.0.CO;2)
- Garreaud R, Vuille M, Clement AC (2003) The climate of the Altiplano: Observed current conditions and mechanisms of past changes. In *Palaeogeography, Palaeoclimatology, Palaeoecology* (Vol. 194, pp. 5–22). [https://doi.org/10.1016/S0031-0182\(03\)00269-4](https://doi.org/10.1016/S0031-0182(03)00269-4)
- Garreaud RCAD, Vuille M, Compagnucci R, et al (2009) Present-day South American climate. *Palaeogeography, Palaeoclimatology, Palaeoecology* 281:180–195. doi: 10.1016/j.palaeo.2007.10.032
- Gent PR, Danabasoglu G, Donner LJ, et al (2011) The Community Climate System Model Version 4. *J Clim* 24:4973–4991. doi: 10.1175/2011jcli4083.1
- Gleckler PJ, Taylor KE, Doutriaux C (2008) Performance metrics for climate models. *J Geophys Res*. doi: 10.1029/2007jd008972
- Grau HR, Aide M (2008) Globalization and land-use transitions in *Latin America. Ecology and Society*. doi: 10.5751/es-02559-130216
- Grimm AM (2011) Interannual climate variability in South America: Impacts on seasonal precipitation, extreme events, and possible effects of climate change. *Stochastic Environmental Research and Risk Assessment*, 25(4), 537–554. <https://doi.org/10.1007/s00477-010-0420-1>
- Haylock MR, Peterson TC, Alves LM, et al (2006) Trends in total and extreme South American rainfall in 1960–2000 and links with sea surface temperature. *J Clim*, 19(8), 1490–1512. <https://doi.org/10.1175/JCLI3695.1>
- Insel N, Poulsen CJ, Sturm C, et al (2013) Climate controls on Andean precipitation $\delta^{18}\text{O}$ interannual variability. *J Geophys Res: Atmospheres* 118:9721–9742. doi: 10.1002/jgrd.50619
- IPCC (2013): *Climate Change 2013: The Physical Science Basis. Contribution of Working Group I to the Fifth Assessment Report of the Intergovernmental Panel on Climate Change* [Stocker, T.F., D. Qin, G. K. Plattner, M. Tignor, S.K. Allen, J. Boschung, A. Nauels, Y. Xia, V. Bex and P.M. Midgley (eds.)]. Cambridge University Press, Cambridge
- Jones CD, Hughes JK, Bellouin N, et al (2011) The HadGEM2-ES implementation of CMIP5 centennial simulations. *Geoscientific Model Development* 4:543–570. doi: 10.5194/gmd-4-543-2011
- Jones C, Carvalho LMV (2013) Climate change in the South American Monsoon System: present climate and CMIP5 projections. *J Clim* 26:6660–6678. doi: 10.1175/jcli-d-12-00412.1
- Lenters JD, Cook KH (1997) On the origin of the Bolivian high and related circulation features of the South American climate. *J Atmos Sci* 54:656–678. doi: 10.1175/1520-0469(1997)054<0656:otootb>2.0.co;2

- Lenters JD, Cook KH (1999) Summertime precipitation variability over South America: Role of the large-scale circulation. *Mon Wea Rev* 127:409–431. doi: 10.1175/1520-0493(1999)127<0409:spvosa>2.0.co;2
- Liebmann B, Kiladis GN, Vera CS, et al (2004) Subseasonal variations of rainfall in South America in the vicinity of the low-level jet east of the Andes and comparison to those in the South Atlantic convergence zone. *J Clim*, 17(19), 3829–3842. [https://doi.org/10.1175/1520-0442\(2004\)017<3829:SVORIS>2.0.CO;2](https://doi.org/10.1175/1520-0442(2004)017<3829:SVORIS>2.0.CO;2)
- Liebmann B, Mechoso CR (2011) The South American Monsoon System. The global monsoon system world scientific series on *Asia-Pacific weather and climate*, 137–157. Doi:10.1142/9789814343411_0009
- Marengo JA, Soares WR, Saulo C, et al (2004) Climatology of the low-level jet east of the Andes as derived from the NCEP-NCAR reanalyses: Characteristics and temporal variability. *J Clim*, 17(12), 2261–2280, doi: 10.1175/1520-0442(2004)017<2261:cotlje>2.0.co;2
- Marengo JA, Liebmann B, Grimm AM, et al (2012) Recent developments on the South American monsoon system. *Int J Clim*. <https://doi.org/10.1002/joc.2254>
- Marengo JA, Chou SC, Torres RR, et al A (2014) Climate change in Central and South America: Recent trends, future projections, and impacts on regional agriculture. CGIAR Research Program on *Climate Change, Agriculture and Food Security* (CAAFS), 73, 93.
- Newman M, Kiladis GN, Weickmann KM, et al (2012) Relative contributions of synoptic and low-frequency eddies to time-mean atmospheric moisture transport, including the role of atmospheric rivers. *J Clim* 25:7341–7361. doi: 10.1175/jcli-d-11-00665.1
- Nogués-Paegle J, Mechoso CR, Fu R, et al (2002) Progress in Pan American CLIVAR Research: Understanding the South American monsoon. *Meteorologica*, 27, 1–30. <https://doi.org/cptec.inpe.br/walmeida/2004/05.13.14.45.34-0>
- Oglesby R, Rowe C, Grunwaldt A, et al (2016) A high-resolution modeling strategy to assess impacts of climate change for Mesoamerica and the Caribbean. *American J Climate Change* 05:202–228. doi: 10.4236/ajcc.2016.52019
- Ovando A, Tomasella J, Rodriguez DA et al (2016) Extreme flood events in the Bolivian Amazon wetlands. *J Hydrology: Regional Studies* 5:25. doi: 10.1016/j.ejrh.2016.01.024
- Penven P (2005) Average circulation, seasonal cycle, and mesoscale dynamics of the Peru Current System: A modeling approach. *J Geophys Res*. doi: 10.1029/2005jc002945
- Raia A, Cavalcanti IFA (2008) The life cycle of the South American monsoon system. *J Clim*, 21(23), 6227–6246. <https://doi.org/10.1175/2008JCLI2249.1>
- Rupp DE, Abatzoglou JT, Hegewisch KC, et al (2013) Evaluation of CMIP5 20th century climate simulations for the Pacific Northwest USA. *J Geophys Res: Atmospheres*. doi: 10.1002/jgrd.50843

- Salazar A, Baldi G, Hirota M, et al (2015) Land use and land cover change impacts on the regional climate of non-Amazonian South America: A review. *Global and Planetary Change*. doi: 10.1016/j.gloplacha.2015.02.009
- Salio P, Nicolini M, Zipser EJ (2007) Mesoscale convective systems over southeastern South America and their relationship with the South American low-level jet. *Mon Wea Rev* 135:1290–1309. doi: 10.1175/mwr3305.1
- Sánchez-Azofeifa GA, Portillo-Quintero C (2011) Extent and drivers of change of neotropical seasonally dry tropical forests. *Seasonally Dry Tropical Forests* 45–57. doi: 10.5822/978-1-61091-021-7_3
- Satyamurty P, Wanzeler da Costa CP, Manzi AO (2013) Moisture source for the Amazon Basin: A study of contrasting years. *Theoretical and Applied Climatology*, 111(1–2), 195–209. <https://doi.org/10.1007/s00704-012-0637-7>
- Seiler C, Hutjes RWA, Kabat P (2013a) Climate variability and trends in Bolivia. *J Applied Meteorology and Climatology* 52:130–146. doi: 10.1175/jamc-d-12-0105.1
- Seiler C, Hutjes RWA, Kabat P (2013b) Likely ranges of climate change in Bolivia. *J Applied Meteorology and Climatology* 52:1303–1317. doi: 10.1175/jamc-d-12-0224.1
- Sheffield J, Barrett AP, Colle B, et al (2013) North American climate in CMIP5 experiments. Part I: Evaluation of historical simulations of continental and regional climatology*. *J Clim* 26:9209–9245. doi: 10.1175/jcli-d-12-00592.1
- Soares WR, Marengo JA (2009) Assessments of moisture fluxes east of the Andes in South America in a global warming scenario. *Int J Clim* 29:1395–1414. doi: 10.1002/joc.1800
- Solman SA, Sanchez E, Samuelsson P, et al (2013) Evaluation of an ensemble of regional climate model simulations over South America driven by the ERA-Interim reanalysis: Model performance and uncertainties. *Clim Dyn*, 41(5–6), 1139–1157. <https://doi.org/10.1007/s00382-013-1667-2>
- Taylor KE, Stouffer RJ, Meehl GA (2012) An overview of CMIP5 and the experiment design. *Bull Am Meteor Soc* 93:485–498. doi: 10.1175/bams-d-11-00094.1
- Trenberth KE, Fasullo JT, Mackaro J (2011) Atmospheric moisture transports from Ocean to land and global energy flows in reanalyses. *J Clim* 24:4907–4924. doi: 10.1175/2011jcli4171.1
- Vera CS, Vigliarolo PK, Berbery EH (2002) Cold season synoptic-scale waves over subtropical South America. *Mon Wea Rev*, 130(3), 684–699. [https://doi.org/10.1175/1520-0493\(2002\)130<0684:CSSSWO>2.0.CO;2](https://doi.org/10.1175/1520-0493(2002)130<0684:CSSSWO>2.0.CO;2)
- Vera C, Baez J, Douglas M, et al (2006) The South American low-level jet experiment. *Bull Am Meteor Soc* 87:63–77. doi: 10.1175/bams-87-1-63
- Vera C, Silvestri G, Liebmann B, González P (2006) Climate change scenarios for seasonal precipitation in South America from IPCC-AR4 models. *Geophys Res Lett*. doi: 10.1029/2006gl025759
- Vicente-Serrano SM, Chura O, López-Moreno JI, et al (2014) Spatio-temporal variability of droughts in Bolivia: 1955-2012. *Int J Clim* 35:3024–3040. doi: 10.1002/joc.4190

- Voldoire A, Sanchez-Gomez E, Méliá DSY, et al (2012) The CNRM-CM5.1 global climate model: description and basic evaluation. *Clim Dyn* 40:2091–2121. doi: 10.1007/s00382-011-1259-y
- Wanzeler da Costa CP, Satyamurty P (2016) Inter-hemispheric and inter-zonal moisture transports and monsoon regimes. *Int J Clim*, 36(15), 4705–4722. <https://doi.org/10.1002/joc.4662>
- Watanabe M, Suzuki T, O’Ishi R, et al (2010) Improved climate simulation by MIROC5: Mean states, variability, and climate sensitivity. *J Clim* 23:6312–6335. doi: 10.1175/2010jcli3679.1
- Watanabe S, Hajima T, Sudo K, et al (2011) MIROC-ESM: model description and basic results of CMIP5-20c3m experiments. *Geoscientific Model Development Discussions* 4:1063–1128. doi: 10.5194/gmdd-4-1063-2011
- Wheeler D (2011) Quantifying vulnerability to climate change: Implications for adaptation assistance. *SSRN Electronic Journal*. doi: 10.2139/ssrn.1824611
- Zanchettin D, Rubino A, Matei D, et al (2012) Multidecadal-to-centennial SST variability in the MPI-ESM simulation ensemble for the last millennium. *Clim Dyn* 40:1301–1318. doi: 10.1007/s00382-012-1361-9
- Zhou J, Lau KM (2001) Principal modes of interannual and decadal variability of summer rainfall over South America. *Int J Clim*, 21(13), 1623–1644. <https://doi.org/10.1002/joc.700>
- Zhou J, Lau KM (1998) Does a monsoon climate exist over South America? *J Clim*, 11(5), 1020–1040. [https://doi.org/10.1175/1520-0442\(1998\)011<1020:DAMCEO>2.0.CO;2](https://doi.org/10.1175/1520-0442(1998)011<1020:DAMCEO>2.0.CO;2)

Table 2.1. CMIP5 models evaluated, and their attributes. Bold-italic models are the ones ultimately chosen for the purpose of downscaling

| Model Name | Spatial Resolution | Center and References |
|--------------------------|---------------------------|--|
| CanESM2 | 2.8 × 2.8 | Canadian Center for Climate Modeling and Analysis, Canada (Arora et al. 2011) |
| <i>CCSM4</i> | 0.94 × 1.25 | National Center for Atmospheric Research, United States (Gent et al. 2011) |
| CNRM-CM5 | 1.4 × 1.4 | Centre National de Recherches Météorologiques / Centre Européen de Recherche et Formation Avancée en Calcul Scientifique, France (Voldoire et al. 2012) |
| HadGEM2-ES | 1.24 × 1.8 | Met Office Hadley Centre (additional HadGEM2-ES realizations contributed by Instituto Nacional de Pesquisas Espaciais), United Kingdom (Jones et al. 2011) |
| IPSL-CM5A-LR | 1.875 × 3.75 | Institut Pierre-Simon Laplace, France (Dufresne et al. 2013) |
| <i>MIROC5</i> | 1.4 × 1.4 | Atmosphere and Ocean Research Institute (The University of Tokyo), National Institute for Environmental Studies, and Japan Agency for Marine- Earth Science and Technology, Japan (Watanabe et al. 2010) |
| MIROC-ESM | 2.8 × 2.8 | Japan Agency for Marine-Earth Science and Technology, Atmosphere and Ocean Research Institute (The University of Tokyo), and National Institute for Environmental Studies, Japan (Watanabe et al. 2011) |
| <i>MPI-ESM-LR</i> | 1.875 × 1.875 | Max-Planck-Institut für Meteorologie (Max Planck Institute for Meteorology), Germany (Zanchettin et al. 2012) |

Table 2.2. Observational and reanalysis datasets

| Observational Dataset | Spatial Resolution | Source and References |
|---|---------------------------|---|
| GPCP, Precipitation | 2.5 × 2.5 | World Climate Research Program, International (Adler et al. 2003) |
| ERA-Interim, Temperature | 0.75 × 0.75 | National Center for Meteorological Research, France (Dee et al. 2011) |
| ERA-Interim, Wind components and Specific Humidity | 0.75 × 0.75 | National Center for Meteorological Research, France (Dee et al. 2011) |

Table 2.3. Mean biases percentage (bias/observation) for CMIP5 simulated precipitation relative to GPCP observations in months of January and July averaged over Bolivia and a larger region representing the continent.

| Model | Bolivia | | Continent | |
|--------------|---------|--------|-----------|--------|
| | Jan | Jul | Jan | Jul |
| MPI-ESM-LR | 10.51 | -12.89 | -7.22 | -68.44 |
| MIROC-ESM | -7.93 | -48.56 | -4.96 | -57.87 |
| MIROC5 | 35.65 | -45.57 | 9.72 | -52.38 |
| IPSL-CM5A-LR | 17.53 | -82.51 | 5.06 | -80.66 |
| HadGEM2-ES | 40.42 | 159.26 | 18.91 | 34.00 |
| CNRM-CM5 | -2.15 | -28.84 | -15.05 | -43.83 |
| CanESM2 | -9.14 | -58.29 | -20.38 | -53.65 |
| CCSM4 | 3.47 | -44.67 | 10.29 | -48.92 |

Table 2.4 January and July biases in CMIP5 simulated temperature relative to ERA-Interim observations averaged over Bolivia and a larger region representing the continent.

| Model | Bolivia | | Continent | |
|--------------|---------|-------|-----------|-------|
| | Jan | Jul | Jan | Jul |
| MPI-ESM-LR | -0.84 | -1.82 | -0.15 | 0.06 |
| MIROC-ESM | 1.80 | 1.03 | -0.53 | -0.23 |
| MIROC5 | 1.25 | 2.21 | 0.45 | 1.10 |
| IPSL-CM5A-LR | 0.55 | -0.93 | -1.28 | -1.38 |
| HadGEM2-ES | -0.51 | -2.33 | -0.15 | -0.54 |
| CNRM-CM5 | -0.35 | -1.42 | 0.03 | -0.38 |
| CanESM2 | 1.16 | 1.61 | 0.51 | 0.30 |
| CCSM4 | 0.62 | 1.62 | 0.05 | 0.21 |

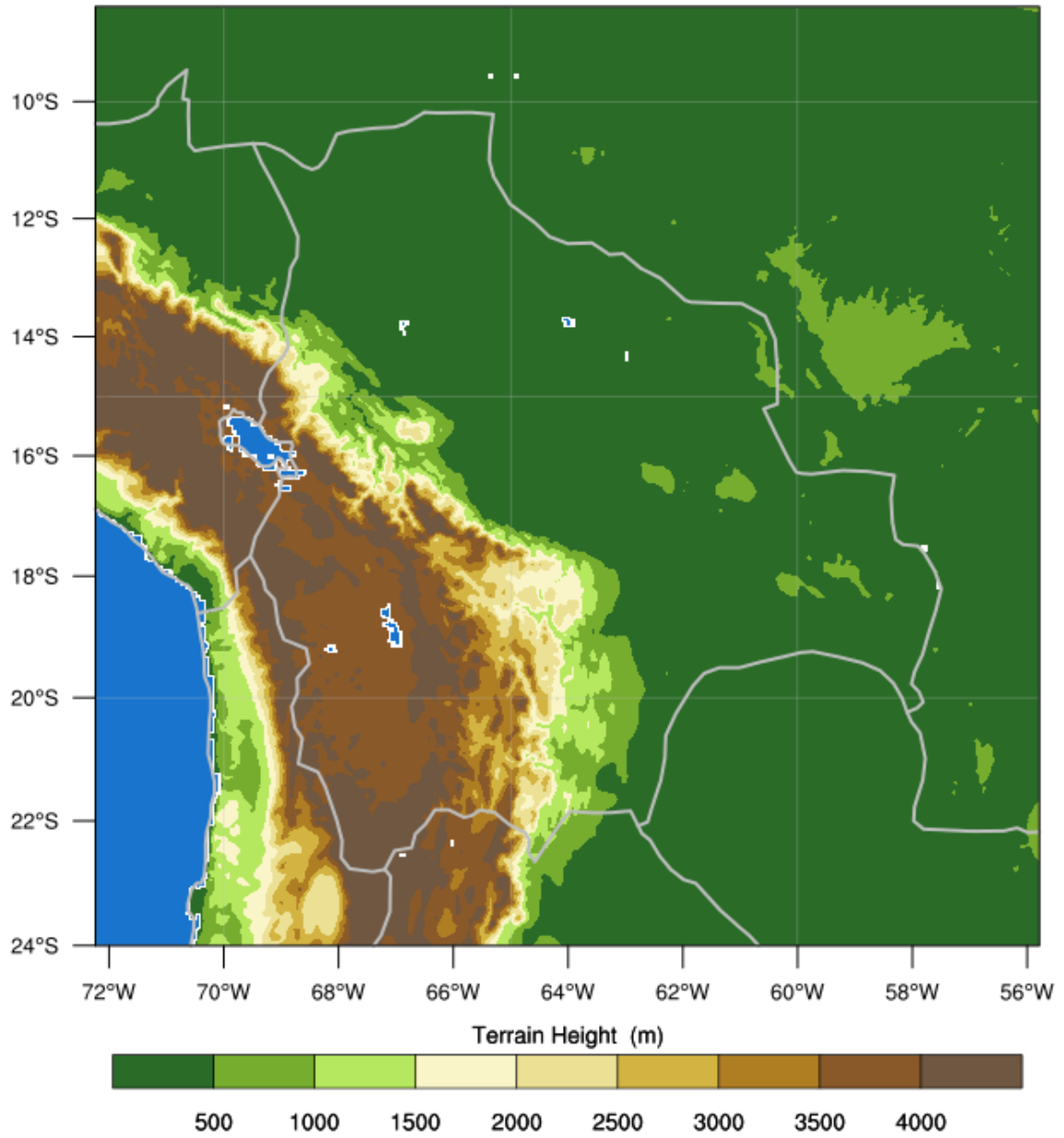


Figure 2.1 Topography of Bolivia. Higher mountains of Andes lie to the west of the country with lowlands to the east. Units are in meters.

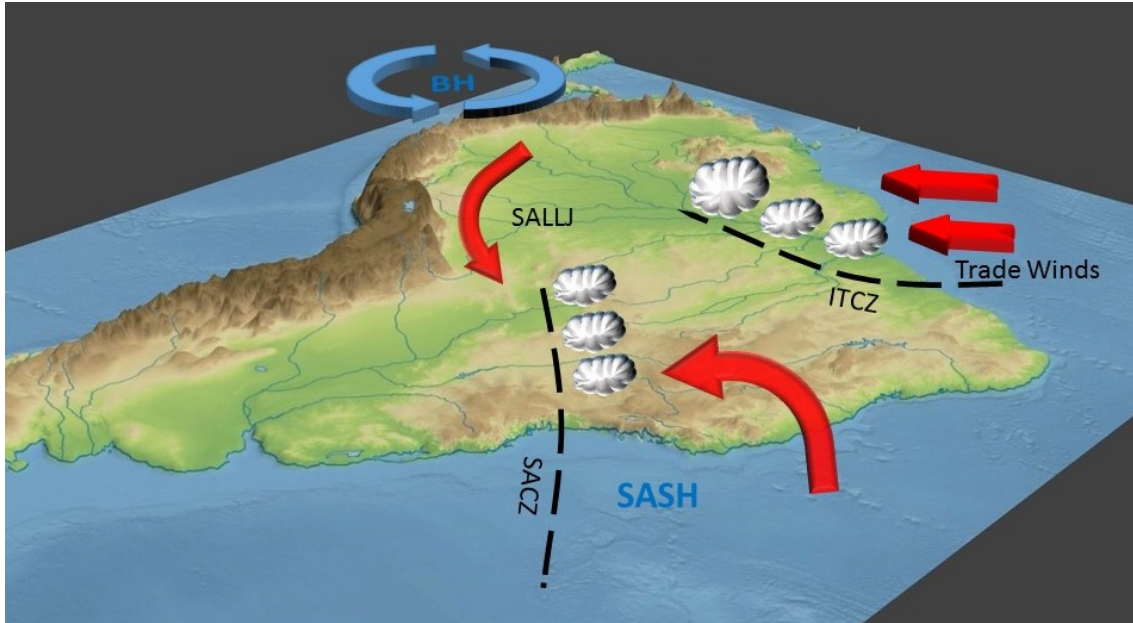


Figure 2.2. Schematic of the large-scale circulation features in DJF season that affect Bolivia's regional climate during the wet months. SASH represents South Atlantic Subtropical High. Red straight arrows show the trade winds blowing to the continent from northeast. The narrow red curved arrow depicts low-level jet, while the thick red arrow shows the northern branch of SASH. The counter-clockwise circulation over the Andes pictures the Bolivian high and dashed black lines illustrate Intertropical Convergence Zone (ITCZ) and South Atlantic Convergence Zone (SACZ).

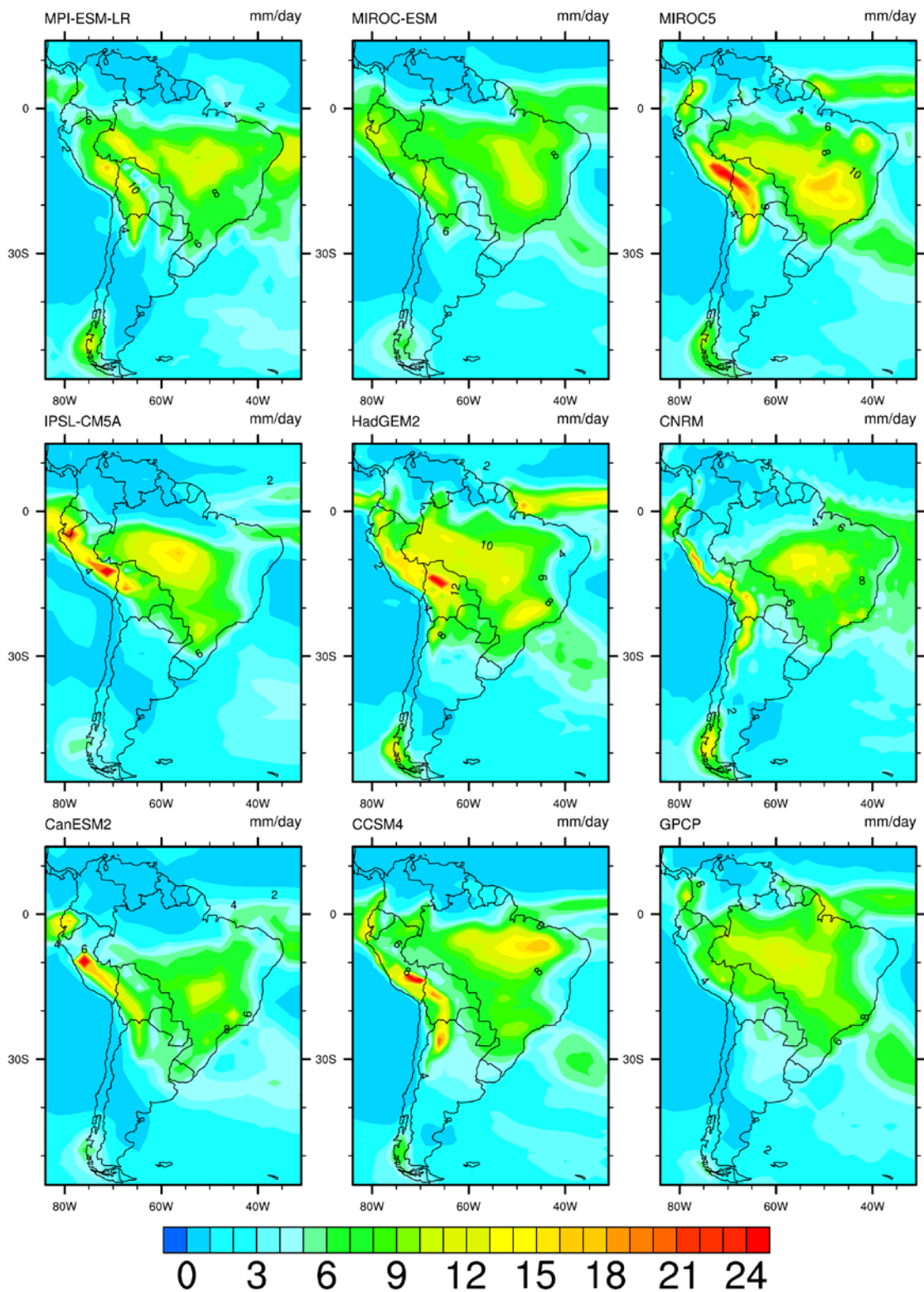


Figure 2.3 Precipitation climatology (1979-2005) for CMIP5 models and GPCP dataset (a) January and (b) July. The model data are shown at their original spatial resolution. Units are in mm/day.

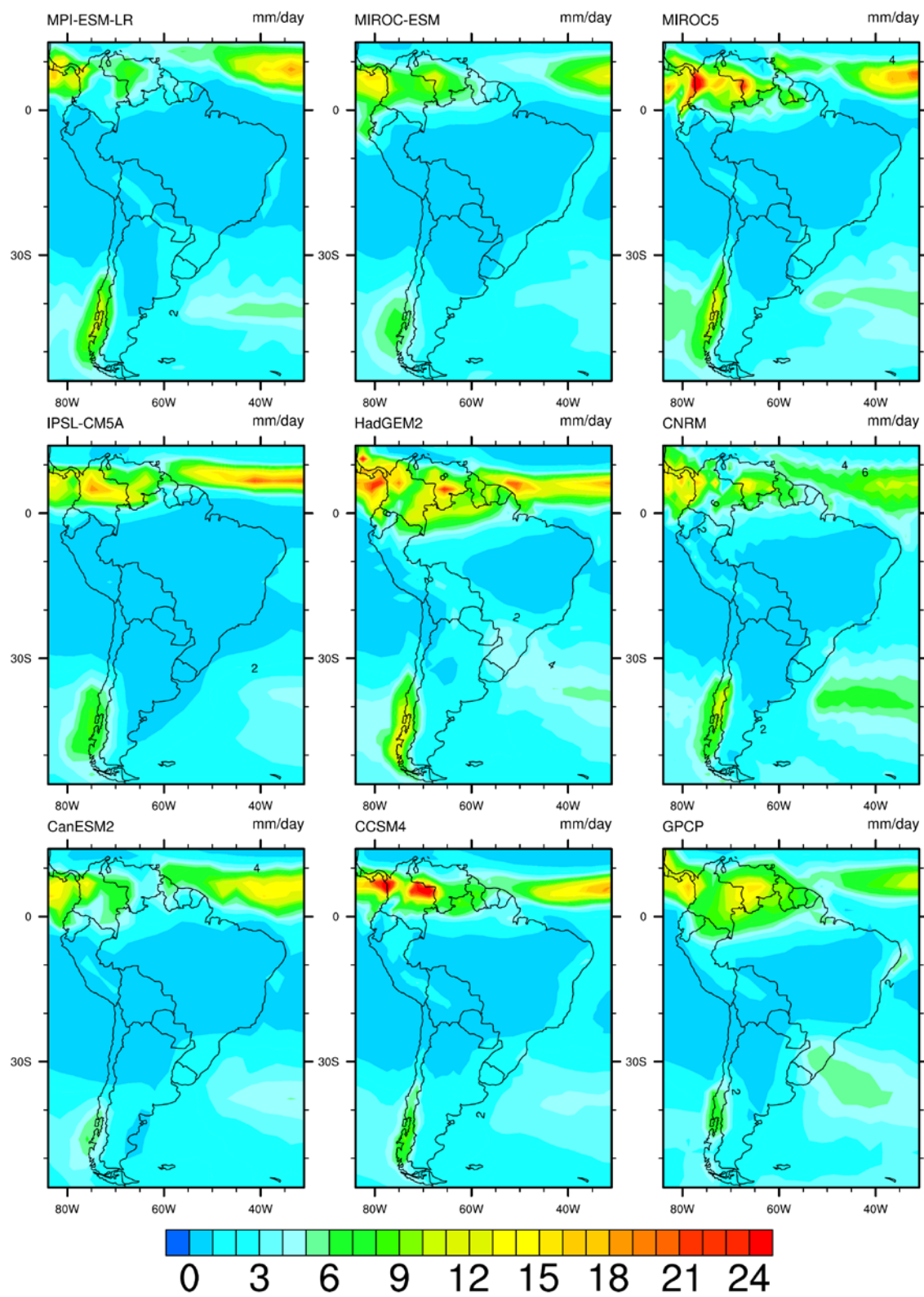


Figure 2.3 (continued)

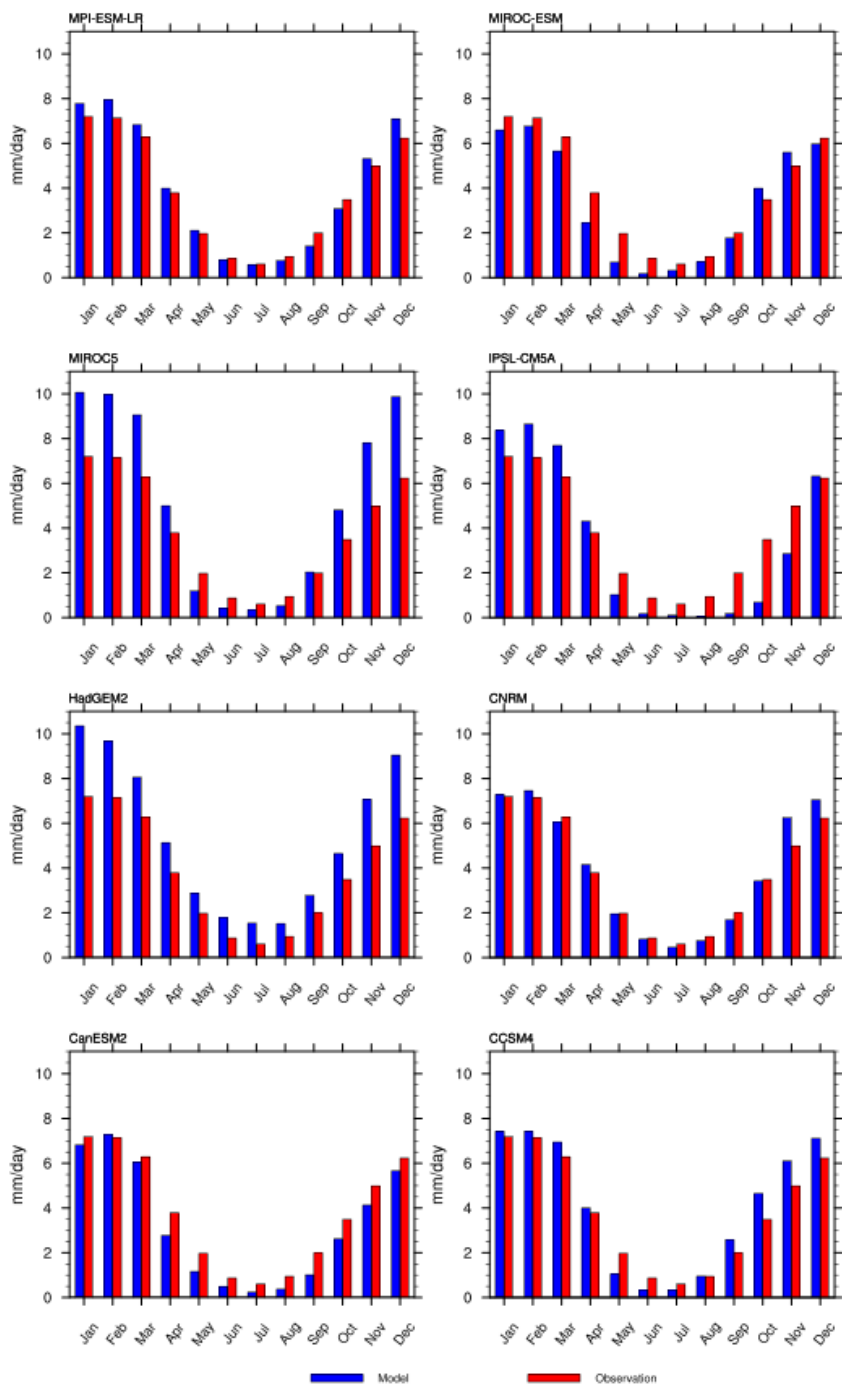


Figure 2.4 Observed and simulated seasonal cycle of monthly precipitation averaged over Bolivia (in mm/day).

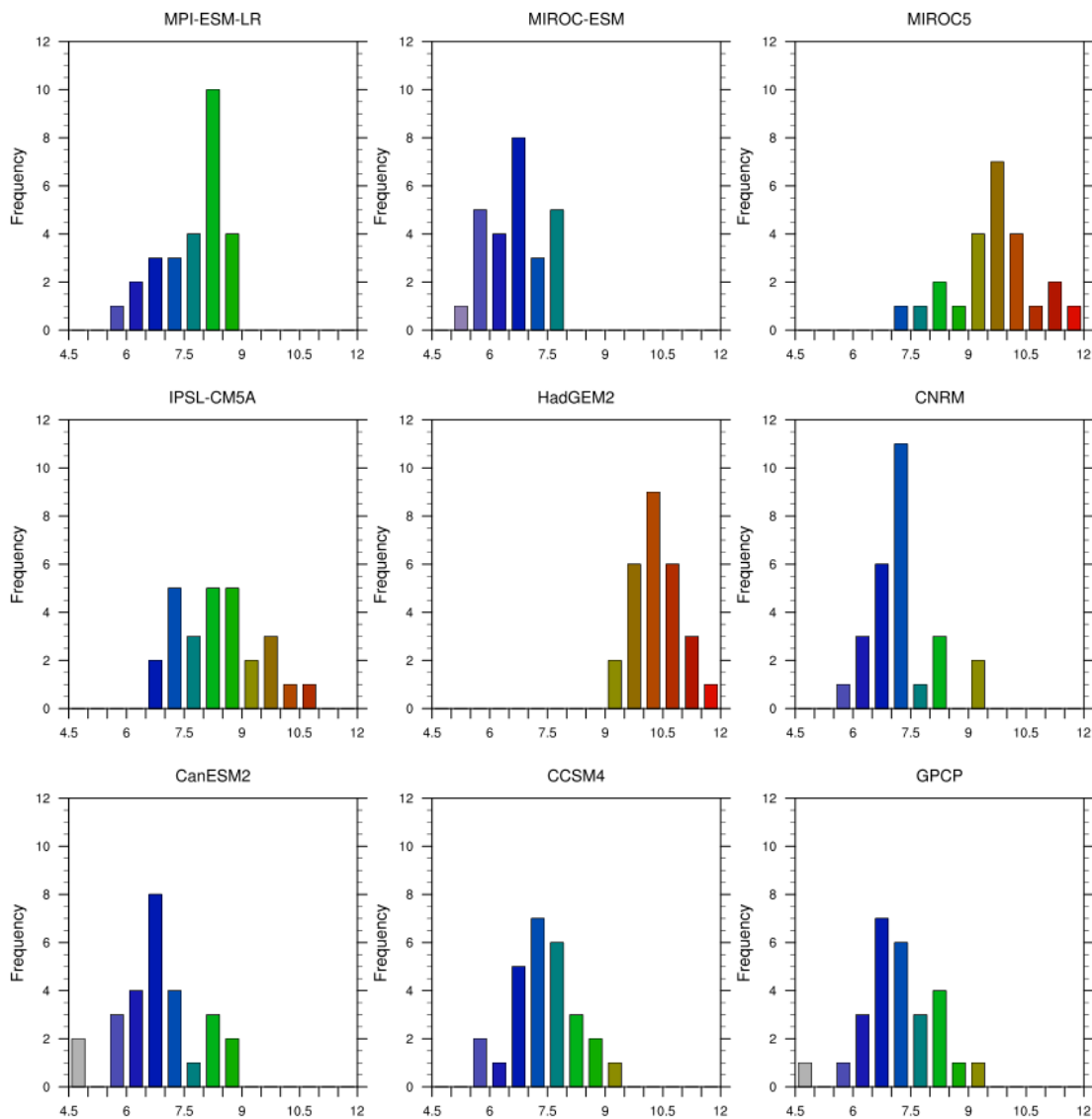


Figure 2.5 Frequency distribution of monthly precipitation for January from 1979-2005, with higher values for precipitation in red and lower values in blue (in mm/day).

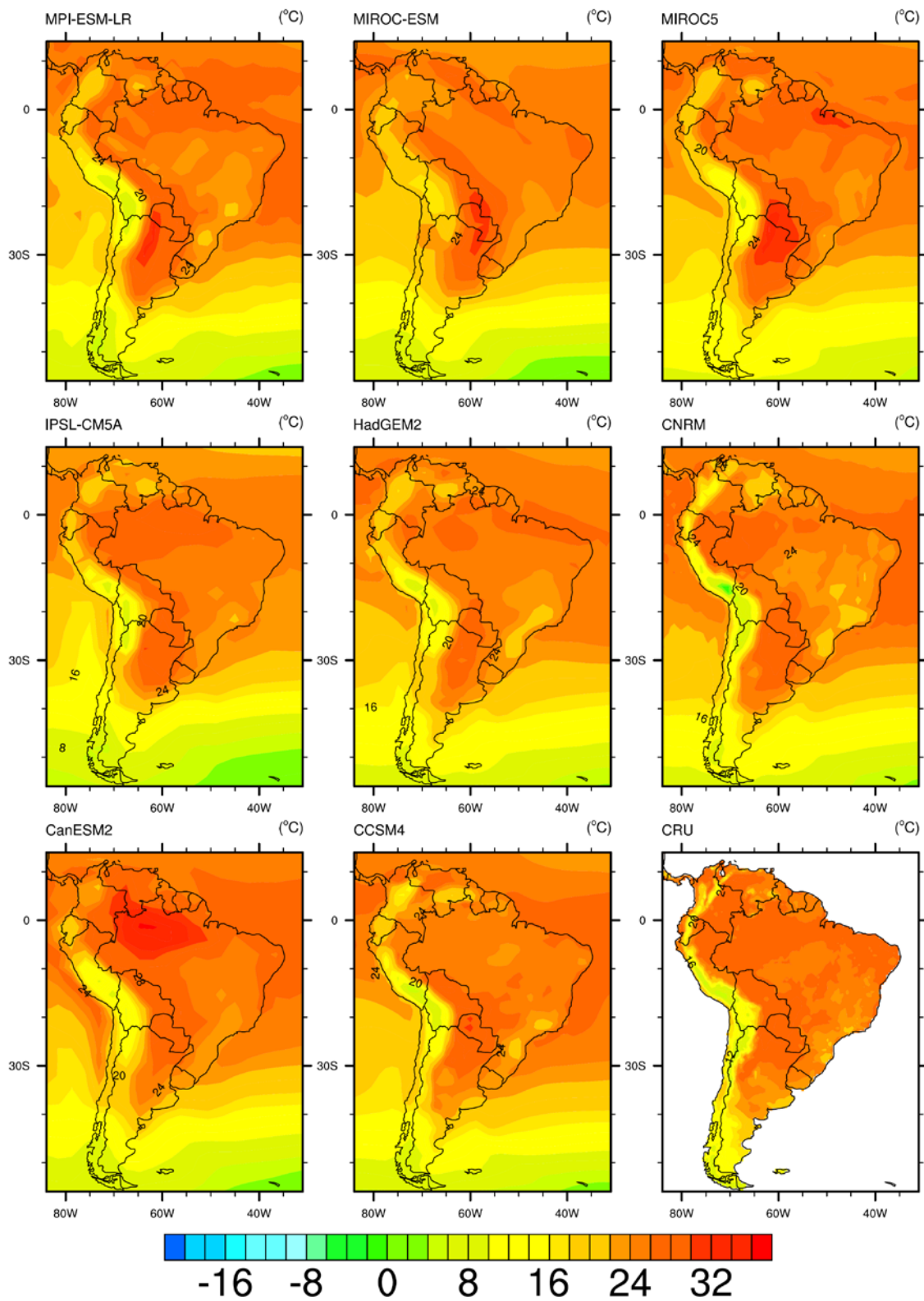


Figure 2.6 Surface temperature climatology (1979-2005) for CMIP5 models and CRU dataset for January (a) and July (b). The model data are shown at their original spatial resolution. Units are in °C.

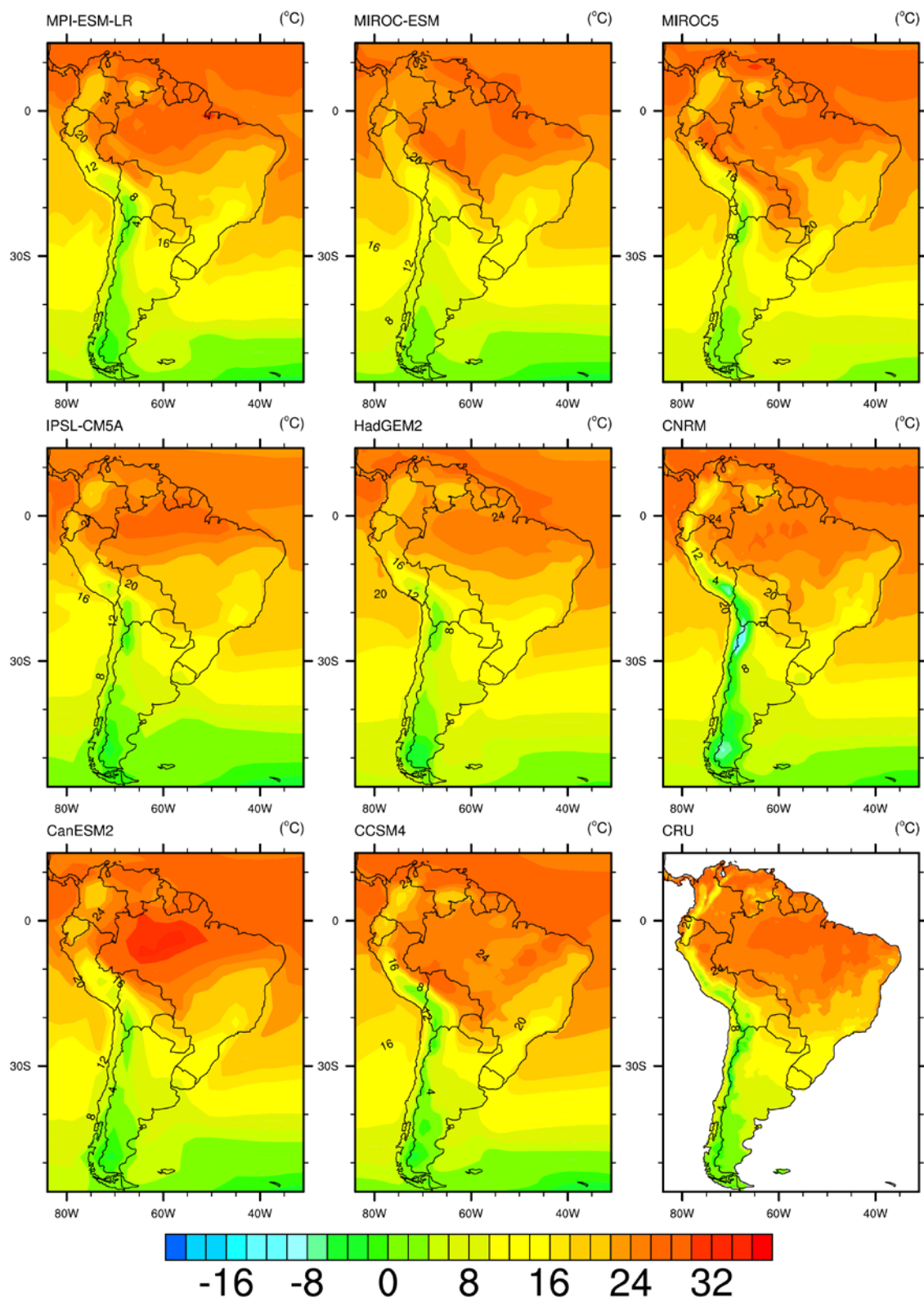


Figure 2.6 (continued)

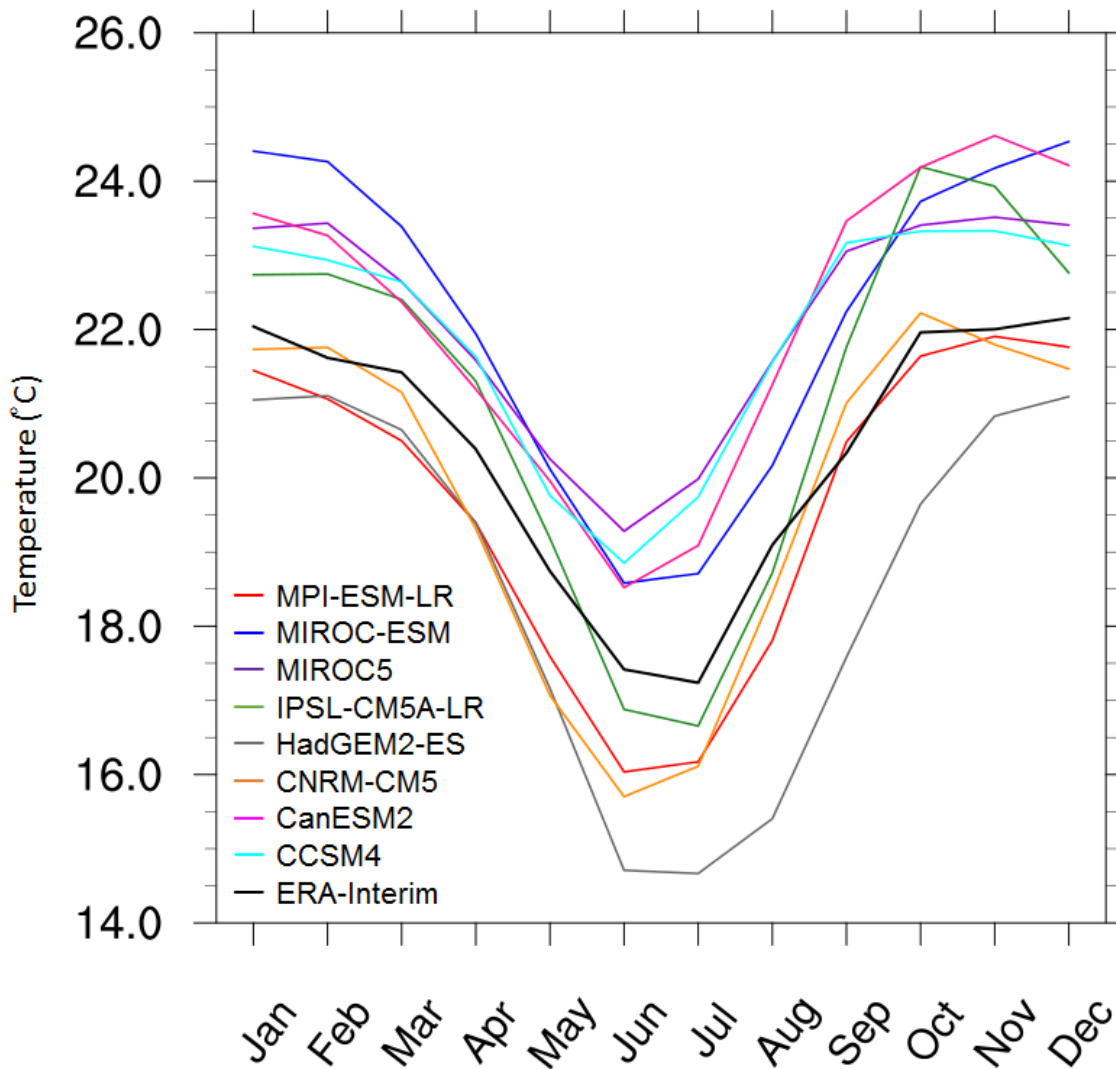


Figure 2.7 Observed and simulated seasonal cycle of monthly temperature averaged over Bolivia (in °C).

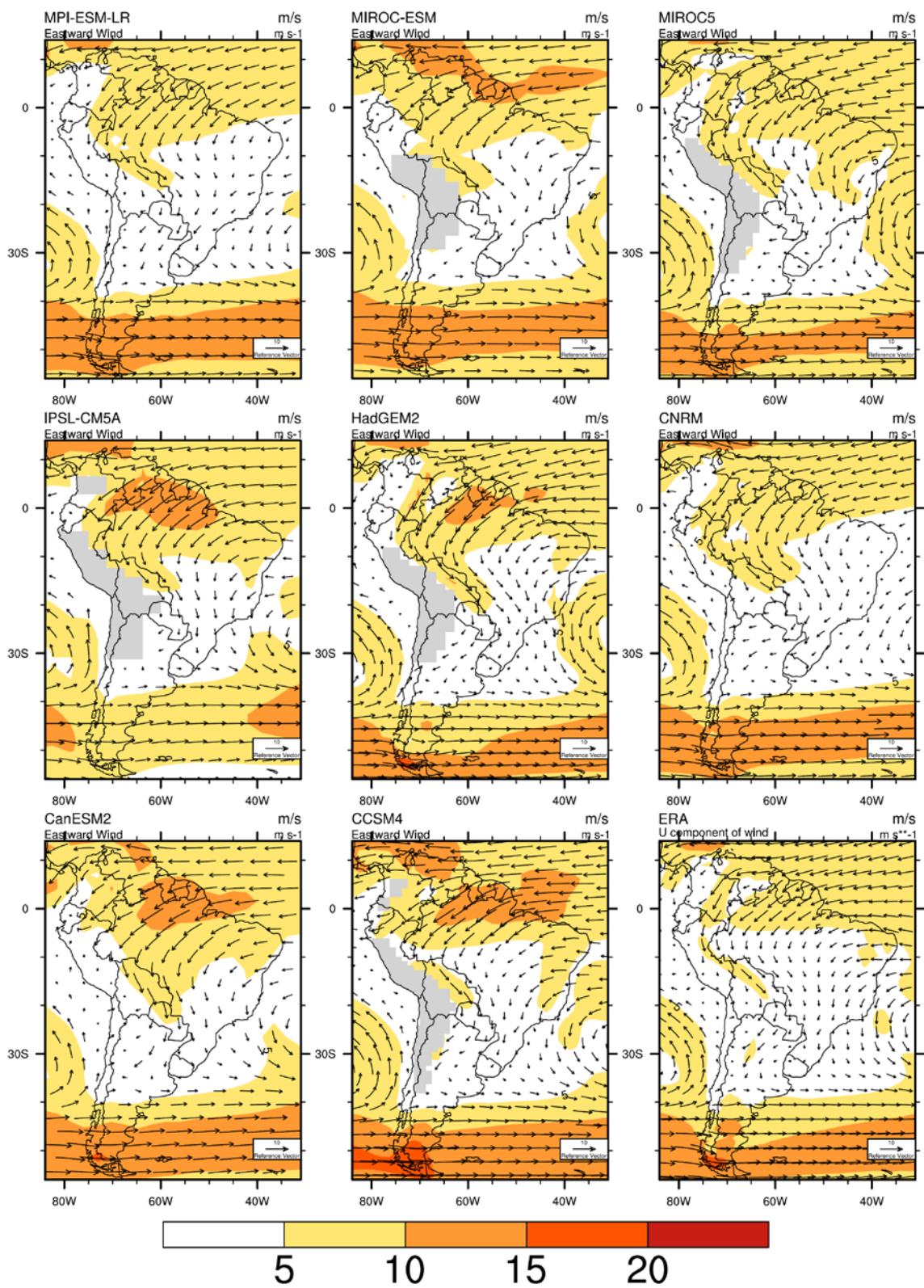


Figure 2.8 Wind vector climatology (1979-2005) at 850 hPa for CMIP5 models and ERA-Interim in January (a) and July (b). The model data are shown at their original spatial resolution.

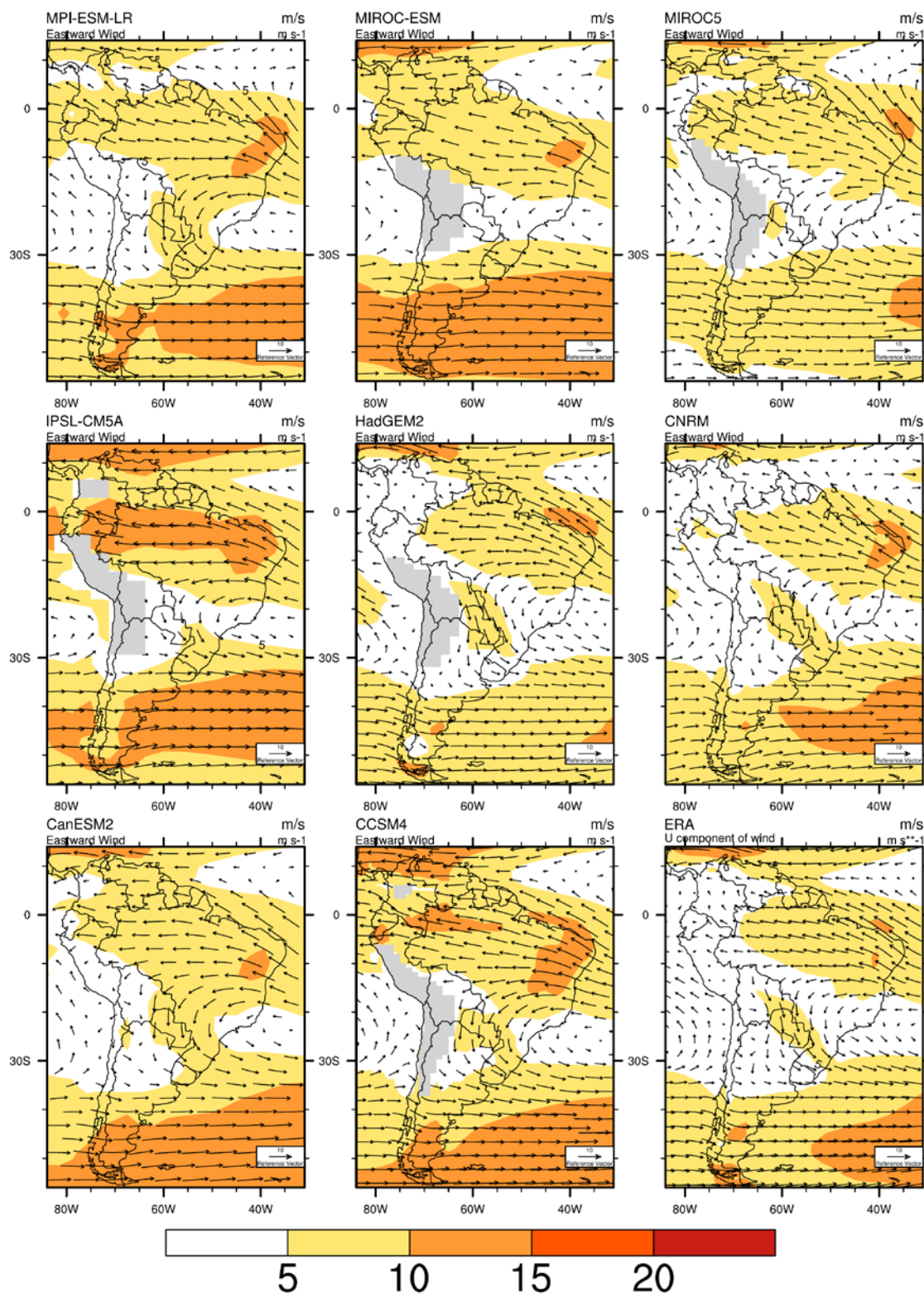


Figure 2.8 (continued)

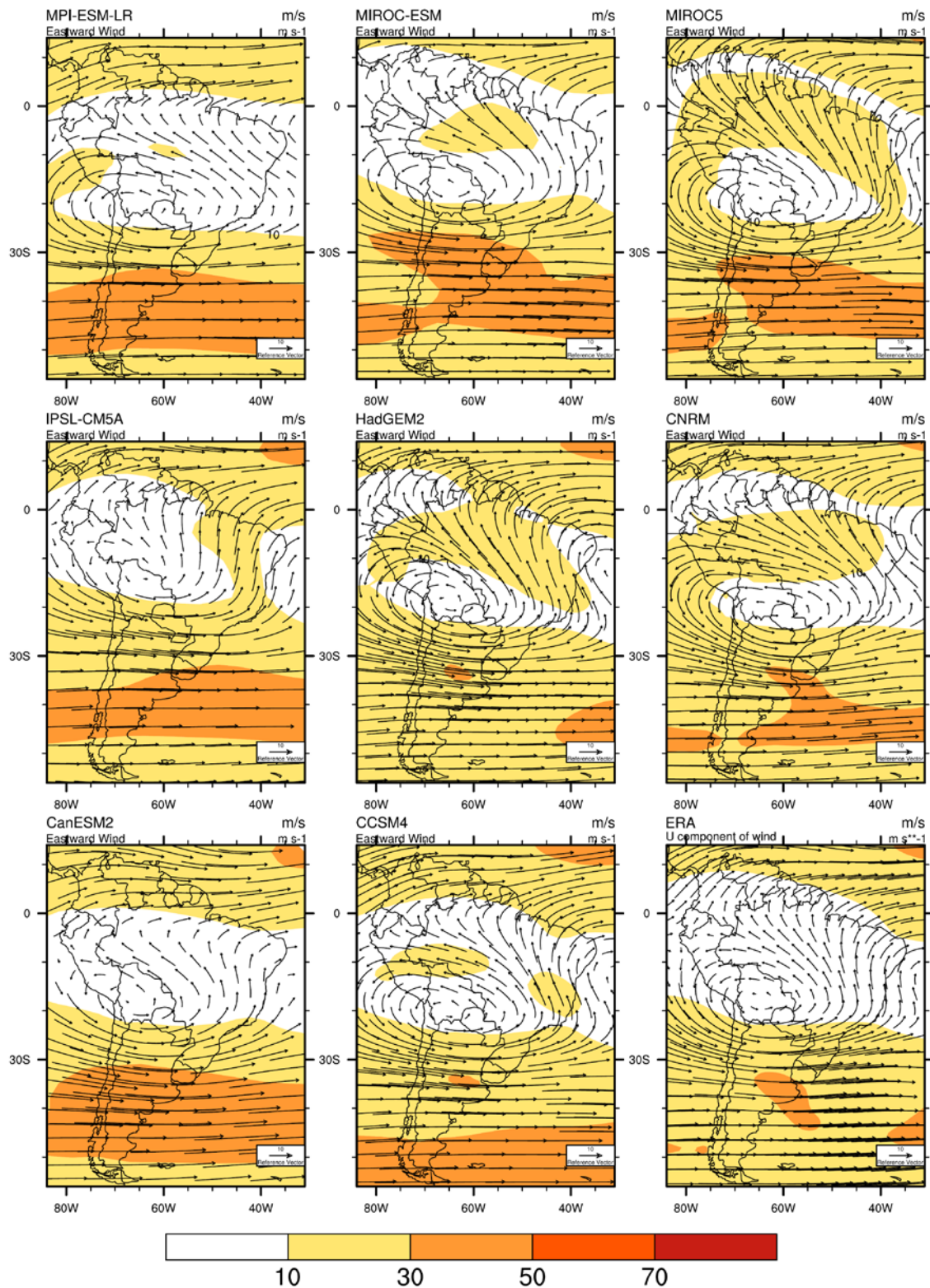


Figure 2.9 Wind vector climatology (1979-2005) at 200 hPa for CMIP5 models and ERA-Interim in January (a) and July (b). The model data are shown at their original spatial resolution.

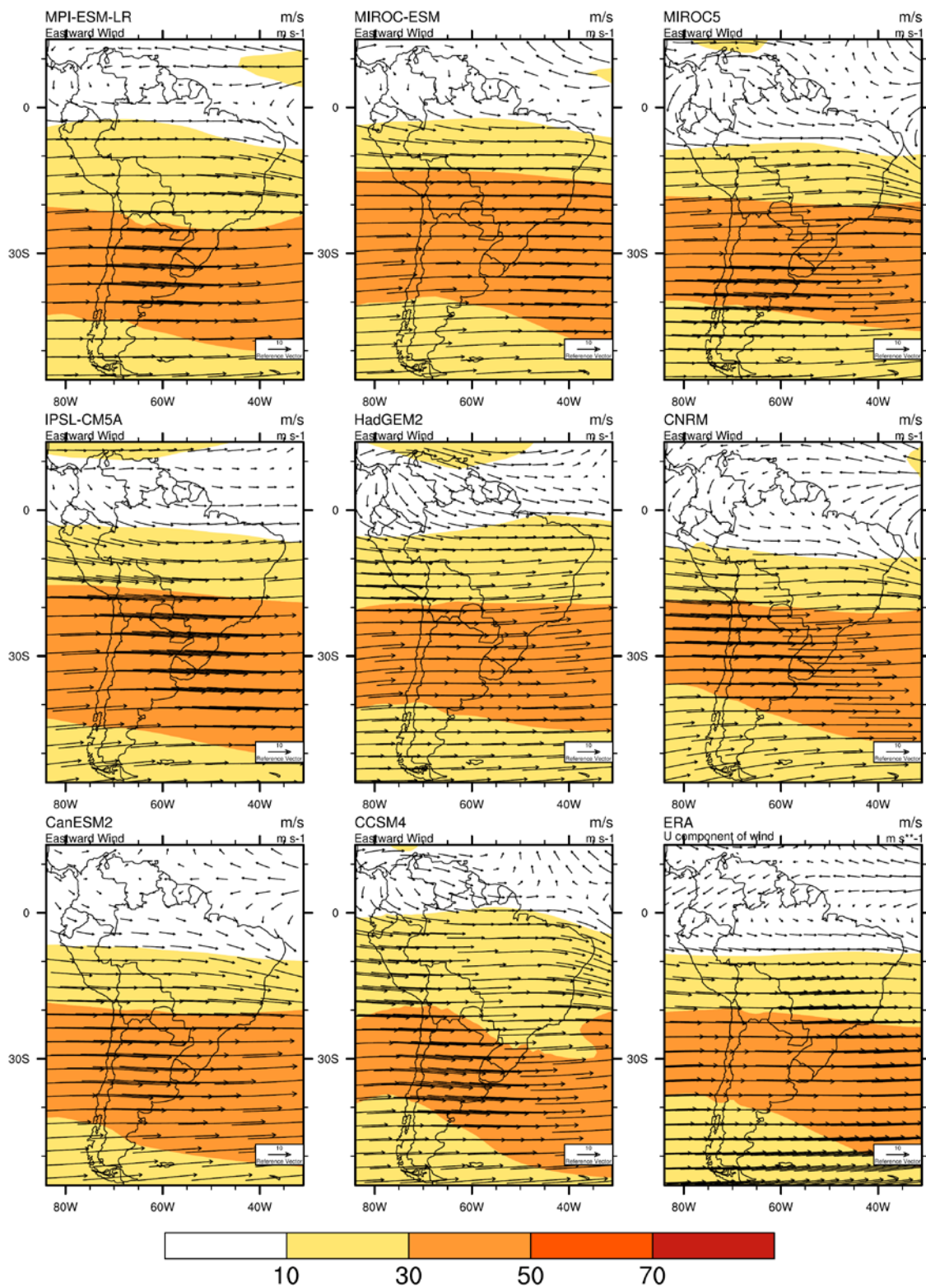


Figure 2.9 (continued)

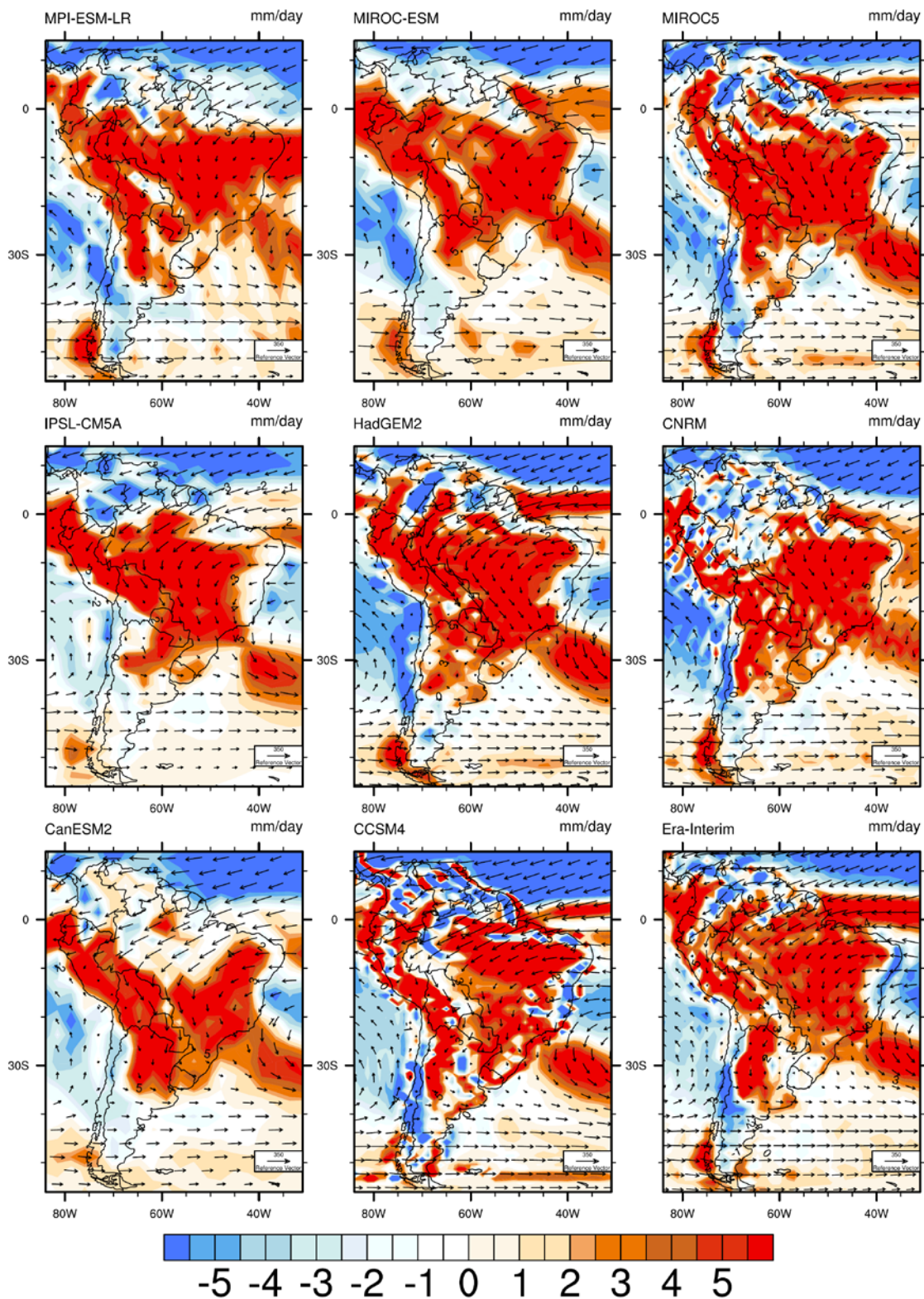


Figure 2.10 Climatology (1979-2005) of vertically integrated moisture transport (vectors) in $\text{kg m}^{-1} \text{s}^{-1}$ and its convergence (contours) in mm/day in January (a) and July (b). The model data are shown at their original spatial resolution.

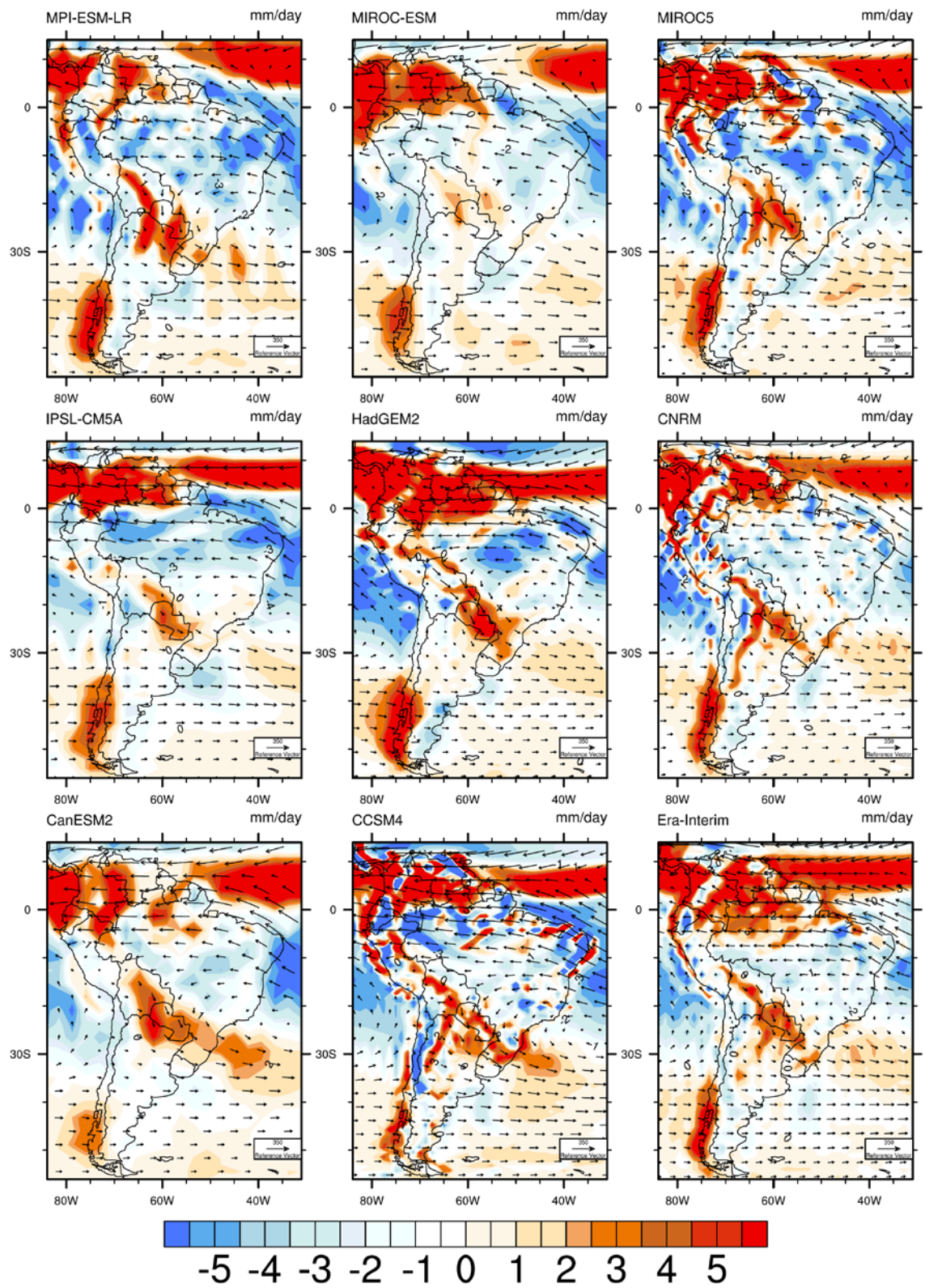


Figure 2.10 (continued)

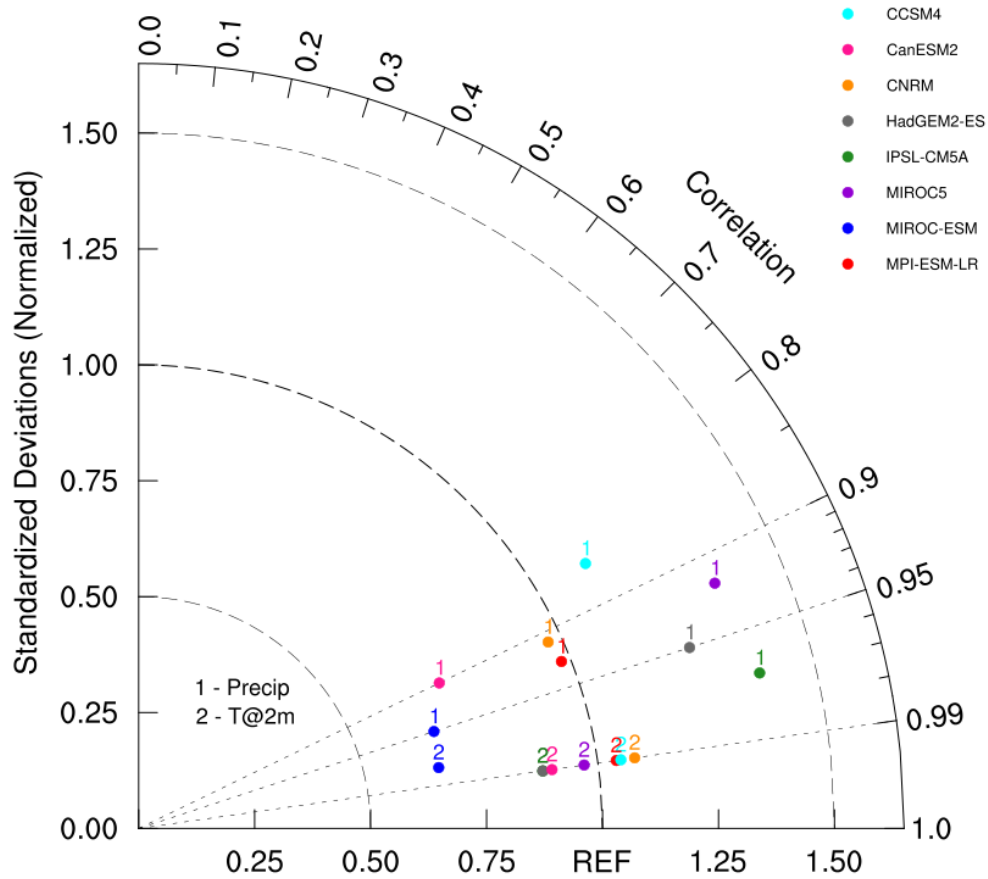


Figure 2.11 Taylor diagram of the spatial pattern of January mean of precipitation and temperature for the eight CMIP5 models over Bolivia. The standard deviations have been normalized relative to the observed values. Each model is represented by a different color specified in the legend and numbers separate variables of precipitation and temperature. All models grids have been regridded to 2.5 degree for this analysis.

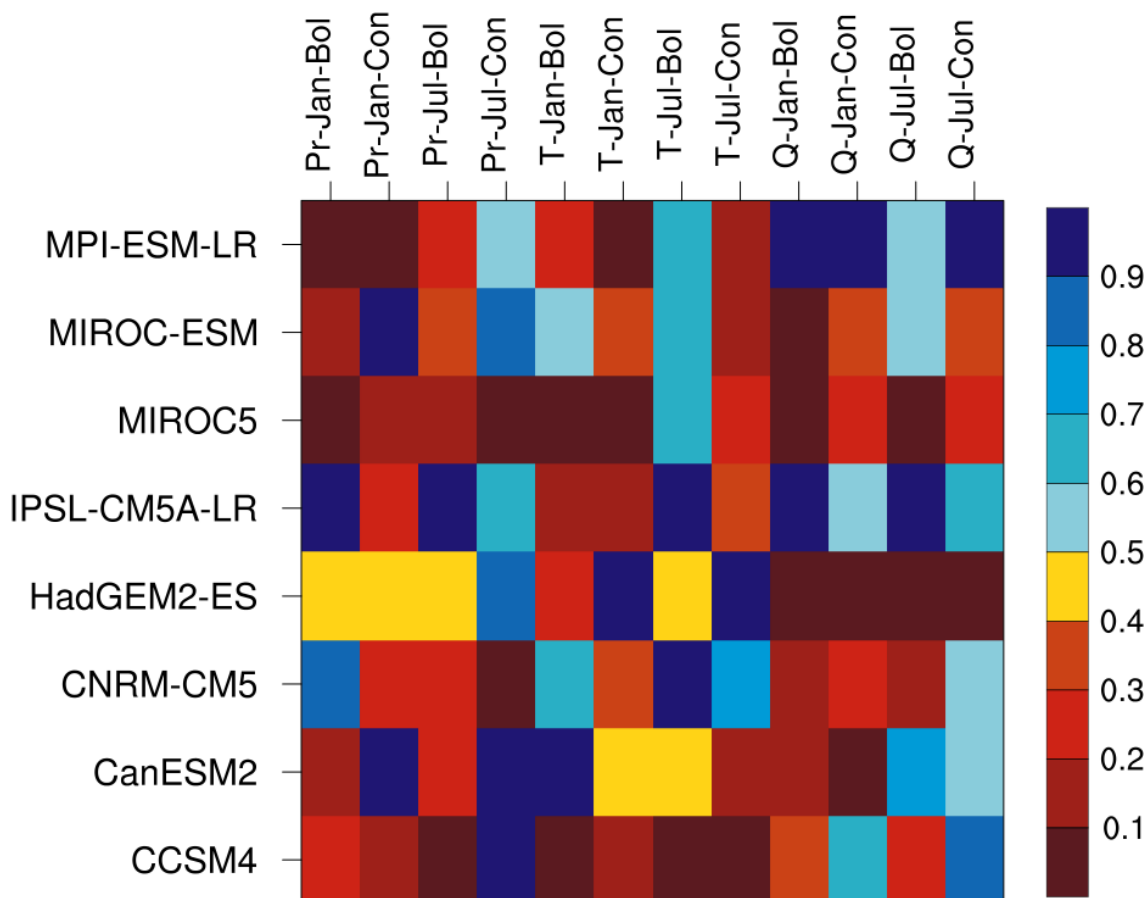


Figure 2.12 Comparison of CMIP5 models across a set of continental (Con) and local (Bol; limited to Bolivia's boundaries) performance metrics based on bias values for precipitation (Pr), temperature (T) and vertically integrated moisture convergence (Q) for January and July. Biases are normalized relative to the range of bias values across models. Red shades represent lower relative bias values and blue shades show higher relative bias values.

Chapter 3

Climate Classification in Bolivia: A Combination of Nonhierarchical and Consensus Clustering Analyses Based on Precipitation and Temperature

Azar M. Abadi¹, Clinton M. Rowe¹ and Marcos Andrade^{2,3}

¹Department of Earth and Atmospheric Sciences, University of Nebraska-Lincoln, Lincoln, Nebraska

²Laboratorio de Física de la Atmósfera, Instituto de Investigaciones Físicas, Universidad Mayor de San Andrés, La Paz, Bolivia

³Department of Atmospheric and Oceanic Science, University of Maryland, College Park, MD, USA

Abstract

Climate regionalization is an inseparable part of many climate change and environmental studies. Delineating climatologically homogeneous regions enhances the utility of such studies and reduces the biases due to the uncertainties associated with climate model outputs at individual grid points which both lead to better understanding of the atmospheric mechanisms affecting a region's climate. Throughout time, researchers and statisticians have developed different methods to perform regionalization in which the techniques are highly dependent on the nature and accessibility of the data. This research aims to divide Bolivia into smaller, coherent climate subdivisions. To achieve this goal, we first apply the nonhierarchical k -means clustering method to precipitation and temperature separately using a gridded observation dataset for Bolivia spanning from 1979 to 2010. The clustering is performed on the two variables separately to avoid arbitrary attribute scaling and information redundancy as well as to gain a better understanding of these individual variables across Bolivia. Consensus clustering then finds the categorical intersection of the two independent clusters to create homogeneous

climate regions. Results from this study show that Bolivia can be divided into ten climatically distinguishable subdivisions largely explicable by topography and latitude, which are the key climate control factors in the region.

3.1. Introduction

Many environmental studies consider some form of regionalization to divide a study area into smaller coherent domains for analysis. In Bolivia, climate impacts on humans are mainly through extreme events such as flood and drought that are often highly spatially localized and can lead to significant economic losses (Seiler et al. 2013a, b). To capture and explore the characteristics of such impacts, we should first divide the region into climatically homogeneous regions on the basis of the most relevant hydro-meteorological variables, so the extent and severity of those impacts and the mechanisms responsible for them can be studied (Dezfuli and Nicholson 2013; Nicholson and Dezfuli 2013).

Scientists have devised different ways to delineate climate regimes. Some widely used approaches include delineation by hydrological basins, geographic boundaries, extent of major atmospheric circulation mechanisms, altitudinal divisions and, as a simpler approach, rectangular areas covering the study area (Korecha and Sorteberg 2013). Depending on the purpose of the study, any of these techniques might perform appropriately. However, the resulting regions are not always representative of distinguishable types of climate.

In Bolivia, using the aforementioned methodologies, the country has been divided into four main regions largely based on the altitudinal gradient and latitudinal change: northern lowlands (aka Amazonia), southern lowlands (aka La Plata basin), Altiplano and valleys (Andrade 2014; Velpuri et al. 2016). More objective methodologies are usually

achieved by some form of the multivariate statistical technique of cluster analysis to promote consistency among studies (Jain et al. 1999; Zhang et al. 2016). To our knowledge, only a few studies have investigated such methodology in South America (Reboita et al. 2010). A technique commonly used in Bolivia and Peru is the regional vector method (RVM) developed by G. Hiez (1977) and incorporated into a hydrological analysis software run by the National Weather Services of these countries. This method has been used in the region in several studies (Hiez 1977; Brunet-Moret 1979). In another study, Velpuri et al. (2016) regionalized Bolivia into homogeneous hydrological regions based on sub-basins and altitudinal datasets. Other examples for South America include Portela et al (2015) which applied principal component analysis (PCA) for drought regionalization in southern Paraguay, Brazil and northern Argentina, and Santos et al (2014) which applied a hierarchical clustering method to distinguish homogeneous precipitation subregions in the Brazilian Amazon.

Being among the countries vulnerable to climate change, such climate classification facilitates studies on regional climate variabilities and the factors influencing those fluctuations. Accordingly, to develop a framework for future studies in Bolivia, this study aims to fill the gap by dividing the country into climate regions with specific climate characteristics using two clustering techniques – independent *k*-means clustering on monthly climatologies of precipitation and temperature followed by a consensus clustering to form a climate regionalization.

The structure of this paper is as follows. Data and clustering approaches are presented in section 2. Section 3 describes the results of the *k*-means and consensus

clustering analysis outcomes and elaborates on the principal findings. Section 5 presents some concluding remarks.

3.2. Data and Methodology

3.2.1 Study Area

Geographically, Bolivia spans from tropical latitudes in the north ($\sim 10^{\circ}\text{S}$) to a subtropical band at the southern edge ($\sim 23^{\circ}\text{S}$). Longitudinally, the boundaries are defined by the high mountains of the central Andes to the west ($\sim 70^{\circ}\text{W}$) and lowlands of La Plata basin to the east ($\sim 56^{\circ}\text{W}$). The distinct position of the country and its heterogeneous topography (Fig. 3.1) expose different parts of the country to different atmospheric circulation mechanisms, influencing temperature and precipitation variability during different months of the year.

3.2.2 Data

Environmental research often requires high resolution, good quality observational climate data, especially in places with a complicated topography such as Bolivia. Andrade (2014) combined reanalysis and satellite data validated by observational data from different sources to create a daily gridded dataset of precipitation and temperature with a spatial resolution of approximately 25 km, from 1979-2010. The data are based on the Climate Forecast System Reanalysis (CFSR), version 1 (Saha et al. 2010), with minimum and maximum temperature and daily precipitation computed from the original 6-hourly reanalysis and interpolated using cubic splines to a $0.25^{\circ} \times 0.25^{\circ}$ spatial resolution. Precipitation data are then adjusted based on a monthly regression against Multi-Satellite TRMM Precipitation Analysis (TMPA; Huffman et al 2007, 2010) applied to the daily, interpolated CFSR data. Both temperature and precipitation data are further adjusted

across four altitudinal zones to increase agreement with in-situ observations from the Bolivian national weather service (SENAMHI), especially in terms of better representing extreme precipitation events. The final, daily, corrected and bias-adjusted data reproduce the climatological distribution of temperature and precipitation across Bolivia. These data have been used for climate change detection across Bolivia (Andrade 2014) and are the basis for the present study.

3.2.3 Methodology

Cluster analysis groups data into smaller subdivisions by combining similar objects (climate stations or grid points) into respective categories and segregating the unlike ones (Gong and Richman 1995). Clustering algorithms can be categorized in two main types of hierarchical and non-hierarchical clustering. The two clustering approaches share a common use of some measure of distance or correlation to perform tests of similarity (small distance, strong correlation) or dissimilarity (large distance, weak correlation) among the objects (here, the individual grid points).

Both hierarchical and non-hierarchical algorithms have advantages and disadvantages, depending on the data structure and available information on the number of outcome clusters and both have been used extensively in atmospheric research. Fovell and Fovell (1993) used a non-hierarchical clustering, often referred to as *k*-means clustering, on temperature and precipitation data to group grid points with similar climate variability in the conterminous United States. This method randomly assigns the objects to a predetermined number of clusters. In the next step, the centroids are computed for each cluster. Then, it repeatedly reassigns the members to clusters with a closer centroid (in climate space) followed by recomputing cluster centroids, until an “optimal”

clustering is achieved. In this approach, closer objects have more influence upon each other. The resulting proximity of the objects (again, in climate space) in this method is of crucial importance especially in georeferenced datasets as it almost guarantees geographical contiguousness of the subregions due to the spatial autocorrelation inherent in the underlying climate data. The major drawback of non-hierarchical cluster analysis is the need for prior knowledge of the number of clusters (Carvalho et al. 2016), or the number of climate regions in our case. Hierarchical methods, on the other hand, proceed hierarchically by either merging smaller clusters at steps (agglomerative, or bottom-up) or dividing the larger clusters into smaller ones (divisive, or top-down) (Rao and Srinivas 2006). The bottom-up approach initially assigns each object to a single-member group and pairs the closest ones in one-way hierarchical steps until all members are in a single group. The top-down method works in the reverse, starting with all members in a single group and repeatedly dividing until each member is in its own group. In either case the user chooses the final number of clusters according to a hierarchical tree diagram or dendrogram (Wilks 2011). Once groups contain more than one member, a variety of methods to measure inter-group distance can be devised, resulting in a family of hierarchical clustering methods. A major disadvantage with these methods is in the deterministic nature of these techniques that there is no capability of reassigning members during subsequent steps, even if a member no longer fits “best” in its assigned group. That is, once groups are joined in an agglomerative method, all members remain in the new group, or once members are split into two groups in a divisive method, they cannot be rejoined.

As mentioned earlier, all clustering approaches share some sort of a tool for assessing the comparability among objects in a form of a dissimilarity measure with the most common ones being Euclidean and Pearson correlation distances (Wilks 2011). The main clustering criterion then would be maximizing (minimizing) the distance between (within) clusters or, inversely, minimizing (maximizing) the correlation between (within) groups.

As hierarchical methods have no provision for reallocating points assigned to “wrong” groups at early stages, in this research we applied nonhierarchical k -means to the monthly climatology of precipitation and temperature. The use of nonhierarchical methods requires *a priori* specification of the number of final clusters, as noted above. Because this is not known for Bolivia temperature and precipitation, k -means was conducted repeatedly over a range of final clusters to determine the optimal number of clusters for each variable. There are many clustering validity indices developed to assist with selecting the optimal number of clusters (Ray and Turi, 1999; Kodinariya and Makwana, 2013). One of the widely used selection methods is the elbow method that optimizes the criterion of the within-cluster sums of squared (WSS) errors that is computed as sum of squared distance between each member of a cluster and the cluster centroid. Changing k (number of clusters) starting from 1, the within-cluster sum of squares is calculated. With increasing k , the error drops dramatically at the beginning and stabilizes after reaching the optimal k (or the “elbow”).

Among the hydrometeorological variables that define a region’s climate, we have chosen precipitation and temperature for the cluster analysis as Fovell (1997) showed that these two variables are generally necessary and sufficient for this type of analysis.

Although clustering methods are capable of multi-variate clustering, we have treated the two variables separately to avoid the need for incommensurable scaling and to gain a better understanding of the structure of each variable separately. However, to minimize the potential error due to large spatial variability, we employed a square root transformation (Richman and Lamb 1985) on the monthly precipitation that by nature follows a gamma distribution to pull in the extremes toward the center (Husak et al. 2007). As temperature data are closer to a normal distribution, no standardization was performed on that variable.

Finally, to create coherent climate regions, the two clustering outcomes must be combined in some way. To this end, Fovell and Fovell (1993) employed an approach called consensus clustering that creates subcategories based upon the intersection of each independent variable's clusters. Assuming m clusters for precipitation dataset and n clusters for temperature datasets, the categorical intersection yields $m \times n$ possible consensus clusters for the outcome. In practice, consensus clustering rarely yields the full number of possible clusters, as some of them are empty due to lack of intersection. Fovell and Fovell (1993) also showed that intersections close to the region boundaries sometimes create small orphaned clusters with few members, not large enough to be considered as distinct climate regions. By reassigning the members of the orphaned clusters to one of the neighboring statistically similar clusters, the spatial consistency of the regions can be improved.

3.3. Results and Discussion

3.3.1 Nonhierarchical Clustering

We begin the regionalization process by creating a matrix containing N rows of objects (the 1468 grid points inside Bolivia) and 24 columns of monthly climatology of square-root precipitation followed by temperature monthly climatology. Each climatology was constructed from the 32-year period (1979 to 2010) of the dataset (Andrade 2014). To select the optimal number of clusters we applied the elbow method to our data (Fig. 3.2). Following the elbow method criterion, we concluded that $k = 4$ gives the optimal number of clusters for both variables as the WSS slows down after partitioning by four clusters in both variables.

Fig. 3.3 represents the four precipitation regions for Bolivia generated by the k -means method, which are each labeled by a numerical value and denoted by a specific color. Separation of regions P1 and P2 is evidence of a precipitation gradient from northern latitudes toward southern latitudes across Bolivia and also of the different mechanisms affecting precipitation in those regions. Region P2 is comprised of three smaller subregions following a similar seasonal climatology of precipitation (Fig. 3.4), but associated with different mechanisms; the eastern sub-region follows the SAMS circulation pattern while the western sub-region is mainly orographic. The southern sub-region is a part of a larger area of higher precipitation caused by Chaco Jet Events (CJE), which is a fundamental component of SAMS (Marengo et al. 2010). Separation between these regions and regions P3 and P4 to the west shows the impact of the altitudinal gradient over the Andes on the precipitation regimes. Fig. 3.5 shows the four temperature regions generated by the same k -means method, each labeled by a numerical value and

designated by a distinct pattern. Similar to the precipitation regions, the temperature regionalization shows mainly the impact of altitudinal change on the temperature distribution across Bolivia.

3.3.2 Consensus Clustering

Table 3.1 summarizes the results of the intersection that creates 16 (4×4) possible precipitation/temperature subtypes or regions; of these possible combinations, five are empty and one is a single-member cluster. Comparing the statistics for these small regions, the isolated cluster was reassigned (black arrow in Table 3.1) to a neighboring region, reducing the total number of populated regions to 10 (Fig. 3.6). These final climate regions are then named from their precipitation category followed by their temperature category (e.g. P4T3).

Boxplots (Fig. 3.7) summarize the statistical properties of annual cycles of precipitation and temperature in each climate region and represent the spatial variability within each region for each month and variable. Region P1T1, encompassing the southern part of Amazonia, covers most of Bolivia's northern and central lowlands and, with 567 grid points, is the largest climate region and includes El Chapare, the region of highest annual rainfall in Bolivia. Region P1T2, a small region covering 22 gridpoints, has very similar precipitation as P1T1 but is located in the Andean foothills of central Bolivia and, thus, has slightly lower temperature in every month. The region of P2T1, covering the eastern lowlands and being a mixture of open scrub woodlands, dry forests and mountain forests, bears some similarity to P1T1 as to precipitation distribution, but with a longer dry season. This region also has higher spatiotemporal variability in temperature and a cold season starting earlier and lasting longer. Proximity to the equator

and the path of the South American Monsoon System (Zhou and Lau 1998; Raia and Cavalcanti 2008; Marengo et al. 2010) exposes these regions to more available atmospheric moisture in the wet months compared to the rest of the country.

Temperature-wise, however, P2T1 shows a greater seasonal change. The inter quartile range (IQR), which is a representative of middle 50% of the data, also shows that temperature is more consistent across P1T1 and P1T2 while in P2T1 there is more spatial variability as noted previously because it includes several non-contiguous subregions. The driest of all regions in the lowlands is P3T1, which has a more pronounced dry season compared to its northern neighbors. This region includes the Gran Chaco or Dry Chaco, an area characterized as extremely dry and hot.

The remaining regions cover more elevated lands with some representing transitional zones between the wetter climates over the lowlands and drier climates in the high valleys. Covering part of Cordillera Real and northern Altiplano, regions P2T2 and P3T3, with lower precipitation and temperatures, separate the wet tropical area to the north from the drier Altiplano to the south. These regions are covered mainly by mountain forests with high spatiotemporal variability in both temperature and precipitation due to the mountainous terrain. Overlaying Cordillera Central, P3T2 and P4T2 are a mixture of high altitude vegetation, dry forests and snow covered mountains, which separate the wetter regions to the east and drier Altiplano to the west. These regions have lower average temperature and precipitation with higher spatiotemporal variability in temperature and shorter and drier wet periods. P4T3, encompassing 178 points, is the largest region on the elevated lands (aka Altiplano) and is distinctively dry and cold. Finally, region P4T4, covering the high mountains in the southern part of the

plateau and high valleys of Cordillera Occidental to the west, is the coldest and driest of all regions in the country. The average precipitation and temperature are lowest among all regions with most of the months being receiving very little or no precipitation in the high barren land or snow covered mountain peaks.

Fig. 3.8 divides the precipitation and temperature characteristics of the homogeneous regions into separate wet (November to March) and dry (May to September) seasons. Precipitation and temperature patterns for each climate region are distinctive in each season, but especially during the wet season when there are greater differences in precipitation among regions. Comparing the wet and dry seasons shows which variable is more important in distinguishing the regions in each season. For example for the largest regions in lowlands, P1T1 and P2T1, the notable change in the wet season is caused by the rainfall amount while in the dry season the influential variable is the temperature as the core in the figure makes a shift to the lower temperature from P1T1 to P2T1.

Lastly, we applied the non-parametric Wilcoxon-Mann-Whitney rank-sum test (Mann and Whitney, 1947) on the time series of monthly precipitation and temperature to verify if the regions are statistically significantly different from each other at the 95% confidence level (Table 3.2). This test was chosen due to its applicability to small samples as well as not requiring normally-distributed data. All regions are distinct with respect to both variables except P2T1 and P3T3. The precipitation distributions in region P2T1 and P2T2 and in regions P3T3 and P3T2 do not show a significant difference while temperature-wise they are different. Even though the regions are not found statistically significant on one of the variables, they still represent distinct climate regions, due to

differences in the other variable. Applying a square-root transformation to the raw precipitation data makes the data less skewed. The transformation reduces the contrast between local maximized precipitation region and the surrounding areas so a region like El Chapare with maximum precipitation is not separated out. However, we should also keep in mind that the data used for this regionalization is not direct observational data but have been derived and adjusted using different sources. In the process, some of the variability has been smoothed out. In addition, the techniques used for finding the regions where precipitation and temperature have homogeneous behavior are not perfect. As a result, the region's boundaries might have some uncertainties. This problem could be especially important for small areas or regions with few observational stations (El Chaco for instance). In spite of this, based on different trials (not discussed here), the large regions obtained from the clustering process seem to be robust.

3.4. Concluding remarks

Regionalization is an important component in many climate-related studies. The objective of the present research is to delineate homogeneous climate regions in Bolivia. First *k*-means approach was applied to 1979-2010 gridded monthly climatologies of temperature and precipitation to construct temperature and precipitation clusters independently. Following the elbow method to find the optimal number of clusters, *k*-means analysis yielded four distinct clusters for precipitation and four different clusters for temperature. Consensus clustering then was applied as the categorical intersection of the two independent cluster sets to derive homogenous regions that are distinct in terms of their precipitation and/or temperature regimes.

Our results show that Bolivia's climate is well represented by ten climatically homogeneous regions largely owing to latitudinal and altitudinal gradients that affect the mechanisms responsible for the seasonal changes in precipitation and temperature. Our findings also show that precipitation and temperature exert more variable weights in different seasons as shown in Fig. 3.8. This regionalization will next be used as a framework to investigate the impacts of climate change in a regional climate downscaling study over Bolivia.

Acknowledgements

We gratefully acknowledge support from the Inter-American Development Bank for the development of tools and techniques used in this research and the UNL Holland Computing Center for computing services and support.

3.5. References

- Andrade MF (2014) La economía del cambio climático en Bolivia: generación de datos meteorológicos de alta resolución para Bolivia. C.E. Ludeña, L. Sanchez-Aragon (eds), Banco Interamericano de Desarrollo, Monografía No. 200, Washington, DC. <http://www.iadb.org/en/publications/publication-detail,7101.html?id=73547>
- Brunet-Moret Y (1979) Homogénéisation des précipitations. *Cahier ORSTOM, Série Hydrologie* 16: 3-4.
- Carvalho MJ, Melo-Gonçalves P, Teixeira JC, Rocha A (2016) Regionalization of Europe based on a k -means cluster analysis of the climate change of temperatures and precipitation. *Physics and Chemistry of the Earth*, 94, 22–28. <https://doi.org/10.1016/j.pce.2016.05.001>
- Dezfuli AK, Nicholson SE (2013) The relationship of rainfall variability in western equatorial africa to the tropical oceans and atmospheric circulation. Part II: The boreal autumn. *Journal of Climate*, 26(1), 66–84. <https://doi.org/10.1175/JCLI-D-11-00686.1>
- Fovell RG (1997) Consensus clustering of U.S. temperature and precipitation data. *Journal of Climate*, 10(6), 1405–1427. [https://doi.org/10.1175/1520-0442\(1997\)010<1405:CCOUST>2.0.CO;2](https://doi.org/10.1175/1520-0442(1997)010<1405:CCOUST>2.0.CO;2)
- Fovell RG, Fovell MYC (1993) Climate zones of the conterminous United States defined using cluster analysis. *Journal of Climate*. [https://doi.org/10.1175/1520-0442\(1993\)006<2103:CZOTCU>2.0.CO;2](https://doi.org/10.1175/1520-0442(1993)006<2103:CZOTCU>2.0.CO;2)
- Gong X, Richman MB (1995) On the application of cluster analysis to growing season precipitation data in North America east of the Rockies. *Journal of Climate*. [https://doi.org/10.1175/1520-0442\(1995\)008<0897:OTAOCA>2.0.CO;2](https://doi.org/10.1175/1520-0442(1995)008<0897:OTAOCA>2.0.CO;2)
- Hiez, G (1977) L'homogénéité des données pluviométriques. *Cahier ORTSTOM, série Hydrologie*, 14:129–172.
- Huffman GJ, Adler RF, Bolvin DT, et al (2007) The TRMM multi-satellite precipitation analysis: quasi-global, multi-year, combined-sensor precipitation estimates at fine scale. *J. Hydrometeor.*, 8(1), 38-55
- Huffman GJ, Adler RF, Bolvin DT, et al (2010) The TRMM multi-satellite precipitation analysis (TMPA). Chapter 1 in *Satellite Rainfall Applications for Surface Hydrology*, F. Hossain and M. Gebremichael, Eds. Springer Verlag, ISBN: 978-90-481-2914-0, 3-22
- Husak GJ, Michaelsen J, Funk C (2007) Use of the gamma distribution to represent monthly rainfall in Africa for drought monitoring applications. *International Journal of Climatology*, 27(7), 935–944. <https://doi.org/10.1002/joc.1441>
- Jain AK, Murty MN, Flynn PJ (1999) Data clustering: a review. *ACM Computing Surveys*, 31(3), 264–323. <https://doi.org/10.1145/331499.331504>
- Kodinariya TM, Makwana PR (2013) Review on determining number of cluster in k -means clustering. *International Journal of Advance Research in Computer Science and Management Studies*, 1(6), 2321–7782.

- Korecha D, Sorteberg A (2013) Validation of operational seasonal rainfall forecast in Ethiopia. *Water Resources Research*, 49(11), 7681–7697. <https://doi.org/10.1002/2013WR013760>
- Mann HB, Whitney DR (1947) On a test of whether one of two random variables is stochastically larger than the other. *Ann. Math. Statistics*, 18(1), 50-60.
- Marengo JA, Liebmann B, Grimm AM et al (2010) Recent developments on the South American monsoon system. *Int J Clim*. doi:10.1002/joc.2254
- Nicholson SE, Dezfuli AK (2013) The relationship of rainfall variability in western equatorial Africa to the tropical oceans and atmospheric circulation. Part I: The boreal spring. *Journal of Climate*, 26(1), 45–65. <https://doi.org/10.1175/JCLI-D-11-00653.1>
- Portela MM, Santos JFD, Silva AT, et al (2015) Drought analysis in southern Paraguay, Brazil and northern Argentina: regionalization, occurrence rate and rainfall thresholds. *Hydrology Research*, 46, 792, doi:10.2166/nh.2014.074.
- Raia A, Cavalcanti IFD (2008) The life cycle of the South American monsoon system. *Journal of Climate*, 21(23), 6227–6246. <https://doi.org/10.1175/2008jcli2249.1>
- Rao AR, Srinivas VV (2006) Regionalization of watersheds by hybrid-cluster analysis. *Journal of Hydrology*, 318(1–4), 37–56. <https://doi.org/10.1016/j.jhydrol.2005.06.003>
- Ray S, Turi RH (1999) Determination of number of clusters in *k*-means clustering and application in colour image segmentation. *Proceedings of the 4th International Conference on Advances in Pattern Recognition and Digital Techniques*, 137–143. <https://doi.org/10.1109/TKDE.2008.158>
- Richman MB, Lamb PJ (1985) Climatic pattern analysis of three- and seven-day summer rainfall in the central United States: some methodological considerations and a regionalization. *Journal of Climate and Applied Meteorology*. [https://doi.org/10.1175/1520-0450\(1985\)024<1325:CPAOTA>2.0.CO;2](https://doi.org/10.1175/1520-0450(1985)024<1325:CPAOTA>2.0.CO;2)
- Reboita MS, Gan MA, Rocha, RP, Ambrizzi T (2010) Regimes de precipitação na América do Sul: uma revisão bibliográfica. *Revista Brasileira de Meteorologia*, 25(2), 185–204. <https://doi.org/10.1590/S0102-77862010000200004>
- Saha S, Murthi S, Pan H et al (2010) The NCEP Climate Forecast System Reanalysis. *Bull. Am. Meteorol. Soc.*, 91, 1015.1057. doi: 10.1175/2010BAMS3001.1
- Santos EB, Lucio PS, Silva CMS (2014) Precipitation regionalization of the Brazilian Amazon. *Atmospheric Science Letters*. <https://doi.org/10.1002/asl2.535>
- Seiler C, Hutjes RWA, Kabat P (2013a) Likely ranges of climate change in Bolivia. *Journal of Applied Meteorology and Climatology*, 52(6), 1303–1317. <https://doi.org/10.1175/JAMC-D-12-0224.1>
- Seiler C, Hutjes RWA, Kabat P (2013b) Climate variability and trends in Bolivia. *Journal of Applied Meteorology and Climatology*, 52(1), 130–146. <https://doi.org/10.1175/JAMC-D-12-0105.1>

- Velpuri NM, Pervez MS, Cushing WM (2016) Hydropower assessment of Bolivia—A multisource satellite data and hydrologic modeling approach: U.S. Geological Survey Open-File Report 2016–1156, 65 p., <http://dx.doi.org/10.3133/ofr20161156>
- Wilks D (2011) Statistical Methods in the Atmospheric Sciences. *International Geophysics Series*. [https://doi.org/10.1016/S0074-7742\(08\)60337-2](https://doi.org/10.1016/S0074-7742(08)60337-2)
- Zhang Y, Moges S, Block P (2016) Optimal cluster analysis for objective regionalization of seasonal precipitation in regions of high spatial–temporal variability: application to western Ethiopia. *Journal of Climate*, 29(10), 3697–3717. <https://doi.org/10.1175/JCLI-D-15-0582.1>
- Zhou J, Lau KM (1998) Does a monsoon climate exist over South America? *Journal of Climate*, 11(5), 1020–1040. [https://doi.org/10.1175/15200442\(1998\)011<1020:DAMCEO>2.0.CO;2](https://doi.org/10.1175/15200442(1998)011<1020:DAMCEO>2.0.CO;2)

Table 3.1. Categorical intersection of precipitation and temperature clusters. Numbers in each cell represents the number of grid points in each climate region (e.g. P1T1 covers 567 grid points). Black arrows indicate the reassignment of the orphan cluster.

| | | P1 | P2 | P3 | P4 |
|---|----|-----|-----|-----|-----|
| ✕ | T1 | 567 | 334 | 102 | 0 |
| + | T2 | 22 | 22 | 116 | 26 |
| ◇ | T3 | 0 | 0 | 25 | 178 |
| ✱ | T4 | 0 | 0 | 1 | 75 |

Table 3.2. Summary of Wilcoxon-Mann-Whitney rank-sum test. P-values lower than 0.05 are shaded in green (orange) for precipitation (temperature).

| | p1t2 | p2t1 | p2t2 | p3t1 | p3t2 | p3t3 | p4t2 | p4t3 | p4t4 |
|------|------|------|------|------|------|------|------|------|------|
| p1t1 | | | | | | | | | |
| p1t2 | | | | | | | | | |
| p2t1 | | | | | | | | | |
| p2t2 | | | | | | | | | |
| p3t1 | | | | | | | | | |
| p3t2 | | | | | | | | | |
| p3t3 | | | | | | | | | |
| p4t2 | | | | | | | | | |
| p4t3 | | | | | | | | | |

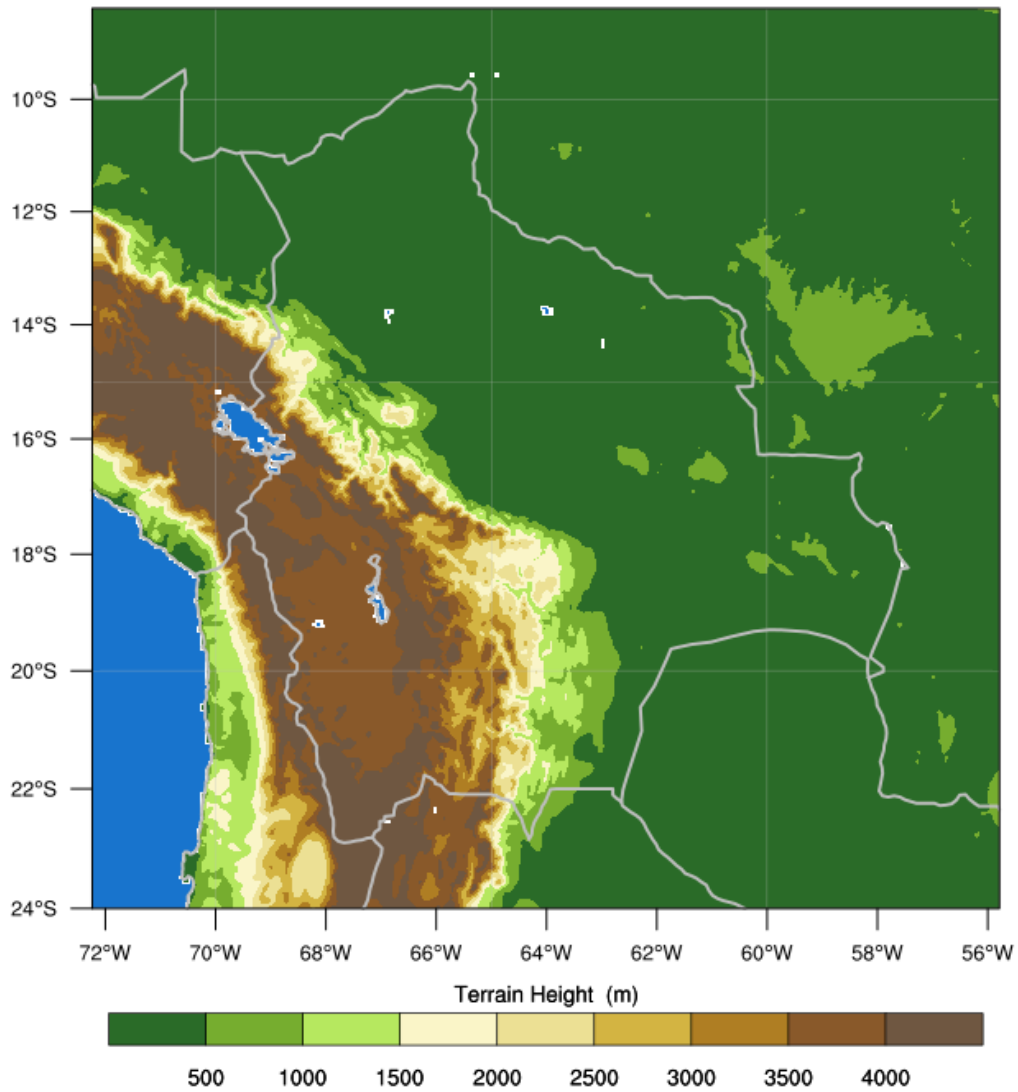


Figure 3.1 Topography of Bolivia. Higher mountains of Andes lie to the west of the country with lowlands to the east. Units are in meters.

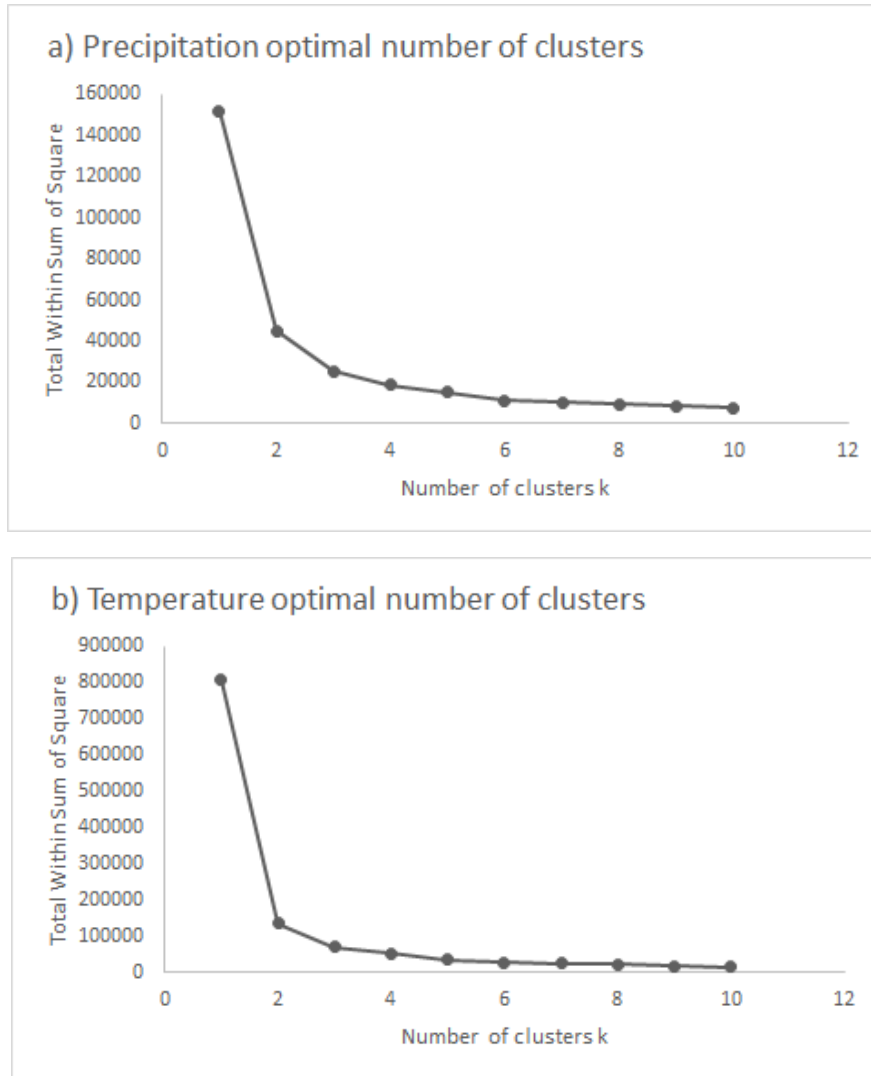


Figure. 3.2 Within-cluster sum of squared errors for 10 clusters of (a) precipitation and (b) temperature.

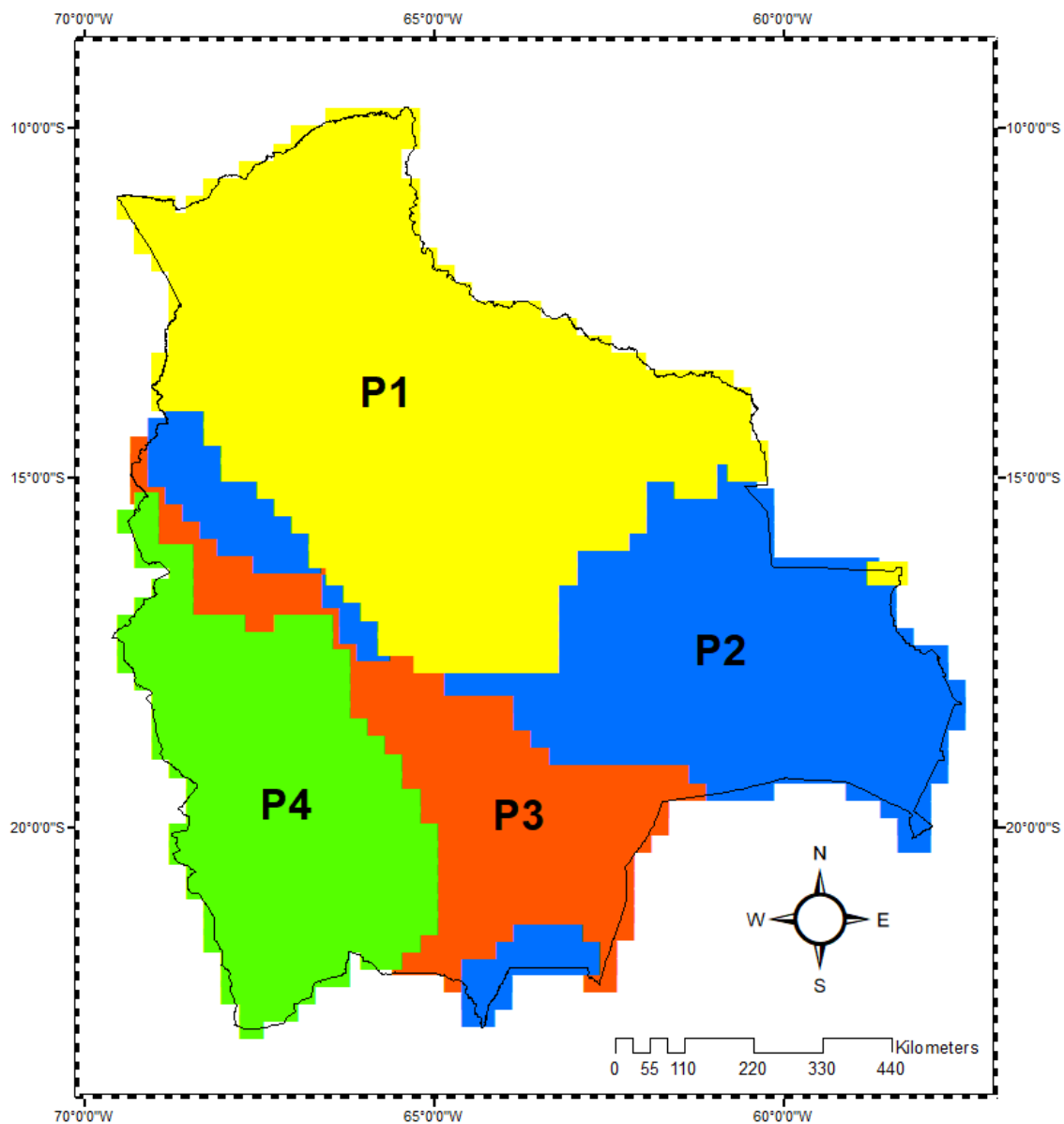


Figure. 3.3 Regionalization of monthly climatology of precipitation over Bolivia. Note that P2 cluster (blue) is not continuous.

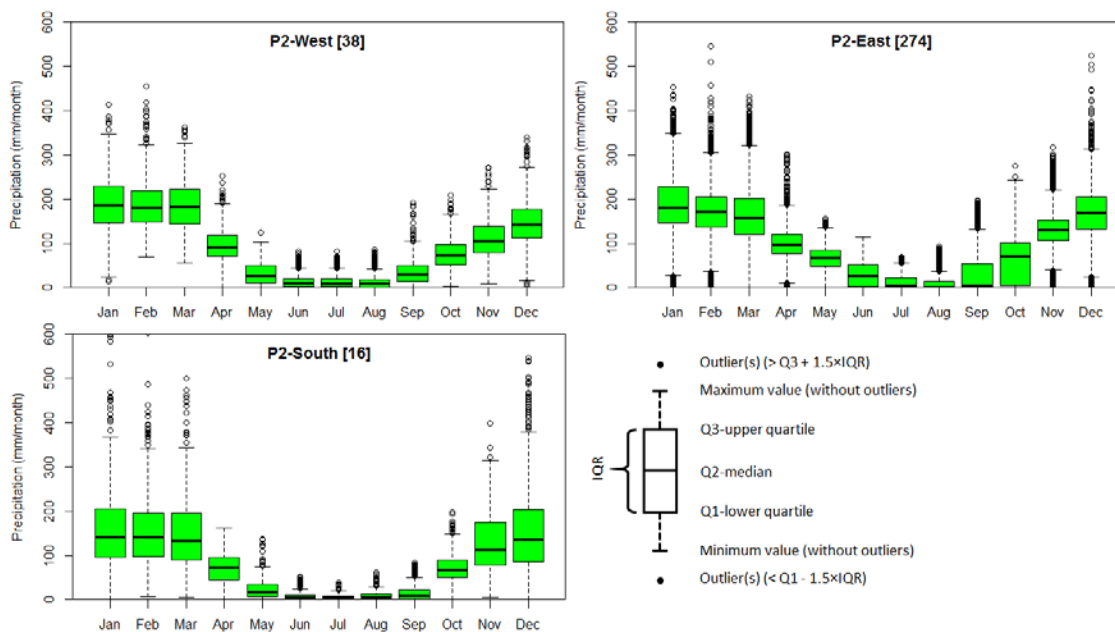


Figure 3.4. Box-and-whisker plot of statistical properties of precipitation in P2 subregions. The numbers in bracket followed by the name of the regions indicate the number of members of each sub-region. Midline is the median of the data with the upper and lower limits of the box being the first and third quartile (25th and 75th percentile) respectively, and denote the interquartile range (IQR). The whiskers extend up to 1.5 times the IQR from the top (bottom) of the box to the furthest datum within that distance. If there are any data beyond that distance, they are represented individually as points ('outliers').

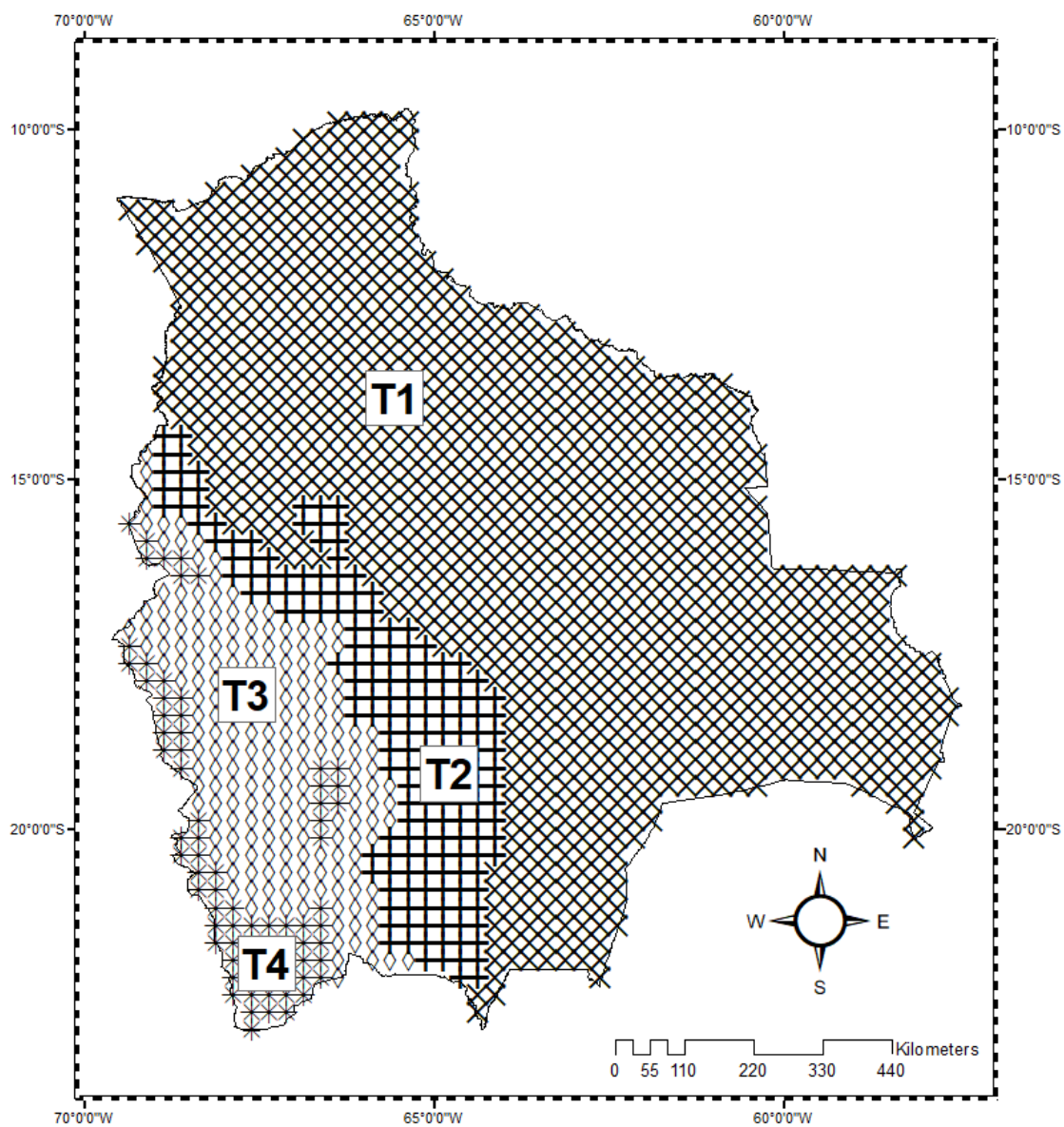


Figure 3.5 Regionalization of monthly climatology of temperature over Bolivia. Note that T4 cluster (asterisk) is not continuous.

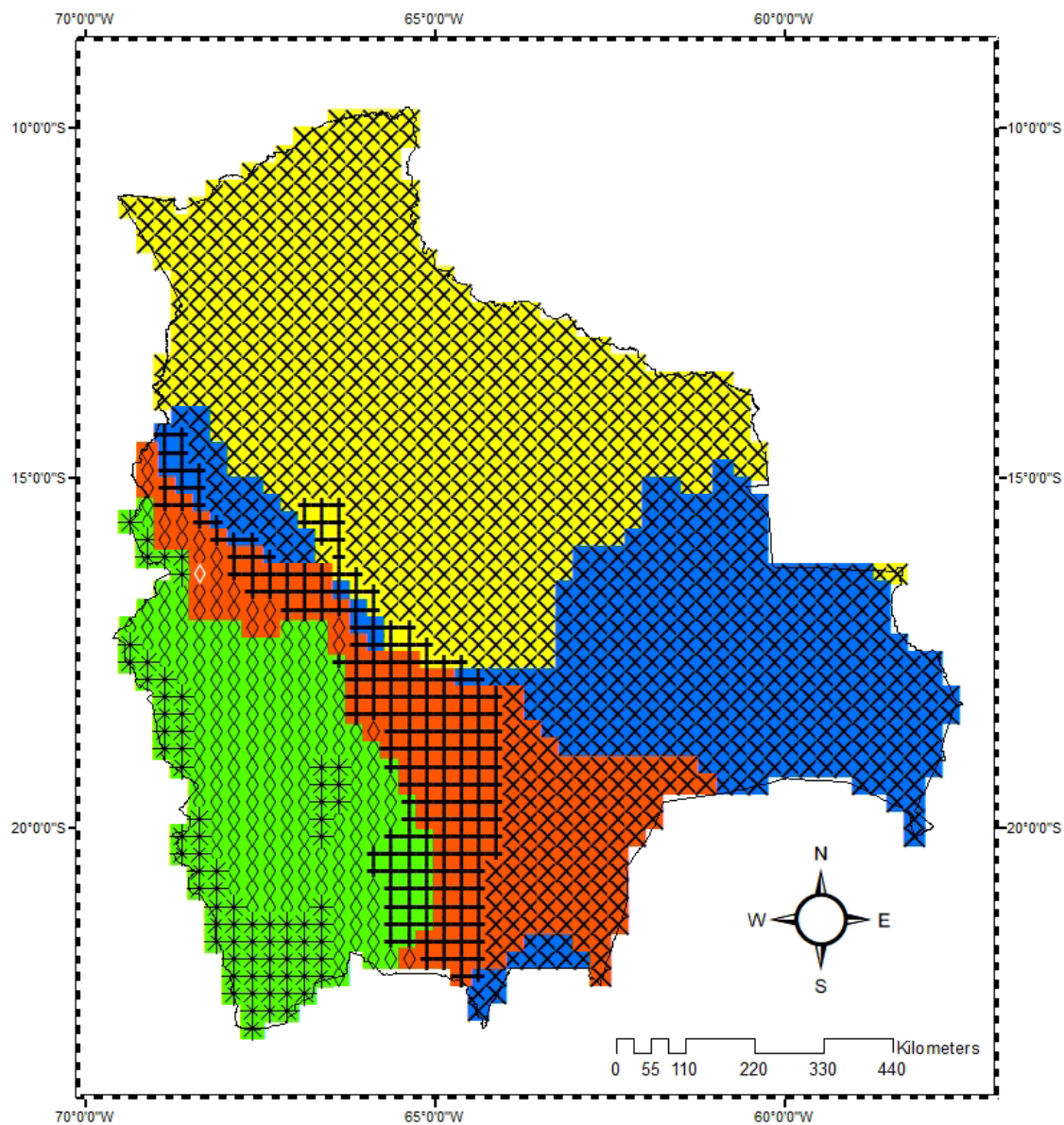


Figure. 3.6. Spatial distribution of final climate regions using *k*-means and consensus clustering techniques. Precipitation clusters are presented in colors and temperature clusters are separated by distinct patterns. White diamond represents the single member cluster of P3T4 which was later reassigned to P3T3.

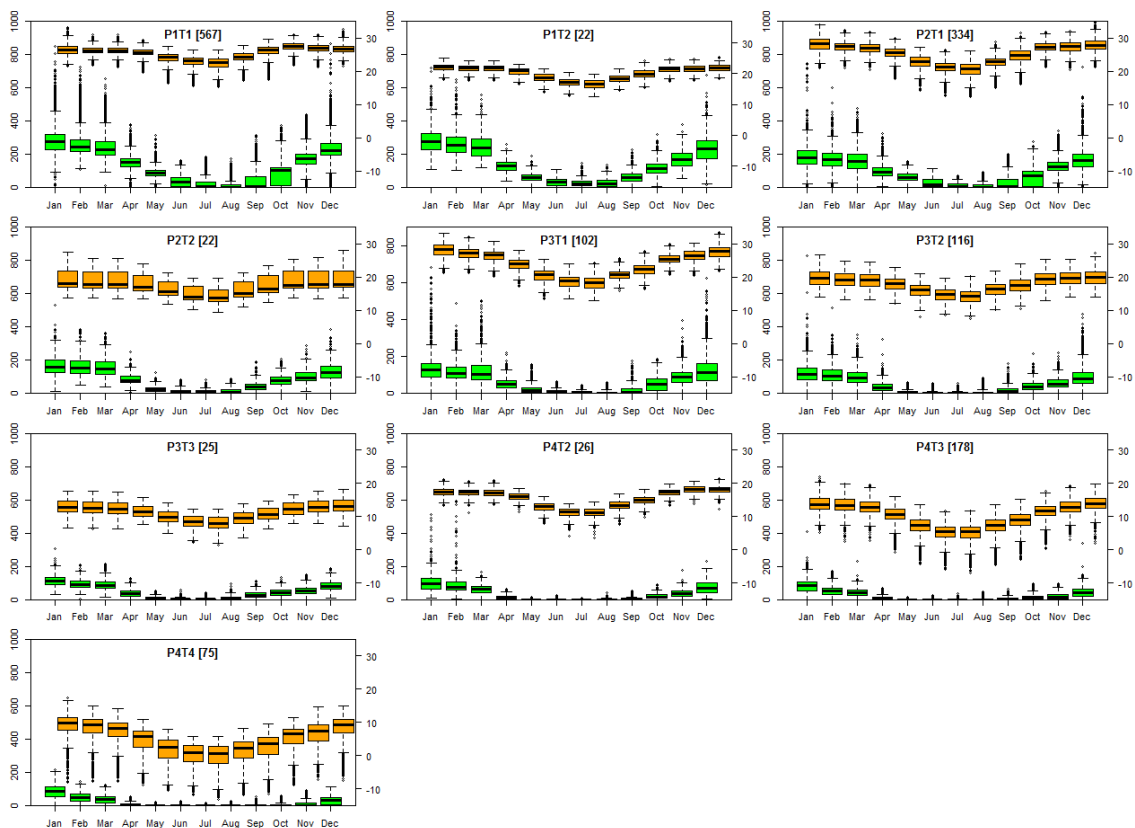


Figure 3.7. Box-and-whisker plot of statistical properties of precipitation (green) and temperature (orange) in outcome climate regions. The numbers in bracket followed by the name of the regions indicate the number of members of each region. First vertical axis scales the precipitation and the second vertical axis represents temperature. See Fig. 3.4 for boxplot details.

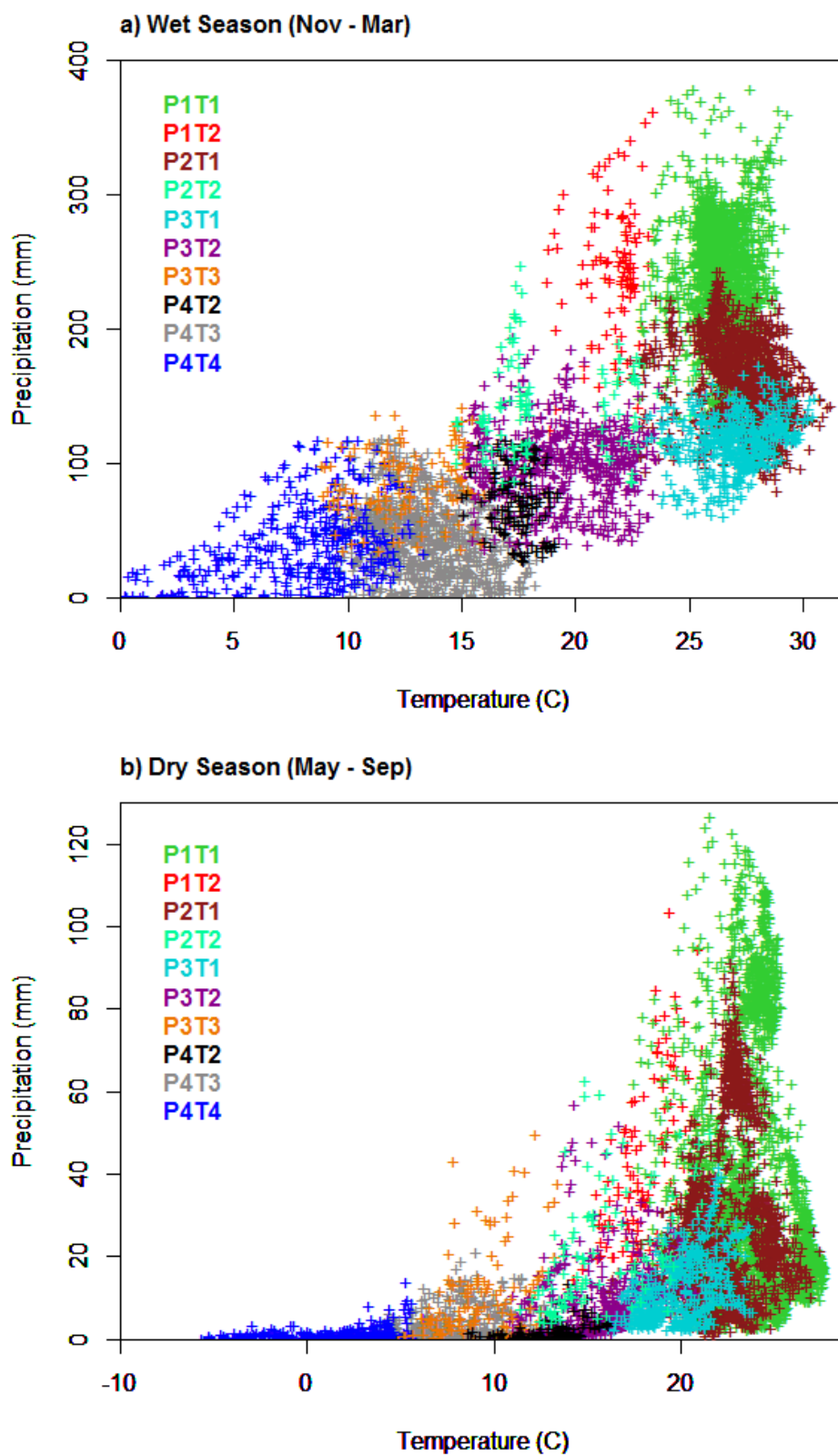


Figure 3.8. Climate characteristics of the homogeneous regions in (a) wet season and (b) dry season. Note that the plots are in different scales.

Chapter 4

Climate Change Impact Assessment over Bolivia Using the WRF High-Resolution Dynamical Downscaling I: Evaluation of the Present-Day Climate

Abstract

Bolivia is a developing country in Latin America which has been listed as one of the most vulnerable countries to climate change and has to pay a high price for a situation for which they have virtually no historical responsibility. This work is part of a more comprehensive evaluation project assessing climate change impacts over Bolivia. The evaluation is done in two steps; of (1) comparing the 33 years of reanalysis-driven WRF vs. observations and (2) 15 years each of three different CMIP5 GCM-driven WRF with observations for three resolutions of 36, 12 and 4 km (d01, d02 and d03, respectively). Comparing the results gain a better understanding of WRF with combined WRF/GCM biases. The results confirm the added value of the downscaled simulations at the higher resolution of 4 km, particularly in higher terrain where the real extent of the topography is not captured in the coarser resolutions of the reanalysis or the GCMs. This evaluation also indicates better agreement in the drier months of JJA where the precipitation is not convective, as the applied convective scheme tends to produce too much rain everywhere. The comparison between reanalysis-driven WRF and the observed values also reveals that the WRF tends to overestimate the extremes as the intensity and frequency of simulated heavy rain events are increased in the model simulations.

4.1. Introduction

Bolivia is a developing country that is listed as one of the poorest countries in Latin America (IPCC 2014). Many Bolivians are already experiencing the consequences of climate change. However, most of the country is not appropriately equipped to adapt to the climate change impacts. Among these key impacts are less food security, reduced water availability from retreating glaciers, more frequent and more severe natural disasters like drought, an increase in mosquito-borne diseases, and forest fires. These impacts threaten the integrity of most Bolivian societies, especially the indigenous people (Oxfam 2009). In a country where the heterogeneous topography is the leading factor in defining the microclimate, to study these impacts on fundamental human needs such as food production, water and energy management and health, policy- and decision-makers should be provided with reliable high-resolution climate data.

Though current global circulation models (GCMs) have proven quite successful in reproducing the large-scale atmospheric circulation pattern, the coarse resolution (~100 km) of the GCMs still poses a particular challenge to target those impacts at local to regional scale (10 km) especially in areas with complex topography and heterogeneous land covers (Soares et al. 2012). Therefore regional climate models (RCMs) are used to provide a higher resolution climate data needed for many impact studies (Sun et al. 2006; Flato 2011). An RCM is a limited-area model that uses the larger-scale climate information provided by GCMs or reanalysis at its lateral boundaries and downscales the input. This downscaling adds regional detail by resolving smaller-scale atmospheric processes (Giorgi and Bates 1989; Sun et al. 2006; chapter 10 Global Climate Models; Christensen et al. 2007) and providing higher resolution of topography and land use.

However, adding value by improving the spatial resolution of the data comes with some limitations as well, as we are introducing a new source of uncertainty by adding a regional climate model. It is an ongoing task among researchers to verify the ability of RCMs to produce physically meaningful results before using their output for climate change impact studies (Castro et al. 2005; Jacob et al. 2007). Therefore, interpretation of the downscaled RCM output should be handled carefully as there are a few different sources of uncertainty involved: (i) parent GCM uncertainties, (ii) regional climate model response through parameterization and internal variability and (iii) emission scenarios (Hawkins and Sutton 2009; Cabre et al. 2015). Investigating all these biases is a demanding task of using different RCMs forced by different GCMs and different representative concentration pathway (RCP) scenarios to account for a broad range of possibilities.

Several studies using regional climate model downscaling have investigated climate change signals in South America, however only a few have focused on Bolivia (Fernandez et al. 2005; Nunes et al. 2008; Urrutia and Vuille 2009; Chou et al. 2011; Seiler 2013). Among them, Urrutia and Vuille (2009), using the Hadley Centre regional climate modeling system (PRECIS) with a 0.44 degree spatial resolution, studied the climate change signal for the tropical Andes. Nunez et al. (2008) used the regional climate model MM5 (grid intervals of 50 km) nested within HasAM3H global model to study climate change over South America. Seiler (2009) implemented and validated 25 km resolution PRECIS simulations for Bolivia. No study, to our knowledge, has focused on Bolivia using a framework of homogeneous climate regions as developed by Abadi et al. (2018b) for improving impact studies at local scale. Our study uses the

Weather Research and Forecasting (WRF) regional climate model to downscale reanalysis and Coupled Model Intercomparison Project Phase 5 (CMIP5) GCM outputs to investigate climate change impacts in Bolivia with a spatial resolution sufficient to capture more realistically the topography of the Andes in Bolivia.

The main objective is to develop a one-way nested dynamical downscaling strategy to set a framework for climate change impact assessment in Bolivia by producing high-resolution, reliable climate information. A prior step to any climate change study is to investigate the ability of the RCM to reproduce the present-day climate as compared to observations. The current chapter focuses on the evaluation of the WRF outputs forced by reanalysis and present-day simulations and from three different CMIP5 GCMs versus observations. The evaluation in this research is focused on wet (DJF) and dry seasons (JJA), respectively.

4.2. Models, Observation and Experiment Design

4.2.1. Study Area and Climate Subregions

Bolivia is a landlocked country located in central South America with extreme topographic variation ranging from the Andes in the west to Amazon Basin lowlands in the northeast (Fig. 4.1). Being on the path of the South American Monsoon System (SAMS), the precipitation in the Amazon Basin to the north is drastically affected by the moisture transferred from the South Atlantic Ocean in the austral summer months (DJF), while the low-level jet to the eastern slope of the Andes channels moisture to the southern lowlands in the wet months (Campetella and Vera 2002; Liebmann et al. 2004; Marengo et al. 2012). Western highlands of the country receive lesser amounts of precipitation year-round, with the Altiplano receiving the least. The temperature pattern is controlled

mainly by the topographic features of the Andes with lower temperatures over the high valleys and higher temperatures in the lowlands.

Previous research (Abadi et al. 2018b) using the impact-related variables of precipitation and temperature showed that the country could be divided into 10 homogeneous climate subregions (Fig. 4.2). In this work we will utilize these climate regions as a framework first to interpret the WRF downscaled outputs and, second, to identify areas where the downscaling fails to reproduce the observational pattern.

4.2.2. Models

4.2.2.1. NNRP

The NCEP/NCAR reanalysis was developed to produce a consistent, global, gridded dataset incorporating observations and numerical weather prediction model output from 1948 through the present. The data covers the globe with the spatial resolution of $2.5^\circ \times 2.5^\circ$ and are available at 6 hour intervals. In this project we used NCEP/NCAR reanalysis project (NNRP) data – which serves as a proxy for the large-scale atmospheric observations that are otherwise lacking (Kalnay et al. 1996) – to initialize the lateral boundary conditions for the smaller scale RCM. It is worth mentioning that several higher resolution reanalysis datasets (e.g., ERA-Interim, CFSv2) were not yet available at the beginning of this project.

4.2.2.2. CMIP5 Global Models

CMIP5 multi-model experiment presents an unprecedented level of information on which to base assessments of climate variability and change (Oglesby et al. 2016). The CMIP5 GCMs were used to simulate both the “present-day” climate as well as make projections for the remainder of this century given three different representative concentration

pathways (RCPs) of greenhouse gas forcing. It is important to note that, in this context, “present-day” is not a simulation of the day-to-day weather and climate that actually occurred during this interval, but rather is representative of conditions that could be expected climatologically. These simulations are used to evaluate how well the GCMs simulate the climate of the region at the beginning of the 21st century. Three GCMs (Table 4.1) were selected based on their relatively superior performance over South America and Bolivia, in particular (Abadi et al. 2018a).

4.2.2.3. WRF Regional Climate Model

The WRF model is a regional model used for both research and operational forecasting (Skamarock et al. 2008). Though originally designed as a mesoscale forecast model, WRF has been adapted for use in climate studies and has become a widely used RCM readily available to the international scientific community. The WRF configuration employed included: parent to nest time and space step ratio of 3 to 1; no feedback from nest to the parent domain; time-varying prescribed sea surface temperature (SST); seasonally varying sea ice, vegetative fraction and albedo; the WSM5 microphysics option; the Kain-Fritsch convective scheme; the YSU PBL physics; the RRTM longwave radiation option; the Dudhia shortwave radiation option; the MM5 Monin-Obukhov surface-layer option (Skamarock et al. 2008); the unified Noah land-surface model (Wang et al. 2013). In this study and in the following chapter, WRF was used in two distinct modes; (i) to evaluate WRF’s ability in simulating the local climate when forced by NNRP global reanalysis and (ii) to downscale GCM projections of 21st century climate change. The latter part is done with WRF forced by output from three different

GCMs, each under three RCPs, for two separate periods: the “present-day”, serving as a base for climate change.

4.2.3. Observational Dataset

4.2.3.1. Station Measurements

As shown in many studies (Soares et al. 2012; Oglesby et al. 2016), comparing the nearest grid point of the model to the observation adds to the reliability of the verification as the model results are compared to the actual instrument measurements. The meteorological observations used for station-to-gridpoint analysis are obtained from Bolivia’s National Service of Meteorology and Hydrology (SENAMHI). There is a total of 300 stations in Bolivia (Fig. 4.2) that measure many hydrometeorological variables including precipitation and surface air temperature on a daily basis. There are some gaps in data coverage, primarily in the remote stations located over the highlands. Originally, 10 stations were selected for the purpose of verifying the downscaled data, each representing one of the 10 climate regions. Ultimately, 4 out of the original 10 were dropped due to intermittent data gaps totaling more than one year (365 days) from 1996 to 2010, since they were sufficiently inadequate for model evaluation.

4.2.3.2. Gridded Observations

Lack of reliable, high-resolution observations has been always a challenge for evaluating model performance especially in mountainous regions and highly dense forested regions such as are found in Bolivia. To address this limitation to some extent, we used a new gridded observational dataset developed for Bolivia (Andrade 2014). Andrade (2014) combined reanalysis and satellite data validated by observational data from different sources to create a daily gridded dataset of precipitation and maximum and minimum

temperatures with a spatial resolution of 0.25° (approximately 25 km), covering the period 1979-2010. In his work, the data are based on the Climate Forecast System Reanalysis (CFSR), version 1 (Saha et al. 2006), with minimum and maximum temperatures and daily precipitation computed from the original six-hourly reanalysis and interpolated using cubic splines to a $0.25^\circ \times 0.25^\circ$ spatial resolution. Precipitation data are then adjusted based on a monthly regression against multi-satellite Tropical Rain Measuring Mission (TRMM) Precipitation Analysis (TMPA; Huffman et al. 2007, 2010) applied to the daily, interpolated CFSR data. Both temperature and precipitation data are further adjusted across four altitudinal zones to increase agreement with in-situ observations from the Bolivia's National Service of Meteorology and Hydrology (SENAMHI), especially in terms of better representing extreme precipitation events. The final, daily, corrected and bias-adjusted data reproduce the climatological distribution of precipitation, maximum and minimum temperatures across Bolivia very well (Andrade 2014).

4.2.4. Experimental Scheme

High spatial resolution is fundamental to capture the regional scale circulation in a region with complex topography as Bolivia. Simulations in this project have been developed over three different domains. The outermost domain (d01, 36 km) covers nearly the entire South American continent to account for the larger scale circulation patterns and serves as a transition to the higher resolution domains. The middle domain (d02, 12km) encompasses almost the entire central part of South America and the innermost domain with the highest resolution (d03, 4 km) covers Bolivia (Fig. 4.1).

The climate change results (Abadi et al. 2018d) were obtained by using the WRF regional climate model to downscale the results from each of the three different GCMs for three different RCPs to evaluate a range of possible changes that may be expected (Moss et al. 2010). The RCP 8.5 scenario was chosen because it represents the largest plausible increase in forcing between now and the end of the century considered by the IPCC AR5 (IPCC 2013) and included in CMIP5. The RCP 2.6 scenario was chosen because it represents the least increase in forcing (likely implausible by now). The RCP 4.5 scenario was chosen as an intermediate scenario. Acknowledging that the different radiative forcings as defined by RCPs do not diverge drastically for the present-day period (2006-2020), we chose the GCM-WRF RCP 4.5 simulations as representative of the present-day climate.

As mentioned above, the downscaling work presented here has been done in two parts with simulations forced by NNRP reanalysis and simulations forced by three different GCMs. We verify the ability of NNRP-WRF downscaling to match the observations (1996-2010), and then evaluate the performance of the GCM-WRF model in reproducing the present-day climate (2006-2020).

Our evaluation is performed in three sections focused on: (i) the capability of WRF to downscale global reanalysis to the station level on a day-to-day basis, (ii) the ability of WRF to simulate the mean spatiotemporal climate patterns and (iii) WRF performance in simulating the interannual variability. The station-based evaluation focuses on comparison of the reanalysis-driven WRF against the station measurements of temperature and precipitation. The performance of the GCM-driven WRF in reproducing the shape of the distributions is evaluated for temperature and precipitation as well as for

the commonly used extreme climate precipitation indices of RX5day and R10mm (Karl et al. 1999; Peterson et al. 2005). These two indices show the maximum five-day precipitation per year and the annual number of precipitation events exceeding 10 mm, respectively. To obtain the daily average temperature from the gridded observational dataset, we took the average of the daily maximum and minimum temperatures which may contribute some uncertainty. This was necessitated because simulated maximum and minimum temperatures could only be estimated from the highest and lowest three-hourly RCM output temperatures, respectively. Furthermore, all the analyses based on area averages have been done using the delineated climate subregions defined in Chapter 3. Seasonal statistics have been calculated separately for the wet (DJF) and dry seasons (JJA). Only results for the 4 km domain (d03) are presented. An evaluation of the downscaling at the other resolutions of 12 and 36 km is presented in Appendix A.

4.3. Results and Discussion

4.3.1. Verification against Station Measurements

The daily values of precipitation and temperature measured at each station and the NNRP-WRF simulated data at the nearest gridpoint at 4 km for the same period (1996-2010) are given in Figs 4.3-4.8. To evaluate the performance of the GCM-driven WRF simulations in reproducing the expected seasonality, we also investigated the daily time-series of precipitation from the GCM-WRF simulations over the period 2006-2020.

Trinidad (Fig 1.1), located on the southern edge of the Amazon basin, is mostly influenced by the South American Monsoon System (SAMS), which causes the area surrounded by forests, lake and rivers, to have a lengthy rainy season and a short dry season. The temperature scatterplot confirms the generally successful performance of

WRF for this station, though it slightly overestimates the magnitude at higher temperatures (Fig 4.3a). The model overestimation is confirmed by the boxplots for the summer months of SON and DJF as the NNRP distribution lies higher compared to the observed distribution (Fig 4.3b). The boxplots also show the higher temperature dispersion with longer tails in JJA, however, in the summer months the data are more centered on the median as the dispersion is lower and the tails are shorter. The GCM-WRF present day simulations are also generally successful in simulating the range and distribution of the observed temperature in wet and dry seasons, with MIROC5 being an exception by overestimating the temperature in all seasons. This temperature pattern repeats itself in the lowlands (San Jose, Fig. 4.4a,b; and San Antonio, Fig 4.5a,b). For stations located in the higher valleys (Sucre, Fig. 4.6a,b; El Alto, Fig. 4.7a,b; and Potosi, Fig. 4.8a,b), the observed temperatures are underestimated by WRF forced by reanalysis and GCMs. This is possibly due to the still coarse resolution of 4 km being unable to resolve the high valleys over the Andes as shown in the elevation differences between the station and the corresponding gridpoint (Table 4.2). For example, the station at Potosi is located more than 300 meters above the nearest gridpoint used for comparison. Also, as all model configurations overestimate precipitation (Fig 4.8c), average temperatures are possibly lower than observed due to increased evapotranspiration. Moreover, the range of temperatures would be decreased in the wetter model environment, resulting in an underestimation of higher temperatures and an overestimation of lower temperatures (Appendix A). Even though precipitation is overestimated in the lowlands as well, soils in those subregions are generally wet year-round, so that evapotranspiration is not significantly increased by the excess precipitation produced by the model.

The comparison of the Trinidad precipitation time series (Fig. 4.3c) shows the successful performance of NNRP-WRF in simulating the well-defined seasonality of the observed precipitation, though it clearly overestimates rainfall to some extent, especially in the rainy seasons. GCM-WRF simulations also show a good agreement with the seasonal pattern of the observation, though generally overestimate precipitation compared to the observed amounts, with the exception of MIROC5, which fails to reproduce the pattern because of large underestimation. The distributions of the RX5day and R10mm indices (Fig. 4.3d) indicate a tendency for WRF-NNRP and all the WRF-GCM simulations except MIROC5 to overestimate the maximum five-day precipitation as the results for R10mm (except for MIROC5) are more or less in the range of the observed values with slight overestimations. The model's tendency to overestimate both the intensity and the frequency of the most extreme precipitation events is evident for all stations (San Jose, Fig.4.4c,d; San Antonio, Fig 4.5c,d; Sucre, Fig. 4.6c,d; El Alto, Fig. 4.7c,d; and Potosi, Fig. 4.8c,d; note that the scales on different station plots are different). The model divergence from observations becomes even more pronounced at higher elevations, especially in calculating the number of days with heavy precipitation (R10mm). This result is common in RCMs, which tend to produce too much rain in terms of both intensity and the frequency of extreme events (Figs 4.3-8d), even at 4 km (refer to Appendix A for other resolution results).

4.3.2. Mean Climate Pattern

All the verification in this section has been done against the gridded observations and are presented in terms of spatial distribution of mean seasonal climatology (Figs. 4.9-10) and the mean annual cycle of precipitation and temperature, area-averaged over the climate

subregions (Figs. 4.11-12). To match the climatology of the observational period and the model simulations, the assumption was made that the climate is nearly stationary and the climatological mean of 1996-2010 (observation and WRF-NNRP simulations) would be close to the climatological mean of 2006-2020 (WRF simulations present-day). Again, only the results for the highest model resolution of 4 km are shown here.

As the observations (top, center) in the rainy season (DJF) confirm, the Amazon basin toward the north, affected by the SAMS (Zhou and Lau 1998; Nogués-Paegle et al. 2002; Vera et al. 2006; Raia and Cavalcanti 2008; Marengo et al. 2012), receives the highest amount of precipitation, which is mainly due to the convective activity in that region. Toward the south, the lowlands receive precipitation mainly caused by another feature of SAMS. Moisture-laden air travelling toward Andes is channeled between the slopes and the thermal Chaco low (the South American Low Level-Jet) and creates a low-level NW-SE oriented convergence band, resulting in precipitation, in the vicinity of the South Atlantic Convergence Zone (SACZ) (Liebmann et al. 2004; Carvalho et al. 2011; Marengo et al. 2012;). The WRF simulations are generally successful in reproducing the spatial pattern of the observations. It is worth noting that the coarser domains of 36 and 12 km underestimate the precipitation over the highlands (Appendix A) while the 4 km, by better resolving the topography, has improved the downscaling in those regions. It is also evident in all the simulations except MIROC5 that WRF tends to overestimate the precipitation in the Amazon basin where most of the precipitation is convective in nature. This behavior repeats itself over the higher terrain as WRF is not identifying the driest region in the Altiplano. The lower amounts of rainfall simulated by MIROC5-WRF is likely attributable to the lateral boundary conditions provided by MIROC5 as the parent

GCM also underestimates the precipitation in the larger-scale (Boulanger et al. 2007; Abadi et al. 2018a). One should note that all the biases represented in this work are relative as the uncertainty in the observations can be large especially in the densely forested areas like Amazonia and mountainous regions like the Andes where reliable high quality data are rare (Torma et al. 2014). In almost all the simulations, the greatest improvement occurs from 12 to 4 km and there is not much change observed going from 36 to 12 km (Appendix A). This finding emphasizes the need for higher resolution simulations, specifically over the high terrain.

WRF-NNRP DJF temperature simulations (Fig 4.9 right column) are in general agreement with observations (Fig 4.9 bottom, center) and have been greatly improved by increasing the resolution (Appendix A), as the temperature is mainly controlled by the topography. Among the GCM-driven simulations, MIROC5 simulations show the warmest biases in the southeastern part of the country, also observed in Jacob et al. (2007). The lack of precipitation in these areas makes the soil drier and increases the sensible heat, resulting in higher surface air temperature.

As illustrated in the observed pattern of the mean winter season precipitation (4.10, top,center), higher amounts of precipitation are limited to the northwest and central part of the country (a.k.a. El Chapare). This pattern follows the inward movement of the South Atlantic High pressure system toward the continent, creating a shift in the wind direction over Bolivia and transports the moisture into northwestern areas. Comparing the NNRP-WRF (Fig 4.10 left column) to observed precipitation, similar to DJF seasonal climatology, higher resolution WRF simulations overestimate the precipitation both in lowlands and highlands. All the coarser GCM-driven simulation drastically underestimate

the precipitation in the Amazon basin (Appendix A). This behavior, not observed in the reanalysis driven simulation, might be inherited from the parent GCMs that, by misplacing the ITCZ, are known for their dry biases over the Amazon basin (Sanchez et al. 2015; Abadi et al. 2018a; Llopart et al. 2018). Temperature in winter months (Fig 4.10 right column) shows a similar pattern of improving with higher resolution simulations over the higher terrain (Appendix A). However, MIROC5-WRF simulations show warmer conditions over Amazonia. This behavior is similar to the parent GCM winter temperature (Abadi et al. 2018a) and is likely the result of drier conditions caused by the underestimation of precipitation by that GCM.

The gradual decrease of precipitation from lowlands to highlands is readily apparent in the observations and NNRP and GCM-WRF simulations (4.11). WRF downscaling simulations are mostly able to capture the seasonality of the precipitation, but they tend to overestimate precipitation greatly almost everywhere, though with lower biases over the drier regions of the Andes. The exception is the simulations forced by MIROC5. Overall, the model-simulated precipitation is in better agreement with observation in the drier months. It is again noticeable that overestimation is larger in magnitude over the lowlands where convective precipitation is dominant.

The outstanding feature in the observed and modeled annual cycle of temperature is that the modeled temperatures are closer to the observations in the lowlands and begin diverging from the observations in elevated terrain (Fig. 4.12). Two reasons contribute to this behavior; (i) the gridded observations are partly based on station measurements, which are sparse in highly elevated terrain, so an overestimation of temperature should be expected in the gridded observation, and (ii) precipitation can be expected to be in the

form of snow in the elevated lands. So, where the models put extra precipitation on the mountainous regions, one can expect to see lower temperatures.

4.3.3. Interannual Variability

Statistics based on monthly time series of gridded observations and WRF simulations over the delimited climate subregions for the “present-day” period (Table 4.3) reveal that almost all of the WRF simulations overestimate precipitation, though the magnitude is improved from 36 to 4 km with MIROC5 being closest to the observations with slight underestimation in the lowlands. The coefficient of variation (CV), defined as the ratio of the standard deviation (SD) to the mean multiplied by 100, shows the extent of variability in relation to the mean. The unitless nature of CV makes it possible to compare the degree of the variability among different regions. The variability of precipitation increases with altitude in the observational dataset, which is not always true for the model simulations. The comparison of CV between different regions also reveals that the WRF simulations underestimate the variability mainly over the elevated lands. Correlation values for the model simulations show a great agreement with the observation (≥ 0.79) almost everywhere with MIROC5-WRF being the exception. Root mean squared error (RMSE) serves as a measure of accuracy between model predictions and the observations. In almost all regions over the Andes, we can see improvements with WRF simulations from 36 to 12 km, as the RMSE decreases.

Results for temperature between the NNRP-WRF simulations and observations show a negative bias almost everywhere increasing with altitude though improving with higher resolution, except for sub-region P3T1. Correlation measurements show a better agreement with observations compared to the precipitation values and are either

unchanged or slightly improved going from 36 to 4 km. RMSE values increase with altitude showing less accuracy in model predictions but again slightly improved with higher resolutions.

Finally, to compare the probability distribution of precipitation among datasets we created quantile-quantile, or QQ, plots. The QQ-plot is a graphical method for comparing the shape of two probability distributions by plotting their quantiles against each other to show if the datasets are coming from the same distribution. The dotted line represents the reference line where ideally the model values shown on the vertical axis perfectly match the observation values shown on the horizontal axis. Comparing the wet-season daily precipitation (Fig 4.13) from NNRP-WRF and GCM-WRF simulations in the present-day (NNRP-WRF and observed: 1996-2010; GCM-WRF 2006-2020) against the observed values in different regions, a noticeable feature is that the model overestimates the precipitation over all regions, but it improves over the higher terrain and also with increasing the resolution (Appendix A). Increasing the resolution does not have the same effect for the lowlands. Again, it is worth mentioning that the reliability of the observed data in high elevation areas and in the highly forested areas of the Amazonia lowlands are questionable as the stations are generally sparse. Another feature shared by all the regions is that the lower tails of the model distributions (representing the frequency of wet days with very low precipitation) are highly overestimated except for MIROC5 in the eastern slopes of the Andes (P2T1, P3T1). This demonstrates that WRF in all domains simulates too many low intensity precipitation events compared to what is actually observed (a.k.a. the drizzle effect; Sun et al. 2006). MIROC5's behavior in those regions might be attributable to the ability of the parent GCM to capture the strength of the SALLJ over

the slopes. Note that the precipitation events from the WRF-GCM simulations are taken from 2006-2020, which, while not directly comparable to the observed period of 1996-2010 on a day-to-day basis, demonstrate how well WRF, driven by GCMs, can reproduce the “present-day” probability distribution of precipitation in the wet season. A related point to consider in interpreting these QQ-plots is that some of the subregions are very small (e.g. P1T2) and only contain a few gridpoints, which may not render a meaningful comparison.

4.4. Summary and Conclusion

Bolivia is a biodiverse country encompassing the wet Amazon rainforests to the north, cold and dry Andes’ Altiplano plateau and high valleys to the west and dry tropical forests and croplands toward the southeast. This abundance and variety of life expose the country to the various impacts of climate change. Coarse future projections of the global models are not reliable at regional scales by themselves, as they do not include the smaller scale circulations at a local scale. To tackle this issue, RCMs are used to downscale the GCM outputs in a limited area. Then the primary question to answer is how much we can trust the regional climate downscaled outputs to develop mitigation and adaptation strategies. The current project investigated the performance of the WRF-downscaled outputs forced by reanalysis and three different GCMs over the present day from 1996 to 2010 and the equivalent “present-day” for the GCMs (2006-2020), assuming the comparability of the two periods. In addition to the evaluation of the WRF in reproducing the present-day climate, this study serves as a baseline for a climate change impact study in Bolivia, studied in a companion paper (Abadi et al. 2018d). The evaluations were done in two aspects of the mean climate and the interannual variability.

The key concluding remarks are as follows. The pair-wise station-gridpoint comparison reveals that there is a better agreement on temperature in lowlands as there is a negative systematic bias in the higher valleys with a different pattern for the two populous cities of El Alto and Potosi in the highlands. Model simulations in those cities not only underestimate the temperature range but also show a lower range in the temperature by underestimating the higher values in the summer months and overestimating the lower temperatures in the winter months. This pattern might be attributable to the poor land cover scheme in the model that cannot resolve the true extent of the urban environment of the two cities or to the wetter conditions simulated by the model.

Generally, the WRF simulations tend to overestimate precipitation in the summer months when the precipitation is mainly convective, while this issue is less pronounced in the drier winter months. This issue might be improved through the use of a different convective scheme parameterization. The QQ-plots results also affirm the higher sensitivity of the elevated regions to the downscaling approach, henceforth the need for higher resolution simulations over the Andes. As the resolution increases, the intensity and the frequency of the heavy rain events get closer to the observed values particularly in the areas with complex topography that confirms the added value of the RCM over the elevated lands. At the lower end of the probability, on the other hand, WRF simulates too many days with low intensity rain events, which has been referred to as the “drizzle effect” in other studies. GCM-driven WRF simulations were able to capture the seasonality of the present-day climate. However, it was evident in these comparisons that GCM-WRF simulations were controlled by the lateral boundary conditions provided by the GCMs conditions, as MIROC5 tended to underestimate the mean precipitation while

CCSM4 and MPI-ESM-LR overestimated the observed climatology (Abadi et al. 2018a). In all these cases, the wet season precipitation biases were amplified by the regional climate model's internal variability.

Finally, a high resolution, high quality observational dataset is the primary requirement for any robust verification. In this study, the WRF performance was evaluated against a relatively coarse resolution (but the highest resolution available for Bolivia) gridded observation ($0.25^{\circ} \times 0.25^{\circ}$). Such a coarse resolution observational dataset adds to the uncertainty in the evaluation especially in the regions where data measurements are rare like the heavily forested lands of Amazonia and high valleys of the Andes. The WRF simulation comparisons against the station measurements were significantly improved with resolution changes from 36 to 4 km as the topography was captured better by WRF. In summary, the WRF model improves the output from coarser resolution reanalysis and GCMs due to higher resolution, especially in the elevated regions, although the results shown in the higher terrains, even at 4 km, still cannot match the observed values closely. To tackle this issue, along with having a better observational dataset, it is suggested to conduct even higher resolution RCM simulations with an updated land surface model to resolve the more realistic topography and land surface condition of the region.

Acknowledgements

We gratefully acknowledge support from the Inter-American Development Bank for the development of tools and techniques used in this research and the UNL Holland Computing Center for computing services and support.

4.5. References

- Abadi AM, Oglesby RJ, Rowe CM et al (2018a) Evaluation of GCMs historical simulations of monthly and seasonal climatology over Bolivia. *Clim Dyn* (2018) 51:733–754
doi: 10.1007/s00382-017-3952-y
- Abadi AM, Rowe CM, Andrade MF (2018b) Climate Classification in Bolivia: A Combination of Nonhierarchical and Consensus Clustering Analyses Based on Precipitation and Temperature
- Andrade MF (2014) La economía del cambio climático en Bolivia: generación de datos meteorológicos de alta resolución para Bolivia. C.E. Ludeña, L. Sanchez-Aragon (eds), Banco Interamericano de Desarrollo, Monografía No. 200, Washington, DC. <http://www.iadb.org/en/publications/publication-detail,7101.html?id=73547>
- Boulanger J, Martinez F, Segura EC (2006) Projection of future climate change conditions using IPCC simulations, neural networks and Bayesian statistics. Part 2: Precipitation mean state and seasonal cycle in South America. *Climate Dynamics*, 28(2-3), 255-271. doi:10.1007/s00382-006-0182-0
- Cabré F, Solman S, Núñez M (2014) Climate downscaling over southern South America for present-day climate (1970-1989) using the MM5 model. Mean, interannual variability and internal variability. *Atmósfera*, 27(2), 117-140. doi:10.1016/s0187-6236(14)71105-1
- Competella CM, Vera CS (2002) The influence of the Andes mountains on the South American low-level flow. *Geophys Res Lett* 29(17):1826.
doi:10.1029/2002GL015451
- Carvalho LMV, Silva A, Jones C et al (2011) Moisture transport and intraseasonal variability in the South America monsoon system. *Clim Dyn* 36(9):1865–1880.
doi:10.1007/s00382-010-0806-2
- Castro CL, Pielke RA Sr, Leoncini G (2005) Dynamical downscaling: an assessment of value added using a regional climate model. *J Geophys Res (Atmospheres)* 110:D05108. doi:10.1029/2004 JD004721
- Chapter 10 Global Climate Models. (1994) *Global Physical Climatology International Geophysics*, 254-285. doi:10.1016/s0074-6142(08)60567-7
- Christensen J, Carter T, Rummukainen M, Amanatidis G (2007) Evaluating the performance and utility of regional climate models: the PRUDENCE project. *Clim Change* 81(1):1–6. doi:10.1007/ s10584-006-9211-6
- Chou SC, Marengo JA, Lyra A, et al (2011) Downscaling of South America present climate driven by 4-member HadCM3 runs. *Clim Dyn*. doi:10.1007/s00382-011-1002-8
- Fernandez JP, Franchito SH, Rao VB (2006) Simulation of the summer circulation over South America by two regional climate models. Part II: A comparison between 1997/1998 El Niño and 1998/1999 La Niña events. *Theoretical and Applied Climatology*, 86(1-4), 261-270. doi:10.1007/s00704-005-0213-5

- Flato GM (2011) Earth system models: An overview. *Wiley Interdisciplinary Reviews: Climate Change*, 2(6), 783-800. doi:10.1002/wcc.148
- Gent PR, Danabasoglu G, Donner LJ et al (2011) The community climate system model version 4. *J Clim* 24:4973–4991. doi:10.1175/2011jcli4083.1
- Giorgi F, Bates GT (1989) The climatological skill of a regional model over complex terrain. *Mon Weather Rev* 117:2325–2347
- Hawkins E, Sutton R (2009) The potential to narrow uncertainty in regional climate predictions. *Bull Am Meteorol Soc* 90(8):1095–1107
- Huffman GJ, Bolvin DT, Nelkin EJ, et al (2007). The TRMM Multisatellite Precipitation Analysis (TMPA): Quasi-Global, Multiyear, Combined-Sensor Precipitation Estimates at Fine Scales. *Journal of Hydrometeorology*, 8(1), 38-55. doi:10.1175/jhm560.1
- Huffman GJ, Adler RF, Bolvin DT, et al (2010) The TRMM multisatellite precipitation analysis (TAMPA). In: Hossain, F., Gebremichael, M. (Eds.), Chapter 1 in *Satellite Rainfall Applications for Surface Hydrology*. Springer Verlag. ISBN: 978-90-481-2914-0, pp. 3–22.
- IPCC (2013) Climate change 2013: the physical science basis. In: Stocker TF, Qin D, Plattner GK, Tignor M, Allen SK, Boschung J, Nauels A, Xia Y, Bex V, Midgley PM (eds) Contribution of working group I to the fifth assessment report of the intergovernmental panel on climate change. Cambridge University Press, Cambridge
- Jacob D, Barring L, Christensen OB, et al (2007) An inter-comparison of regional climate models for Europe: model performance in present-day climate. *Clim Change* 81:31–52
- Kalnay E, et al (1996) The NCEP/NCAR 40-year reanalysis project, *Bull. Am. Meteorol. Soc.*, 77, 437–470.
- Karl TR, Nicholls N, Ghazi A (1999) CLIVAR/GCOS/WMO Workshop on Indices and Indicators for Climate Extremes Workshop Summary. *Weather and Climate Extremes*, 3-7. doi:10.1007/978-94-015-9265-9_2
- Liebmann B, Kiladis GN, Vera CS, et al (2004) Subseasonal variations of rainfall in South America in the vicinity of the lowlevel jet east of the Andes and comparison to those in the South Atlantic convergence zone. *J Clim* 17(19):3829–3842. doi:10.1175/1520-0442(2004)0172.0.CO;2
- Llopart M, Reboita M, Coppola E, et al (2018) Land Use Change over the Amazon Forest and Its Impact on the Local Climate. *Water*, 10(2), 149. doi:10.3390/w10020149
- Marengo JA, Liebmann B, Grimm AM, et al (2012) Recent developments on the South American monsoon system. *Int J Clim*. doi:10.1002/joc.2254
- Moss RH, et al (2010) The next generation of scenarios for climate change research and assessment, *Nature*, 463(7282), 747–756
- Nogués-Paegle J, Mechoso CR, Fu R, et al (2002) Progress in Pan American CLIVAR research: understanding the South American monsoon. *Meteorologica* 27:1–30

- Nuñez MN, Solman SA, Cabré MF (2008) Regional climate change experiments over southern South America. II: Climate change scenarios in the late twenty-first century. *Climate Dynamics*, 32(7-8), 1081-1095. doi:10.1007/s00382-008-0449-8
- Oglesby R, Rowe C, Grunwaldt A, et al (2016) A High-Resolution Modeling Strategy to Assess Impacts of Climate Change for Mesoamerica and the Caribbean. *American Journal of Climate Change*, 05(02), 202-228. doi:10.4236/ajcc.2016.52019
- Oxfam (2009) Bolivia climate change, poverty and adaptation. <https://www.oxfam.org/sites/www.oxfam.org/files/bolivia-climate-change-adaptation-0911.pdf>
- Peterson TC (2005) Climate change indices, *WMO Bull.*, 54, 82–86.
- Raia A, Cavalcanti IFA (2008) The life cycle of the South American monsoon system. *J Clim* 21(23):6227–6246. doi:10.1175/2008JCLI2249.1
- Sánchez E, Solman S, Remedio AR, et al (2015). Regional climate modelling in CLARIS-LPB: A concerted approach towards twentyfirst century projections of regional temperature and precipitation over South America. *Climate Dynamics*, 45(7-8), 2193-2212. doi:10.1007/s00382-014-2466-0
- Saha S, Nadiga S, Thiaw, et al (2006). The NCEP Climate Forecast System. *Journal of Climate*, 19(15), 3483-3517. doi:10.1175/jcli3812.1
- Seiler C, Hutjes RWA, Kabat P (2013) Climate variability and trends in Bolivia. *J Appl Meteorol Climatol* 52:130–146. doi:10.1175/jamc-d-12-0105.1
- Skamarock (2008) A Description of the Advanced Research WRF Version 3
- Sun Y, Solomon S, Dai A, Portmann RW (2006) How often does it rain? *Journal of Climate* 19: 916–934, DOI: 10.1175/JCLI3672.1.
- Torma C, Giorgi F, Coppola E (2015) Added value of regional climate modeling over areas characterized by complex terrain-Precipitation over the Alps. *Journal of Geophysical Research: Atmospheres*, 120(9), 3957-3972. doi:10.1002/2014jd022781
- Urrutia R, Vuille M (2009) Climate change projections for the tropical Andes using a regional climate model: Temperature and precipitation simulations for the end of the 21st century. *Journal of Geophysical Research*, 114(D2). doi:10.1029/2008jd011021
- Vera C, Baez J, Douglas M, et al (2006b) The South American lowlevel jet experiment. *Bull Am Meteor Soc* 87:63–77. doi:10.1175/bams-87-1-63
- Watanabe S, Hajima T, Sudo K, et al (2011) MIROC-ESM: model description and basic results of CMIP5-20c3m experiments. *Geosci Model Dev Discuss* 4:1063–1128. doi:10.5194/gmdd-4-1063-2011
- Zanchettin D, Rubino A, Matei D, et al (2012) Multidecadal-to-centennial SST variability in the MPI-ESM simulation ensemble for the last millennium. *Clim Dyn* 40:1301–1318. doi:10.1007/s00382-012-1361-9
- Zhou J, Lau KM (1998) Does a monsoon climate exist over South America? *J Clim* 11(5):1020–1040. doi:10.1175/1520-0442(1998)0112.0.CO;2

Table 4.1. Attributes of the selected GCMs

| Model Name | Horizontal resolution | Center and References |
|-------------------|------------------------------|---|
| CCSM4 | 0.94×1.25 | National Center for Atmospheric Research, United States (Gent et al. 2011) |
| MIROC5 | 1.4×1.4 | Atmosphere and Ocean Research Institute (The University of Tokyo), National Institute for Environmental Studies, and Japan Agency for Marine-Earth Science and Technology, Japan (Watanabe et al. 2010) |
| MPI-ESM-LR | 1.875×1.875 | Max-Planck Institute for Meteorology, Germany (Zanchettin et al. 2012) |

Table 4.2. Stations geographical details

| Region | Station | Department | Latitude | Longitude | Elevation (m) | |
|---------------|----------------|-------------------|-----------------|------------------|----------------------|------------|
| | | | | | Obs | d03 |
| P1T1 | Trinidad | Beni | -14.8 | -64.9 | 156 | 154 |
| P2T1 | San Jose | Santa Cruz | -17.8 | -60.7 | 284 | 297 |
| P3T1 | San Antonio | Santa Cruz | -20.0 | -63.2 | 600 | 613 |
| P3T2 | Sucre | Chuquisaca | -19.0 | -65.3 | 2904 | 2846 |
| P3T3 | El Alto | La Paz | -16.5 | -68.2 | 4071 | 4007 |
| P4T3 | Potosi | Potosi | -19.5 | -65.7 | 4100 | 3782 |

Table 4.3. Verification of the statistics for selected regions. Units for precipitation and temperature are mm/day and °C, respectively. The statistics presented in the table are calculated based on the monthly datasets over the “present-day” period.

| P1T1 | | | | | |
|----------------------|------------|----------------------|---------------------|------------------------|-----------------------|
| Precipitation | | | | | |
| | Obs | NNRP 4 km | MPI 4 km | MIROC5 4 km | CCSM4 4 km |
| Mean | 3.14 | 9.62 | 8.75 | 2.50 | 9.62 |
| Stdev | 2.37 | 6.67 | 7.04 | 2.44 | 7.53 |
| CV | 75.48 | 69.33 | 80.46 | 97.60 | 78.27 |
| RelBias | | 206.53 | 178.65 | -20.3 | 206.26 |
| Corr | | 0.87 | 0.81 | 0.43 | 0.82 |
| RMSE | | 8.04 | 7.71 | 2.65 | 8.65 |
| Mean | 25.46 | 25.17 | 25.04 | 28.15 | 25.86 |
| Stdev | 3.06 | 2.07 | 2.52 | 2.47 | 2.50 |
| CV | 12.02 | 8.22 | 10.06 | 8.77 | 9.67 |
| Bias | | -0.29 | -0.42 | 2.69 | 0.40 |
| Corr | | 0.74 | 0.57 | 0.72 | 0.61 |
| RMSE | | 2.09 | 2.66 | 3.44 | 2.52 |

| P1T2 | | | | | |
|----------------------|------------|----------------------|---------------------|------------------------|-----------------------|
| Precipitation | | | | | |
| | Obs | NNRP 4 km | MPI 4 km | MIROC5 4 km | CCSM4 4 km |
| Mean | 2.68 | 16.78 | 14.64 | 2.86 | 18.00 |
| Stdev | 2.28 | 11.23 | 10.23 | 2.90 | 13.87 |
| CV | 85.0 | 66.92 | 69.88 | 101.0 | 77.06 |
| RelBias | | 524.8 | 445.2 | 6.46 | 570.4 |
| Corr | | 0.82 | 0.76 | 0.18 | 0.82 |
| RMSE | | 16.94 | 14.72 | 3.34 | 19.48 |
| Mean | 21.95 | 17.19 | 16.71 | 19.27 | 17.57 |
| Stdev | 2.83 | 1.72 | 2.27 | 2.91 | 2.20 |
| CV | 12.8 | 10.01 | 13.58 | 15.10 | 12.52 |
| Bias | | -4.76 | -5.24 | -2.68 | -4.38 |
| Corr | | 0.91 | 0.79 | 0.81 | 0.78 |
| RMSE | | 4.98 | 5.52 | 3.21 | 4.72 |

| P2T1 | | | | | |
|----------------------|------------|----------------------|---------------------|------------------------|-----------------------|
| Precipitation | | | | | |
| | Obs | NNRP 4 km | MPI 4 km | MIROC5 4 km | CCSM4 4 km |
| Mean | 3.52 | 7.69 | 6.90 | 1.29 | 7.77 |
| Stdev | 2.73 | 5.49 | 5.38 | 1.37 | 6.24 |
| CV | 77.5 | 71.39 | 77.97 | 106.2 | 80.31 |
| RelBias | | 118.1 | 95.95 | -63.33 | 120.4 |
| Corr | | 0.87 | 0.87 | 0.26 | 0.86 |
| RMSE | | 5.38 | 4.72 | 3.51 | 5.92 |
| Mean | 22.4 | 22.05 | 21.66 | 24.34 | 22.49 |
| Stdev | 2.13 | 2.35 | 2.73 | 3.23 | 2.76 |
| CV | 9.48 | 10.66 | 12.60 | 13.27 | 12.27 |
| Bias | | -0.41 | -0.80 | 1.87 | 0.03 |
| Corr | | 0.87 | 0.76 | 0.81 | 0.75 |
| RMSE | | 0.96 | 1.57 | 2.35 | 1.38 |

| P2T2 | | | | | |
|----------------------|------------|-------------|-------------|---------------|--------------|
| Precipitation | | | | | |
| | | NNRP | MPI | MIROC5 | CCSM4 |
| | Obs | 4 km | 4 km | 4 km | 4 km |
| Mean | 2.13 | 9.45 | 8.14 | 1.88 | 10.19 |
| Stdev | 1.92 | 6.09 | 5.50 | 1.86 | 7.41 |
| CV | 90.14 | 64.44 | 67.57 | 98.94 | 72.72 |
| RelBias | | 344.83 | 283.14 | -11.5 | 379.44 |
| Corr | | 0.84 | 0.80 | 0.37 | 0.84 |
| RMSE | | 8.65 | 7.30 | 2.12 | 9.98 |
| Mean | 17.32 | 15.12 | 14.40 | 15.10 | 15.28 |
| Stdev | 2.47 | 1.55 | 2.09 | 2.67 | 1.99 |
| CV | 14.26 | 10.25 | 14.51 | 17.68 | 13.02 |
| Bias | | -2.20 | -2.92 | -2.22 | -2.04 |
| Corr | | 0.94 | 0.84 | 0.81 | 0.85 |
| RMSE | | 2.48 | 3.21 | 2.72 | 2.42 |

| P3T1 | | | | | |
|----------------------|------------|-------------|-------------|---------------|--------------|
| Precipitation | | | | | |
| | | NNRP | MPI | MIROC5 | CCSM4 |
| | Obs | 4 km | 4 km | 4 km | 4 km |
| Mean | 2.81 | 6.58 | 5.47 | 0.85 | 7.12 |
| Stdev | 2.24 | 4.73 | 4.13 | 1.10 | 5.51 |
| CV | 79.72 | 71.88 | 75.50 | 129.41 | 77.39 |
| RelBias | | 134.35 | 94.94 | -69.72 | 153.75 |
| Corr | | 0.83 | 0.78 | 0.42 | 0.83 |
| RMSE | | 4.91 | 3.84 | 2.82 | 5.78 |
| Mean | 16.99 | 18.19 | 17.87 | 18.90 | 18.38 |
| Stdev | 1.94 | 2.39 | 2.79 | 3.40 | 2.77 |
| CV | 11.42 | 13.14 | 15.61 | 17.99 | 15.07 |
| Bias | | 1.20 | 0.89 | 1.92 | 1.40 |
| Corr | | 0.92 | 0.85 | 0.84 | 0.85 |
| RMSE | | 1.55 | 1.78 | 2.81 | 2.06 |

| P3T2 | | | | | |
|----------------------|------------|-------------|-------------|---------------|--------------|
| Precipitation | | | | | |
| | | NNRP | MPI | MIROC5 | CCSM4 |
| | Obs | 4 km | 4 km | 4 km | 4 km |
| Mean | 2.02 | 7.01 | 6.03 | 1.68 | 7.67 |
| Stdev | 1.86 | 4.75 | 4.33 | 1.69 | 5.72 |
| CV | 92.0 | 67.76 | 71.81 | 100.6 | 74.58 |
| RelBias | | 246.4 | 197.6 | -17.1 | 278.6 |
| Corr | | 0.83 | 0.77 | 0.50 | 0.80 |
| RMSE | | 6.02 | 5.07 | 1.81 | 7.13 |
| Mean | 15.3 | 13.51 | 12.69 | 12.61 | 13.60 |
| Stdev | 2.28 | 1.53 | 2.07 | 2.57 | 1.95 |
| CV | 14.9 | 11.32 | 16.31 | 20.38 | 14.34 |
| Bias | | -1.80 | -2.61 | -2.69 | -1.70 |
| Corr | | 0.95 | 0.86 | 0.80 | 0.87 |
| RMSE | | 2.04 | 2.86 | 3.11 | 2.04 |

| P3T3 | | | | | |
|----------------------|------------|-------------|-------------|---------------|--------------|
| Precipitation | | | | | |
| | | NNRP | MPI | MIROC5 | CCSM4 |
| | Obs | 4 km | 4 km | 4 km | 4 km |
| Mean | 1.21 | 5.44 | 4.68 | 2.51 | 6.27 |
| Stdev | 1.33 | 3.19 | 3.24 | 1.88 | 4.31 |
| CV | 109.92 | 58.64 | 69.23 | 74.90 | 68.74 |
| RelBias | | 348.13 | 285.39 | 107.15 | 417.03 |
| Corr | | 0.82 | 0.76 | 0.65 | 0.77 |
| RMSE | | 4.78 | 4.2 | 1.93 | 6.09 |
| Mean | 14.65 | 7.59 | 6.27 | 5.46 | 7.88 |
| Stdev | 2.77 | 1.58 | 2.01 | 1.59 | 1.66 |
| CV | 11.42 | 13.14 | 15.61 | 17.99 | 15.07 |
| Bias | | -7.06 | -8.38 | -9.19 | -6.77 |
| Corr | | 0.94 | 0.87 | 0.71 | 0.86 |
| RMSE | | 7.19 | 8.49 | 9.40 | 6.95 |

| P4T2 | | | | | |
|----------------------|------------|-------------|-------------|---------------|--------------|
| Precipitation | | | | | |
| | | NNRP | MPI | MIROC5 | CCSM4 |
| | Obs | 4 km | 4 km | 4 km | 4 km |
| Mean | 1.26 | 5.37 | 4.79 | 2.36 | 6.12 |
| Stdev | 1.40 | 3.34 | 3.34 | 1.97 | 4.48 |
| CV | 111.11 | 62.20 | 69.73 | 83.47 | 73.20 |
| RelBias | | 325.57 | 279.12 | 87.07 | 384.36 |
| Corr | | 0.78 | 0.75 | 0.64 | 0.76 |
| RMSE | | 4.76 | 4.30 | 1.88 | 6.00 |
| Mean | 14.68 | 9.62 | 8.30 | 7.34 | 9.74 |
| Stdev | 2.76 | 1.42 | 1.93 | 1.87 | 1.66 |
| CV | 18.80 | 14.76 | 23.25 | 25.48 | 17.04 |
| Bias | | -5.06 | -6.38 | -7.34 | -4.94 |
| Corr | | 0.93 | 0.87 | 0.74 | 0.85 |
| RMSE | | 5.06 | 6.38 | 7.34 | 4.94 |

| P4T3 | | | | | |
|----------------------|------------|-------------|-------------|---------------|--------------|
| Precipitation | | | | | |
| | | NNRP | MPI | MIROC5 | CCSM4 |
| | Obs | 4 km | 4 km | 4 km | 4 km |
| Mean | 0.81 | 3.62 | 2.87 | 2.03 | 4.47 |
| Stdev | 0.97 | 2.41 | 2.40 | 1.81 | 3.54 |
| CV | 119.7 | 66.57 | 83.62 | 89.16 | 79.1 |
| RelBias | | 347.4 | 255.7 | 150.8 | 453.1 |
| Corr | | 0.85 | 0.74 | 0.73 | 0.78 |
| RMSE | | 3.26 | 2.73 | 1.77 | 4.63 |
| Mean | 12.84 | 7.79 | 6.47 | 5.57 | 8.21 |
| Stdev | 2.99 | 2.06 | 2.51 | 1.92 | 2.02 |
| CV | 23.29 | 26.44 | 38.79 | 34.47 | 24.60 |
| Bias | | -5.05 | -6.37 | -7.28 | -4.63 |
| Corr | | 0.95 | 0.88 | 0.81 | 0.89 |
| RMSE | | 5.05 | 6.37 | 7.28 | 4.63 |

| P4T4 | | | | | |
|----------------------|------------|-------------|-------------|---------------|--------------|
| Precipitation | | | | | |
| | | NNRP | MPI | MIROC5 | CCSM4 |
| | Obs | 4 km | 4 km | 4 km | 4 km |
| Mean | 0.60 | 3.10 | 2.99 | 2.55 | 4.66 |
| Stdev | 0.77 | 2.24 | 2.48 | 2.17 | 3.77 |
| CV | 128 | 72.26 | 82.94 | 85.10 | 80.90 |
| RelBias | | 414.2 | 396.2 | 322.5 | 672.5 |
| Corr | | 0.83 | 0.76 | 0.77 | 0.78 |
| RMSE | | 3.00 | 3.08 | 2.55 | 5.16 |
| Mean | 9.99 | 6.22 | 5.01 | 4.08 | 6.93 |
| Stdev | 3.01 | 2.38 | 2.73 | 2.16 | 2.24 |
| CV | 30.1 | 38.26 | 54.49 | 52.94 | 32.32 |
| Bias | | -3.77 | -4.97 | -5.91 | -3.06 |
| Corr | | 0.95 | 0.89 | 0.83 | 0.90 |
| RMSE | | 3.92 | 5.15 | 6.15 | 3.36 |

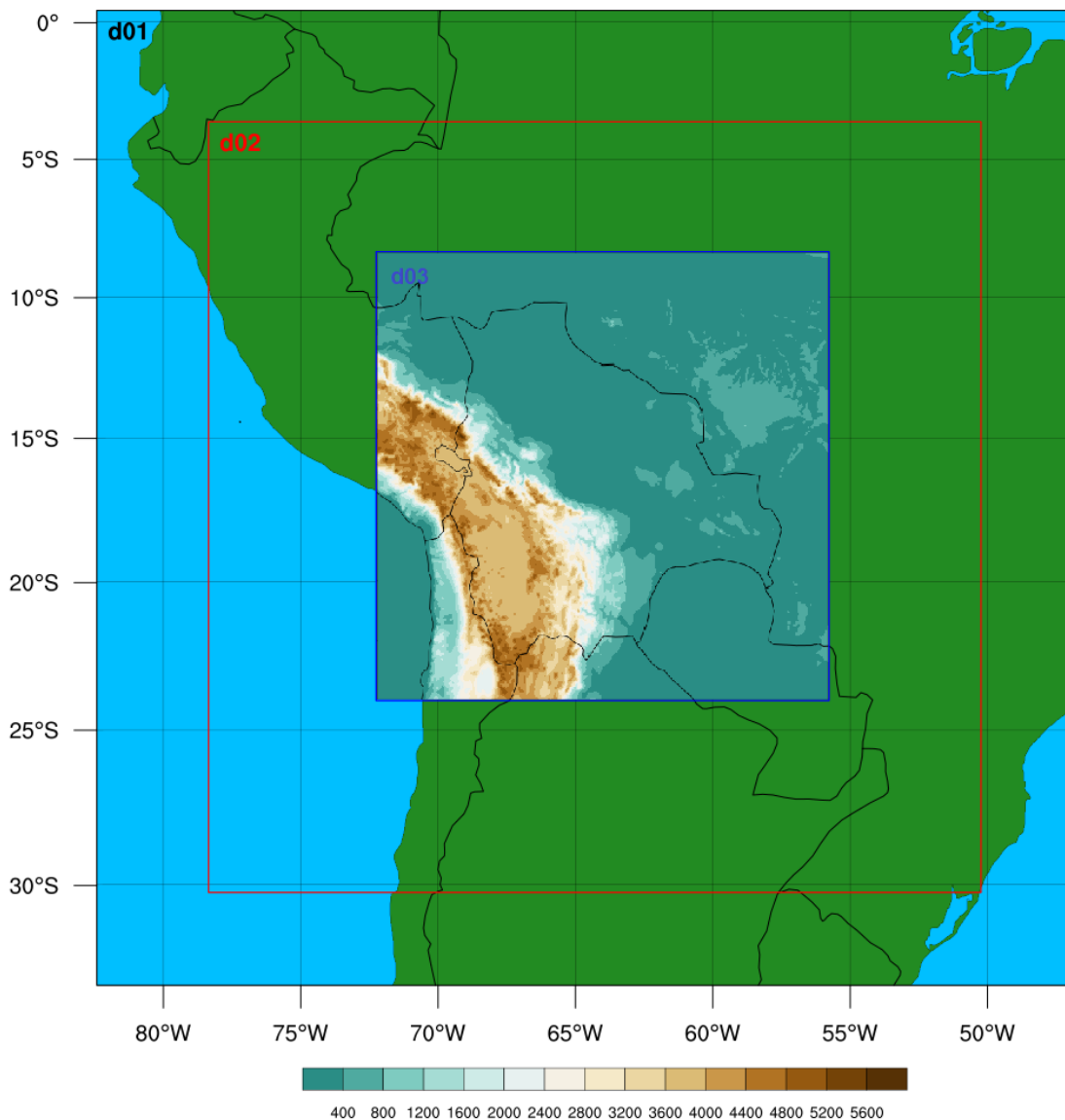


Figure 4.1. Topography of Bolivia. Higher mountains of Andes lie to the west of the country with lowlands to the east. Units are in meters. Black (outer), red and blue (inner) boxes represent the domains with different resolutions of 36, 12 and 4 km, respectively.

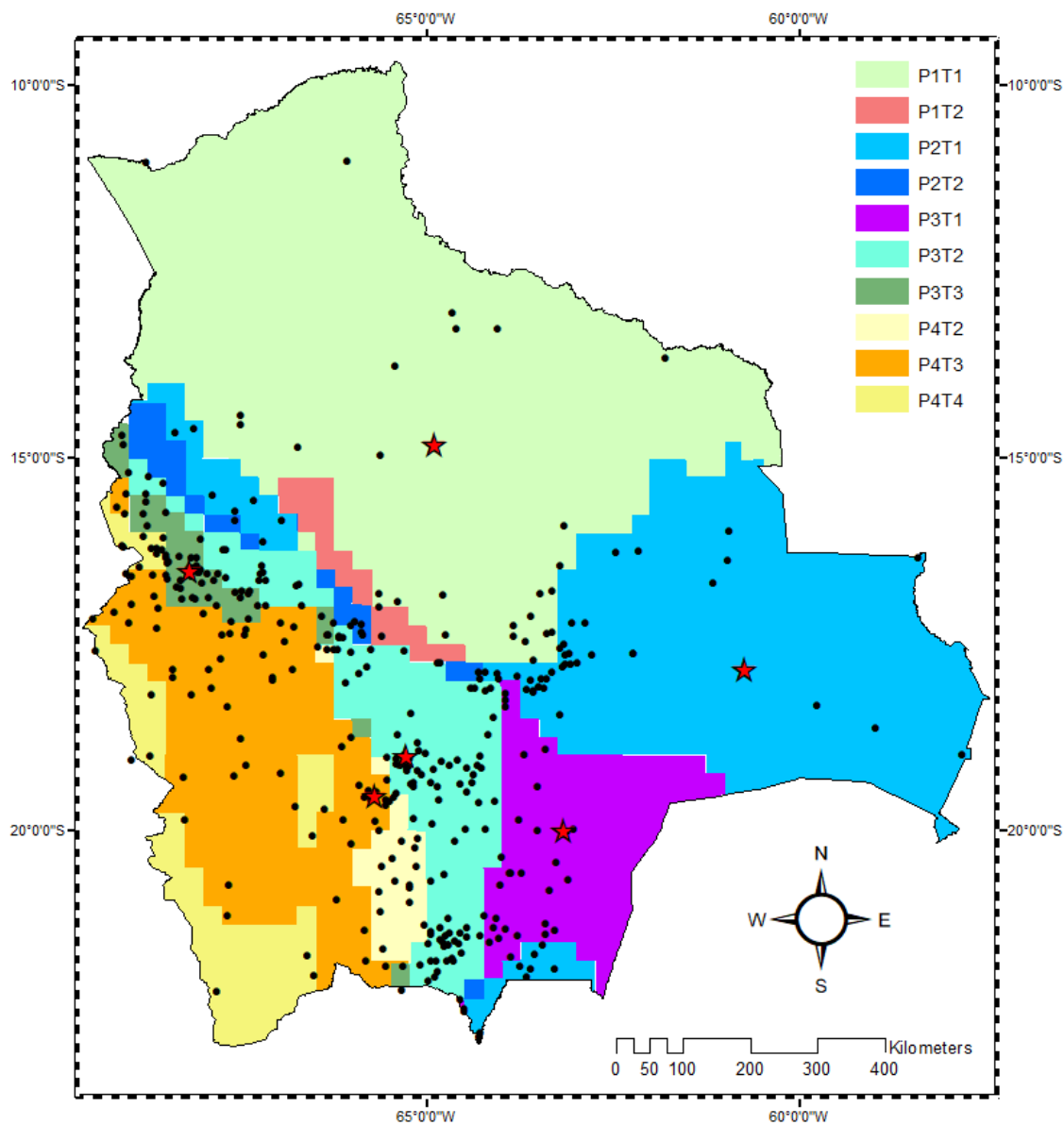


Figure 4.2. Homogeneous climate subregions. The regions are labeled following the associated precipitation and temperature clusters ordered from the highest amount of precipitation in the Amazon basin to the lowest amount in Altiplano. The dots show the geographical position of the meteorological stations over the country. The stars represent the selected stations for station-to-gridpoint analysis.

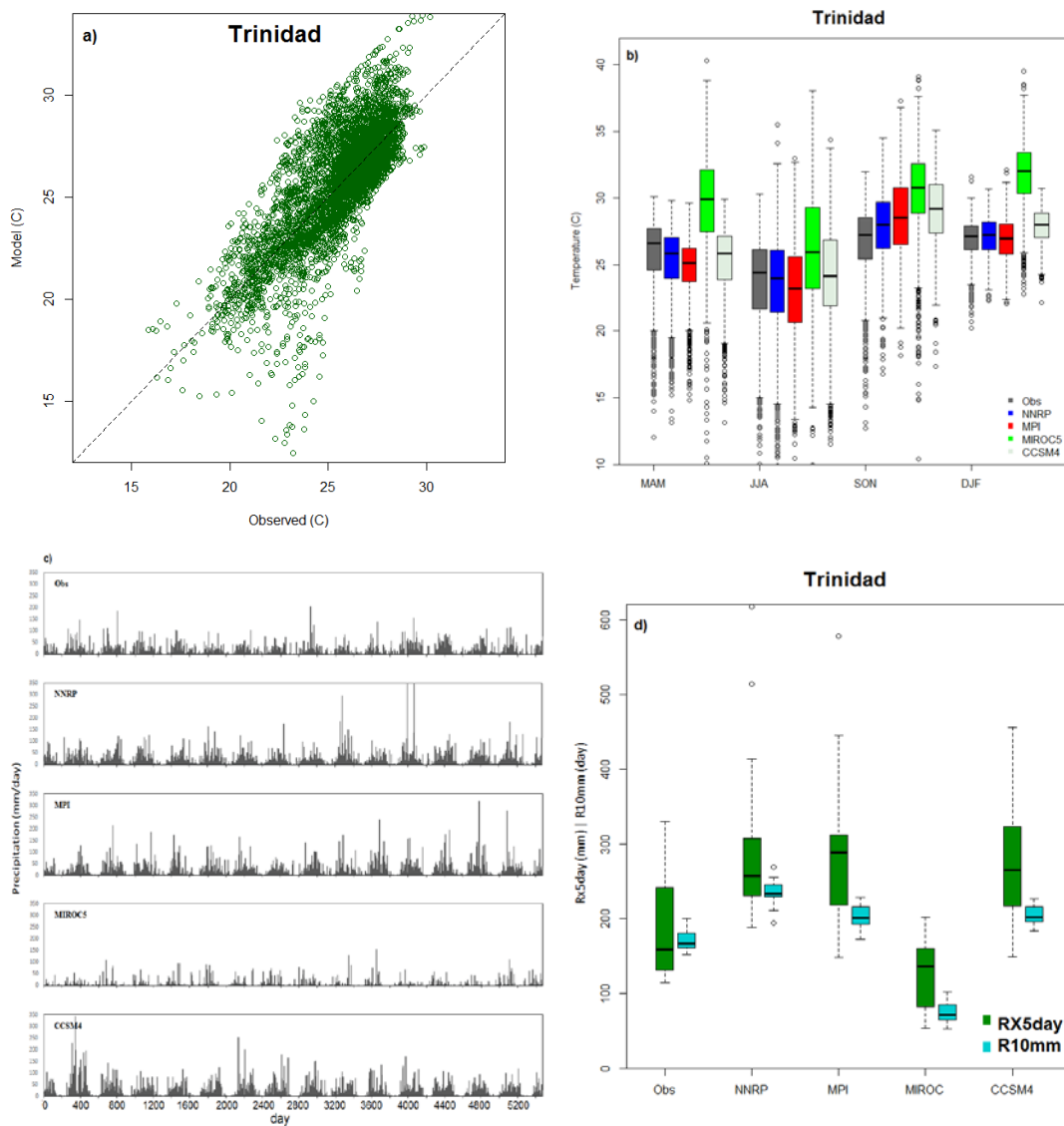


Figure 4.3. Trinidad, (a) temperature scatterplot for NNRP-WRF and station measurements, (b) boxplots of temperature distribution simulated by NNRP-WRF and GCM-WRF for the four season, (c) precipitation time series of observed versus NNRP-WRF and GCM-WRF simulations for the period of 1996-2010 for the observation and reanalysis and 2006-2020 for the GCM-driven simulations, and (d) boxplot comparison of extreme indices of RX5day and R10mm for the reanalysis and GCM driven WRF simulations against the observed. See Fig. 3.4 for boxplot details.

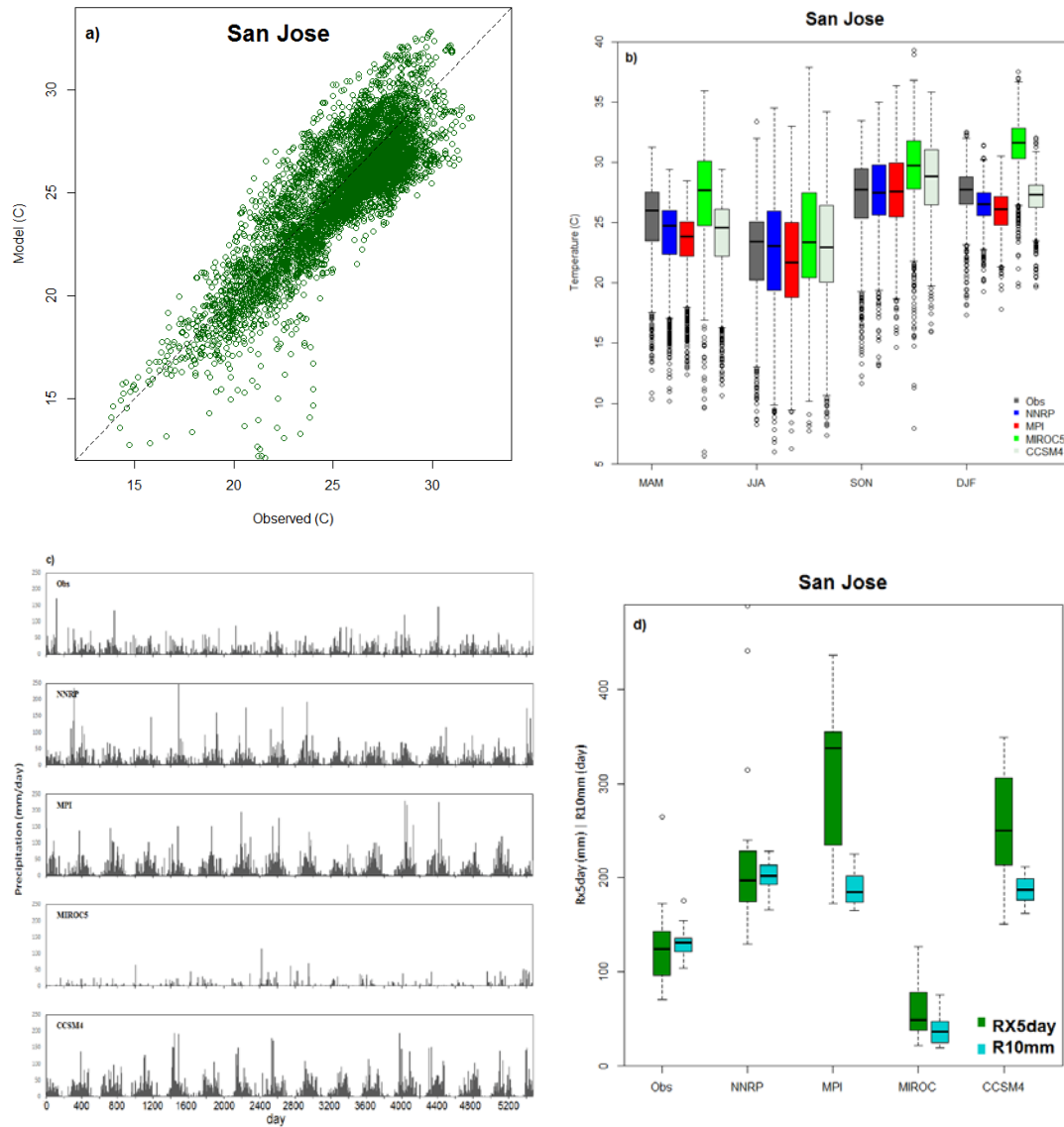


Figure 4.4. San Jose, (a) temperature scatterplot for NNRP-WRF and station measurements, (b) boxplots of temperature distribution simulated by NNRP-WRF and GCM-WRF for the four season, (c) precipitation time series of observed versus NNRP-WRF and GCM-WRF simulations for the period of 1996-2010 for the observation and reanalysis and 2006-2020 for the GCM-driven simulations, and (d) boxplot comparison of extreme indices of RX5day and R10mm for the reanalysis and GCM driven WRF simulations against the observed. See Fig. 3.4 for boxplot details.

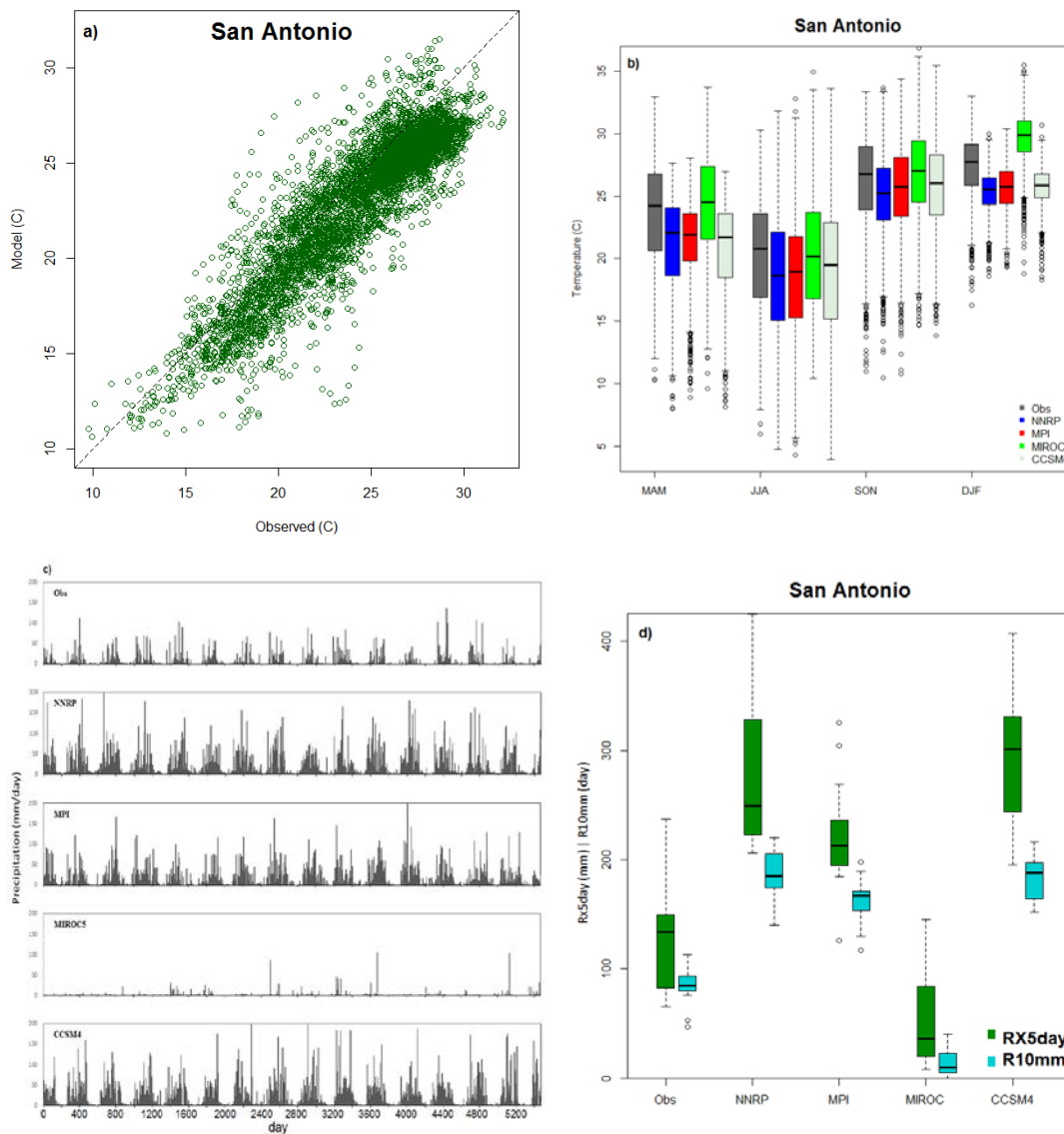


Figure 4.5. San Antonio, (a) temperature scatterplot for NNRP-WRF and station measurements, (b) boxplots of temperature distribution simulated by NNRP-WRF and GCM-WRF for the four season, (c) precipitation time series of observed versus NNRP-WRF and GCM-WRF simulations for the period of 1996-2010 for the observation and reanalysis and 2006-2020 for the GCM-driven simulations, and (d) boxplot comparison of extreme indices of RX5day and R10mm for the reanalysis and GCM driven WRF simulations against the observed. See Fig. 3.4 for boxplot details.

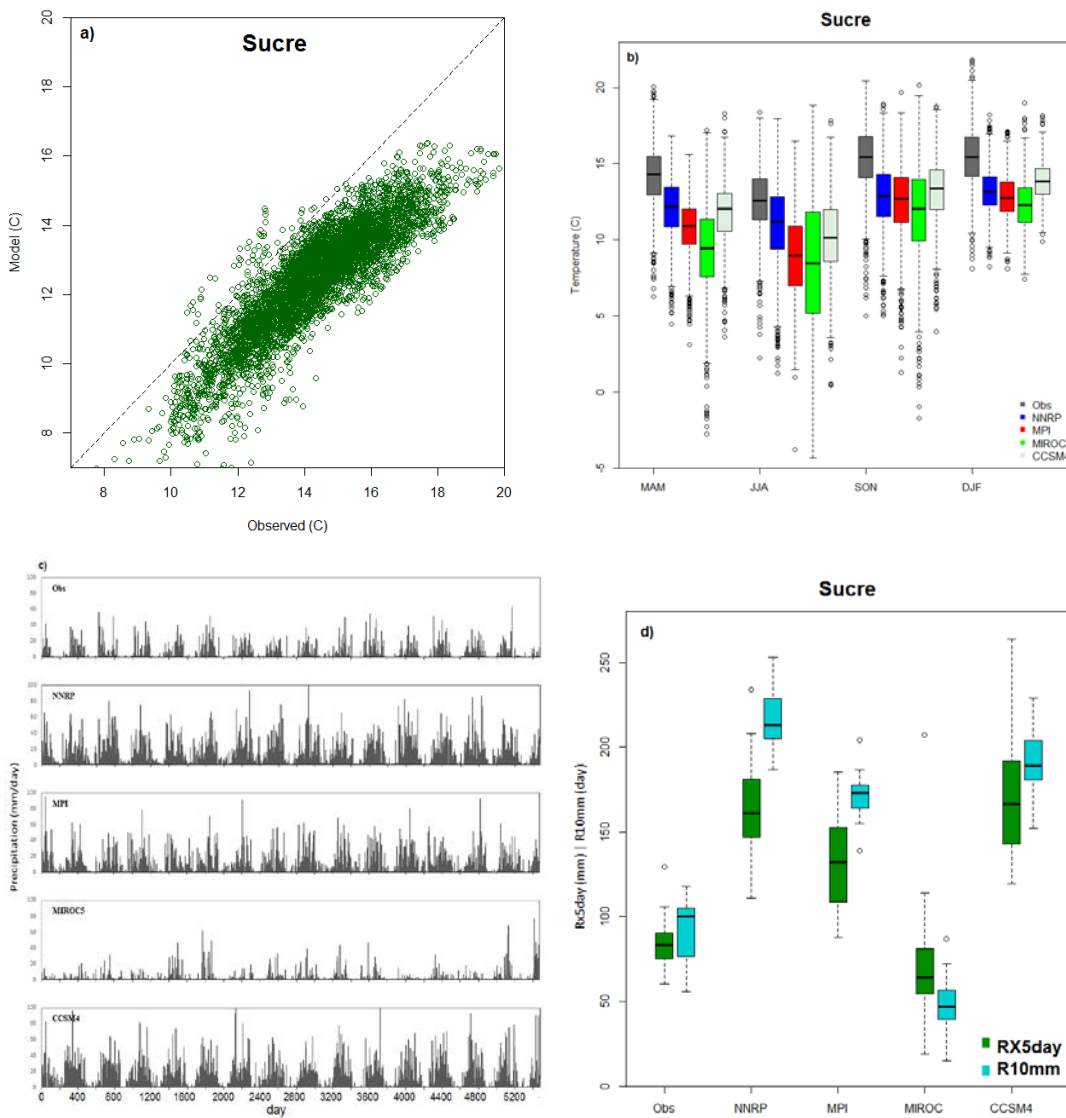


Figure 4.6. Sucre, (a) temperature scatterplot for NNRP-WRF and station measurements, (b) boxplots of temperature distribution simulated by NNRP-WRF and GCM-WRF for the four season, (c) precipitation time series of observed versus NNRP-WRF and GCM-WRF simulations for the period of 1996-2010 for the observation and reanalysis and 2006-2020 for the GCM-driven simulations, and (d) boxplot comparison of extreme indices of RX5day and R10mm for the reanalysis and GCM driven WRF simulations against the observed. See Fig. 3.4 for boxplot details.

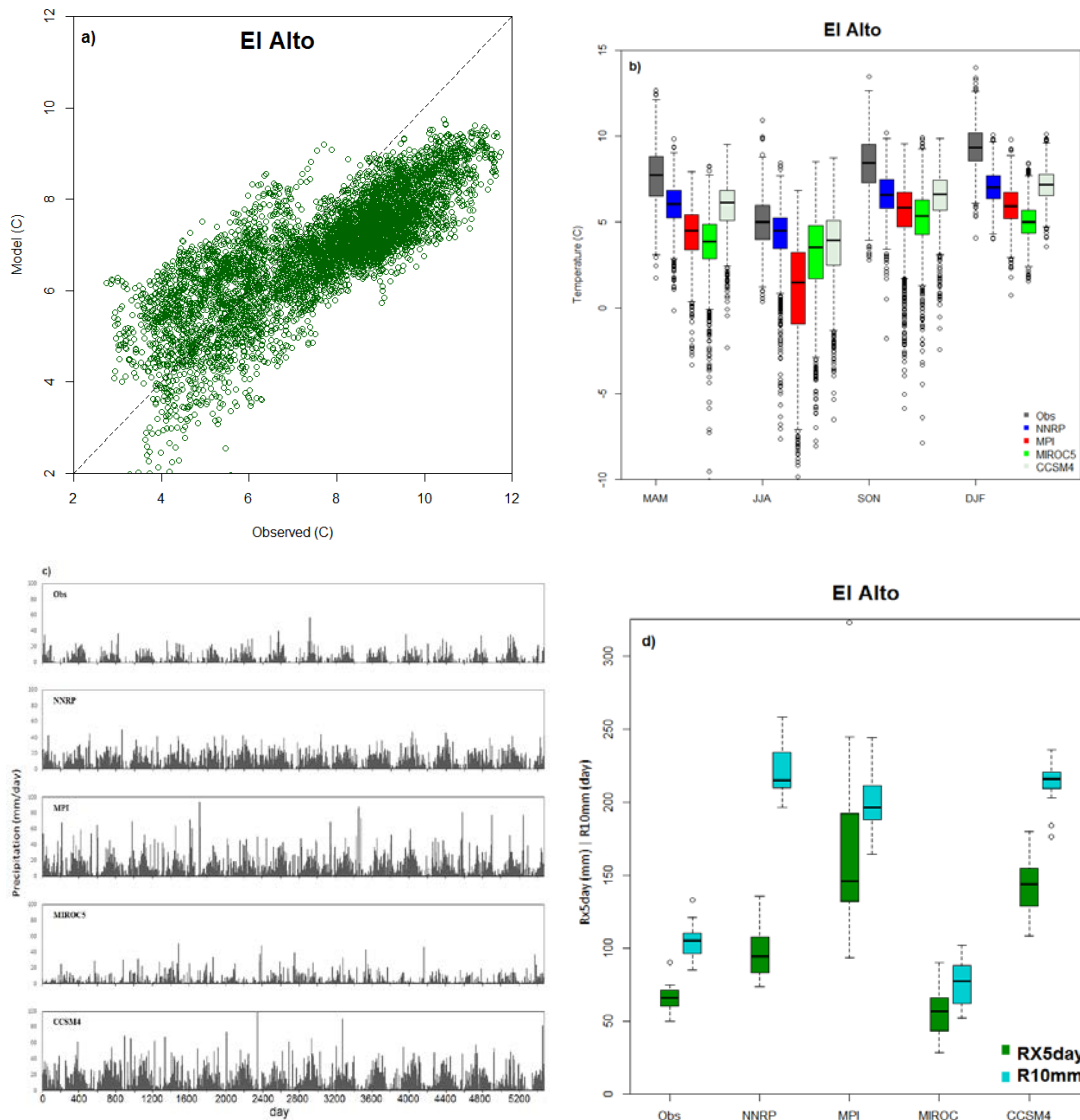


Figure 4.7. El Alto, (a) temperature scatterplot for NNRP-WRF and station measurements, (b) boxplots of temperature distribution simulated by NNRP-WRF and GCM-WRF for the four season, (c) precipitation time series of observed versus NNRP-WRF and GCM-WRF simulations for the period of 1996-2010 for the observation and reanalysis and 2006-2020 for the GCM-driven simulations, and (d) boxplot comparison of extreme indices of RX5day and R10mm for the reanalysis and GCM driven WRF simulations against the observed. See Fig. 3.4 for boxplot details.

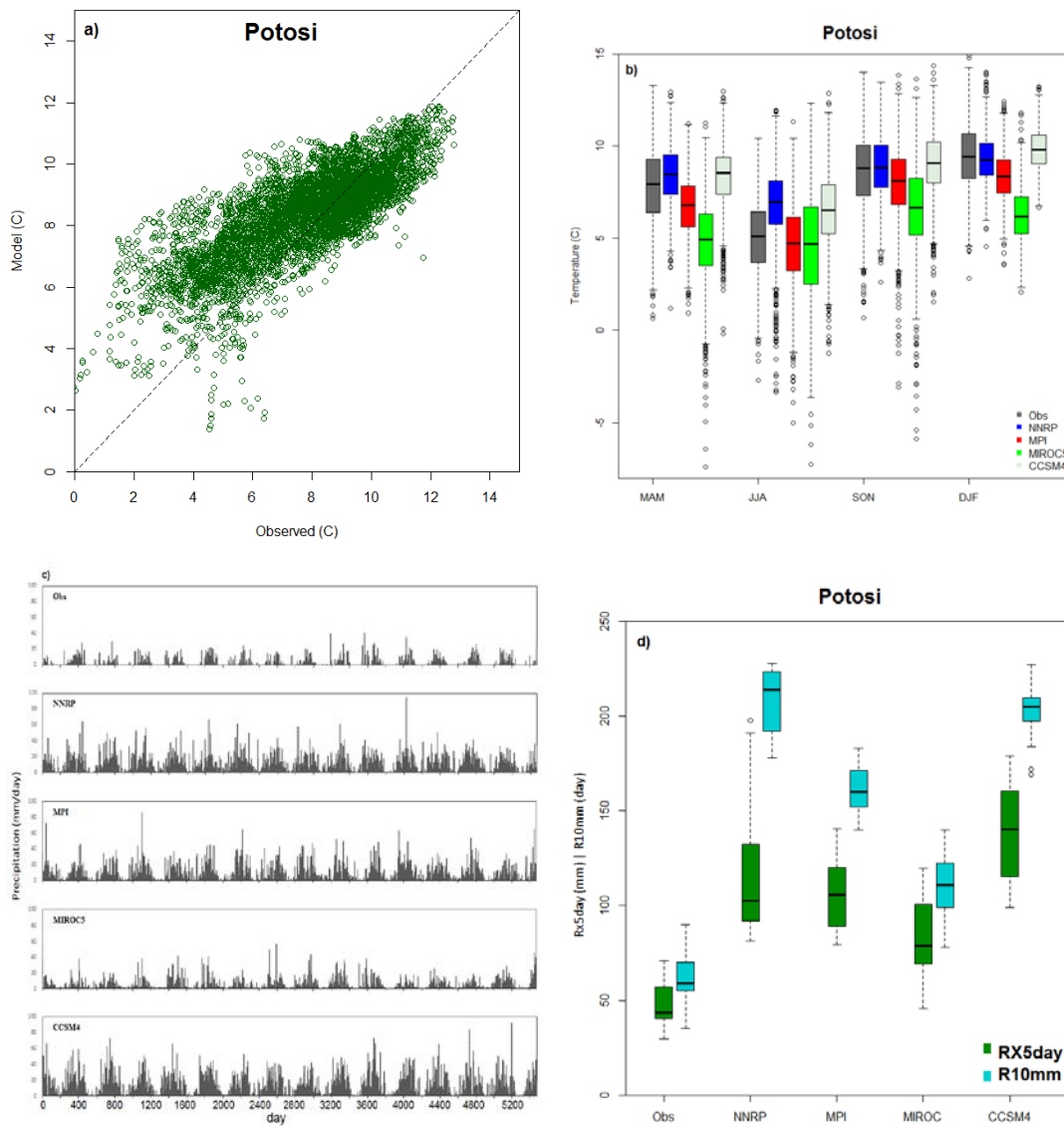


Figure 4.8. Potosi, (a) temperature scatterplot for NNRP-WRF and station measurements, (b) boxplots of temperature distribution simulated by NNRP-WRF and GCM-WRF for the four season, (c) precipitation time series of observed versus NNRP-WRF and GCM-WRF simulations for the period of 1996-2010 for the observation and reanalysis and 2006-2020 for the GCM-driven simulations, and (d) boxplot comparison of extreme indices of RX5day and R10mm for the reanalysis and GCM driven WRF simulations against the observed. See Fig. 3.4 for boxplot details.

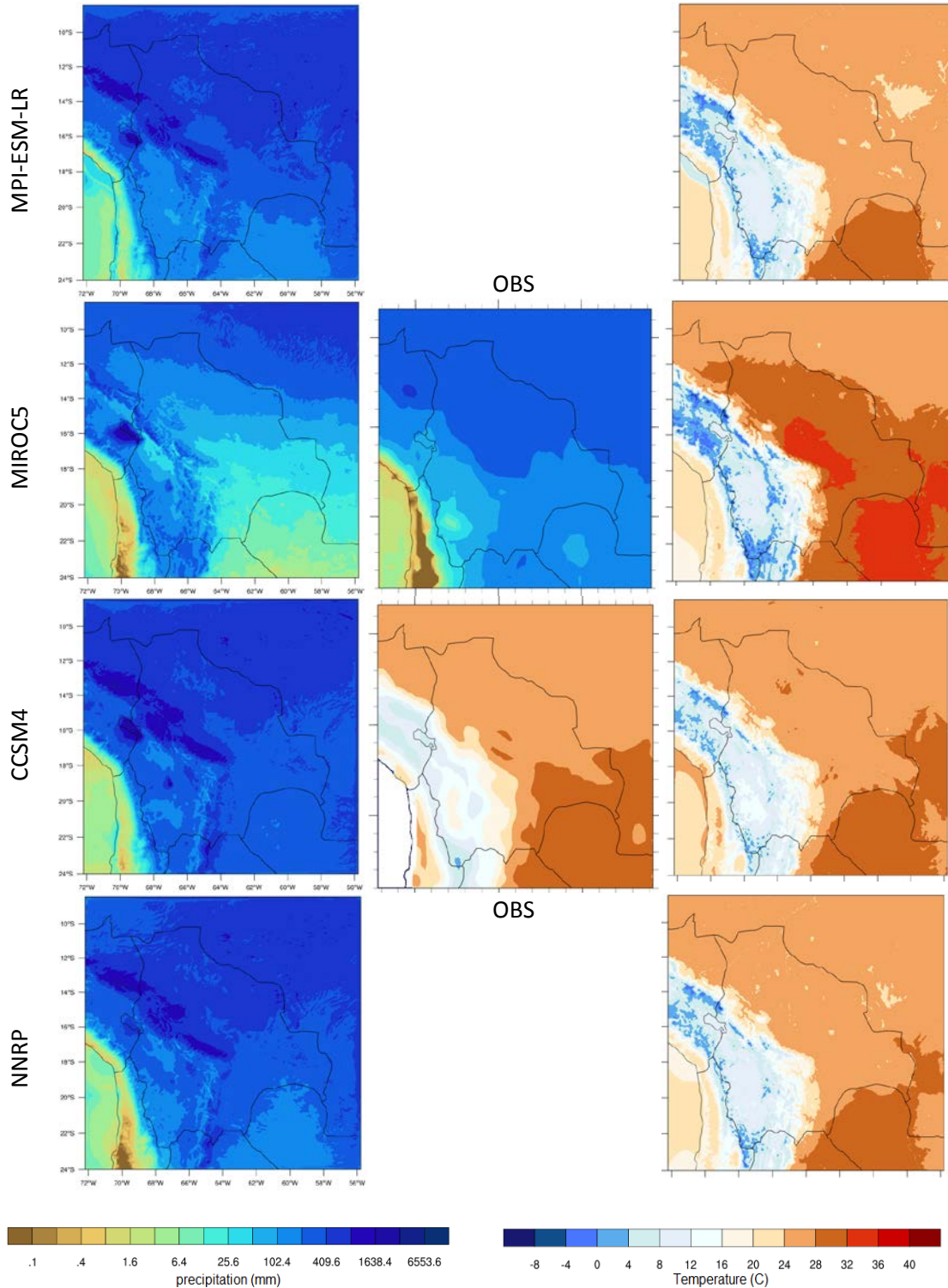


Figure 4.9. Wet season (DJF) climatological mean of precipitation (mm/month) and temperature (degree C) for observed, 1996-2010 versus reanalysis-driven WRF, 1996-2010 (bottom left for precipitation and bottom right for temperature) and GCM-driven WRF, 2006-2020 (left column for precipitation and right column for temperature). The original spatial resolutions of modeled and observed datasets have been used (25 km for the observed and 4 km for the WRF simulations).

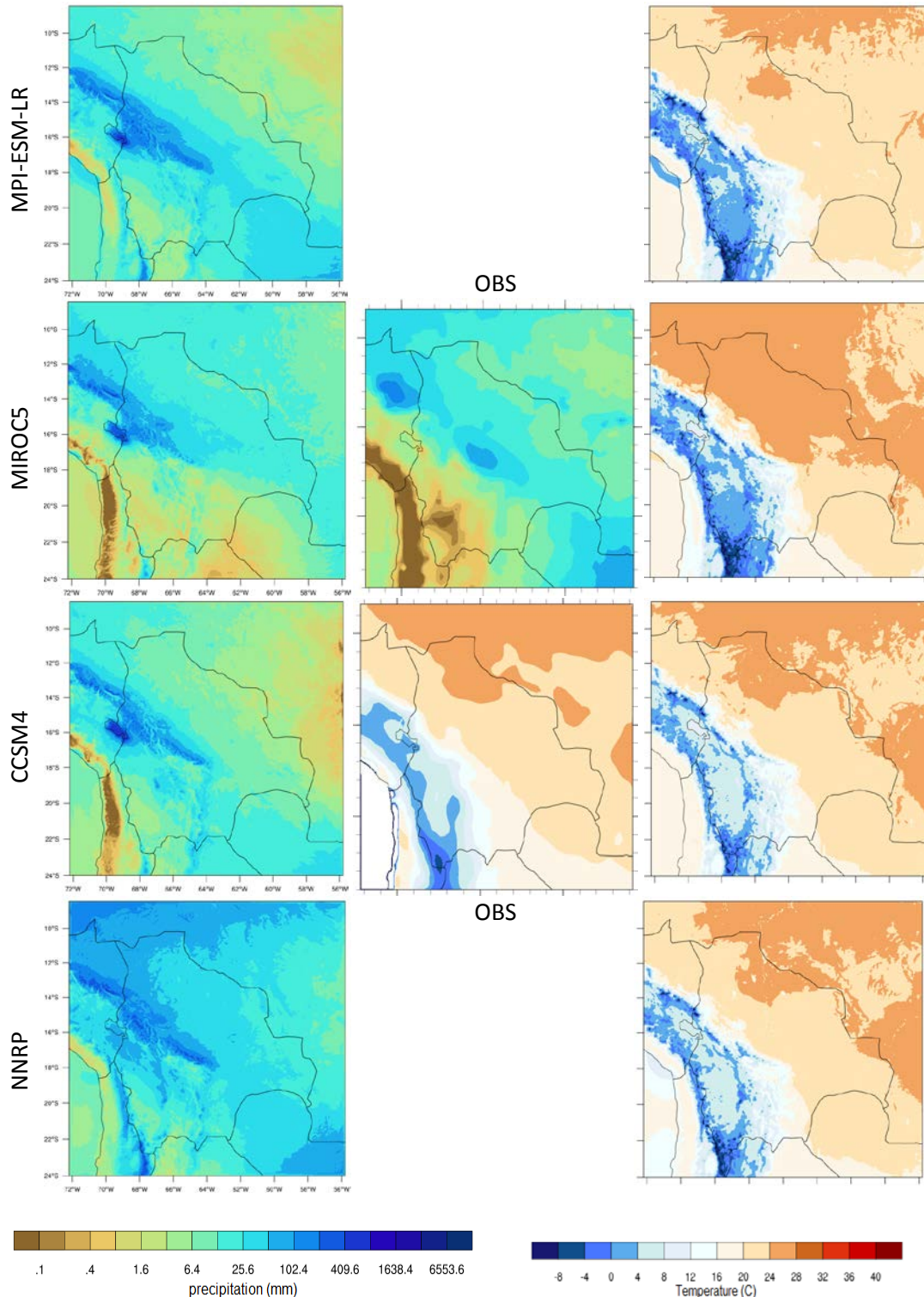


Figure 4.10. Dry season (JJA) climatological mean of precipitation (mm/month) and temperature (degree C) for observed, 1996-2010 versus reanalysis-driven WRF, 1996-2010 (bottom left for precipitation and bottom right for temperature) and GCM-driven WRF, 2006-2020 (left column for precipitation and right column for temperature). The original spatial resolutions of modeled and observed datasets have been used (25 km for the observed and 4 km for the WRF simulations).

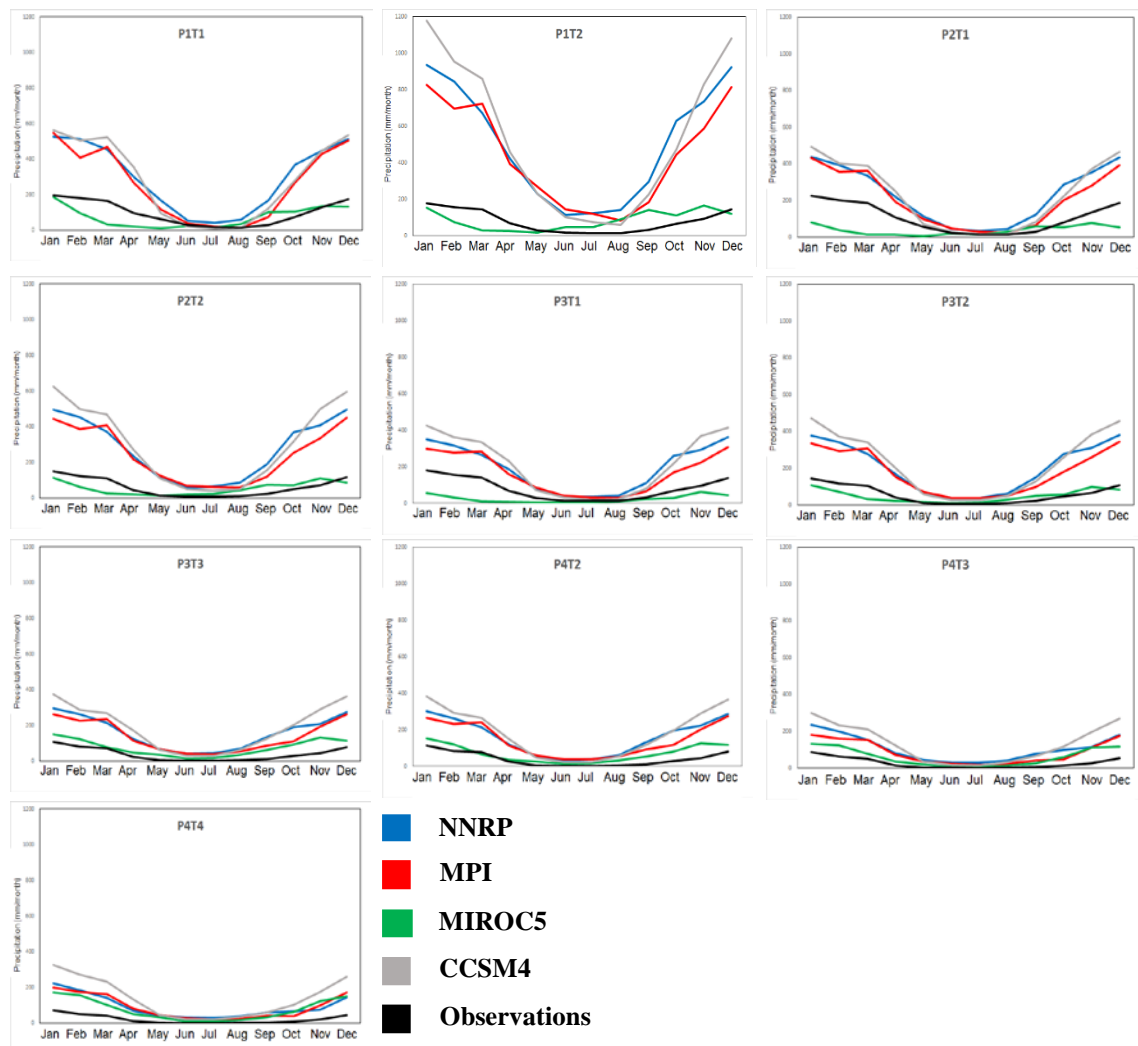


Figure 4.11. Mean annual cycle of precipitation (mm/month) for present day climate (Observed: 1996-2010, Modeled: 2006-2020) over the defined climate regions. The original spatial resolutions of modeled and observed datasets have been used.

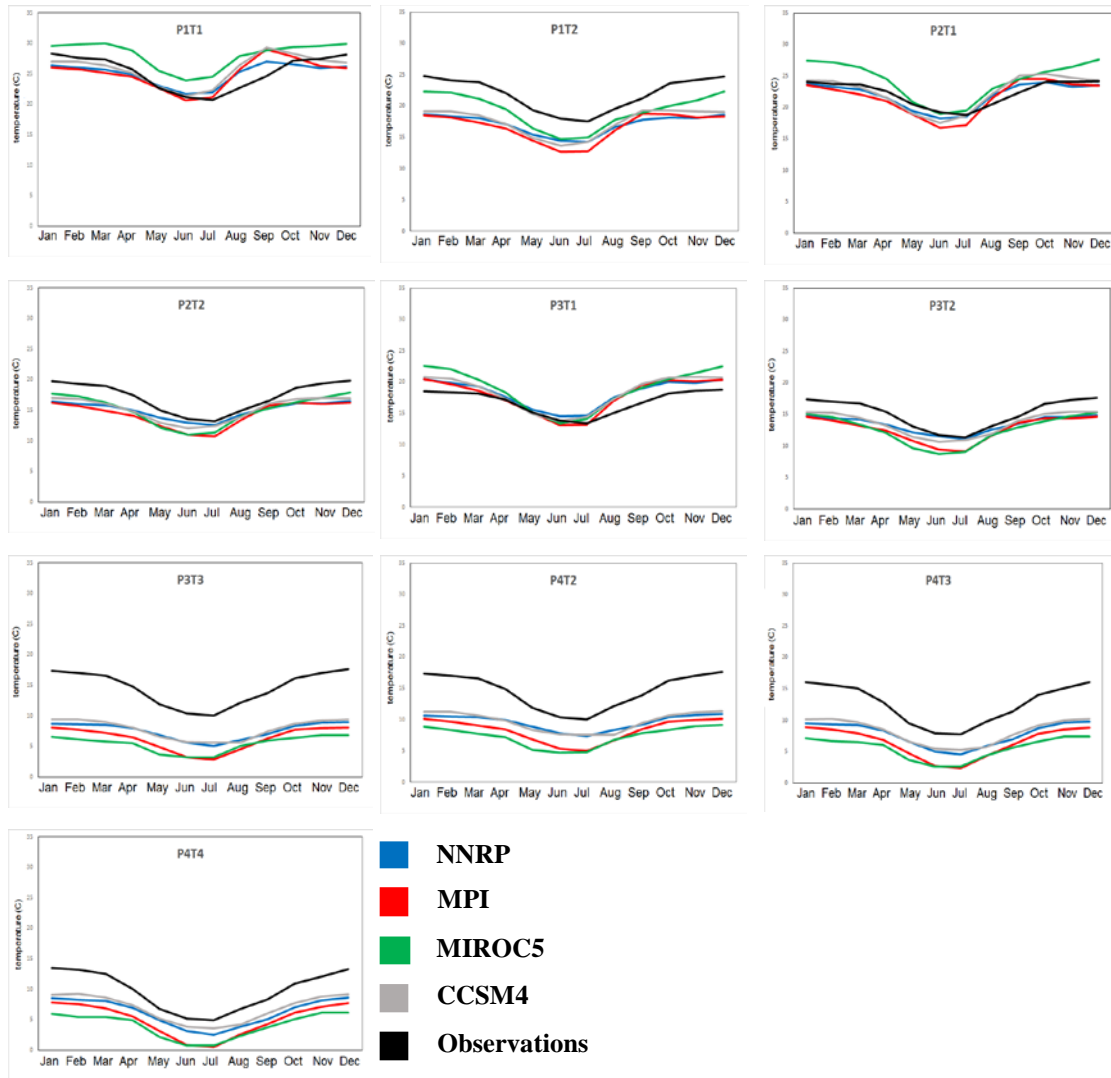


Figure 4.12. Mean annual cycle of temperature (degree C) for present day climate (Observed: 1996-2010, Modeled: 2006-2020) over the defined climate regions. The original spatial resolutions of modeled and observed datasets have been used.

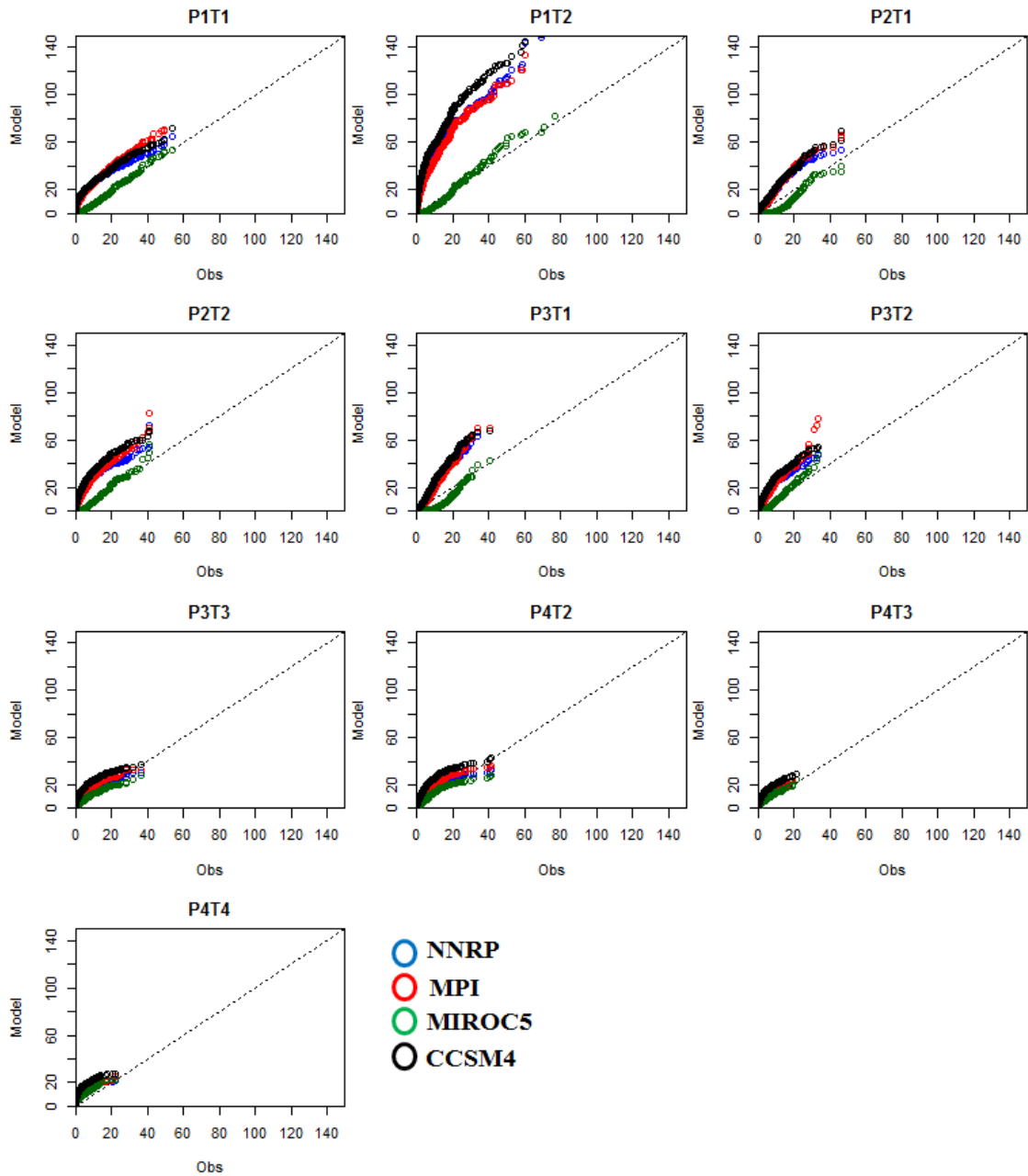


Figure 4.13. QQ-plot of WRF simulations forced by reanalysis and GCMs against observed data for the wet season (DJF) daily precipitation over the defined climate regions. Dashed lines illustrate the perfect match between models and observation. The original spatial resolutions of modeled and observed datasets have been used (Obs: 25 km; Model: 4 km).

Chapter 5

Climate Change Impact Assessment over Bolivia Using the WRF High-Resolution Dynamical Downscaling II: A Case Study for Drought

Abstract

Bolivia is a vulnerable developing country impacted by climate change for several basic reasons. First, the country is among the poorest in Latin America with the highest percentage of indigenous people. Second, its geographic location, with climatically variable and bio-diverse regions, exposes it to different impacts of climate change. Finally, the physical features of the land are undergoing irreversible changes such as deforestation in the Amazonian lowlands and glacier retreat in the highlands. The current paper is the third part of a three-part project that provides an overview of projected changes in the mean climate and climate extremes, sixty years into the future. Since coarse resolution global climate models (GCMs) cannot adequately resolve regional scale features such as topography and local scale circulations, we used the Weather, Research and Forecasting (WRF) regional climate model to dynamically downscale the output of three CMIP5 GCMs under three representative concentration pathways (RCPs) to account for a range of possible future climate outcomes. Our results demonstrate that the whole country will suffer from further warming with varying magnitude. The already arid higher terrain, having the highest temperature increase, will also experience reduced precipitation that leads to accelerated retreat of the glaciers. The flood-prone lowland region of El Chapare, with the highest annual rainfall at present, will experience even higher rainfall in the future, making that region more vulnerable to the hazards of landslides, loss of crops, and damage to homes and infrastructures.

5.1. Introduction

As reported by many studies, the frequency of extreme climate events worldwide has been changing rapidly in recent decades (Easterling et al. 2000; Frich et al. 2002; Cai et al. 2014). Meanwhile, developing countries are, and will continue to be, strongly impacted by these changes as they are challenged to adapt to these fast-growing changes due to limited financial and technological resources. Bolivia, among these developing countries and having a biodiverse climate of wet Amazonia to the north and the barren high plateau of Altiplano to the west, is already experiencing the consequences of climate change in its more vulnerable regions primarily in the form of costly hazards of flooding and drought in the lowlands and highlands, respectively. Oxfam (2009) classifies the overall impacts in five main categories in Bolivia, involving reduced food security, accelerated glacial retreat constraining the water availability, more frequent and more intense natural hazards, increases in the frequency of forest fires, and increases in mosquito-borne diseases.

Little research has targeted these impacts across Bolivia in detail (Francou et al. 2003; Vuille et al. 2008; Chevalier et al. 2010; Seiler et al. 2013). The focus of most of these studies is on changes in the tropical glaciers over the Andes and the impact on water supply or on deforestation in Amazonia as one of earth's largest sinks of carbon dioxide. Studying such impacts requires the use of future climate projections that have been made available from global climate model (GCM) simulations with an approximate resolution of 100 km over the globe. The current challenge comes because these coarse resolution models cannot adequately resolve the topography and regional scale features such as circulations and land cover types that are more closely entangled with the impacts.

Therefore, to study the impacts at more regional scales, we need to downscale the output of those coarser resolution GCMs in a physically meaningful manner.

Dynamical downscaling is a commonly used approach to derive finer spatial resolution climate data from the coarser GCM outputs. In this approach, a limited area regional climate model (RCM), fed by the GCM outputs at its boundaries, simulates more realistic finer resolution outputs by incorporating higher resolution topography and land use information and explicitly including smaller-scale atmospheric processes (Sun et al. 2006). A large number of RCM simulations of future climate change have been carried out for South America with different RCMs but none, to our knowledge, has focused on Bolivia with resolutions higher than 0.44° (Nunes et al. 2008; Marengo et al. 2009; Urrutia and Vuille 2009; Chou et al. 2011).

The most comprehensive strategy for downscaling is one that investigate uncertainties involved in regional climate models, parent GCMs, and different emission scenarios. To account for all these uncertainties, different RCMs should be initialized by different GCMs for different representative concentration pathways (RCPs), making the downscaling approach very computationally expensive. Therefore in most of the regional climate studies, only one or two GCMs are used to force a single RCM at a moderate spatial resolution. The current research outperforms most past studies by using the Weather Research and Forecasting (WRF) regional climate model forced by three GCMs, each under three different RCPs, projecting alternative climate futures at three resolutions of 36, 12 and 4 km. The important questions to answer are: (1) how well are the GCMs producing the large-scale atmospheric circulation, as any errors will be transferred to the higher resolution simulations through the boundaries, (2) how well is the RCM

simulating the observed (present day) climate, and (3) what differences in future climate projections come about depending on different RCPs. Answering the first question, Abadi et al. (2018a) evaluated the performance various CMIP5 GCMs in reproducing the larger-scale atmospheric pattern in South America and, more particularly, in Bolivia. The second question was recently answered in a companion paper evaluating the WRF model ability in reproducing the present day climate (Abadi et al. 2018c). As the third phase of this project, this paper aims to answer the third question and assess the climate change impacts in Bolivia.

This initial assessment is presented as a case study of potential changes in drought duration, magnitude, and severity under different emission scenarios since drought is of critical concern to the country and the international community. It also has recently forced the government of Bolivia to declare a state of emergency due to water shortages in large swaths of the country.

5.2. Data and Experiment Design

5.2.1. Study Area and the Climate Subregions

Bolivia is located in South America, bordering Brazil to the north and east, Peru to the northwest, Chile to the southwest, Argentina to the south, and Paraguay to the southeast (Fig. 5.1). Positioned between 9-22°S and 57-70°W, Bolivia has a tropical climate mainly influenced by the South American Monsoon System (SAMS; Marengo et al. 2009; Chou et al. 2011) with higher annual rainfall in the lowlands of Amazonia and drier conditions in the Altiplano, over the higher terrain of Andes. The wet season is from November to April in the austral summer with the highest amount occurring in the Chapare lowlands of Cochabamba, which receive more than 5500 mm per year, on average. The dry season

starts in May and lasts until October (austral winter). Altitudinal and latitudinal gradients control the climate variability in Bolivia as the Andes act as a barrier to moisture-laden flow coming from the Atlantic Ocean and limit the moisture content in the higher elevated lands and valleys.

The regional analysis in this paper is conducted for ten homogeneous climate regions defined in Abadi et al. (2018b). These ten regions provide a framework for discussion of potential future climate change and its impact in Bolivia.

5.2.2. Reanalysis and Observational Datasets

5.2.2.1. Gridded Observations

High quality, reliable observational data are relatively scarce in Bolivia as the densely forested Amazonia to the north and complex topography of the Andes to the west restrict the availability of the stations in those regions with lack of people and resources. To tackle this issue, Andrade (2014) combined Tropical Rainfall Measuring Mission (TRMM) satellite data (Scheel et al., 2010) and Climate Forecast System Reanalysis (CFSR) data (Saha et al. 2006), verified by surface observations obtained from the National Service of Meteorology and Hydrology (SENAMHI) of Bolivia, to generate a gridded dataset of temperature and precipitation, covering the whole country with a spatial resolution of $0.25^{\circ} \times 0.25^{\circ}$ and spanning the years 1979-2010. While the gridded dataset provides both maximum and minimum temperature, downscaling simulations provided temperature at three-hourly intervals, which were averaged to produce a daily average temperature. For comparison, the gridded observed daily average temperature was estimated as the average of the maximum and minimum temperatures, potentially introducing some biases in the resulting evaluation.

5.2.2.2. NCEP/NCAR Reanalysis Project

To gain an understanding of any biases induced by the WRF regional climate model, we use NCEP/NCAR Reanalysis Project (NNRP) as a forcing to initialize and provide lateral boundary conditions for WRF. Incorporating observations and numerical weather prediction model outputs, the reanalysis data offer the boundary conditions in a horizontal resolution of $2.5^{\circ} \times 2.5^{\circ}$ and vertical resolution of 17 levels on a six-hourly basis from 1948 to present (Kalnay et al., 1996). Here, we note that the higher resolution reanalysis data sets were not available at the time the study began. In the current study, the gridded observational data set and the WRF-NNRP downscaling are used to evaluate the WRF simulations forced by GCMs in simulating the historical patterns of the drought in the country.

5.2.3. Forcing CMIP5 Global Models

The CMIP5 (Coupled Model Intercomparison Project phase 5) experiment aims to improve the understanding of climate and to provide estimates of future climate change (Meehl et al. 2014). In this research, the regional climate model is forced by three CMIP5 models that successfully simulate the large-scale circulation of South America (Abadi et al. 2018 a). These GCMs (Table 5.1) were used in downscaling by WRF in two 15-year periods: (i) 2006-2020, representing the present day climate (baseline for climate change analysis) and (ii) 2066-2080, representing the future projections. It is worth mentioning that the “present day” simulations cannot be compared with the real observations as they are only representative of the climatologically expected conditions in that period and not the day-to-day weather that actually occurred.

5.2.4. Regional Climate Model

The WRF model has been used in many downscaling climatological studies around the world (Leung and Qian, 2009; Chotamonsak et al. 2011). Here, WRF simulations were performed using version 3.3 of the model with 29 vertical levels up to 50 hPa. Physics options employed include the unified Noah LSM (Chen and Dudhia 2001), the WSM5 microphysics option, the Kain-Fritsch convective scheme (Kain, 2004), the YSU PBL physics (Hong et al. 2006), the Rapid Radiative Transfer Model (RRTM) longwave radiation option, the Dudhia shortwave radiation option and the MM5 Monin-Obukhov surface-layer option. The model was one-way nested with no feedback from nest to the parent domain, and with time varying sea surface temperature (SST), sea ice, vegetative fraction and albedo.

5.2.5. Experiment Design and Methodology

In this study, the WRF model simulations were initialized in two distinct modes (i) forced by NNRP for the period of 1979-2012, in which the results are comparable with the real observational datasets as they are forced by the reanalysis data and (ii) forced by outputs from the above-mentioned three GCMs for the two periods of 2006-2020 and 2066-2080 considering three different RCPs (RCP2.6, RCP4.5 and RCP8.5). The simulations were done over three different domains: (i) an outermost domain of 36 km (d01) covering most of South America to capture the large-scale circulation, as the convective precipitation mechanism, especially in Amazonia, is part of a larger scale atmospheric circulation; (ii) a middle domain of 12 km (d02); and (iii) the innermost domain of 4 km (d03) covering all of Bolivia (Fig. 5.1; Table 5.2). The analysis is done for the two impact-related variables of precipitation and temperature in two aspects: (i) investigating the change in

the mean climate simulated by the three GCMs applying three RCPs, shown as the spatial distribution of the differences between the present day climate and the future projections; and (ii) on a regional scale, exploring the extreme aspect of the climate and projected climate change.

To perform the latter, our results focus on the probability distribution changes between the two periods, as well as changes in selected climate indices. To study the climate extremes, we selected the most relevant precipitation-based indices from the Expert Team on Climate Change Detection and Indices (ETCCDI; Klein Tank et al. 2009; Zhang et al. 2011). As the temperature-based indices were defined based on maximum and minimum temperatures that, due to the reason explained earlier, are not available from the RCM downscaling, we were unable to investigate changes in those indices. The climate extreme indices of RX5day and R10mm were chosen representing the maximum five-day precipitation and heavy precipitation days, respectively (Table 5.3).

Finally, because drought is one of the natural hazards that has the largest impacts on the socioeconomic situation in the country, we investigated the spatiotemporal pattern of drought events and its changes in the context of climate change in Bolivia. Nam et al. (2015) applied run theory to identify drought events based on the standardized precipitation evapotranspiration index (SPEI) at three different time scales of 1-, 6-, and 12-month. Following their methodology, we identified drought events in the downscaling simulations to evaluate the ability of WRF to produce the observed pattern of short- and long-term droughts when forced by NNRP or present-day GCMs and to evaluate changes in drought under future climate change scenarios. Run theory, presented by Yevjevich

(1967), is a widely applied approach to time series of drought indices to single out drought events and investigate their components and statistical properties. The statistical properties (Nam et al. 2015) explored in this method are (i) the drought duration, counting the months from the starting point of the event where the deficit crosses the specified threshold until the end of the event; (ii) the drought magnitude, or the cumulative deficiency of the drought index falling below a specified threshold; and (iii) the drought severity which is the ratio of the magnitude to the duration of the drought event (Fig. 5.3).

A drought index is a quantitative measure developed for monitoring drought condition and classification. Various drought indices have been proposed in the scientific community depending on various variables such as precipitation, soil moisture and evapotranspiration (e.g. Palmer 1965; McKee et al. 1993; Vicente-Serrano et al. 2010). In the current study, given the complex topography of Bolivia and the variety of the climate types from humid in the lowlands to arid in the Altiplano, and the importance of drought on the agriculture sector (Vicente-Serrano et al. 2010), we have used the SPEI (Vicente-Serrano et al. 2014) monthly values at three different time scales (i.e., 1-, 6- and 12-months). The work is done to (i) evaluate the performance of the WRF model to simulate the present day spatiotemporal pattern of drought, and (ii) to detect changes in the statistical properties of drought events between the present day and future projections. For the change detection, our analysis is focused only on the 12-month SPEI to account for the biodiversity in the vegetation type from the Amazon broadleaf forests and shrublands to the north to more cultivated vegetation types to the south and higher elevations, as they have various responses to water balance (Yu et al. 2014; Ivits et al.

2014; Li et al. 2015; Feng et al. 2017). Drought classification based on the SPEI values is summarized in Table 5.4.

SPEI values are calculated based on the monthly water balance (precipitation minus potential evapotranspiration) and time series are developed for three periods of 1996-2010 (observational data set), 2006-2020 (present day WRF simulations) and 2066-2080 (WRF future climate simulations). According to the scientific literature, there are approximately 50 methods to estimate potential evapotranspiration (ET_0) varying according to the required input meteorological variables or developed for specific geographical locations (Grismer et al. 2002; Lu et al. 2005). Among the commonly used methods are the Penman-Monteith equation (Penman 1948; Allen et al. 1994), and two temperature-based methods of Thornthwaite (1948) and Hargreaves-Samani (1994). The two latter methods are more appropriate for regions lacking reliable meteorological data, like Bolivia, as they only require the maximum and minimum temperature. The Hargreaves method was later modified by Droogers and Allen (2002), correcting ET_0 using precipitation data. In this research, we have used the modified-Hargreaves (Droogers and Allen 2002) method to calculate potential evapotranspiration and, henceforth, the SPEI.

All the above-mentioned analyses are done for the wet (DJF) and dry (JJA) seasonal averages and only the highest resolution of 4 km is presented for the purpose of studying the impacts (Abadi et al. 2018c).

5.3. Results and Discussion

We first examine the change in the seasonal, climatological mean pattern of precipitation and temperature in the wet and dry seasons and then we present the results for changes in the climate extreme characteristics.

5.3.1. Changes in Mean Climate

Wet-season (DJF) precipitation change from present-day (2006-2020) to projected future (2066-2080) for the three RCPs reveals that all the models in almost all the scenarios predict near-normal to somewhat drier conditions on the highlands, not changing drastically with increasing the emission scenarios (Fig. 5.4). The Amazon region and the dry tropical forests to the east will experience wetter conditions especially for RCP4.5 and RCP8.5. MIROC5 provides an exception, predicting a change toward drier condition for the whole country especially with RCP2.6 and RCP8.5 (Fig. 5.4). This behavior by MIROC5 was expected as that GCM tends to underestimate the precipitation greatly (Abadi et al. 2018c). MPI and CCSM4 agree by putting the largest positive change on the western part of Amazonia (the Chapare lowlands of Cochabamba), the wettest region in Bolivia. According to these results, lowlands can expect more flooding that increases the risk of hazards such as landslide on the slopes and crop damage in the flatter regions. It also shows that drought conditions can get worse over the higher elevated lands where some of the agricultural products are grown. Wet-season temperature changes from the present day to the future projections show consistent warming across the country with larger increases of 2-3°C for the higher RCPs. The largest temperature increases will occur over the highlands where existing glaciers are already threatened (Fig. 5.5).

Changes in precipitation for the austral winter months (JJA) are much smaller across the country and are generally less than 10 mm (Fig. 5.6). The exception is western Amazonia with relatively larger decreases that become more pronounced in the higher RCPs. This region is expected to receive more precipitation in the summer months and, thus, will experience enhanced seasonality in precipitation. These results are in agreement with other studies done for South America (Marengo et al. 2009). As was the case for austral summer, almost all the models in all emission scenarios predict warmer winters over the higher valleys of Andes and the lowlands of Amazonia (Fig. 5.7). The sole exception is WRF-MPI, which projects some cooling in the lowest emission scenario over the areas receiving the largest increases in precipitation. The present day and future projection maps for both seasons are provided in Appendix B.

5.3.2. Changes in Extremes

This section investigates the change in the extreme indices of precipitation and change in the frequency distribution of precipitation and temperature in the wet and dry seasons. All the results in this section are presented on a regional scale for each climate subregion. The calculations are done for all the gridpoint time series in a region for the 15-year period of the present day and future simulations. Fig. 5.8 shows the change in the distribution of the RX5day between present day and future climate simulations for three GCMs and three RCPs for the 10 climate subregions. As Silmann et al. (2013) pointed out, this index is often used to examine flood risks as heavy rain conditions in consecutive days can contribute to flood conditions (Frich et al. 2002). The square roots of the index are shown on the vertical axis to capture the smaller changes of the arid regions on the same scale as the wetter areas of Amazonia. One noticeable feature shared

by almost all models is the shift toward higher values in the lowlands and the small changes toward lower values in the higher valleys of Andes (Fig. 5.8). This result is in agreement with the future wetter conditions over the Amazonia and the future drier conditions over the Andes presented in the previous section. Another noticeable change is the higher dispersion of the RX5day distribution in the lowlands while the distributions on the higher terrains is more centered on the median.

The R10mm index is representative of the wet part of the precipitation distribution, however does not describe extreme precipitation (Silmann et al. 2013). Quite interestingly, almost all the models in all RCPs and in all the regions show almost no change from present-day to future climates. Whatever changes are evident, however, are toward reduced numbers of heavy precipitation days and become more pronounced in the higher emission scenarios (Fig. 5.9). This means that, in general, the number of days with heavy precipitation will decrease in the future so the wet part of the precipitation does not contribute to the increased risk of flooding in the lowlands in particular but the increased extreme precipitation events frequency is more responsible for the results shown in the previous section.

The probability distribution of precipitation (Fig. 5.10) for the present day and future climate projections under RCP8.5 for three GCMs and three RCPs in the wet season (DJF) show agreement on the lower tail of the precipitation distribution for all subregions and only start diverging toward the higher tail representing the high extreme values. Comparison of the higher tails of all three sets of simulations forced by GCMs shows that the probability of the extreme events is increasing from the lowlands toward the high valleys. That shows the extreme precipitation frequency change is more pronounced in

the highlands compared to the lowlands and the probabilities are even higher in the higher emission scenarios (see Appendix B for RCP 2.6 and 4.5). Temperature probability distributions (Fig. 5.11) for all models clearly show the shift toward higher temperatures in the future projections, and are most pronounced in RCP8.5.

Changes in the probability distributions of the precipitation for the dry season (Fig. 5.12) are similar to those for wet season precipitation distributions at the low end, with little change. The models do not agree on the change between the present day and future for the higher ends of the distributions as MPI shows an increase and MIROC5 and CCSM4 show decrease in the higher ends. Temperature distribution changes (Fig. 5.13) again show clear shifts to the higher values, similar to the DJF distribution changes. All the models in all the scenarios agree in projecting warming for all the regions with RCP 8.5 showing the greatest increase (see Appendix B for RCP 2.6 and 4.5).

5.3.3. Drought Assessment

This section evaluates the WRF model performance in reproducing the historical evolution of the drought events that occurred from 1979 to 2010. We also investigate the change in the statistical properties of drought events including trend, duration, magnitude and severity between the present day and the future climate projections.

5.3.3.1. Drought Event Identification

Following the strategy presented in Nam et al. (2015), we set the threshold for drought identification at a SPEI value of -0.5. Any SPEI value below this level is considered a drought event and the rest will be considered as non-drought events. Time series of 1-, 6-, and 12-month SPEI (Figs. 5.14-16, respectively) for the 10 climate subregions spanning from 1979 to 2010 indicate that the downscaling performs reasonably well in terms of

capturing drought. As expected, the 1-month SPEI shows higher frequency drought events compared to the longer term of 6- and 12-month SPEI time series as the shorter time scales like 1-month does not adapt to the memory of the system under study. The observed time series match the historical records of drought events in Bolivia especially in the more arid regions of higher terrain like P4T3 (Vicente-Serrano et al. 2014) with a wet period from 1979 to 1990 and drought periods from 1995 to 2005. The observed SPEI also confirm the decadal nature of drought in the country (Fig. 5.15 left column). Comparing the results from Amazonia to Altiplano, a temporal shift is noticeable as it takes higher valleys longer to respond to the water deficit (Fig. 5.15 left column). Comparing the length of drought events between Amazonia and Altiplano also reveals that drought duration decreases, though, the intensity increases with increasing elevation. NNRP-WRF simulations, unanimously underestimate the number of drought events and their intensity. This pattern is almost predictable, as the WRF model tends to overestimate precipitation across the country. There are also some uncertainties involved in these results as the NNRP-WRF has a 4-km resolution and observational gridded dataset has a coarser resolution of 25 km. WRF simulations tend to overestimate precipitation while the measurements likely are underestimated by the gridded observational dataset. The only major discrepancy between the observed dataset and NNRP-WRF simulations is the underestimated extent of the major drought of 1995-2005 especially in the lowlands.

5.3.3.2. Statistical Properties of Drought Events under Climate Change

Changes in the statistical properties of drought events (consecutive sequence of monthly SPEI values ≤ -0.5) include changes in the number of droughts, drought duration, drought magnitude, and drought severity in the context of climate change. The annual average of 12-month SPEI for each subregion (Fig. 5.17) illustrates the changes in the drought events between observed SPEI, SPEI based on the present day simulations using NNRP and the three GCMs, as well as the equivalent values for the future projections under different RCPs. As the present day GCM-driven WRF simulations do not diverge significantly under different RCPs, only the values for RCP 4.5 are presented for simplicity and, for the future, only the two higher RCPs are shown.

The number of droughts simulated by WRF in the present day is underestimated in the more arid regions. It is also evident that the models do not agree on the sign of the change as one model shows an increase and the others show decreases. The MPI model shows a decrease in the lowlands an increase in the higher terrain. MIROC5 shows a negative trend across the country with higher emissions. CCSM4 shows an increase in the lowlands and decrease over the higher elevated regions.

Changes in lowland drought duration (Fig. 5.18, left), drought magnitude (middle) and the drought severity (right) show a decrease in drought duration agreed by all models while the magnitude trend sign varies among the models, two showing increases and MIROC5 showing a decrease. Drought severity shows mainly positive changes shared by almost all models with MPI showing a slight decrease. On the other hand, in the higher elevated regions, the models unanimously project longer duration, magnitude and severity for drought events.

Overall, droughts in lowlands are getting shorter with increased severity. In higher terrain and the Altiplano, the duration, magnitude and severity of drought events all will increase, confirming the higher sensitivity of the mountainous regions to climate change. The projected climate change over the higher mountains makes the poor communities of the higher elevated lands more vulnerable to global warming.

5.4. Summary and Concluding Remarks

This paper assesses several aspects of climate change in Bolivia, a developing country listed as one of the most vulnerable countries to climate change due to its socioeconomic situation. To this end, a comprehensive dynamical downscaling strategy was developed including the WRF regional climate model and 4 sets of forcings of NCEP/NCAR Reanalysis Project (NNRP) and three CMIP5 GCMs: MPI-ESM-LR, MIROC5 and CCSM4. The WRF model boundary conditions were initialized by (i) the NNRP for the period of 1979-2010 to quantify the internal bias of the WRF model and (ii) the GCMs under three RCPs of 2.6, 4.5 and 8.5 to simulate the present day climate (a.k.a. reference period: 2006-2020) and future period of 2066-2080, through downscaling. The assessment is done through investigating the change in the mean climatic pattern and extremes as the difference between future projection and the reference period. As one of the costliest hazards affecting all regions in the country, drought characteristics including changes in annual number, duration, magnitude and severity were also examined in the context of climate change by applying an SPEI drought index and following the run theory.

Investigating the change in the mean climate affirms the common statement that the “wet gets wetter and dry gets drier” in Bolivia as the WRF model simulations almost

unanimously project increases in precipitation and temperature in the lowlands, particularly over western Amazonia, however the already dry elevated lands get drier and warmer. These projected changes will add to the vulnerabilities of the flood-prone regions of the lowlands to a higher risk of flooding and the drought-prone regions in the highlands to drier conditions as well as faster glacier retreat, exacerbating impacts on the regions' water supplies.

Our analysis of climate extremes shows projected increase of the RX5day indices in the lowlands with little to no decrease in the highlands while the R10mm index, representing the wetter part of the precipitation distribution, show negative changes across the region. This result is robust evidence that the potential risk of flooding in the lowlands will be increased due to more frequent extreme events in the future, particularly under higher emission scenarios.

Examining the probability distribution of precipitation shows higher frequency of extreme events on the highlands as the higher tail of the probability density function in the highlands lies above the ones from the lowlands. The shifts toward more extreme values toward the end of the century remain uncertain, as models do not agree on the projections. Temperature probability distributions, on the other hand, clearly show projected warming across the country in both wet and dry seasons.

Finally, the drought hazard analysis reveals that droughts in higher terrains are shorter but more severe compared to the lowlands. The change in the statistical properties of drought events between the present day and 60 years into the future generally shows that the lowlands droughts are getting shorter in length and more severe. As for the highlands, the changes in drought duration, magnitude and severity are all positive,

confirming the higher sensitivity of the mountainous regions to climate change. The study presented here could help policy- and decision-makers in the country develop more-applicable mitigation and adaptation strategies for the vulnerable, hazard-prone regions of Bolivia.

Acknowledgements

We gratefully acknowledge support from the Inter-American Development Bank for the development of tools and techniques used in this research and the UNL Holland Computing Center for computing services and support. The authors would also like to thank Marcos Andrade for producing and making available the observational gridded dataset over Bolivia.

5.5. References

- Abadi AM, Oglesby RJ, Rowe CM et al (2018a) Evaluation of GCMs historical simulations of monthly and seasonal climatology over Bolivia. *Clim Dyn* 51:733–754 doi: 10.1007/s00382-017-3952-y
- Abadi AM, Rowe CM, Andrade MF (2018b) Climate classification in Bolivia: A combination of nonhierarchical and consensus clustering analyses based on precipitation and temperature, *Int. J. Climatology*, submitted.
- Abadi AM, Rowe CM (2018c) Climate change impact assessment over Bolivia using the WRF high-resolution dynamical downscaling I: Evaluation of the present-day climate, *J. Climate*, in preparation.
- Abadi AM, Rowe CM, Hayes M (2018d) Climate change impact assessment over Bolivia using the WRF high-resolution dynamical downscaling II: A case study for drought, *J. Climate*, in preparation.
- Andrade MF (2014) La economía del cambio climático en Bolivia: generación de datos meteorológicos de alta resolución para Bolivia. C.E. Ludeña, L. Sanchez-Aragon (eds), *Banco Interamericano de Desarrollo*, Monografía No. 200, Washington, DC. <http://www.iadb.org/en/publications/publication-detail,7101.html?id=73547>
- Allen RG, Smith M, Pereira LS, Perrier A, (1994) An update for the calculation of reference evapotranspiration. *ICID Bulletin of the International Commission on Irrigation and Drainage*, 35–92.
- Cai W, Borlace S, Lengaigne M, et al (2014) Increasing frequency of extreme El Niño events due to greenhouse warming. *Nature Climate Change*, 4(2), 111-116. doi:10.1038/nclimate2100
- Chen F, Dudhia J (2001) Coupling an advanced land surface–hydrology model with the Penn State–NCAR MM5 modeling system. Part I: model implementation and sensitivity. *Monthly Weather Review*, 129(4), 569-585. doi:10.1175/1520-0493(2001)1292.0.co;2
- Chotamonsak C, Salathé EP, Kreasuwan J, et al (2011) Projected climate change over Southeast Asia simulated using a WRF regional climate model. *Atmospheric Science Letters*, 12(2), 213-219. doi:10.1002/asl.313
- Chevallier P, Pouyaud B, Suarez W, et al (2010) Climate change threats to environment in the tropical Andes: Glaciers and water resources. *Regional Environmental Change*, 11(S1), 179-187. doi:10.1007/s10113-010-0177-6
- Chou SC, Marengo JA, Lyra A, et al (2011) Downscaling of South America present climate driven by 4-member HadCM3 runs. *Clim Dyn*. doi:10.1007/s00382-011-1002-8
- Droogers P, Allen RG (2002) Estimating reference evapotranspiration under inaccurate data conditions. *Irrigation and Drainage Systems* 16: 33–45.
- Easterling DR, Evans JL, Groisman PY, et al (2000) Observed variability and trends in extreme climate events: A brief review. *Bulletin of the American Meteorological Society*, 81(3), 417-425. doi:10.1175/1520-0477(2000)0812.3.co;2

- Feng, S., Trnka, M., Hayes, M., & Zhang, Y. (2017). Why do different drought indices show distinct future drought risk outcomes in the U.S. Great Plains? *Journal of Climate*, 30(1), 265-278. doi:10.1175/jcli-d-15-0590.1
- Francou B (2003) Tropical climate change recorded by a glacier in the central Andes during the last decades of the twentieth century: Chacaltaya, Bolivia, 16°S. *Journal of Geophysical Research*, 108(D5). doi:10.1029/2002jd002959
- Frich P, Alexander L, Della-Marta P, et al (2002) Observed coherent changes in climatic extremes during the second half of the twentieth century. *Climate Research*, 19, 193-212. doi:10.3354/cr019193
- Gent PR, Danabasoglu G, Donner LJ et al (2011) The community climate system model version 4. *J Clim* 24:4973–4991. doi:10.1175/2011jcli4083.1
- Grismer ME, Orang M, Snyder R, et al (2002) Pan evaporation to reference evapotranspiration conversion methods. *Journal of Irrigation and Drainage Engineering*, 128(3), 180-184. doi:10.1061/(asce)0733-9437(2002)128:3(180)
- Hargreaves GH (1994) Defining and using reference evapotranspiration. *Journal of Irrigation and Drainage Engineering* 120: 1132–1139
- Hong S, Noh Y, Dudhia J (2006) A new vertical diffusion package with an explicit treatment of entrainment processes. *Monthly Weather Review*, 134(9), 2318-2341. doi:10.1175/mwr3199.1
- Ivits E, Horion S, Fensholt R, et al (2013) Drought footprint on European ecosystems between 1999 and 2010 assessed by remotely sensed vegetation phenology and productivity. *Global Change Biology*, 20(2), 581-593. doi:10.1111/gcb.12393
- Kain JS (2004) The Kain–Fritsch convective parameterization: An update. *Journal of Applied Meteorology*, 43(1), 170-181. doi:10.1175/1520-0450(2004)0432.0.co;2
- Kalnay, E, et al (1996) The NCEP/NCAR 40-year reanalysis project, *Bull. Am. Meteorol. Soc.*, 77, 437–470.
- Klein Tank AMG, Zwiers FW, Zhang X (2009) Guidelines on analysis of extremes in a changing climate in support of informed decisions for adaptation. WCDMP-72, WMO-TD/No.1500; 56 pp
- Leung LR, Qian Y (2009) Atmospheric rivers induced heavy precipitation and flooding in the western U.S. simulated by the WRF regional climate model. *Geophysical Research Letters*, 36(3). doi:10.1029/2008gl036445
- Li Z, Zhou T, Zhao X, et al (2015) Assessments of drought impacts on vegetation in China with the optimal time scales of the climatic drought index. *International Journal of Environmental Research and Public Health*, 12(7), 7615-7634. doi:10.3390/ijerph120707615
- Lu J, Sun G, McNulty SG, et al (2005) A comparison of six potential evapotranspiration methods for regional use in the southeastern United States. *Journal of the American Water Resources Association*, 41(3), 621-633. doi:10.1111/j.1752-1688.2005.tb03759.x
- Marengo JA, Jones R, Alves LM, et al (2009) Future change of temperature and precipitation extremes in South America as derived from the PRECIS regional

- climate modeling system. *International Journal of Climatology*, 29(15), 2241-2255. doi:10.1002/joc.1863
- McKee TB, Doesken NJ, Kleist J (1993) The relationship of drought frequency and duration to time scale. In: Preprints, 8th *Conference on Applied Climatology*, American Meteorological Society, Anaheim, CA, pp. 179–184
- Meehl GA, Moss R, Taylor KE, et al (2014) Climate model intercomparisons: Preparing for the next phase. *Eos, Transactions American Geophysical Union*, 95(9), 77-78. doi:10.1002/2014eo090001
- Nam W, Hayes MJ, Svoboda MD, et al (2015) Drought hazard assessment in the context of climate change for South Korea. *Agricultural Water Management*, 160, 106-117. doi:10.1016/j.agwat.2015.06.029
- Núñez MN, Solman SA, Cabré MF (2008) Regional climate change experiments over southern South America. II: Climate change scenarios in the late twenty-first century. *Climate Dynamics*, 32(7-8), 1081-1095. doi:10.1007/s00382-008-0449-8
- Oxfam (2009) Bolivia climate change, poverty and adaptation. <https://www.oxfam.org/sites/www.oxfam.org/files/bolivia-climate-change-adaptation-0911.pdf>
- Palmer WC (1965) Meteorological drought. In: Research Paper 45. U.S. Department of Commerce, Washington, D.C
- Penman HL (1948) Natural evaporation from open water, bare soil and grass. *Proceedings of the Royal Society A: Mathematical, Physical and Engineering Sciences*, 193(1032), 120-145. doi:10.1098/rspa.1948.0037
- Saha S, Nadiga S, Thiaw C, et al (2006) The NCEP climate forecast system. *Journal of Climate*, 19(15), 3483-3517. doi:10.1175/jcli3812.1
- Scheel ML, Rohrer M, Huggel C, et al (2010) Evaluation of TRMM multi-satellite precipitation analysis (TMPA) performance in the central Andes region and its dependency on spatial and temporal resolution. *Hydrology and Earth System Sciences Discussions*, 7(5), 8545-8586. doi:10.5194/hessd-7-8545-2010
- Seiler C, Hutjes RW, Kabat P (2013) Likely ranges of climate change in Bolivia. *Journal of Applied Meteorology and Climatology*, 52(6), 1303-1317. doi:10.1175/jamc-d-12-0224.1
- Sillmann J, Kharin VV, Zhang X, et al (2013) Climate extremes indices in the CMIP5 multimodel ensemble: Part 1. Model evaluation in the present climate. *Journal of Geophysical Research: Atmospheres*, 118(4), 1716-1733. doi:10.1002/jgrd.50203
- Stocker TF, Dahe Q, Plattner GK (2013) *Climate Change 2013: The Physical Science Basis. Working Group I Contribution to the Fifth Assessment Report of the Intergovernmental Panel on Climate Change*; Summary for Policymakers (IPCC, 2013); IPCC: Bern, Switzerland, 2013; pp. 1–33.
- Sun Y, Solomon S, Dai A, Portmann RW (2006) How often does it rain? *Journal of Climate* 19: 916–934, DOI: 10.1175/JCLI3672.1.
- Thornthwaite CW (1948) An approach toward a rational classification of climate. *Geographical Review* 38: 55–94. doi:10.2307/2107309.

- Urrutia R, Vuille M (2009) Climate change projections for the tropical Andes using a regional climate model: Temperature and precipitation simulations for the end of the 21st century. *Journal of Geophysical Research*, 114(D2). doi:10.1029/2008jd011021
- Vicente-Serrano SM, Beguería S, López-Moreno JI (2010) A multiscalar drought index sensitive to global warming: The standardized precipitation evapotranspiration index. *Journal of Climate*, 23(7), 1696-1718. doi:10.1175/2009jcli2909.1
- Vicente-Serrano SM, Chura O, López-Moreno JI, et al (2014) Spatio-temporal variability of droughts in Bolivia: 1955-2012. *International Journal of Climatology*, 35(10), 3024-3040. doi:10.1002/joc.4190
- Vogel A, Scherer-Lorenzen M, Weigelt A (2012) Grassland resistance and resilience after drought depends on management intensity and species richness. *PLoS ONE*, 7(5). doi:10.1371/journal.pone.0036992
- Vuille M, Francou B, Wagnon P, et al (2008) Climate change and tropical Andean glaciers: Past, present and future. *Earth-Science Reviews*, 89(3-4), 79-96. doi:10.1016/j.earscirev.2008.04.002
- Watanabe S, Hajima T, Sudo K, et al (2011) MIROC-ESM: model description and basic results of CMIP5-20c3m experiments. *Geosci Model Dev Discuss* 4:1063–1128. doi:10.5194/gmdd-4-1063-2011
- Yevjevich V (1967) An objective approach to definition and investigations of continental hydrologic droughts. In: Hydrology Paper No. 23. Colorado State University, Fort Collins, USA.
- Yu M, Li Q, Hayes MJ, Svoboda MD et al (2013) Are droughts becoming more frequent or severe in China based on the Standardized Precipitation Evapotranspiration Index: 1951-2010? *International Journal of Climatology*, 34(3), 545-558. doi:10.1002/joc.3701
- Zanchettin D, Rubino A, Matei D et al (2012) Multidecadal-to-centennial SST variability in the MPI-ESM simulation ensemble for the last millennium. *Clim Dyn* 40:1301–1318. doi:10.1007/s00382-012-1361-9
- Zhang X, Alexander L, Hegerl GC, et al (2011) Indices for monitoring changes based on daily temperature and precipitation data. *WIREs Clim. Change* 2: 851–870, DOI: 10.1002/wcc.147.

Table 5.1 Attributes of the selected GCMs

| Model Name | Horizontal resolution | Center and References |
|------------|-----------------------|---|
| CCSM4 | 0.94×1.25 | National Center for Atmospheric Research, United States (Gent et al. 2011) |
| MIROC5 | 1.4×1.4 | Atmosphere and Ocean Research Institute (The University of Tokyo), National Institute for Environmental Studies, and Japan Agency for Marine-Earth Science and Technology, Japan (Watanabe et al. 2010) |
| MPI-ESM-LR | 1.875×1.875 | Max-Planck Institute for Meteorology, Germany (Zanchettin et al. 2012) |

Table 5.2 Downscaling Simulations Summary

| Domains | Model & Scenarios | Years | |
|-------------|-------------------|---------------------------------|----------------------------|
| | Historical NNRP | 1979-2012 | |
| | MPI-RCP 2.6 | Present-day 2006-2020 | Future 2066-2080 |
| | MPI-RCP 4.5 | | |
| | MPI-RCP 8.5 | | |
| d01 (36 km) | MIROC5-RCP 2.6 | | |
| d02 (12 km) | MIROC5-RCP 4.5 | | |
| d03 (4 km) | MIROC5-RCP 8.5 | | |
| | CCSM4-RCP 2.6 | | |
| | CCSM4-RCP 4.5 | | |
| | CCSM4-RCP 8.5 | | |

Table 5.3 Selected climate extreme indices' attributions (Zhang et al. 2011)

| Label | Name | Index Definition | Unit |
|--------|--------------------------|--|------|
| RX5day | Max 5 day precipitation | Maximum consecutive 5-day precipitation per year | mm |
| R10mm | Heavy precipitation days | Annual Count where precipitation exceeds 10 mm | days |

Table 5.4 Drought classification based on the Standardized Precipitation Evapotranspiration Index (SPEI)

| SPEI | Drought Classification |
|--------------|------------------------|
| ≥ 2.0 | Extremely wet |
| 1.5 – 1.99 | Very wet |
| 1.0 – 1.49 | Moderately wet |
| 0.5 – 0.99 | Slightly wet |
| -0.49 – 0.49 | Near normal |
| -0.99 – -0.5 | Mild dry |
| -1.49 – -1.0 | Moderately dry |
| -1.99 – -1.5 | Severely dry |
| ≤ -2.0 | Extremely dry |

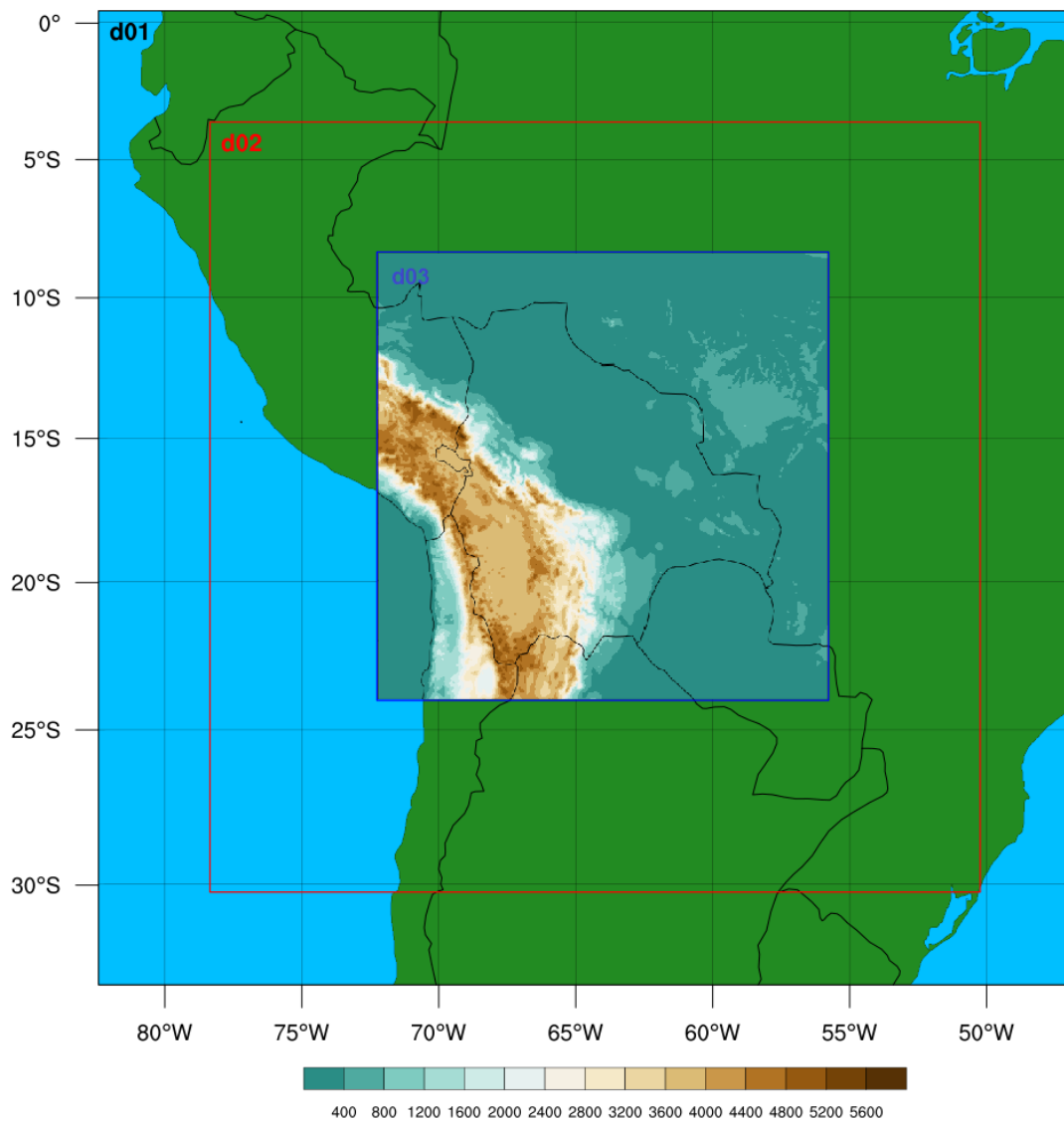


Figure 5.1. Topography of Bolivia. Higher mountains of Andes lie to the west of the country with lowlands to the east. Units are in meters. Black (outer), red and blue (inner) boxes represent the domains with different resolutions of 36, 12 and 4 km, respectively (Abadi et al. 2018b).

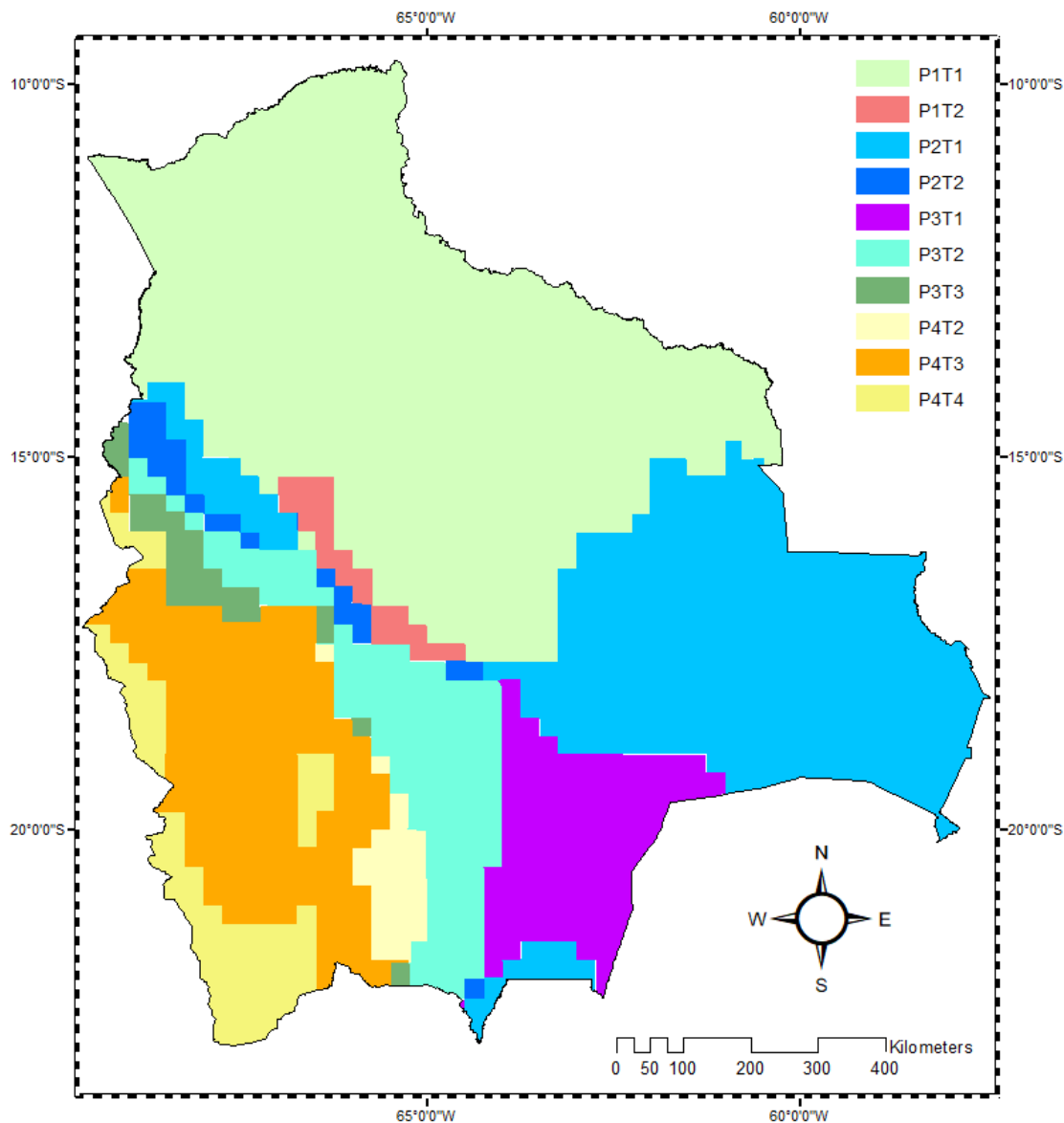


Figure 5.2. Homogeneous climate subregions. The regions are labeled following the associated precipitation and temperature clusters ordered from the highest amount of precipitation in the Amazon basin to the lowest amount in Altiplano (Abadi et al. 2018b)

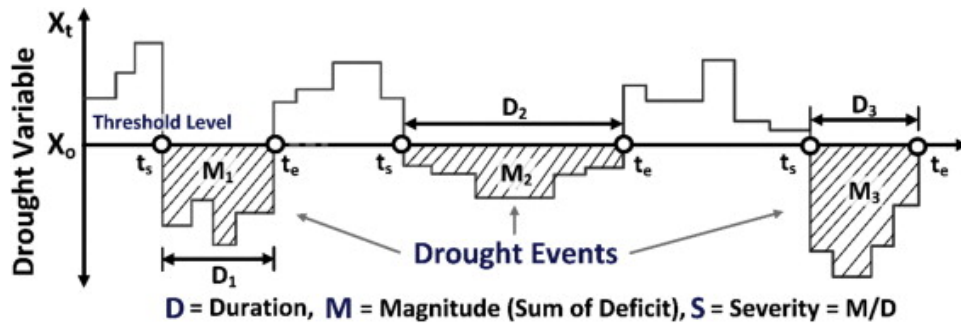


Figure 5.3. Drought characteristics using the Run theory. X_0 denotes the threshold level of the drought index (from Nam et al. 2015)

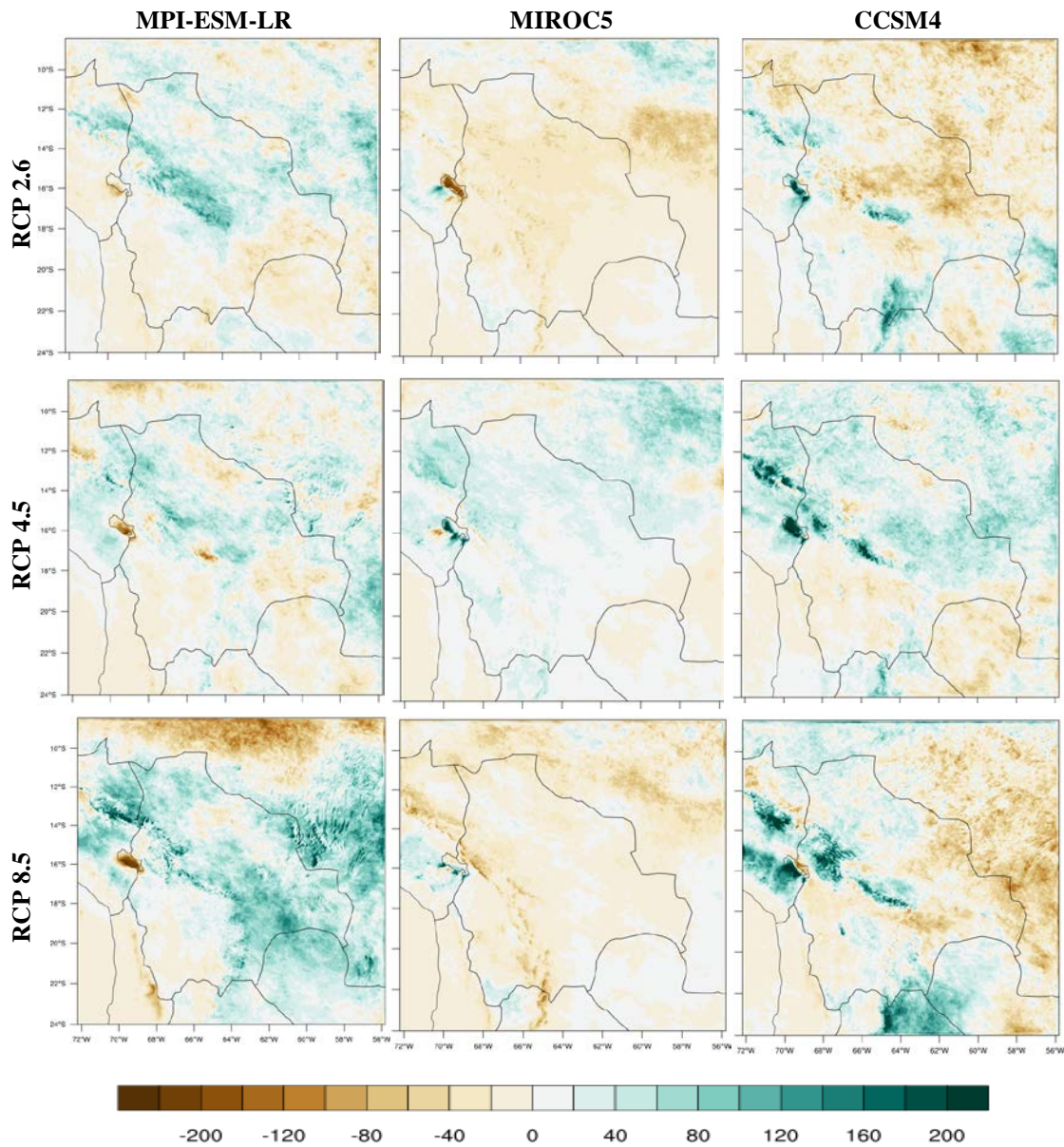


Figure 5.4. Mean seasonal change of precipitation during DJF over 2066-2080 displayed as differences (in mm) relative to the reference period (2006-2020) for three GCMs shown on the columns: MPI-ESM-LR (left), MIROC5 (middle) and CCSM4 (right) and three RCPs specified in different rows: RCP 2.6 (top), RCP 4.5 (middle) and RCP 8.5 (bottom).

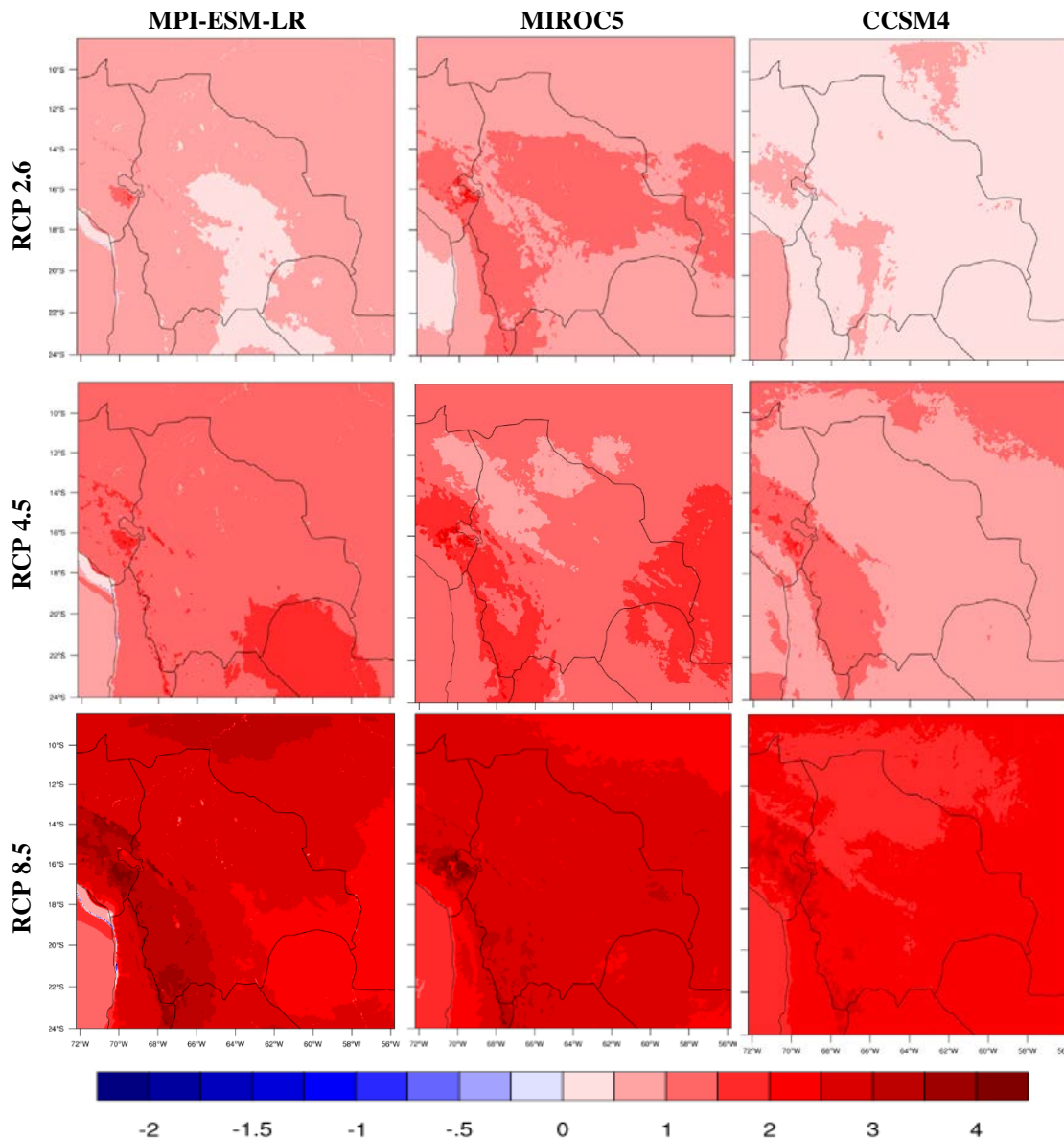


Figure 5.5. Mean seasonal change of temperature during DJF over 2066-2080 displayed as differences (in degree C) relative to the reference period (2006-2020) for three GCMs shown on the columns: MPI-ESM-LR (left), MIROC5 (middle) and CCSM4 (right) and three RCPs specified in different rows: RCP 2.6 (top), RCP 4.5 (middle) and RCP 8.5 (bottom).

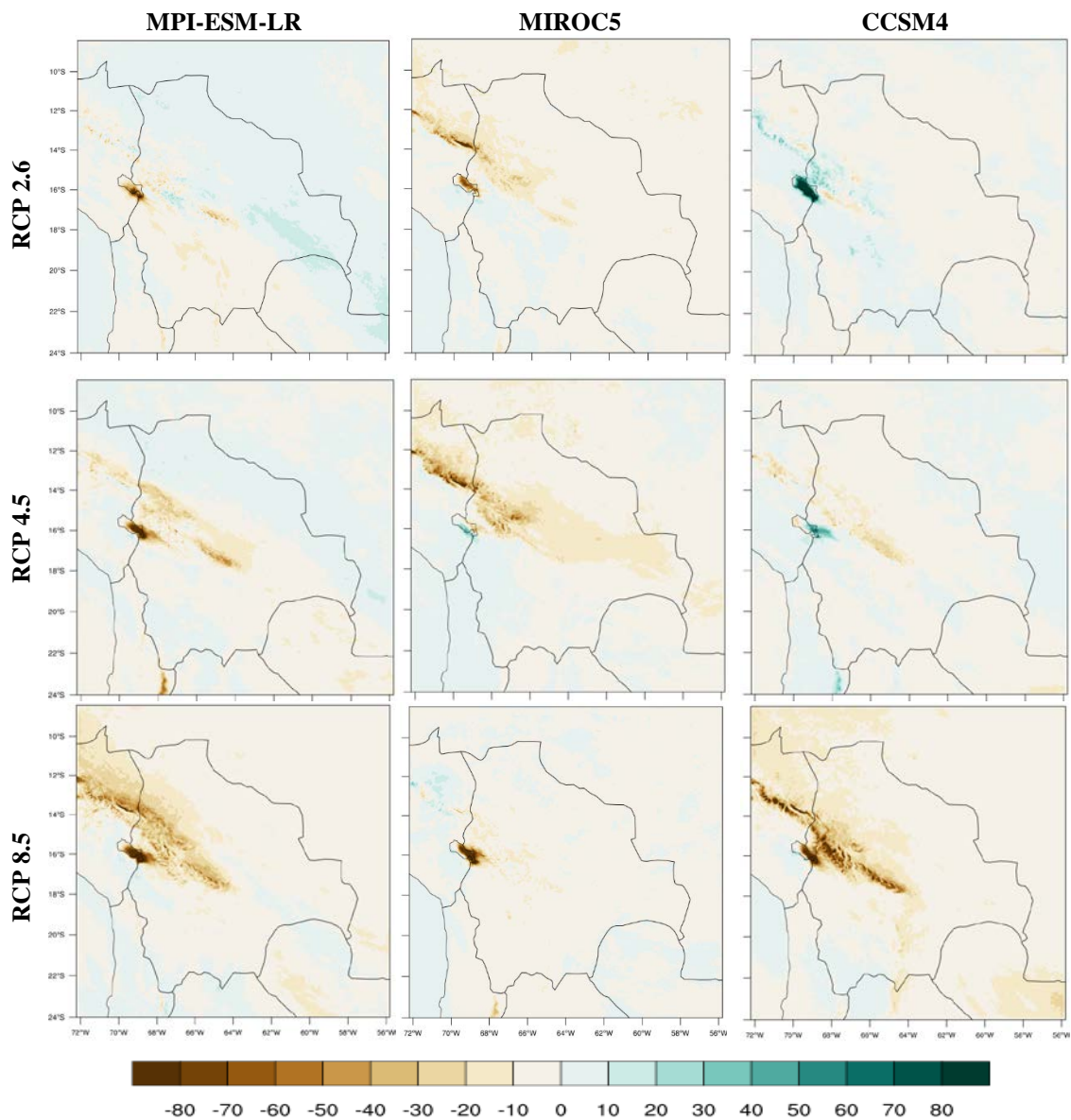


Figure 5.6. Mean seasonal change of precipitation during JJA over 2066-2080 displayed as differences (in mm) relative to the reference period (2006-2020) for three GCMs shown on the columns: MPI-ESM-LR (left), MIROC5 (middle) and CCSM4 (left) and three RCPs specified in different rows: RCP 2.6 (top), RCP 4.5 (middle) and RCP 8.5 (bottom).

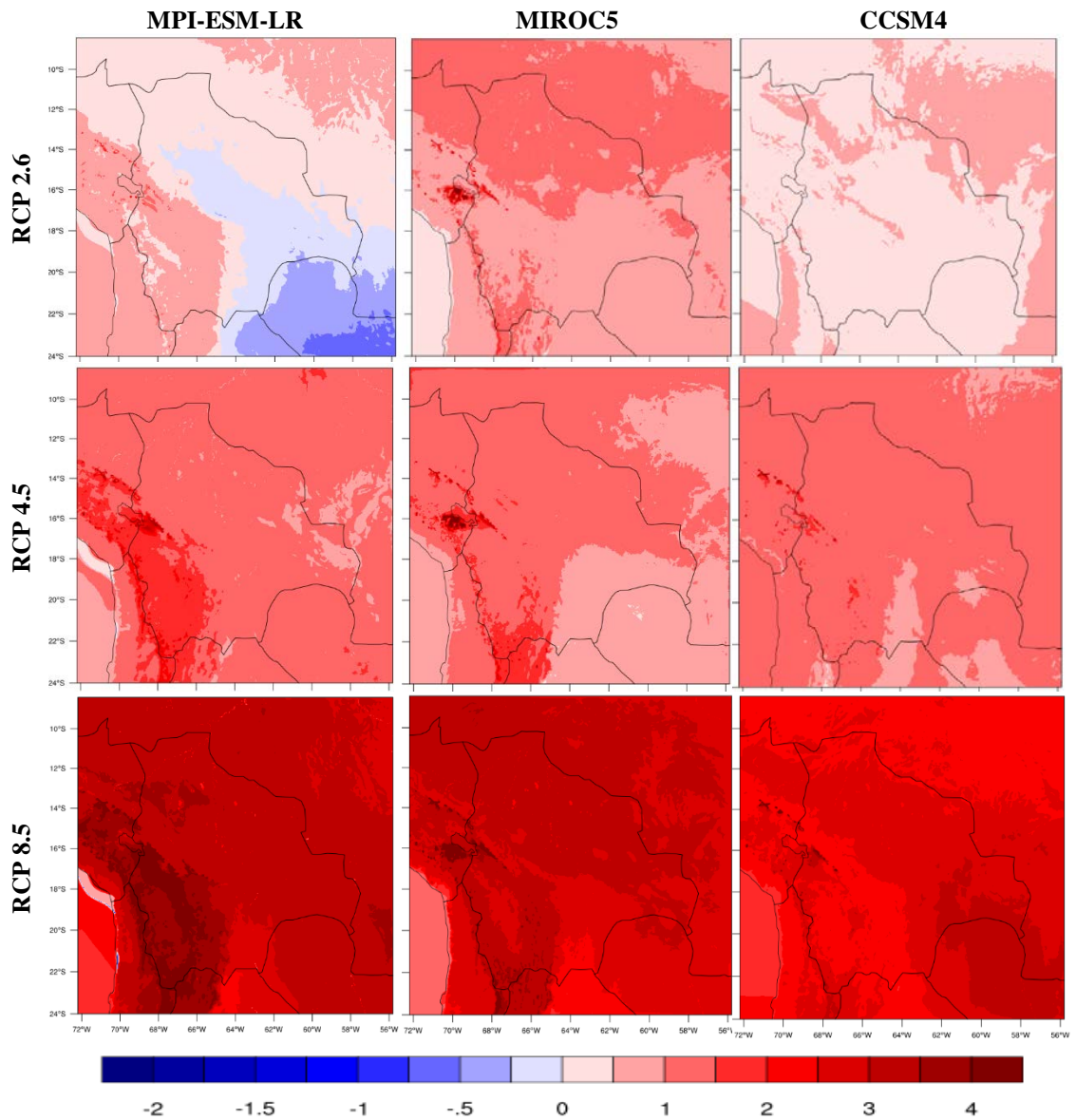


Figure 5.7. Mean seasonal change of temperature during JJA over 2066-2080 displayed as differences (in degree C) relative to the reference period (2006-2020) for three GCMs shown on the columns: MPI-ESM-LR (left), MIROC5 (middle) and CCSM4 (left) and three RCPs specified in different rows: RCP 2.6 (top), RCP 4.5 (middle) and RCP 8.5 (bottom).

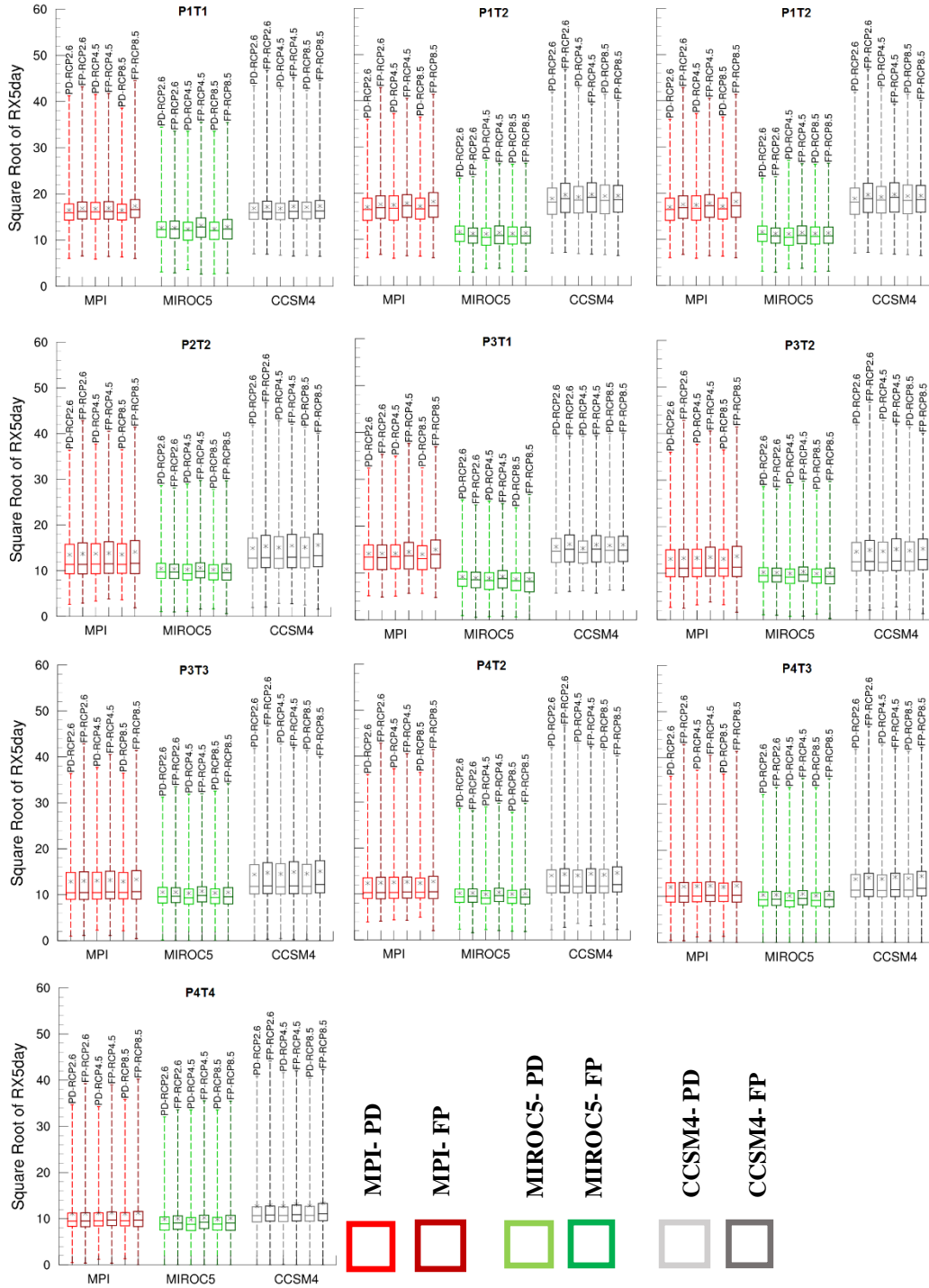


Figure 5.8. Regional present day (PD) RX5day index (in mm) values and the future projections (FP) for three GCMs and three RCPs. Boxes indicate the interquartile range for the RX5day index values over 15 years considering all the gridpoints in the region. See Fig. 3.4 for boxplot details.

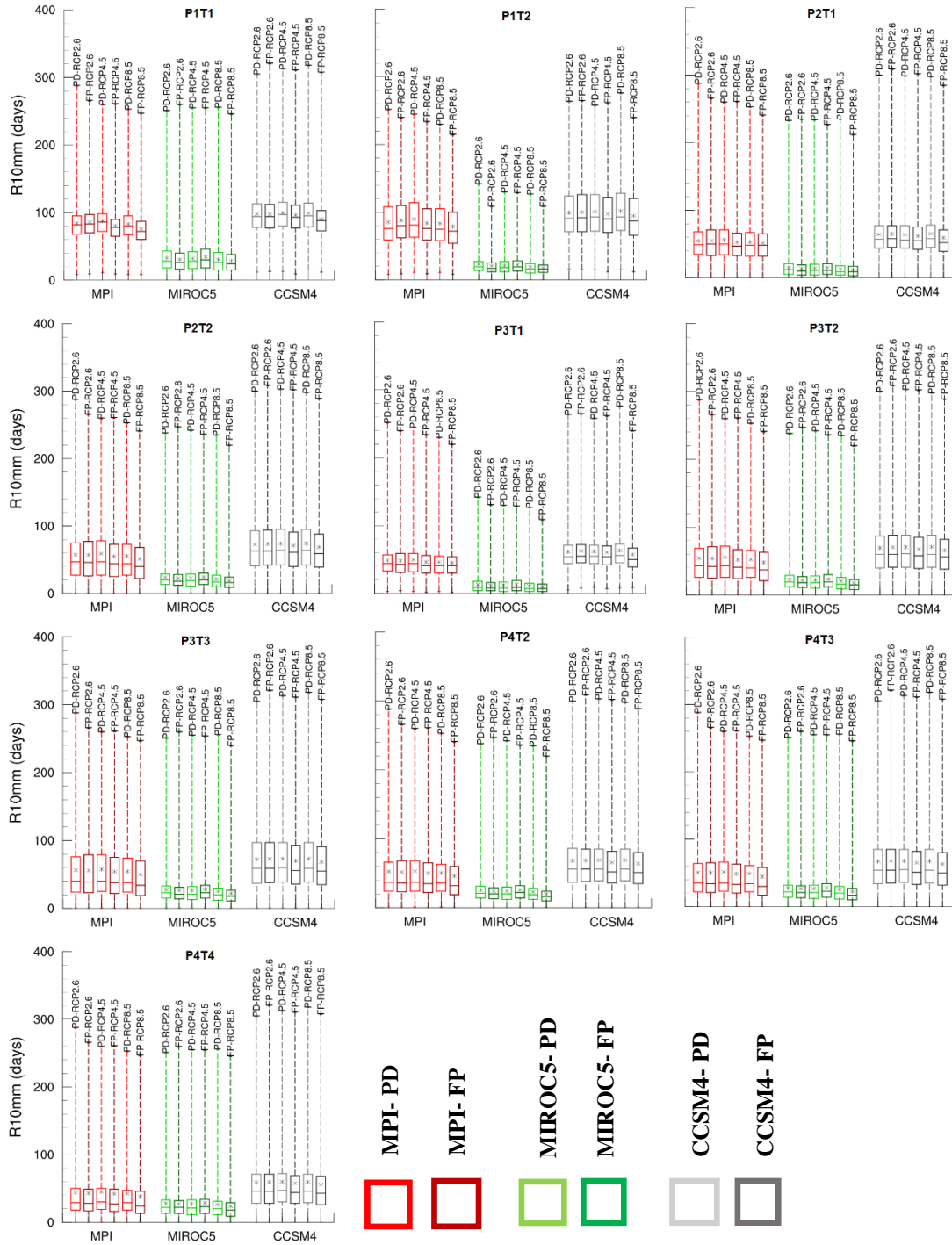


Figure 5.9. Regional present day (PD) R10mm index (in days) values and the future projections (FP) for three GCMs and three RCPs. Boxes indicate the interquartile range for the R10mm index values over 15 years considering all the gridpoints in the region. See Fig. 3.4 for boxplot details.

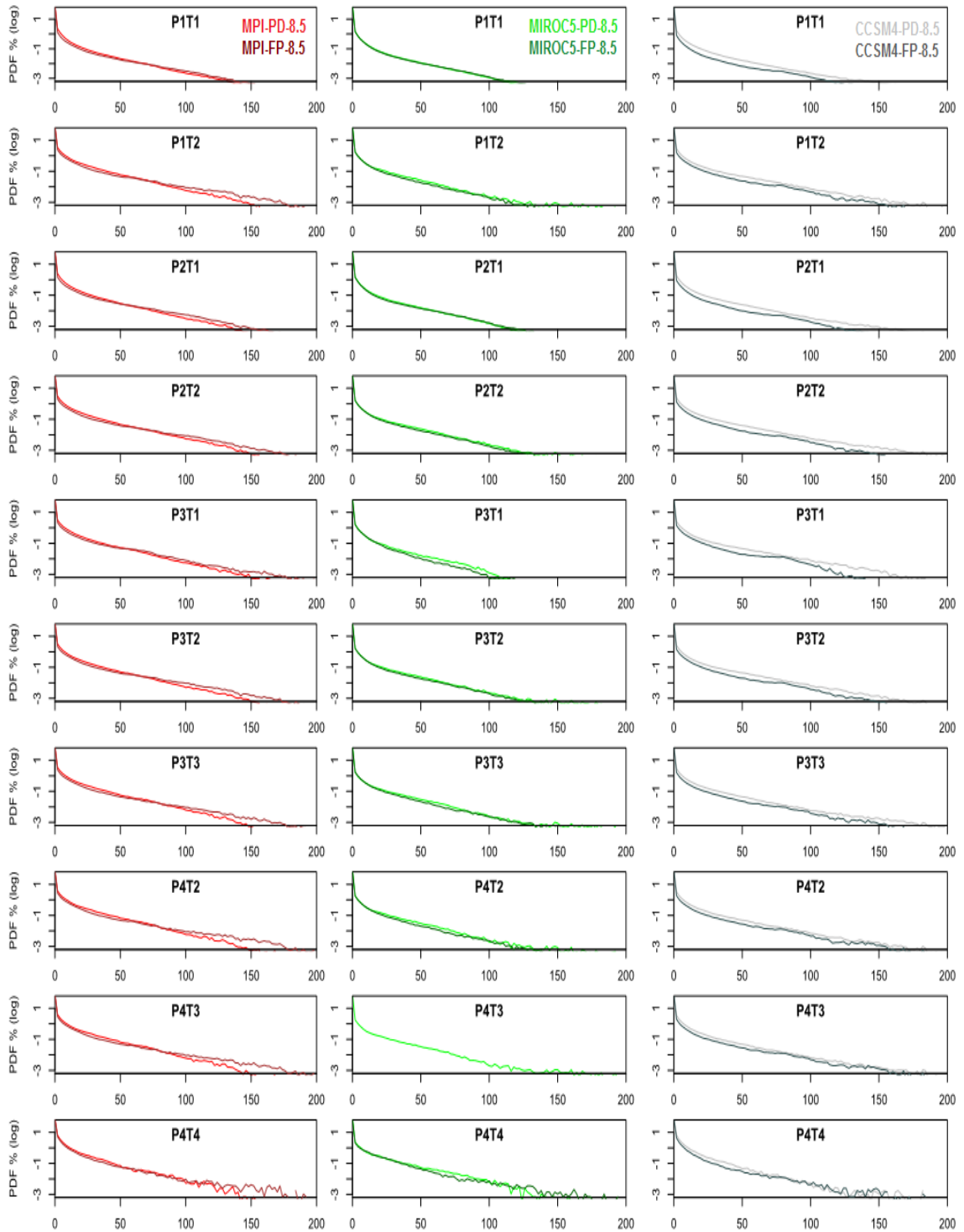


Figure 5.10. Frequency distributions of daily precipitation for present day (PD) and future projections (FP) under RCP 8.5 during DJF season for ten climate subregions. Each column represents a GCM-driven WRF simulations: MPI-ESM-LR (left), MIROC5 (middle) and CCSM4 (right). The vertical axis is shown on the log scale.

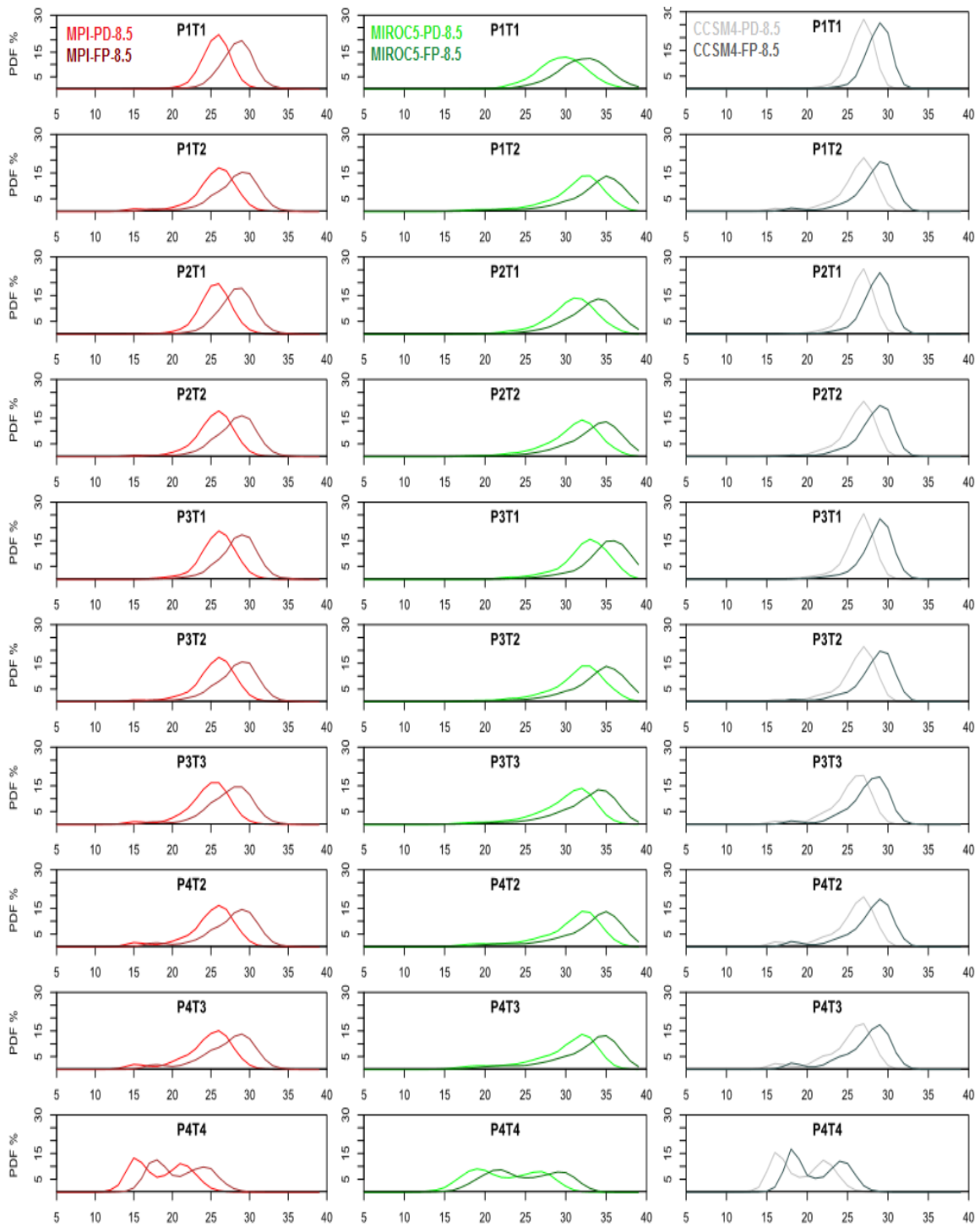


Figure 5.11. Frequency distributions of daily temperature for present day (PD) and future projections (FP) under RCP 8.5 during DJF season for ten climate subregions. Each column represents a GCM-driven WRF simulations: MPI-ESM-LR (left), MIROC5 (middle) and CCSM4 (right).

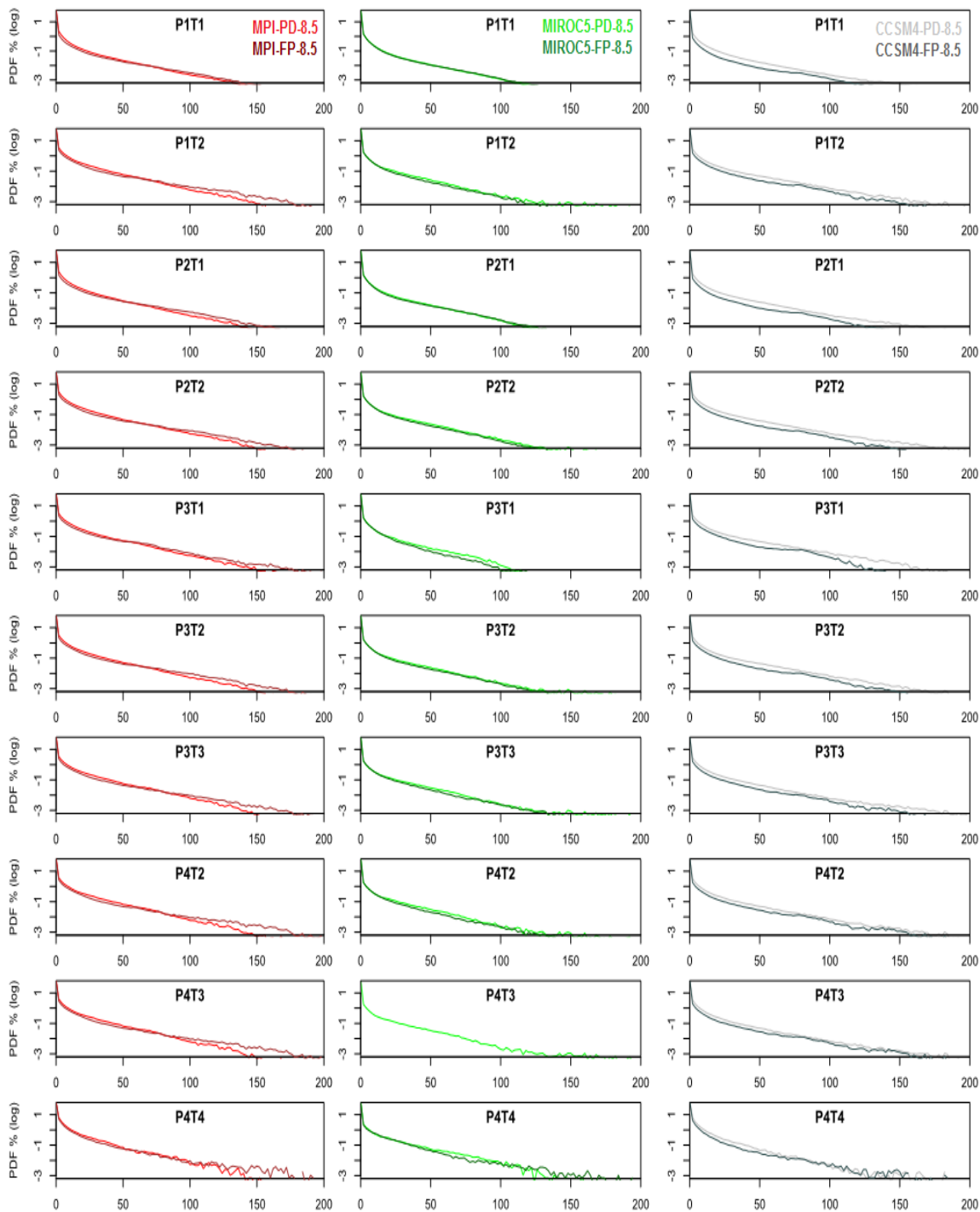


Figure 5.12. Frequency distributions of daily precipitation for present day (PD) and future projections (FP) under RCP 8.5 during JJA season for ten climate subregions. Each column represents a GCM-driven WRF simulations: MPI-ESM-LR (left), MIROC5 (middle) and CCSM4 (right). The vertical axis is shown on the log scale.

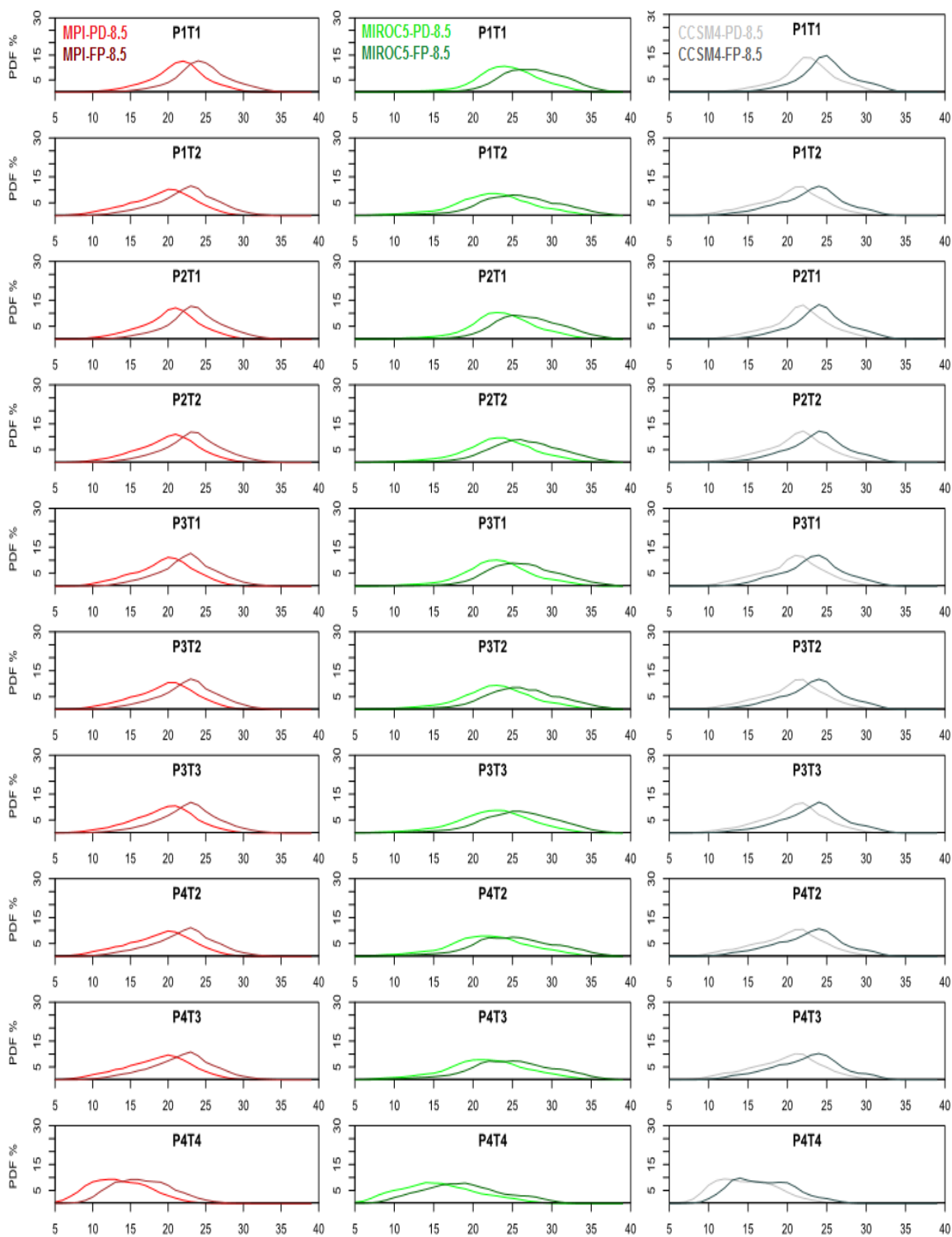


Figure 5.13. Frequency distributions of daily temperature for present day (PD) and future projections (FP) under RCP 8.5 during JJA season for ten climate subregions. Each column represents a GCM-driven WRF simulations: MPI-ESM-LR (left), MIROC5 (middle) and CCSM4 (right).

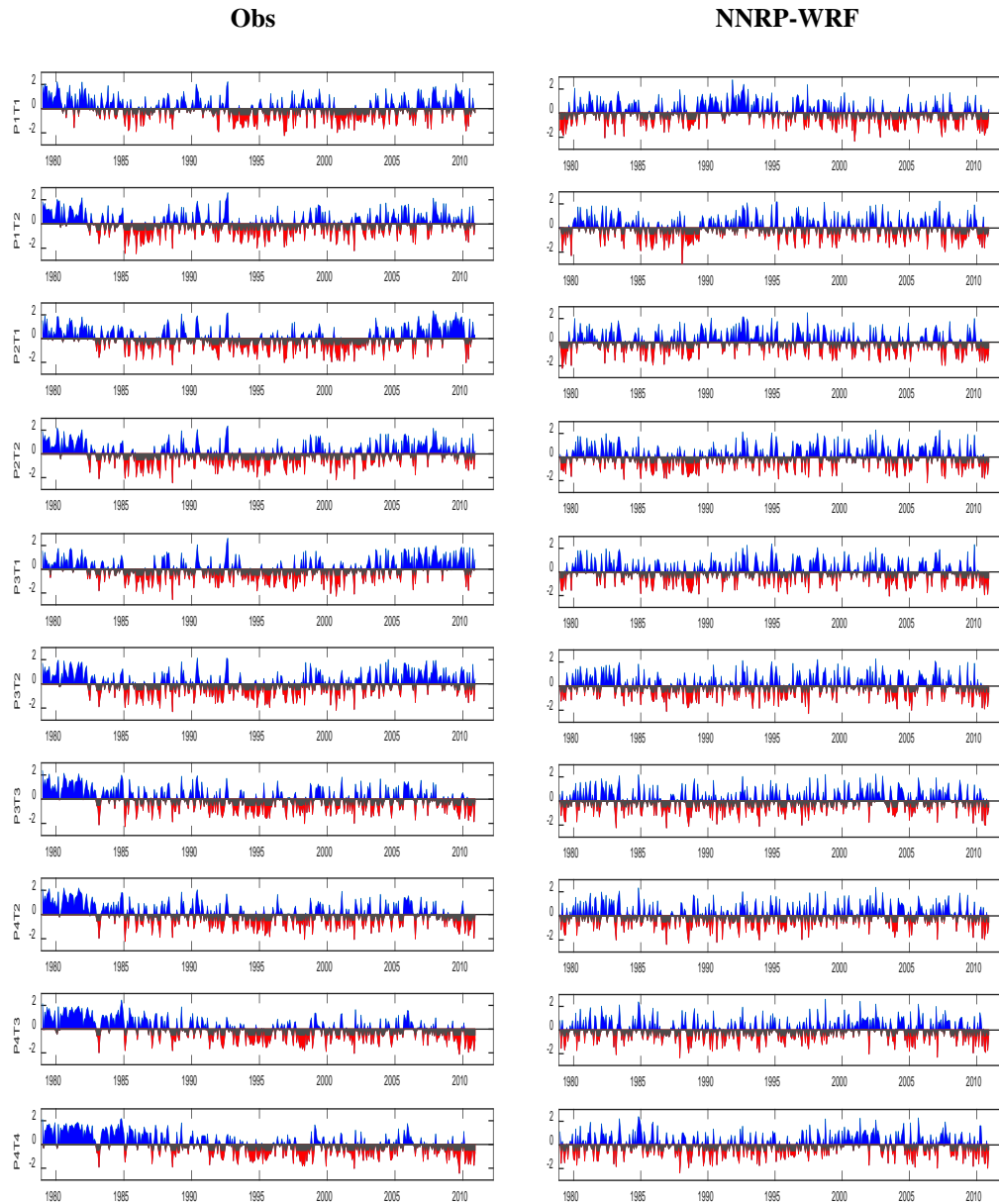


Figure 5.14. Time series of 1-month SPEI using observations (left) and NNRP-driven WRF (right) for the period of 1979-2012. The gray shading represent $-0.5 \leq \text{SPEI} \leq 0$ as the blue and red shadings show the wet and dry years with respectively SPEI values > 0 and ≤ -0.5 .

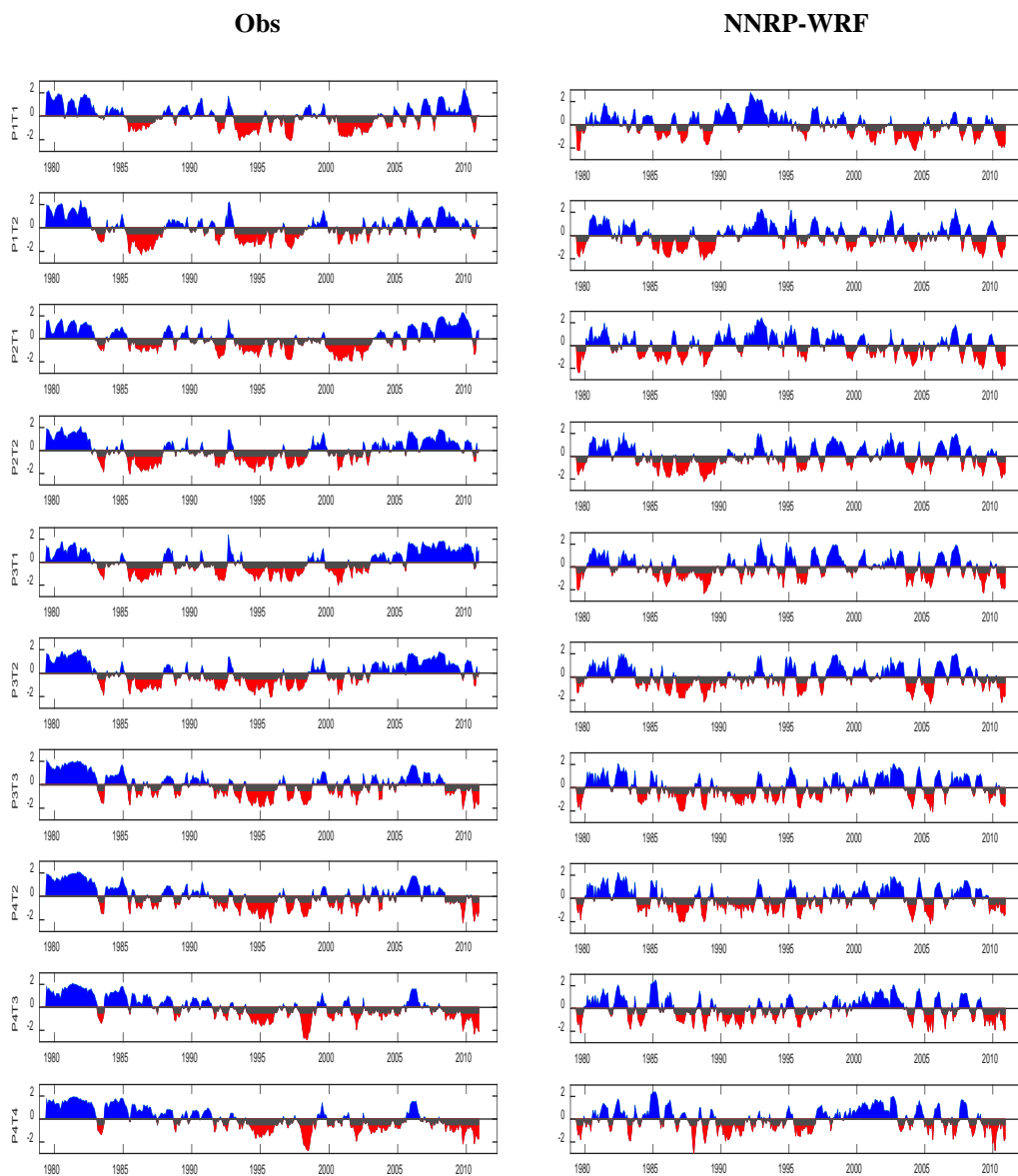


Figure 5.15. Time series of 6-month SPEI using observations (left) and NNRP-driven WRF (right) for the period of 1979-2012. The gray shading represent $-0.5 \leq \text{SPEI} \leq 0$ as the blue and red shadings show the wet and dry years with respectively SPEI values > 0 and ≤ -0.5 .

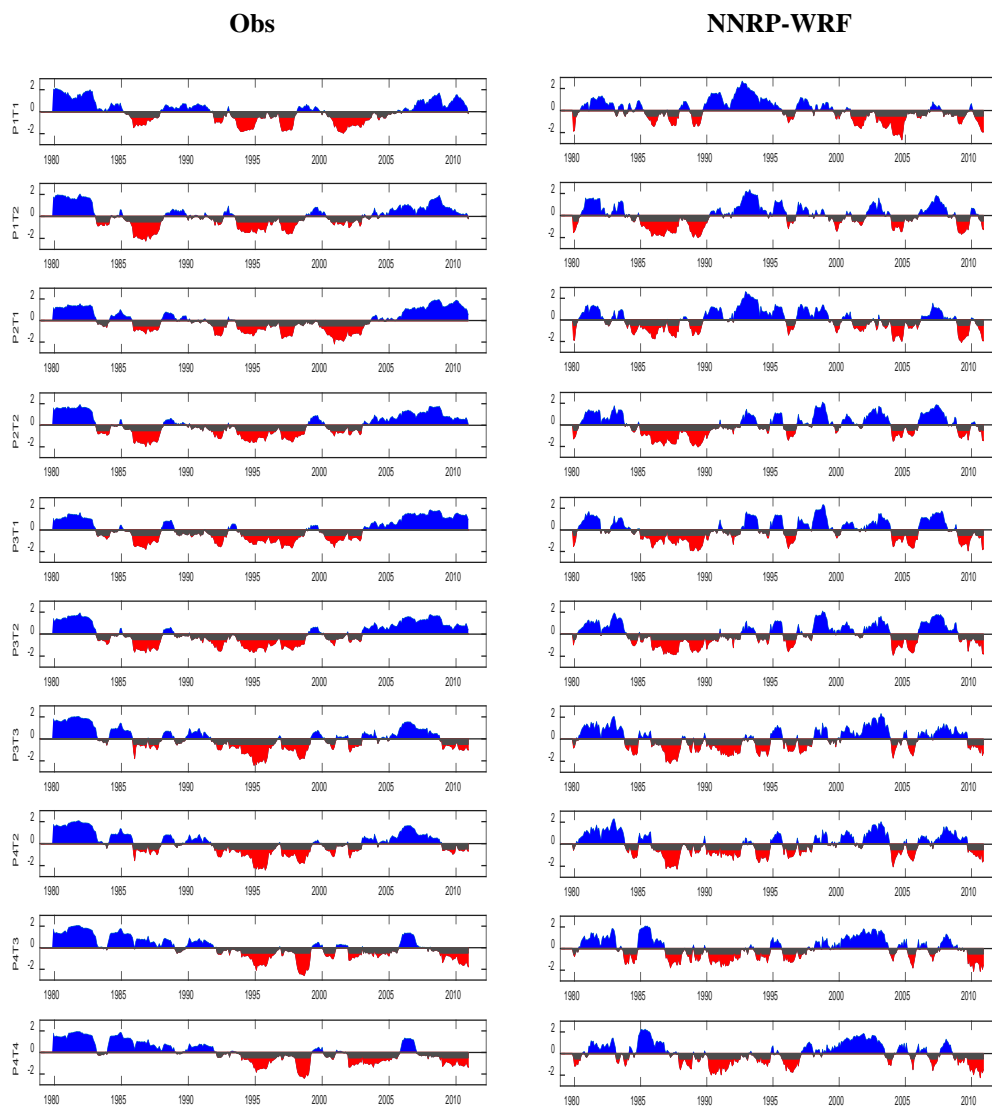


Figure 5.16. Time series of 12-month SPEI using observations (left) and NNRP-driven WRF (right) for the period of 1979-2012. The gray shading represent $-0.5 \leq \text{SPEI} \leq 0$ as the blue and red shadings show the wet and dry years with respectively SPEI values > 0 and ≤ -0.5 .

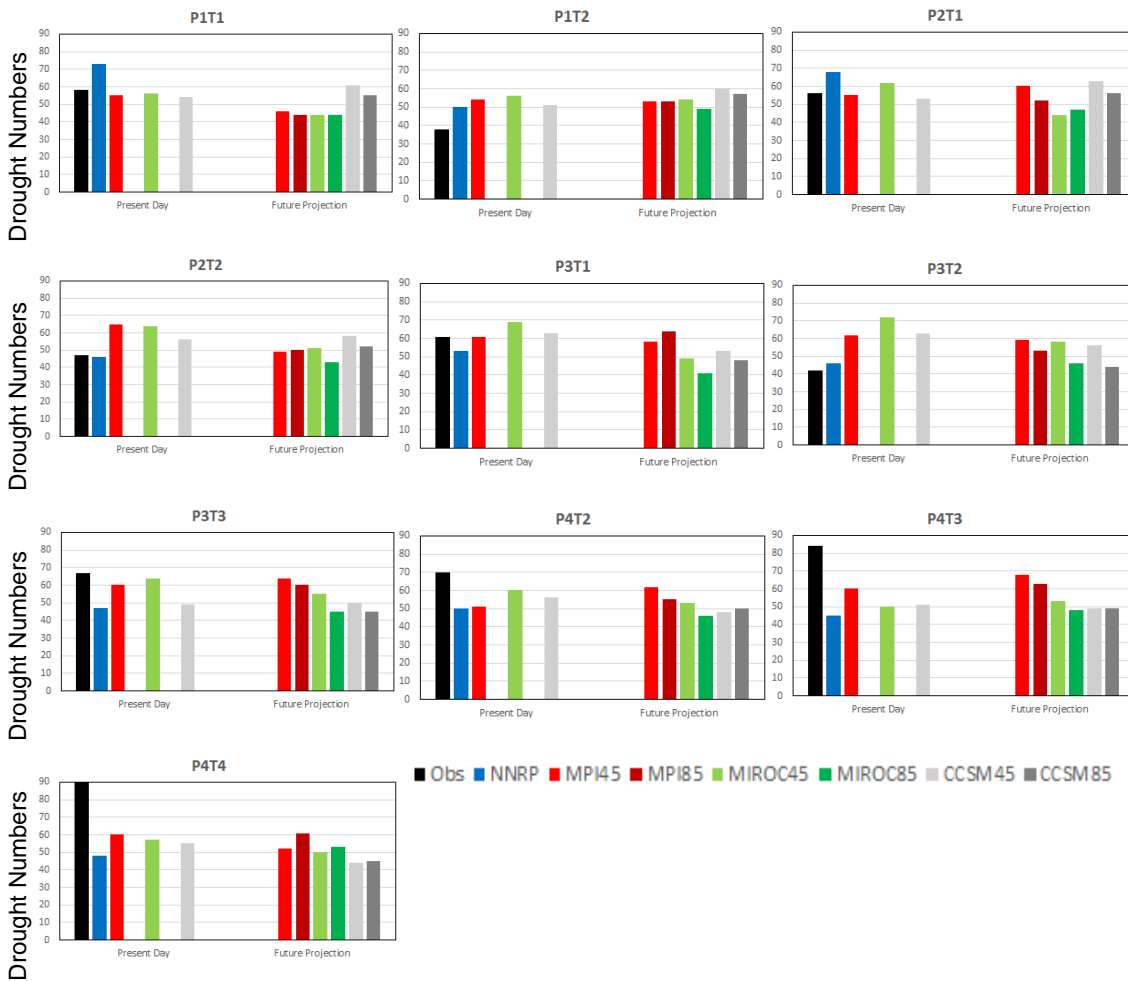


Figure 5.17. Temporal change in the number of drought events defined by SPEI values ≤ -0.5 . The results are presented in two sections of “Present Day” (2006-2020) and “Future Projection” (2088-2080). For simplicity, only the results for RCP 4.5 are shown for the present day and future projection results are presented in RCP 4.5 and RCP 8.5. The Observation (1996-2010) and NNRP-driven WRF (1996-2010) are shown for evaluating the ability of GCM-driven WRF simulations in reproducing the results in their equivalent present day.

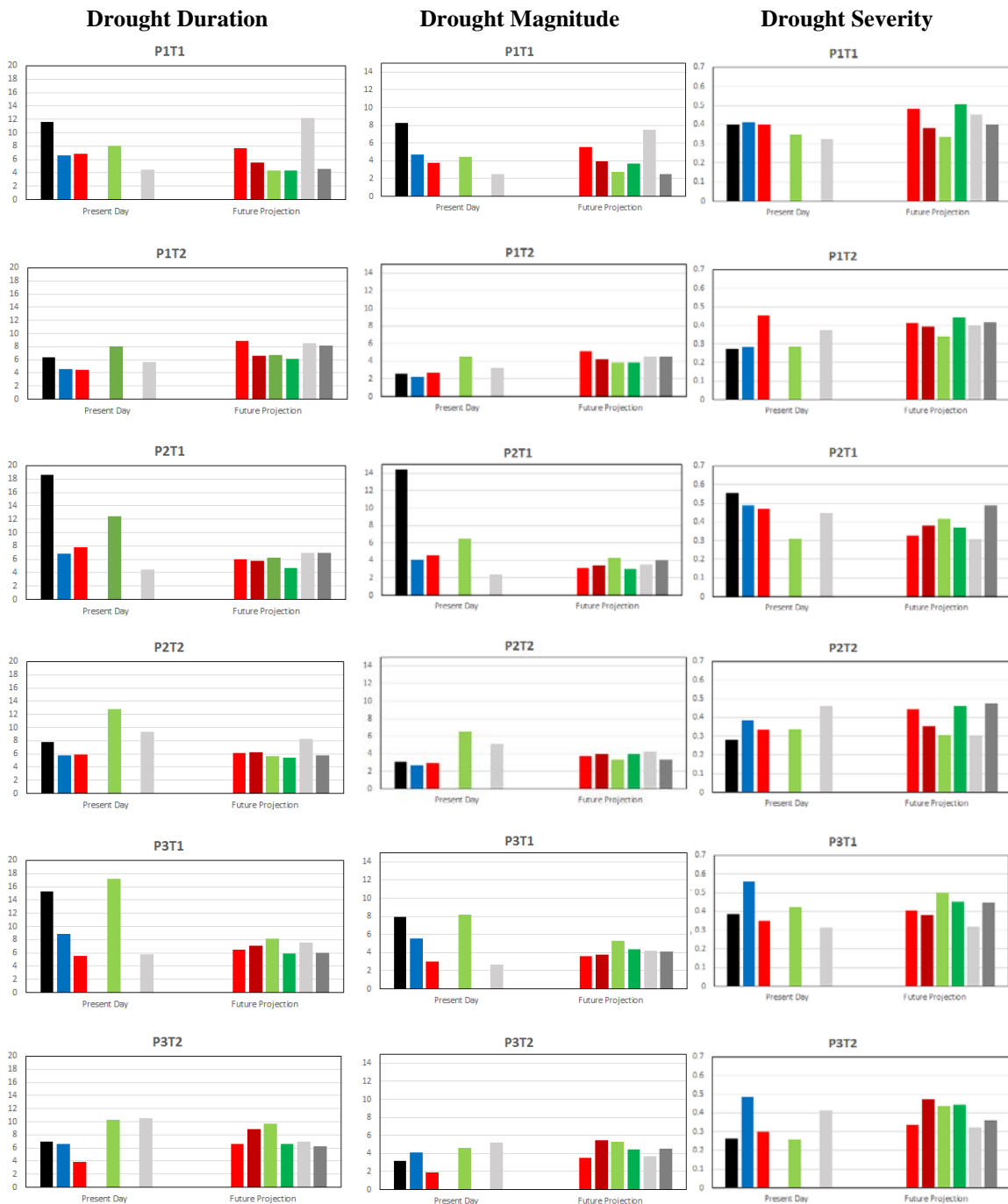


Figure 5.18. Temporal change in the drought statistical characteristics of duration, magnitude and severity. The results are presented in two sections of “Present Day” (2006-2020) and “Future Projection” (2066-2080). For simplicity, only the results for RCP 4.5 are shown for the present day and future projection results are presented in RCP 4.5 and RCP 8.5. The Observation (1996-2010) and NNRP-driven WRF (1996-2010) are shown for evaluating the ability of GCM-driven WRF simulations in reproducing the results in their equivalent present day.

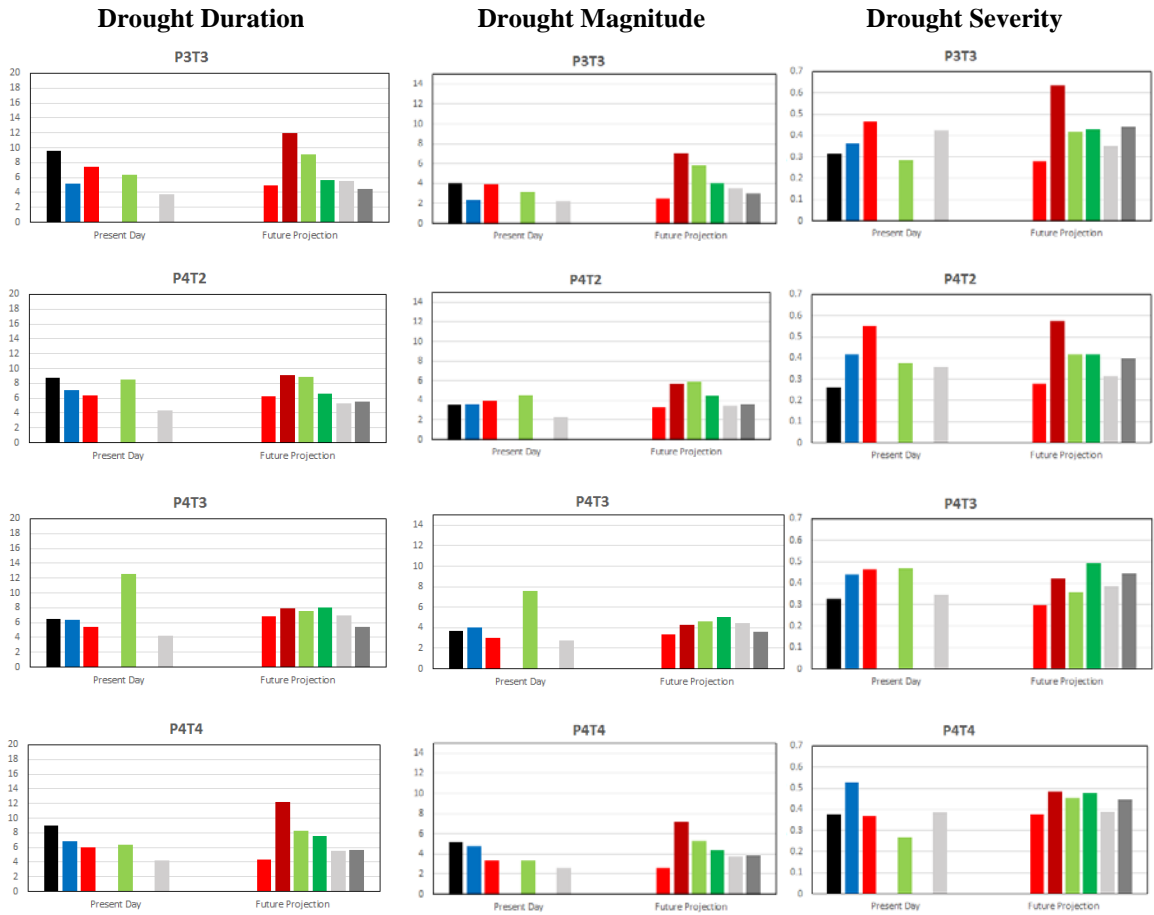


Figure 5.18. (Continued)

Chapter 6

Conclusions

Bolivia is home to almost 11 million people and a huge variety of floral and faunal species living in a range of climates from the tropical wet and humid Amazon rainforests in the lowlands to the polar desert type climate in the elevated Altiplano in the Andes, which hosts one of the largest glaciated area in the tropics. A large portion of the country, particularly the rural areas, relies on the agriculture as of their only source of subsistence.

Among these societies, the most vulnerable to climate change are the poor people from the higher valleys, where water availability is a challenge, and the communities residing in the flood-prone regions along the riverbeds in the lowlands. The low incomes and limited resources of such communities make those communities more vulnerable to the impact of climate change as they cannot develop adaptation plans to mitigate such impacts. Therefore, an understanding of how the biodiverse microclimates of Bolivia might respond to climate change is of significant importance to the scientific community, policymakers, and inhabitants.

Climate change assessment is a process demanding high resolution future climate data to study the impacts at local scales where they are felt. Due to the computational constraint on the power of the supercomputers such high resolution climate data are not readily available over the entire globe and are only presented in coarse resolution of 100-200 km in GCM outputs. To fill this gap in impact studies and to provide a better understanding of the regional climate, scientists have developed regional climate models, operating similar to GCMs but over a limited domain, to downscale such coarse resolution data to finer scales (<10 km) to assess climate change on regional scales. In the downscaling process, the uncertainties emerge from different sources including the parent

GCMs, the regional climate model internal structure, emission scenarios representing alternative futures and observational datasets.

This study applies a comprehensive dynamical downscaling strategy using the WRF regional climate model to assess the potential climate change impacts in Bolivia in the latter part of the current century. Beginning with eight GCMs with well-documented performance in simulating the historical circulation over South America, an evaluation in terms of temperature and precipitation, lower- and upper-level winds, and vertically integrated moisture transport was conducted, with a specific focus on Bolivia during its wet and dry seasons. The results show the successful performance of three GCMs (MPI-ESM-LR, MIROC5 and CCSM4) in reproducing the larger atmospheric circulation of South America including Bolivia (Abadi et al. 2018a). The atmospheric circulation resulting from these coarse global model simulations can then be used for initializing the WRF model.

Prior to evaluating the ability of WRF in proper downscaling, a climate classification was developed using a combined approach of nonhierarchical k -means and consensus clustering techniques on precipitation and temperature observational datasets (Abadi et al. 2018b). This approach yielded ten homogeneous climate subregions for Bolivia that were then used as a framework for the remainder of the study. The shape and extent of the final climate regions show the influence of the South American Monsoon System on the precipitation as the rainfall rate is highest in Amazonia and drops toward the higher terrain of the Altiplano. The regions are also distinguished by the gradual decrease in the temperature from in the lowlands toward the highlands. This regionalization allows for the evaluations of downscaling results over these climatically

homogeneous regions of Bolivia, rather than over the entire country or more arbitrary zonations.

Evaluation of the reanalysis- and the GCM-driven WRF downscaling simulations for the present day climate shows that these simulations are controlled principally by the forcing data, as MIROC5-WRF simulations were different from the other WRF simulations and largely mirrored the differences among the forcing datasets. For the present-day climate, evaluation of WRF downscaled data, reveals that the WRF model tends to overestimate precipitation mainly in the summer months when the precipitation is convective in nature (Abadi et al. 2018c). However, comparing the results in different spatial resolutions of 36, 12 and 4 km clearly illustrate the value added by the higher resolutions simulations, particularly in the regions with complex topography (Appendix A), as the frequency and intensity of heavy precipitation events gets closer to the observed. These results reaffirm the need for higher resolution climate data for proper impact studies.

As one of the most robust evaluating techniques, we also performed comparisons between the station measurements and the nearest model grid points. The six selected stations are scattered across the country with Trinidad and San Jose located in the northern and eastern lowlands and the rest lie on the higher terrain. This evaluation showed that, though the WRF simulations improve with higher resolutions over the Andes, there are still some disagreements with the model simulations versus observations. These biases will potentially decrease by using a higher resolution observational datasets as well as increasing the resolution of the simulations. Evaluations

on the regional scale render the same results showing improvement with higher resolution simulations over the Andes.

Finally, an investigation into the change in the mean climatic pattern and extremes as the difference between future projections and the reference period was performed (Abadi et al. 2018d). RCM projections generally show precipitation and temperature increases in the lowlands, especially in one of the wettest regions of the country, El Chapare, and precipitation decreases and more pronounced temperature increases over the highlands, where water shortage and rapid deglaciation is already a concern. This affirms the common statement that the “wet gets wetter and dry gets drier.” These projected changes will add to the vulnerabilities of the flood-prone regions of the lowlands to a higher risk of flooding and the drought-prone regions in the highlands to drier conditions as well as faster glacier retreat, exacerbating impacts on the regions’ water supplies. Additionally, drought characteristic changes show that lowland droughts are getting shorter in length but becoming more severe, while for the highlands, the changes in duration, magnitude and severity of drought are all positive which confirms the higher sensitivity of the mountainous regions to climate change.

Confirming the results in the World Bank Group climate change study on Bolivia (2010), our findings add more confidence in the taken adaptation measures. The World Bank study shows that improving agricultural practices have higher priority in the lowlands than water management, as water is more abundant in those regions. In contrast, the higher valleys, already suffering from water shortages, put priority on water management, followed by improved agricultural and livestock practices. The results presented in this dissertation show that existing measures should be expanded in the

higher valleys as higher temperature and lower rainfall will result in greater agricultural loss, crop and animal diseases, and health consequences. The situation in the lowlands is quite opposite as our results confirm a wetter scenario. Although the soybean production will benefit from a warmer and wetter climate in the lowlands (World Bank 2010), the region should be more prepared for the potential crop loss and damage due to the increased extreme precipitation events.

In conclusion, the present study restates the significance of providing reliable, high-resolution climate data in impact studies. It is hoped that the results here will be improved by even higher spatial resolution climate data and eventually lead to modified mitigation and adaptation strategies to minimize the adverse impacts of climate change in the more vulnerable regions of Bolivia. Moreover, the methodology used here is completely transferable to other regions of the world and can be utilized to provide similar high-resolution data for policy- and decision-makers in those regions.

References

- Abadi AM, Oglesby RJ, Rowe CM et al (2018a) Evaluation of GCMs historical simulations of monthly and seasonal climatology over Bolivia. *Clim Dyn* (2018) 51:733–754
doi: 10.1007/s00382-017-3952-y
- Abadi AM, Rowe CM, Andrade MF (2018b) Climate classification in Bolivia: A combination of nonhierarchical and consensus clustering analyses based on precipitation and temperature
- Abadi AM, Rowe CM, Oglesby RJ (2018c) Climate change impact assessment over Bolivia using the WRF high-resolution dynamical downscaling I: Evaluation of the present-day climate
- Abadi AM, Rowe CM, Hayes M (2018d) Climate change impact assessment over Bolivia using the WRF high-resolution dynamical downscaling II: A case study for drought
- World Bank (2010) Adaptation to climate change vulnerability assessment and economic aspects - Plurinational state of Bolivia (English). Washington, DC: World Bank.
<http://documents.worldbank.org/curated/en/642891468162260845/Adaptation-to-climate-change-vulnerability-assessment-and-economic-aspects-BR-Plurinational-state-of-Bolivia>

Appendices

A. This section provides the supplementary material for chapter 4.

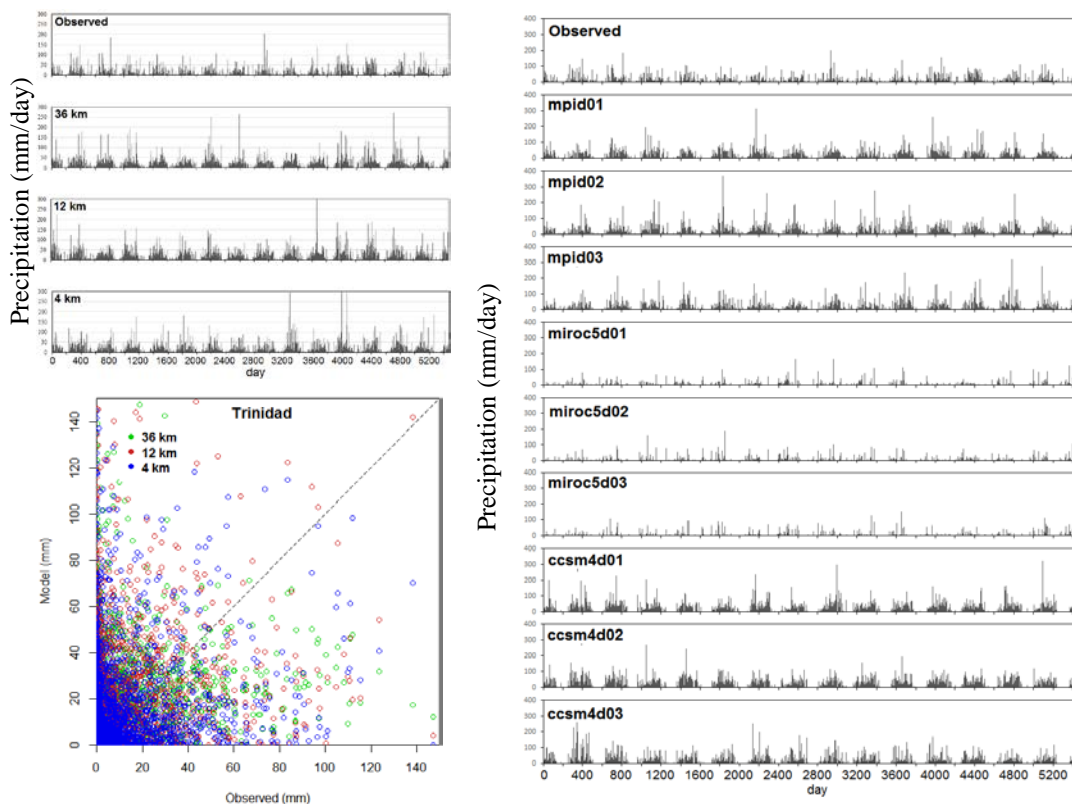


Figure A.1 Trinidad, (a) precipitation time series of observed versus reanalysis-driven WRF for the period of 1996-2010, (b) precipitation scatterplot of reanalysis-driven WRF versus observed, and (c) precipitation time series of observed (1996-2010) versus GCM-driven WRF for the period of 2006-2020.

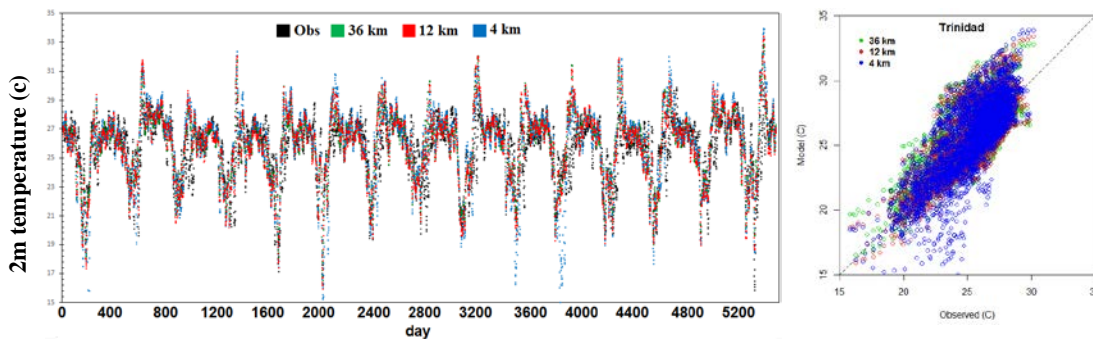


Figure A.2 Trinidad, (a) temperature time series (10-day running average) of observed versus reanalysis-driven WRF for the period of 1996-2010, (b) temperature scatterplot of reanalysis-driven WRF versus observed.

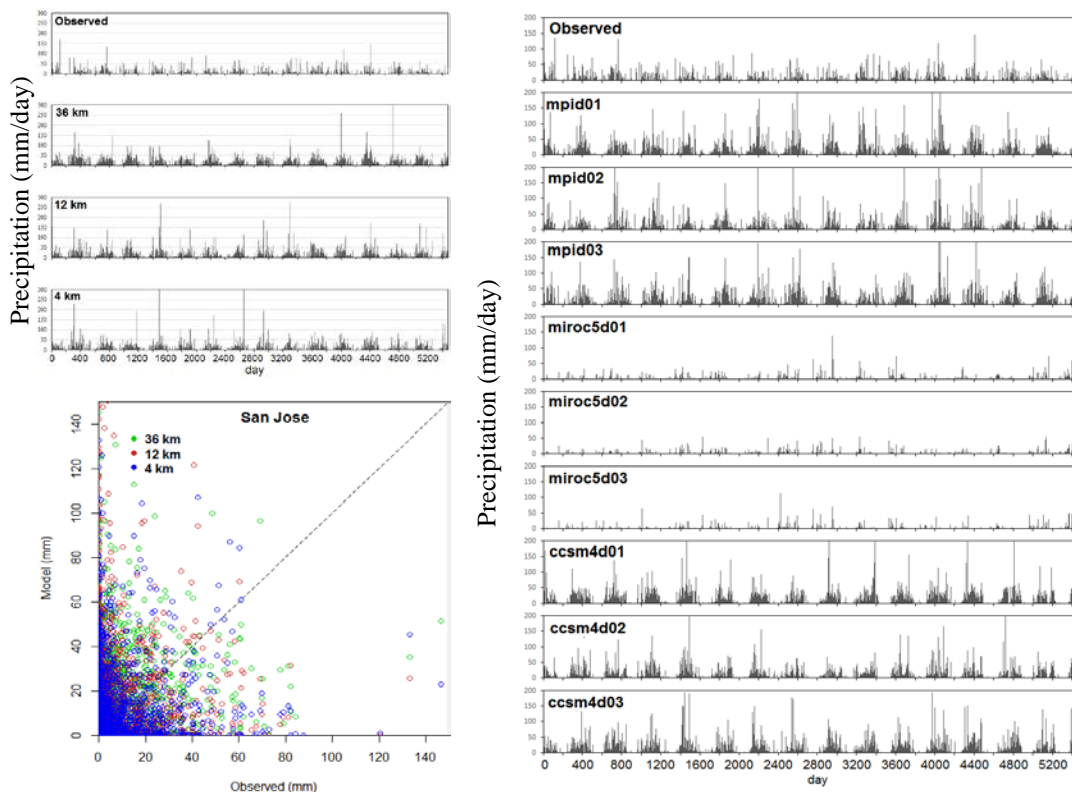


Figure A.3 San Jose, (a) precipitation time series of observed versus reanalysis-driven WRF for the period of 1996-2010, (b) precipitation scatterplot of reanalysis-driven WRF versus observed and (c) precipitation time series of observed (1996-2010) versus GCM-driven WRF for the period of 2006-2020

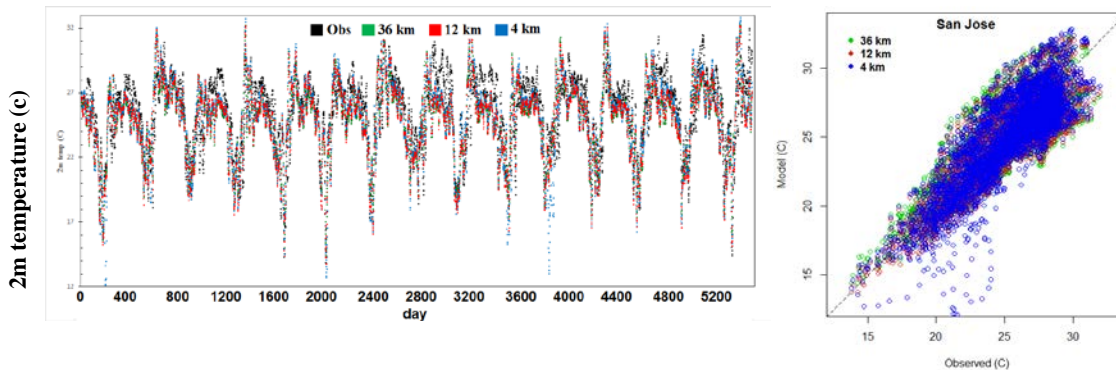


Figure A.4 San Jose, (a) temperature time series (10-day running average) of observed versus reanalysis-driven WRF for the period of 1996-2010, (b) temperature scatterplot of reanalysis-driven WRF versus observed

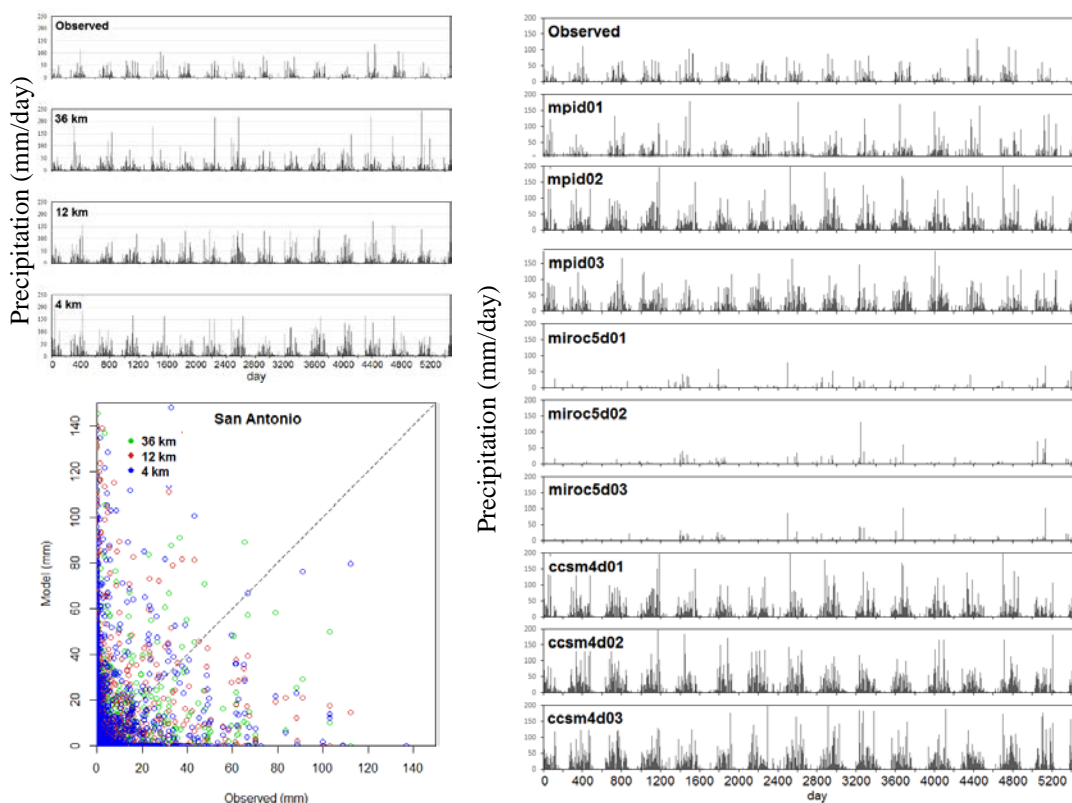


Figure A.5 San Antonio, (a) precipitation time series of observed versus reanalysis-driven WRF for the period of 1996-2010, (b) precipitation scatterplot of reanalysis-driven WRF versus observed and (c) precipitation time series of observed (1996-2010) versus GCM-driven WRF for the period of 2006-2020

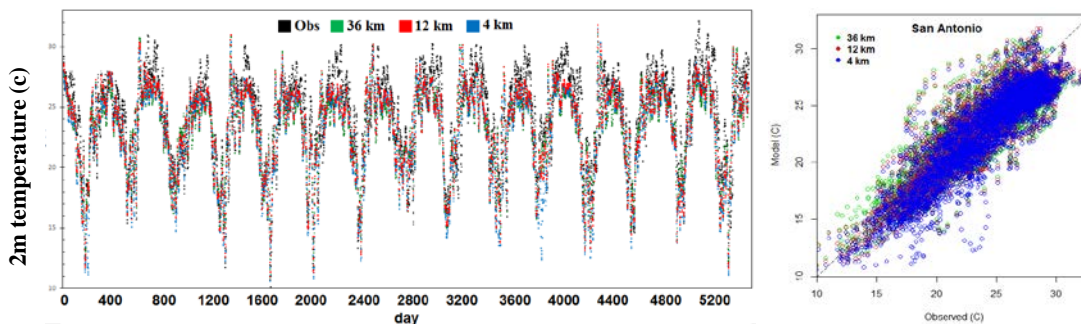


Figure A.6 San Antonio, (a) temperature time series (10-day running average) of observed versus reanalysis-driven WRF for the period of 1996-2010, (b) temperature scatterplot of reanalysis-driven WRF versus observed

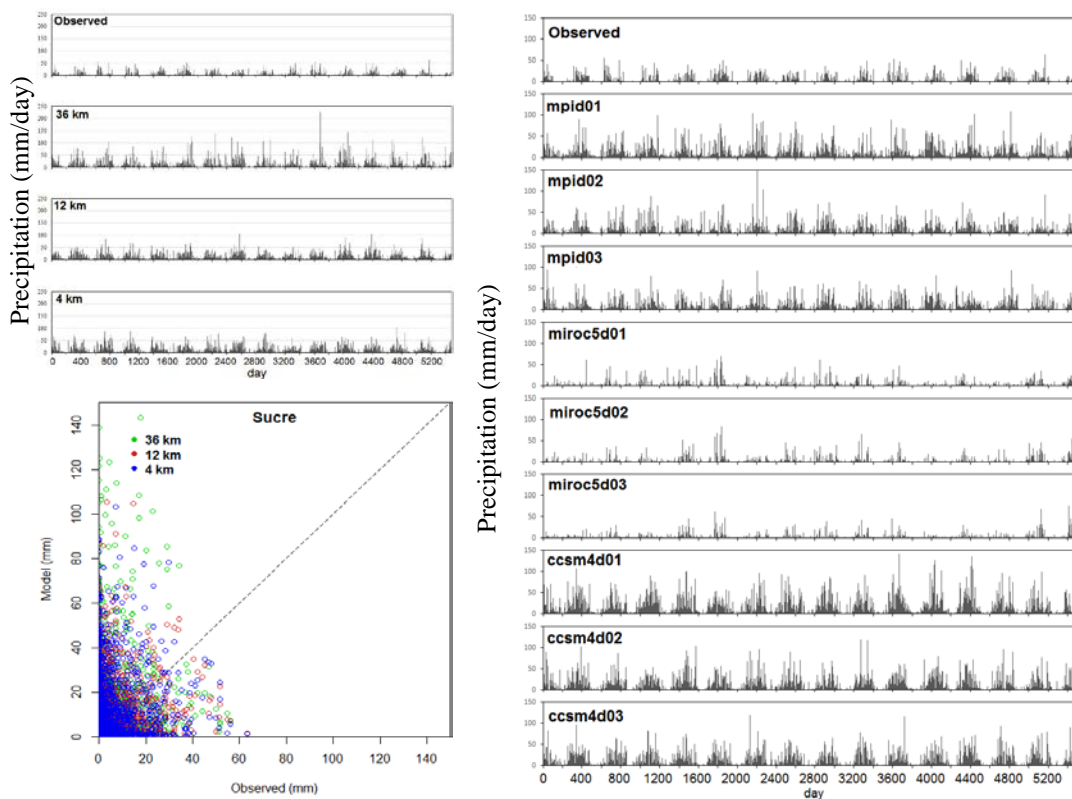


Figure A.7 Sucre, (a) precipitation time series of observed versus reanalysis-driven WRF for the period of 1996-2010, (b) precipitation scatterplot of reanalysis-driven WRF versus observed and (c) precipitation time series of observed (1996-2010) versus GCM-driven WRF for the period of 2006-2020

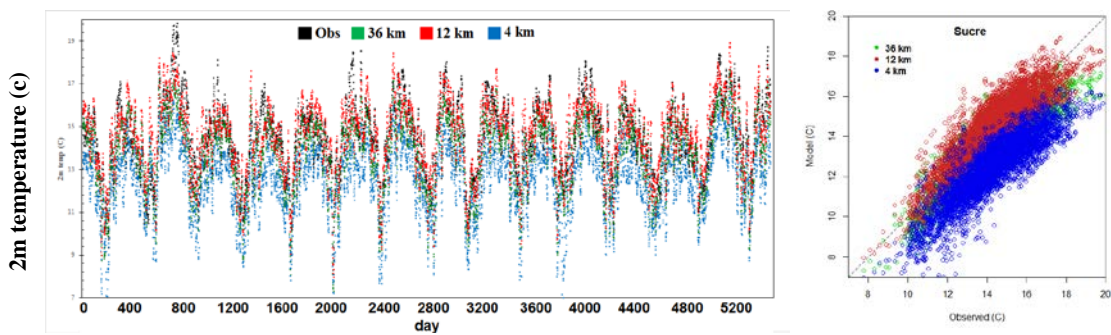


Figure A.8 Sucre, (a) temperature time series (10-day running average) of observed versus reanalysis-driven WRF for the period of 1996-2010, (b) temperature scatterplot of reanalysis-driven WRF versus observed

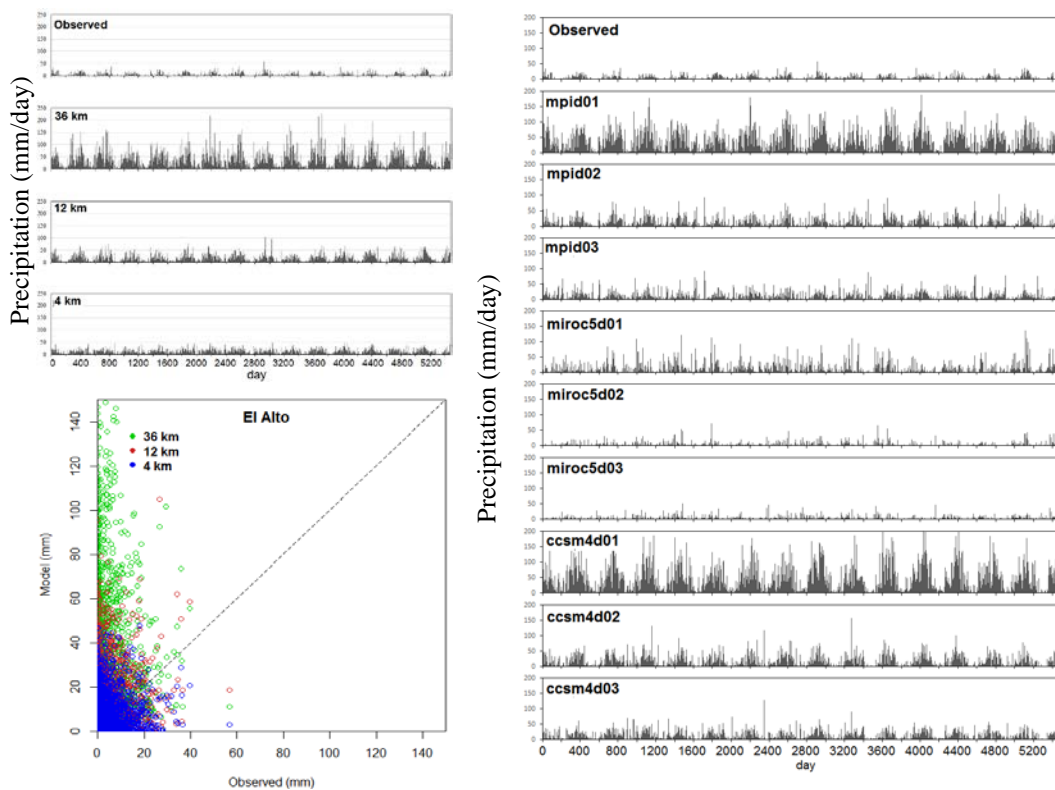


Figure A.9 El Alto, (a) precipitation time series of observed versus reanalysis-driven WRF for the period of 1996-2010, (b) precipitation scatterplot of reanalysis-driven WRF versus observed and (c) precipitation time series of observed (1996-2010) versus GCM-driven WRF for the period of 2006-2020

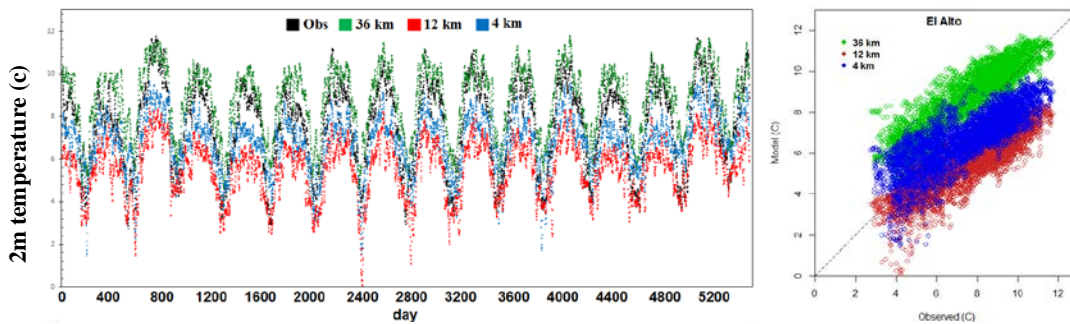


Figure A.10 El Alto, (a) temperature time series (10-day running average) of observed versus reanalysis-driven WRF for the period of 1996-2010, (b) temperature scatterplot of reanalysis-driven WRF versus observed

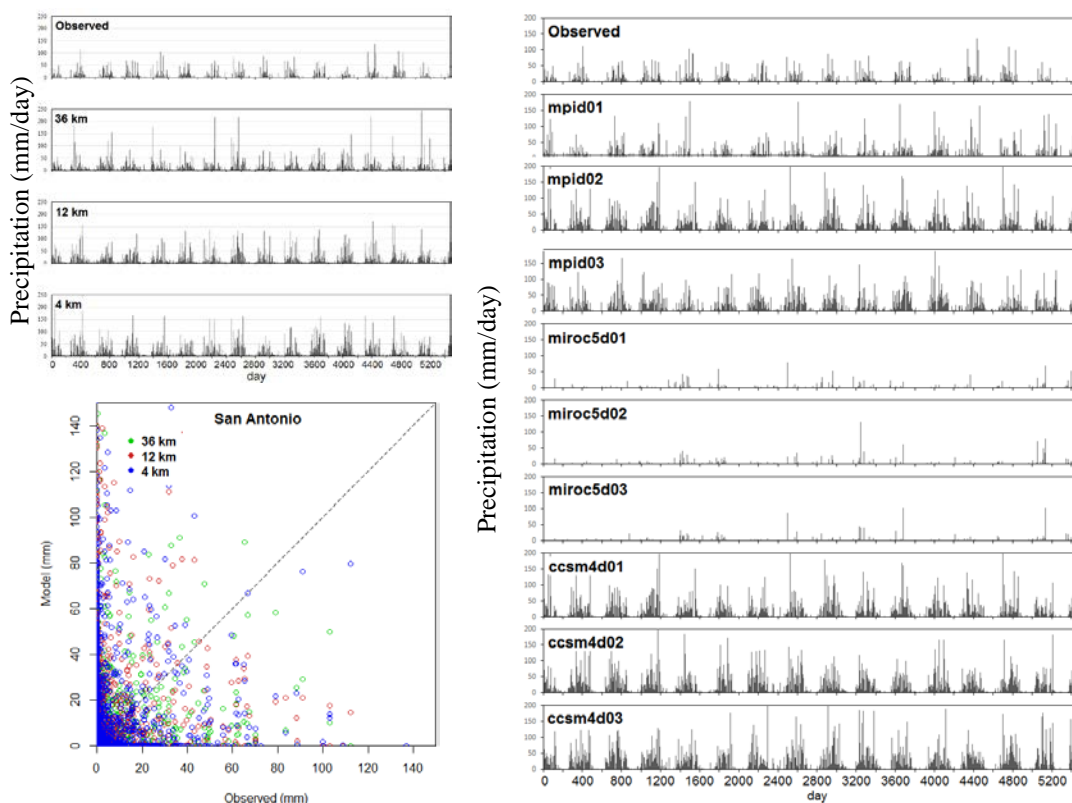


Figure A.11 Potosi, (a) precipitation time series of observed versus reanalysis-driven WRF for the period of 1996-2010, (b) precipitation scatterplot of reanalysis-driven WRF versus observed and (c) precipitation time series of observed (1996-2010) versus GCM-driven WRF for the period of 2006-2020

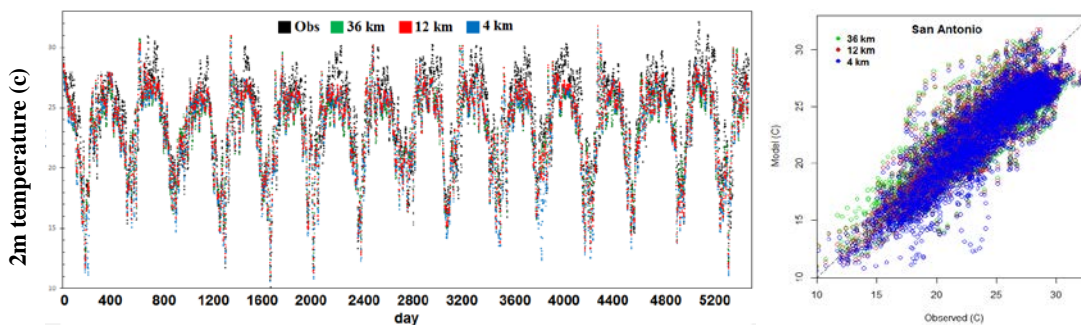


Figure A.12 Potosi, (a) temperature time series (10-day running average) of observed versus reanalysis-driven WRF for the period of 1996-2010, (b) temperature scatterplot of reanalysis-driven WRF versus observed

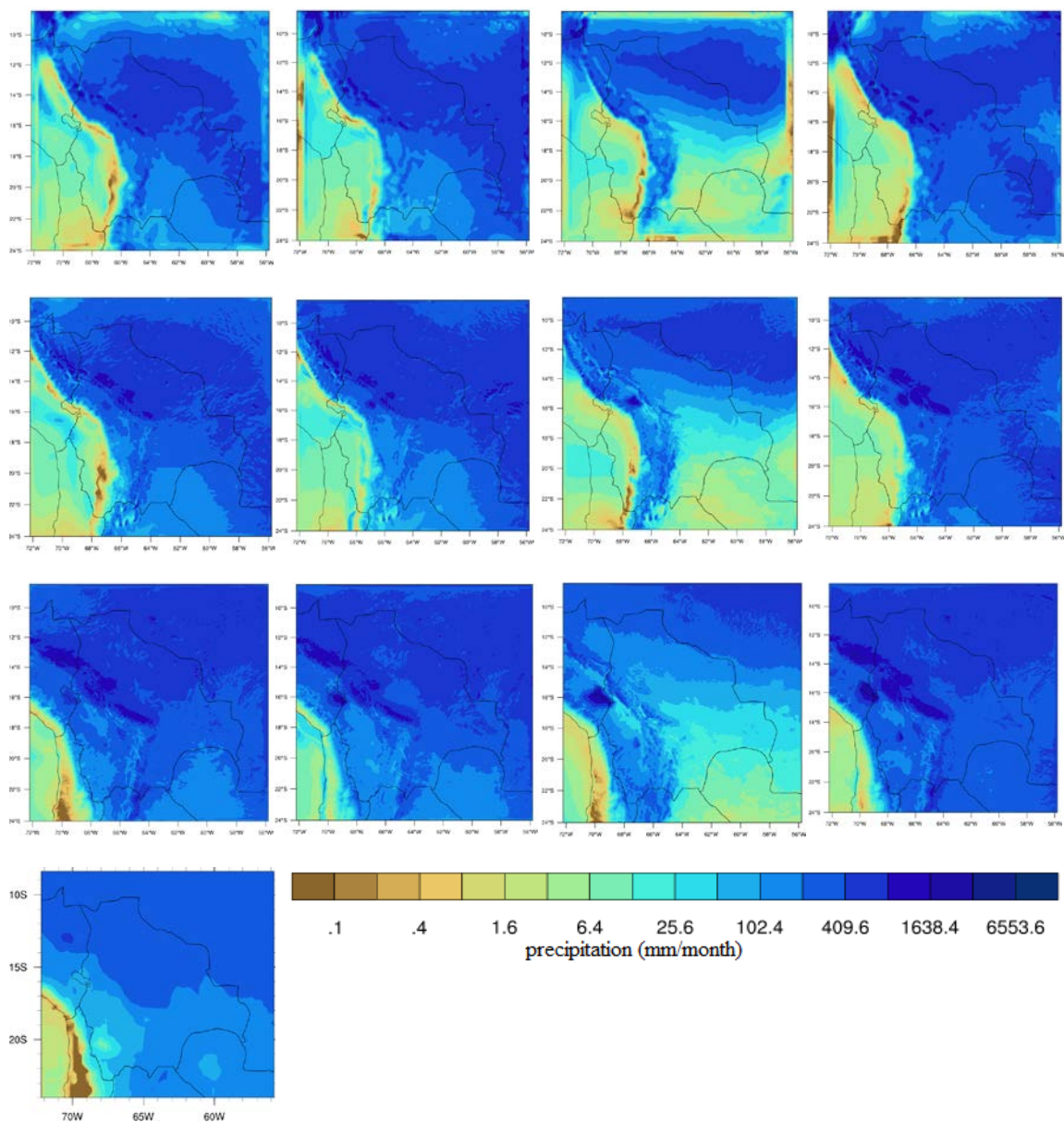


Figure A.13 Wet season (DJF) climatological mean of precipitation (mm/month) for observed, 1996-2010 (4th row) versus reanalysis-driven WRF, 1996-2010 (1st column) from lower resolution of 36 km (1st row) to 4 km (3rd row) and GCM-driven WRF, 2006-2020; MPI (2nd column), MIROC (3rd column) and CCSM4 (4th column). The original spatial resolutions of modeled and observed datasets have been used.

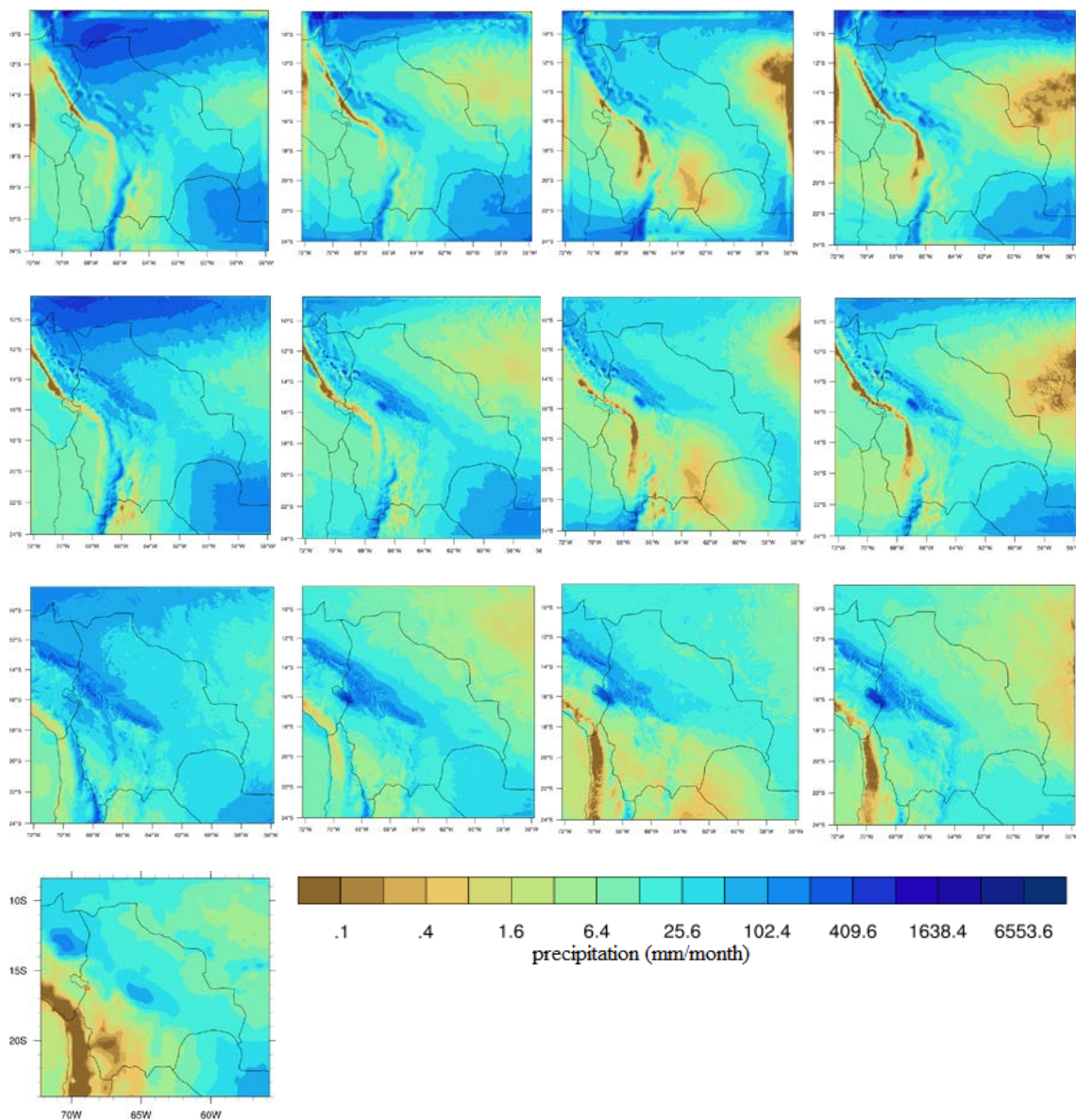


Figure A.14 Dry season (DJF) climatological mean of precipitation (mm/month) for observed, 1996-2010 (4th row) versus reanalysis-driven WRF, 1996-2010 (1st column) from lower resolution of 36 km (1st row) to 4 km (3rd row) and GCM-driven WRF, 2006-2020; MPI (2nd column), MIROC (3rd column) and CCSM4 (4th column). The original spatial resolutions of modeled and observed datasets have been used.

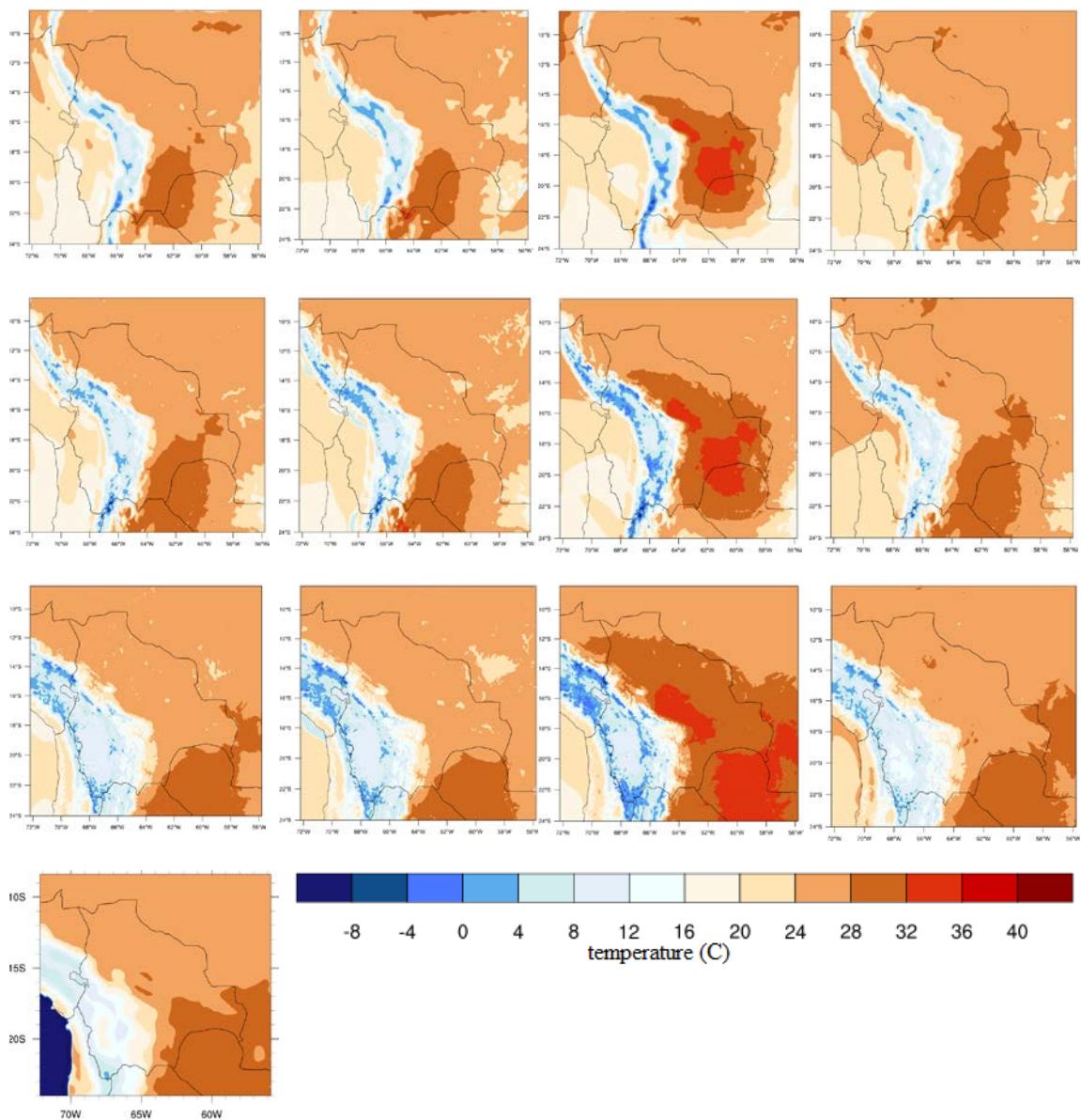


Figure A.15 Summer (DJF) climatological mean of temperature (degree C) for observed, 1996-2010 (4th row) versus reanalysis-driven WRF, 1996-2010 (1st column) from lower resolution of 36 km (1st row) to 4 km (3rd row) and GCM-driven WRF, 2006-2020; MPI (2nd column), MIROC (3rd column) and CCSM4 (4th column). The original spatial resolutions of modeled and observed datasets have been used.

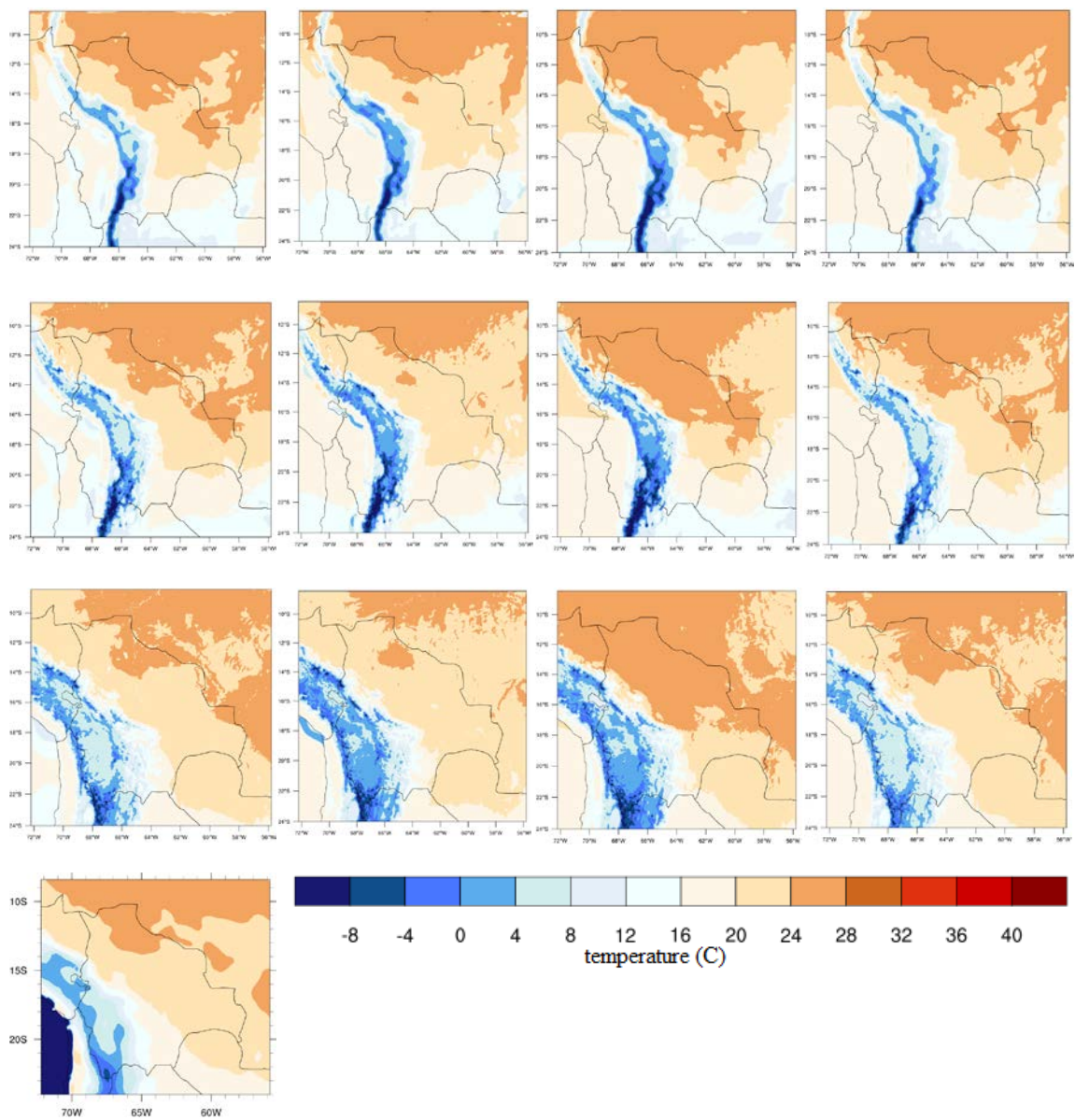


Figure A.16 Winter (DJF) climatological mean of temperature (degree C) for observed, 1996-2010 (4th row versus reanalysis-driven WRF, 1996-2010 (1st column)) from lower resolution of 36 km (1st row) to 4 km (3rd row) and GCM-driven WRF, 2006-2020; MPI (2nd column), MIROC (3rd column) and CCSM4 (4th column). The original spatial resolutions of modeled and observed datasets have been used.

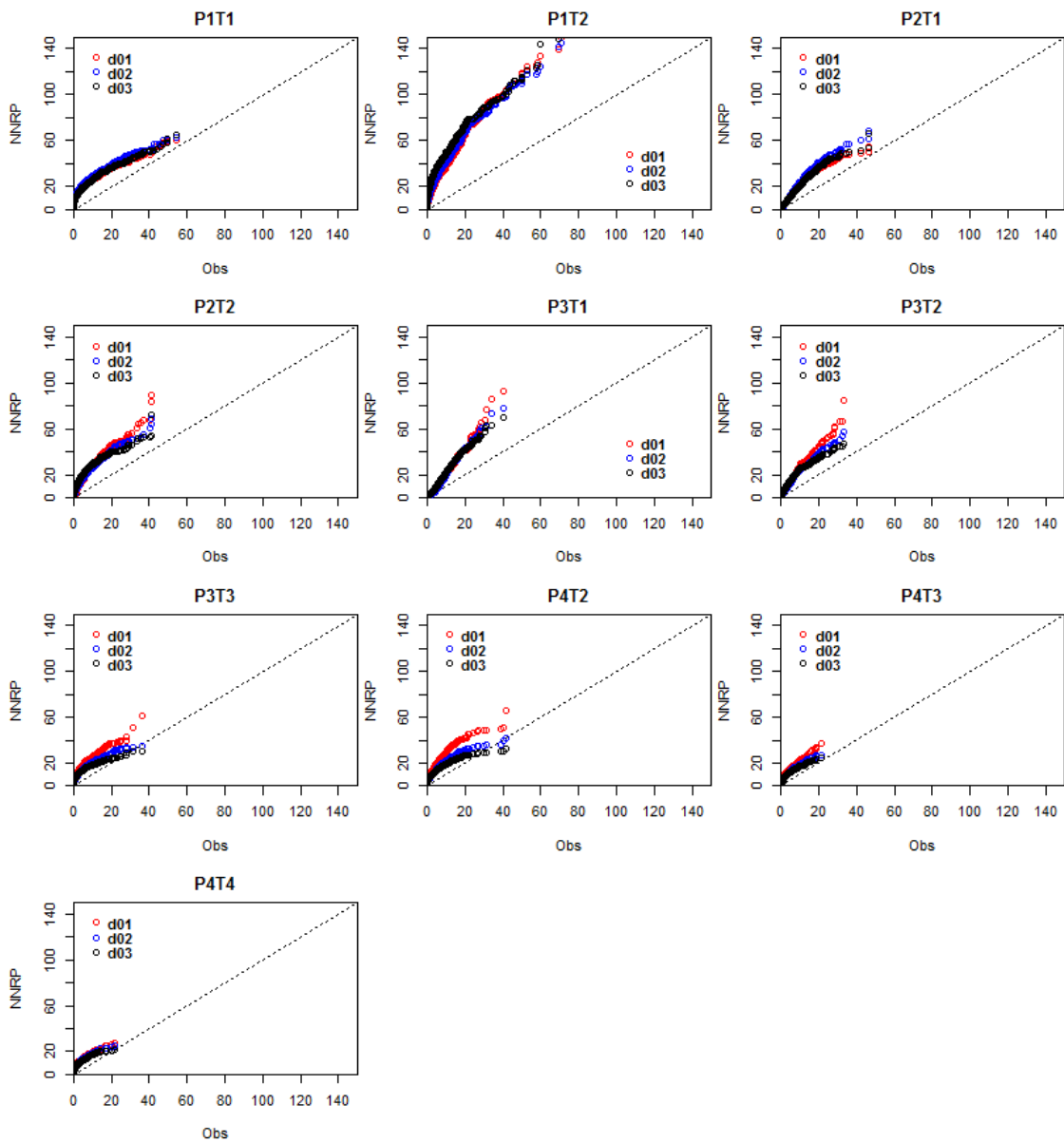


Figure A.17 QQ-plot of NNRP-driven WRF versus observed data for the wet season (DJF) daily precipitation over the defined climate regions. Dashed lines illustrate the perfect match between models and observation. The original spatial resolutions of modeled and observed datasets have been used.

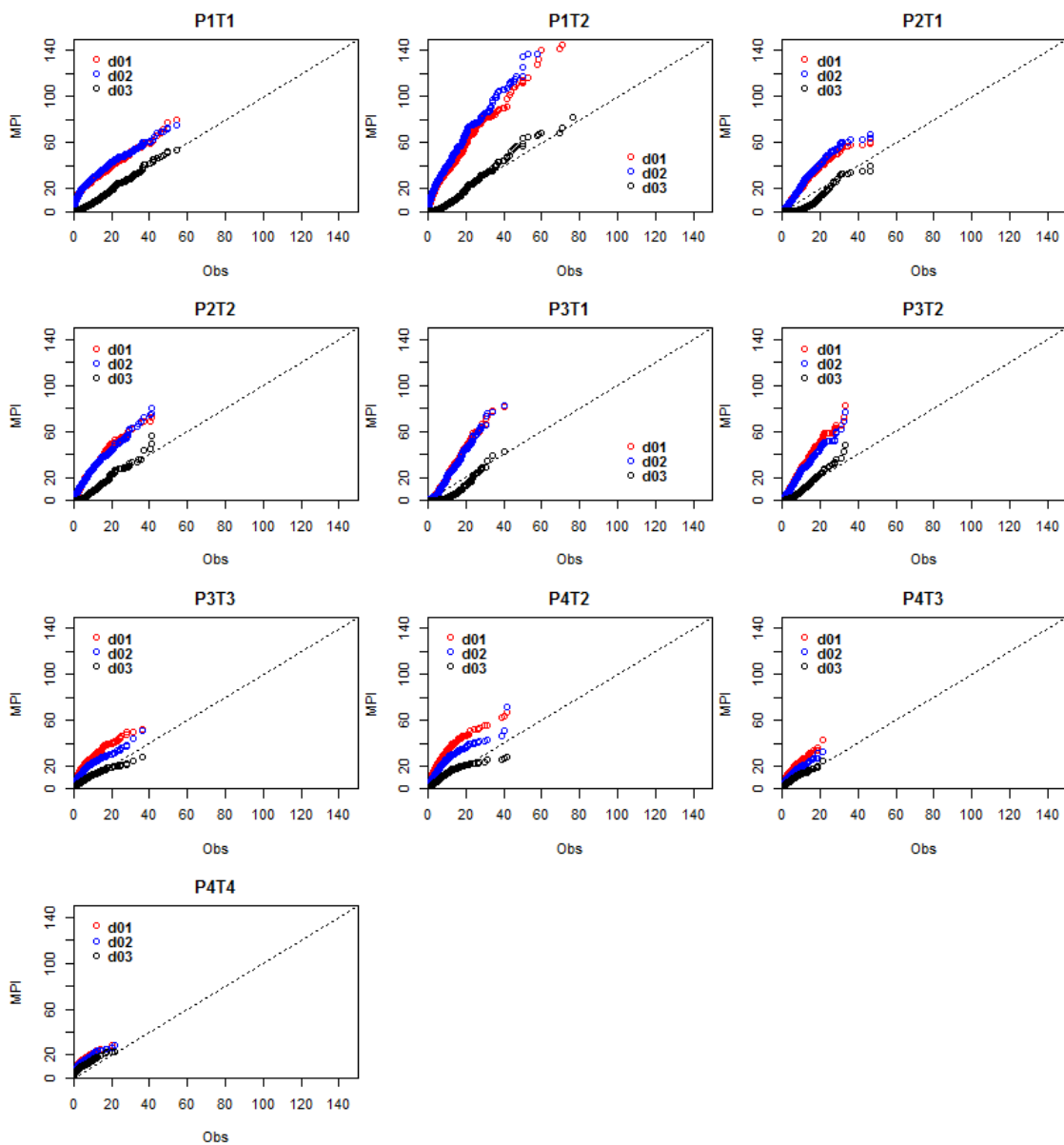


Figure A.18 QQ-plot of MPI-driven WRF versus observed data for the wet season (DJF) daily precipitation over the defined climate regions. Dashed lines illustrate the perfect match between models and observation. The original spatial resolutions of modeled and observed datasets have been used.

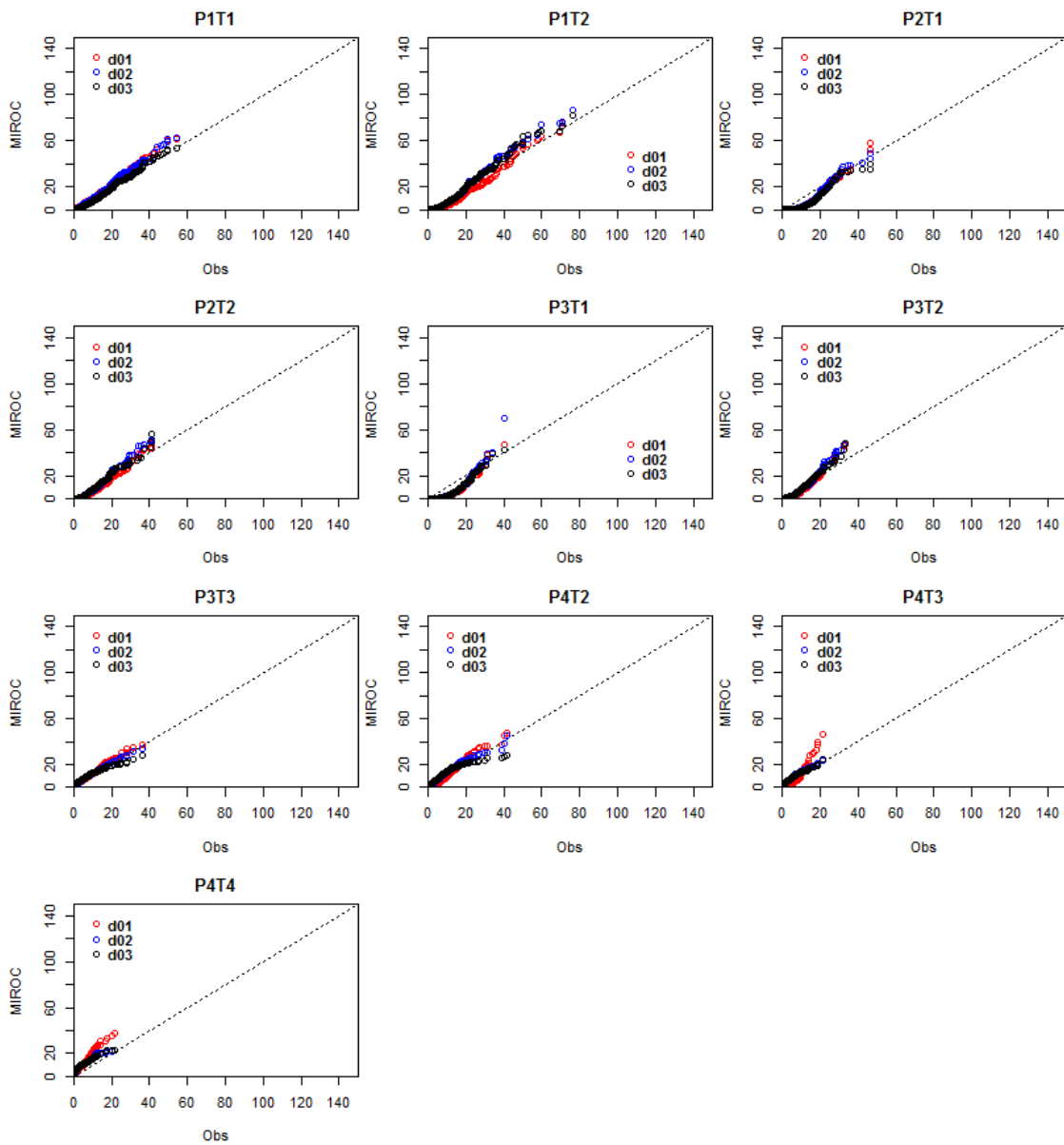


Figure A.19 QQ-plot of MIRPC5-driven WRF versus observed data for the wet season (DJF) daily precipitation over the defined climate regions. Dashed lines illustrate the perfect match between models and observation. The original spatial resolutions of modeled and observed datasets have been used.

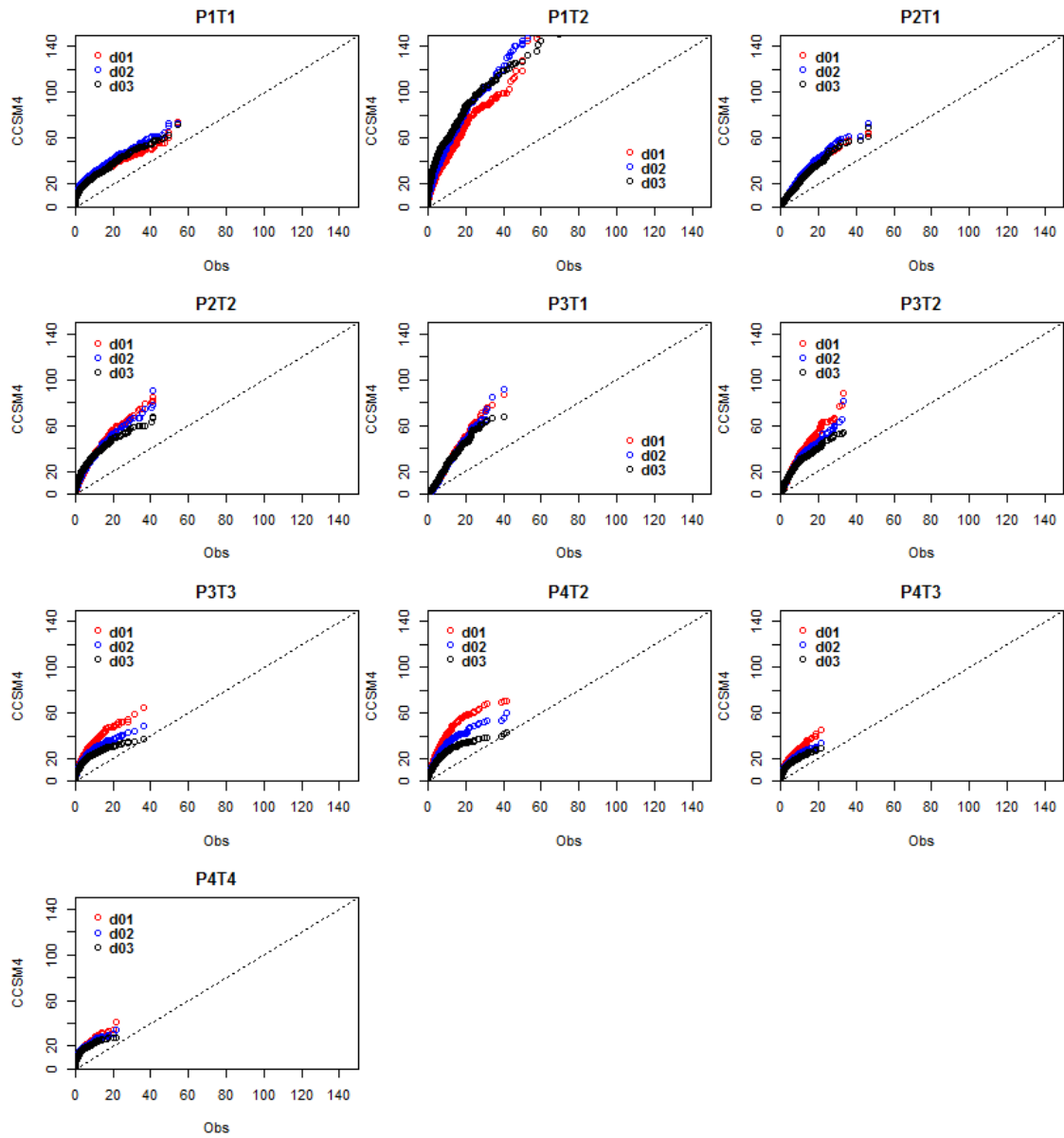


Figure A.20 QQ-plot of CCSM4-driven WRF versus observed data for the wet season (DJF) daily precipitation over the defined climate regions. Dashed lines illustrate the perfect match between models and observation. The original spatial resolutions of modeled and observed datasets have been used.

B. This section provides the supplementary material for chapter 5.

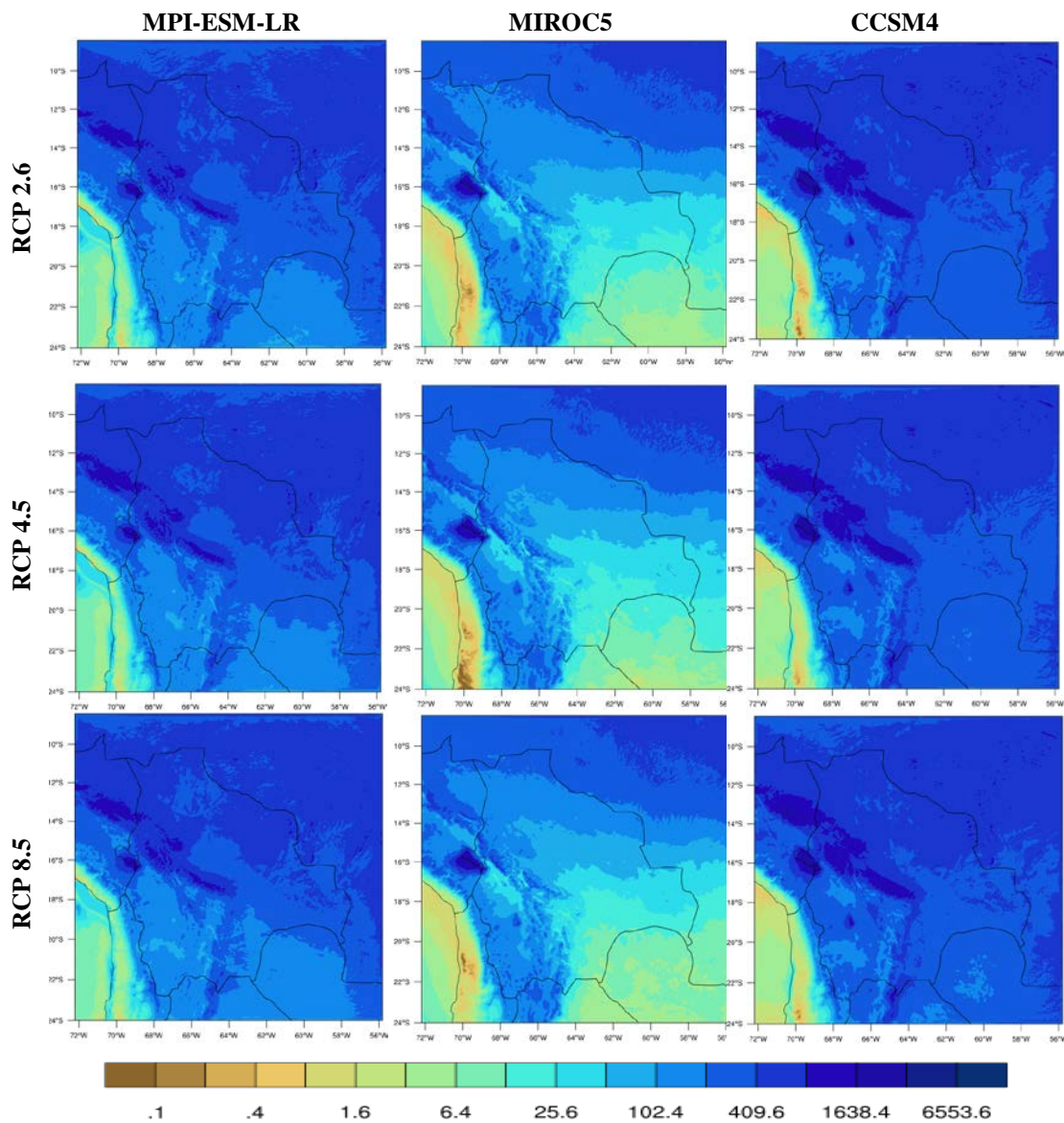


Figure B.1 Mean seasonal average of precipitation during DJF over 2006-2020 representing the present day climate (in mm) for three GCMs shown on the columns: MPI-ESM-LR (left), MIROC5 (middle) and CCSM4 (right) and three RCPs specified in different rows: RCP 2.6 (top), RCP 4.5 (middle) and RCP 8.5 (bottom).

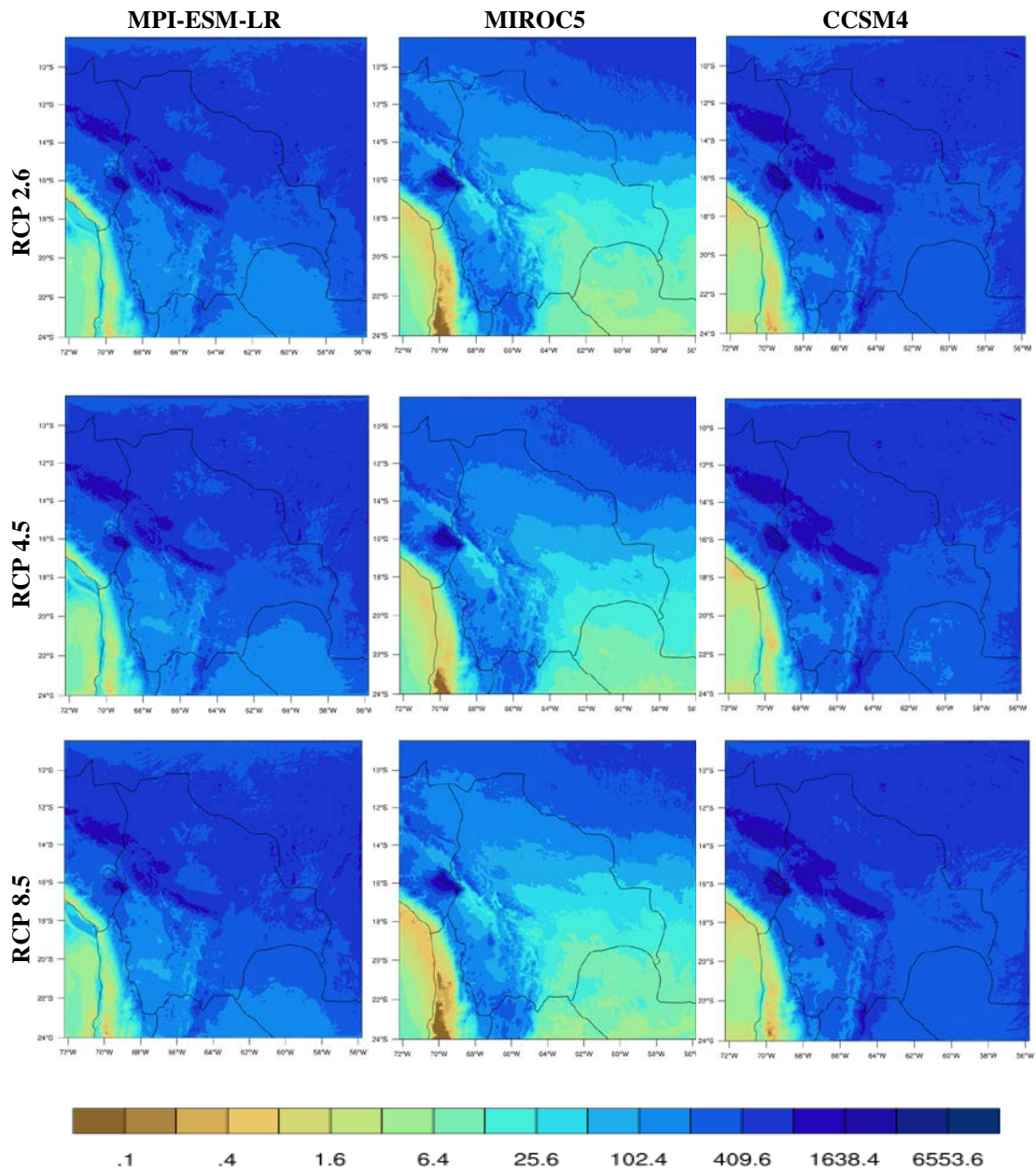


Figure B.2 Mean seasonal average of precipitation during DJF over 2066-2080 representing the future climate (in mm) for three GCMs shown on the columns: MPI-ESM-LR (left), MIROC5 (middle) and CCSM4 (right) and three RCPs specified in different rows: RCP 2.6 (top), RCP 4.5 (middle) and RCP 8.5 (bottom).

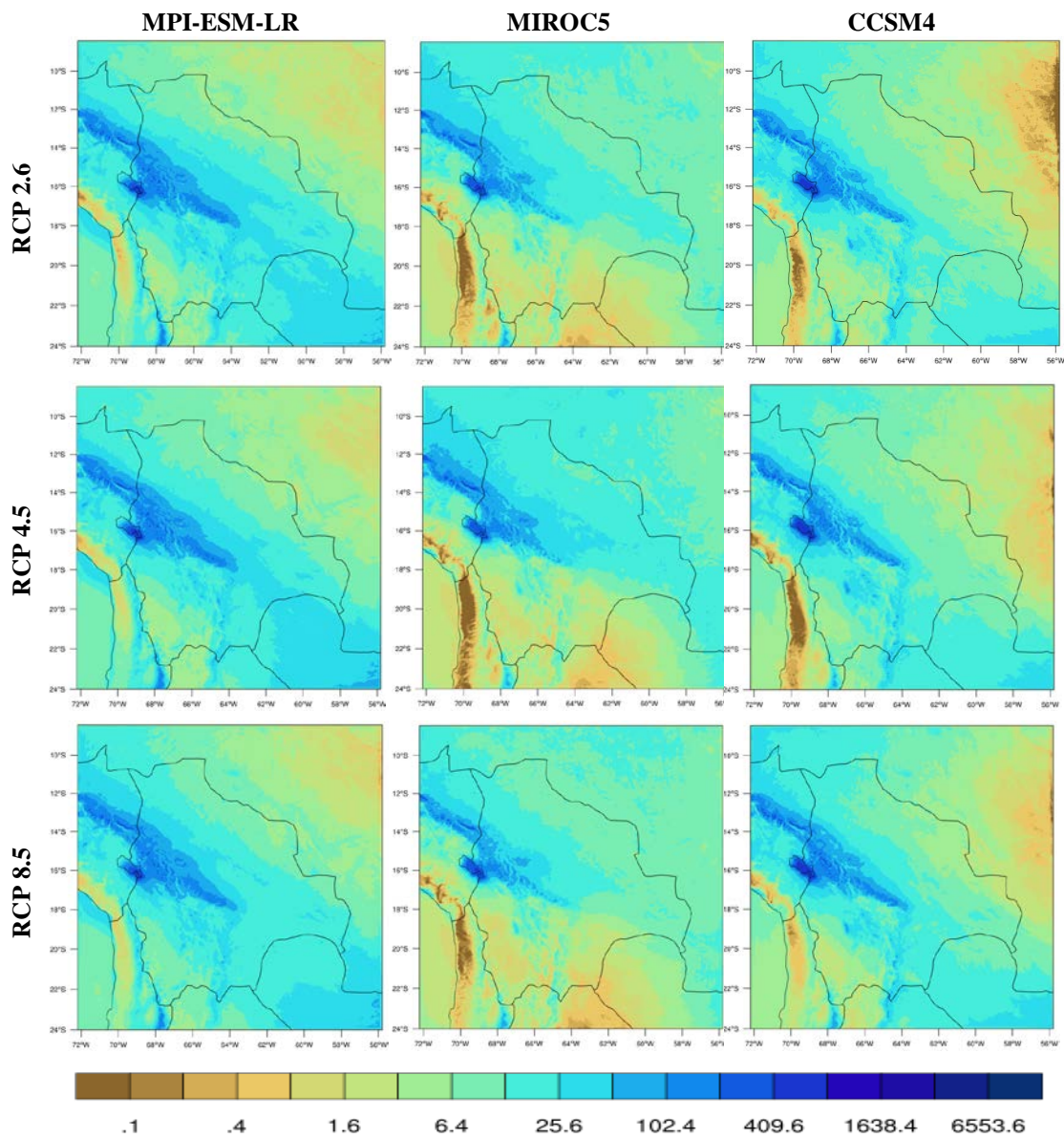


Figure B.3 Mean seasonal average of precipitation during JJA over 2006-2020 representing the present day climate (in mm) for three GCMs shown on the columns: MPI-ESM-LR (left), MIROC5 (middle) and CCSM4 (right) and three RCPs specified in different rows: RCP 2.6 (top), RCP 4.5 (middle) and RCP 8.5 (bottom).

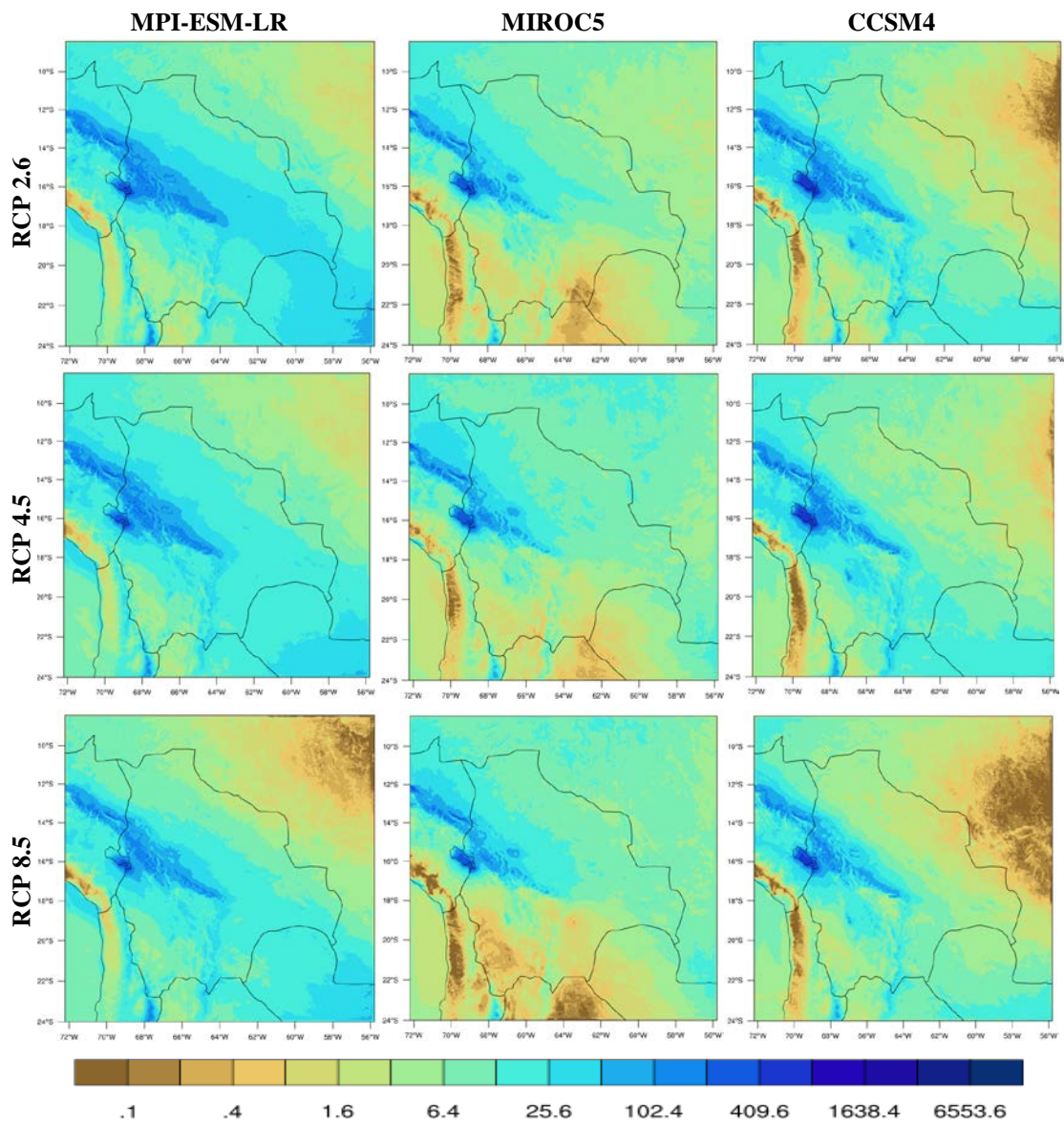


Figure B.4 Mean seasonal average of precipitation during JJA over 2066-2080 representing the future climate (in mm) for three GCMs shown on the columns: MPI-ESM-LR (left), MIROC5 (middle) and CCSM4 (right) and three RCPs specified in different rows: RCP 2.6 (top), RCP 4.5 (middle) and RCP 8.5 (bottom).

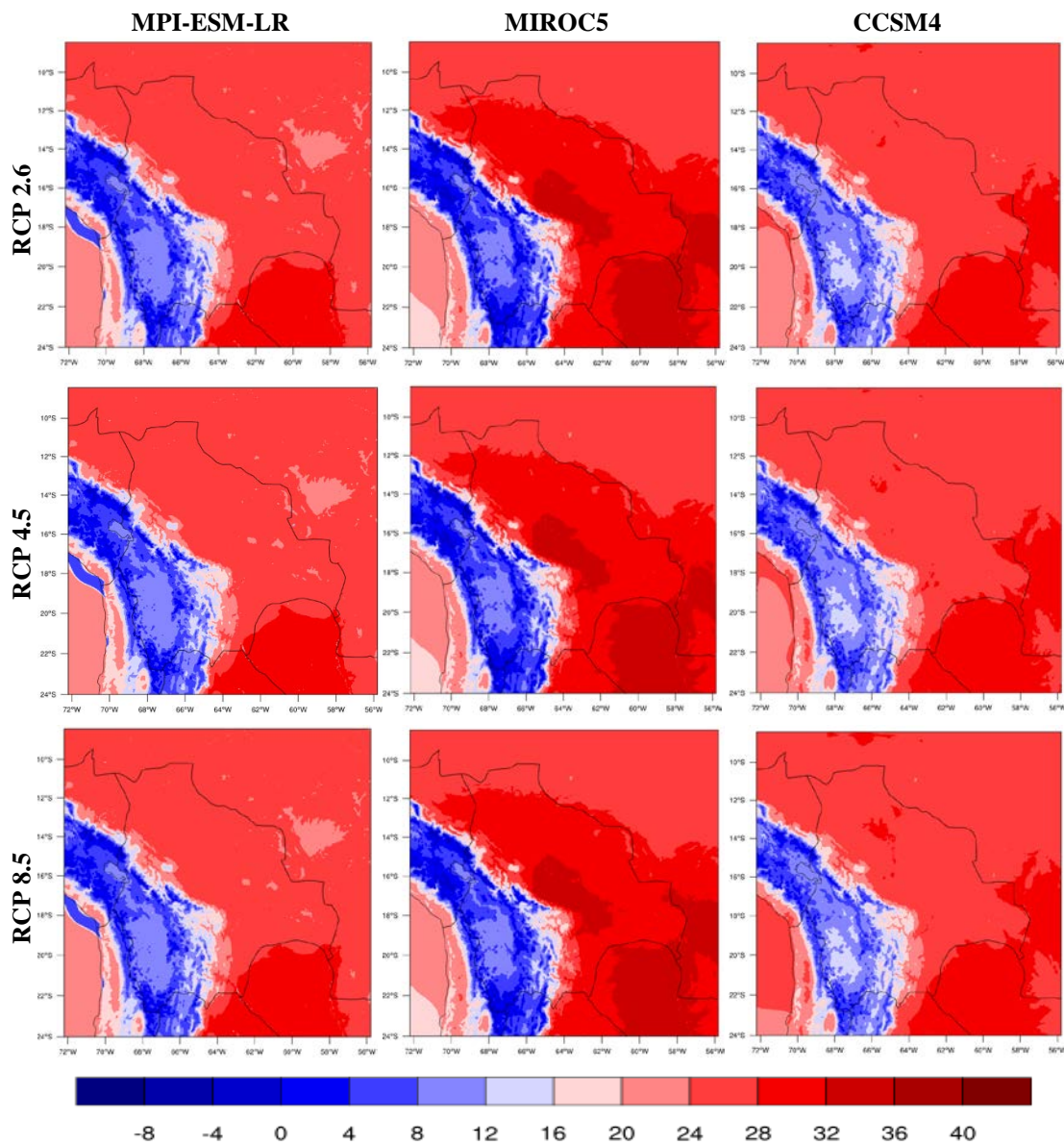


Figure B.5 Mean seasonal average of temperature during DJF over 2006-2020 representing the present day climate (in mm) for three GCMs shown on the columns: MPI-ESM-LR (left), MIROC5 (middle) and CCSM4 (right) and three RCPs specified in different rows: RCP 2.6 (top), RCP 4.5 (middle) and RCP 8.5 (bottom).

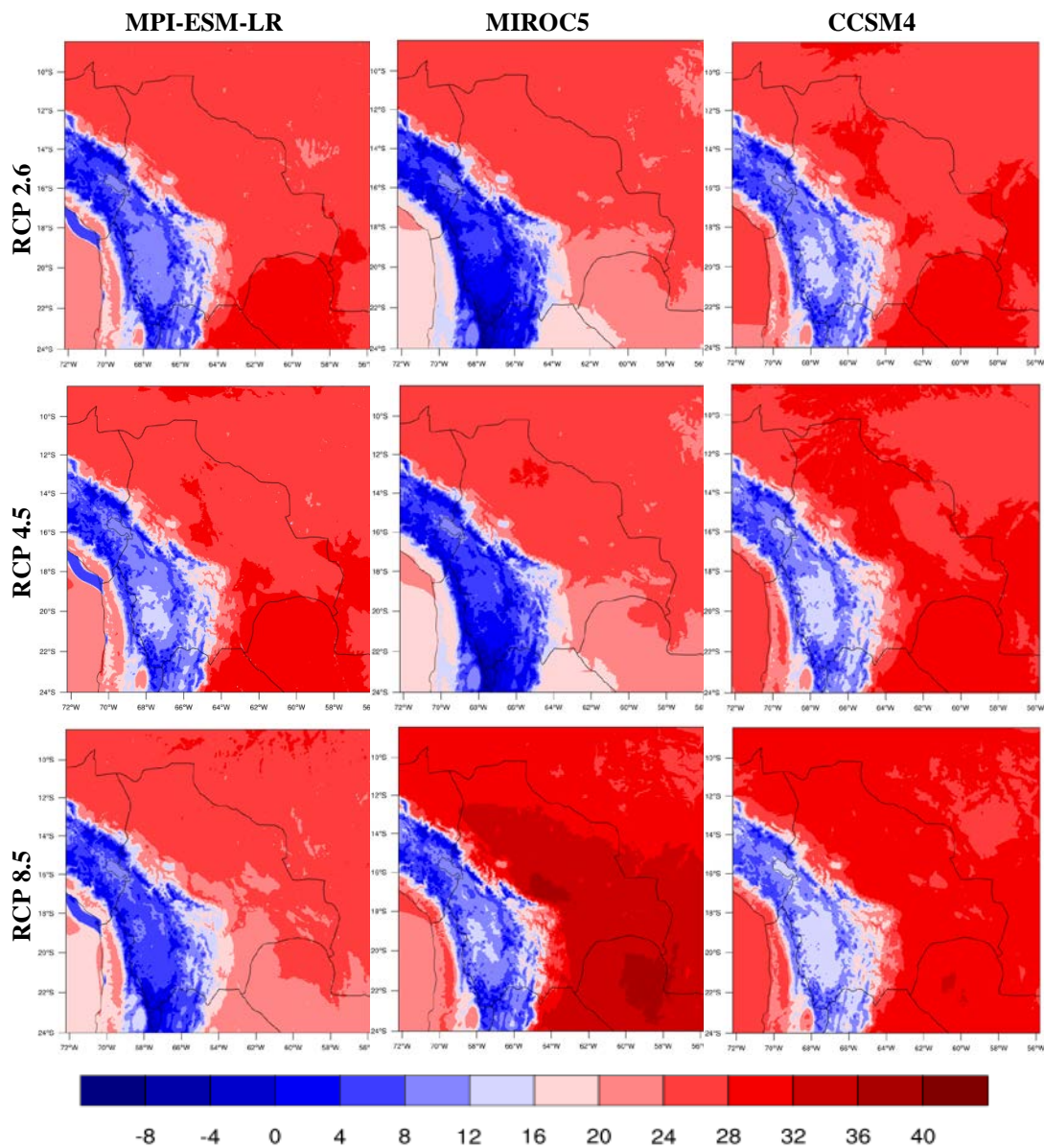


Figure B.6 Mean seasonal average of temperature during DJF over 2066-2080 representing the future climate (in mm) for three GCMs shown on the columns: MPI-ESM-LR (left), MIROC5 (middle) and CCSM4 (right) and three RCPs specified in different rows: RCP 2.6 (top), RCP 4.5 (middle) and RCP 8.5 (bottom).

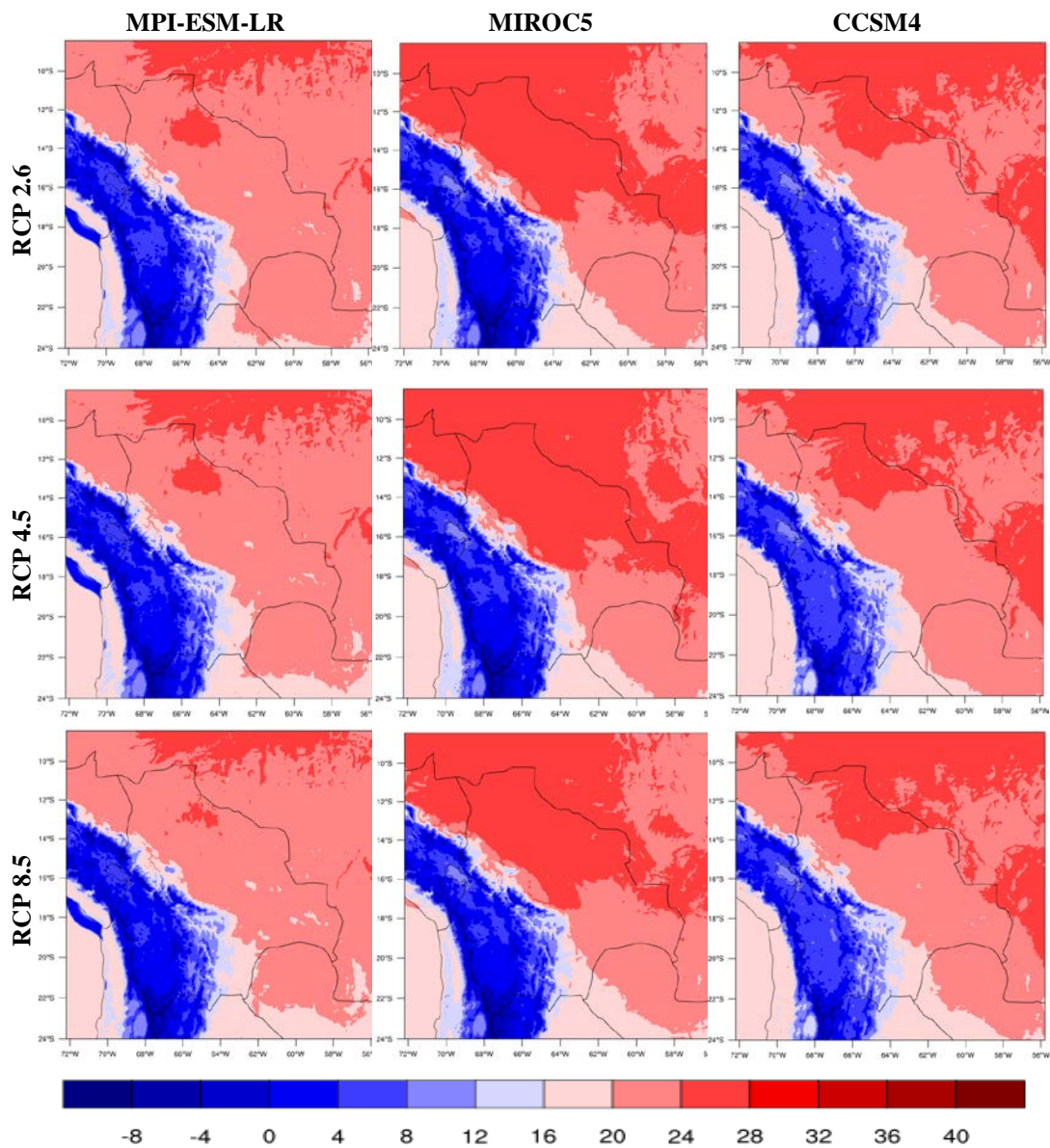


Figure B.7 Mean seasonal average of temperature during JJA over 2006-2020 representing the present day climate (in mm) for three GCMs shown on the columns: MPI-ESM-LR (left), MIROC5 (middle) and CCSM4 (right) and three RCPs specified in different rows: RCP 2.6 (top), RCP 4.5 (middle) and RCP 8.5 (bottom).

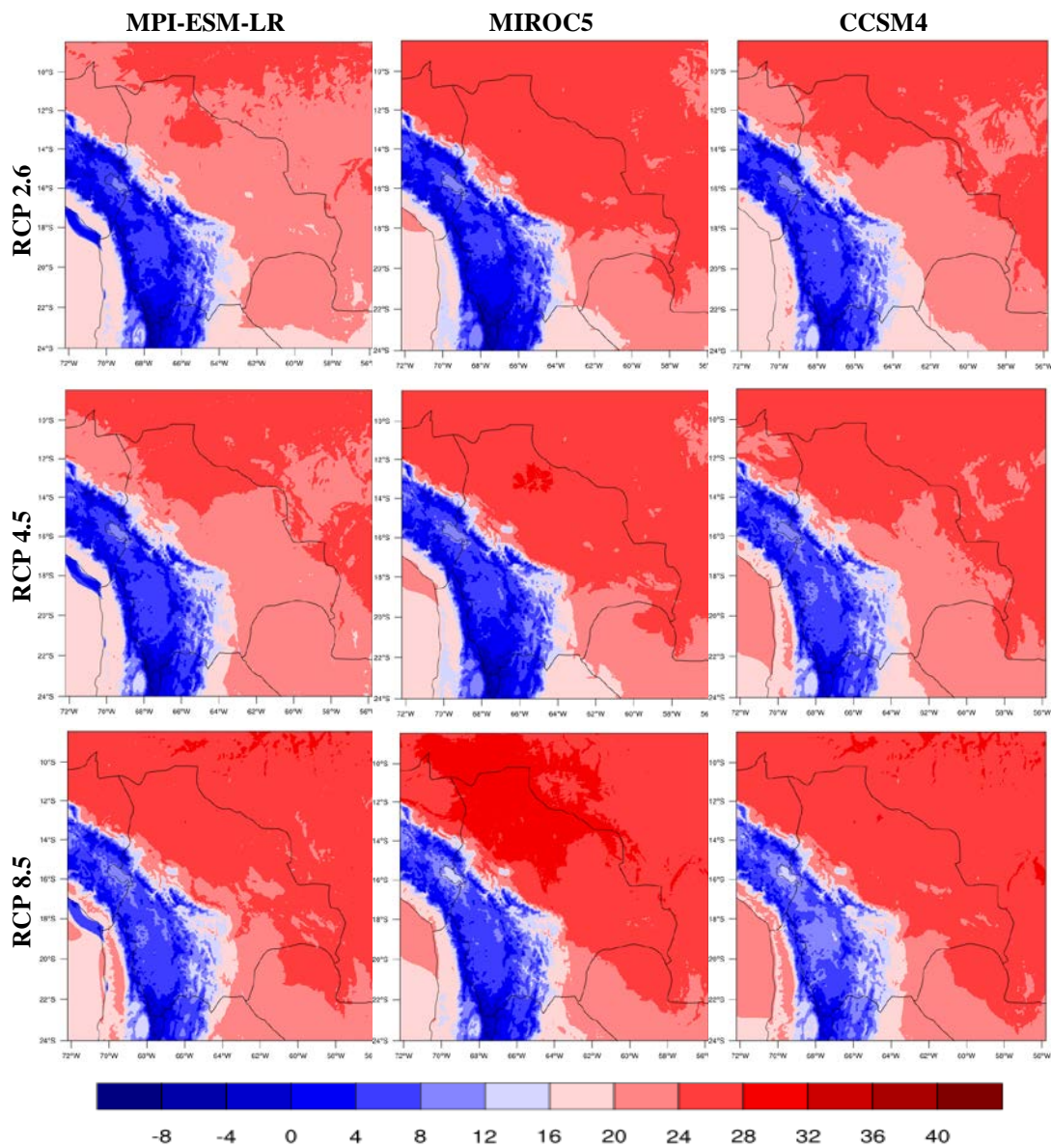


Figure B.8 Mean seasonal average of temperature during JJA over 2066-2080 representing the future climate (in mm) for three GCMs shown on the columns: MPI-ESM-LR (left), MIROC5 (middle) and CCSM4 (right) and three RCPs specified in different rows: RCP 2.6 (top), RCP 4.5 (middle) and RCP 8.5 (bottom).